KANSAS GEOLOGICAL SURVEY
OPEN-FILE REPORT 95-37

HYDROSTRATIGRAPHIC CONTROLS ON GROUND-WATER FLOW AND THE DISTRIBUITON OF CHLORIDE IN THE UPPER DAKOTA AQUIFER OF SOUTHWESTERN ELLIS COUNTY, KANSAS

by

Martin E. Smith

Disclaimer

The Kansas Geological Survey does not guarantee this document to be free from errors or inaccuracies and disclaims any responsibility or liability for interpretations based on data used in the production of this document or decisions based thereon. This report is intended to make results of research available at the earliest possible date, but is not intended to constitute final or formal publications.

Kansas Geological Survey
1930 Constant Avenue
University of Kansas
Lawrence, KS 66047-3726

Hydrostratigraphic Controls on Ground-Water Flow and the Distribution of Chloride in the Upper Dakota Aquifer of Southwestern Ellis County, Kansas

by

Martin Everett Smith

B.S., Michigan State University, 1992

Submitted to the Department of
Geology and the Faculty of the
Graduate School of The University
of Kansas in partial fulfillment
of the requirements for the degree
of Master of Science.

_____
Professor in Charge

_____

_____
Committee Members

_____
for the Department

Date Accepted: _____

Abstract

In southwestern Ellis County, the upper Dakota aquifer (Dakota Formation) is composed of a complex arrangement of sandstone lenses (aquifer subunits) encased in mudstone (aquitard subunits). The interconnection and distribution of the these aquifer subunits are poorly understood. The problem of water resources development is compounded by the presence of a saline-water, transition zone in the eastern portion of the county. This project investigated both the geologic heterogeneity of the upper Dakota aquifer and the flow and transport processes in the study area.

The subsurface was investigated using 1,131 gamma-ray logs. The upper Dakota aquifer was divided into three zones, and the cumulative aquifer subunit thickness was determined for each. Directional semivariograms were used to determine the spatial correlation of the aquifer subunits along specific orientations. The analysis shows the high degree of local variability in thickness values at the local scale. Block kriging was then used to determine the arrangement of aquifer subunits within each zone and was incorporated into the modeling as heterogeneity. Results indicate that the lowest zone should have the highest degree of interconnection, while areas of interconnection in the middle and upper zones are patchy. However, the middle zone showed a strong east-west trend in its areas of interconnection, while the upper zone had a slight north-south trend.

Modeling results indicate that the lowest zone of the Dakota Formation is the most transmissive. Furthermore, the hydraulic conductivity was 100 times lower in the north-south than the east-west direction, resulting in a highly elliptical cone of depression during pumping. Therefore, wells should be located farther away from each other in the east-west direction to avoid overlapping cones of depression. Finally, there should be no regional deterioration in water quality due to pumping over a ten year period.

Different model configurations were used to evaluate end-member transport processes in the study area. Advection dominates transport in the interconnected aquifer subunits, and lateral flow from the west controls the chloride distribution. However, diffusion dominates transport in the areas isolated from the regional flow system, and the specified chloride concentration of the lower aquitard controls the chloride distribution.

TABLE OF CONTENTS

Page

ABSTRACT ii

TABLE OF CONTENTS iv

LIST OF FIGURES vii

LIST OF TABLES xi

ACKNOWLEDGMENTS xii

CHAPTER 1. INTRODUCTION 1

CHAPTER 2. HYDROGEOLOGIC SETTING 5

2.1. Previous Work 5

2.2. Physiography 5

2.3. Geologic Framework 5

2.4. Hydrostratigraphy 10

2.5. Ground-Water Flow in the Upper Dakota Aquifer 12

2.6. Salinity in the Upper Dakota Aquifer 16

2.7. Summary of Hydrogeologic Setting 31

CHAPTER 3. ANALYSIS OF THE DAKOTA AQUIFER FRAMEWORK 32

3.1. Subsurface Data 32

3.1.1. Gamma-Ray Logs 32

3.1.2. Elevation and Thickness of Hydrostratigraphic Units 34

3.2. Subdivision of the Upper Dakota Aquifer 34

3.2.1. Three Zones of the Upper Dakota Aquifer 34

3.2.2. Method Used to Distinguish Aquifer and Aquitard Subunits 40

3.2.3. The Percentages of Aquifer Subunits by Zone 42

3.3. Geostatistics 51

3.3.1. Background 51

3.3.2. Results of Semivariograms 58

3.3.3. Kriging 63

CHAPTER 4. MODEL DESCRIPTION AND INPUT PARAMETERS 69
4.1. Conceptual Model of Ground-Water Flow and Mass Transport 69
4.2. Description of Numerical Modeling Programs 72
4.3. Model Domain and Boundary Conditions 75
4.3.1. Model Grid and Layers 75
4.3.2. Boundary Conditions for the Flow Model 76
4.3.3. Boundary Conditions for the Transport Model 81
4.4. Model Input Data 81
4.4.1. Water-Level Data 83
4.4.2. Water Quality Data 84
4.4.3. Hydrogeologic Properties 86
4.4.3a. Hydraulic Conductivities 88
4.4.3b. Storativities 89
4.4.3c. Transport Properties 89
CHAPTER 5. MODEL CALIBRATION AND RESULTS 91
5.1. Introduction 91
5.2. Calibration of the Steady-State Flow Field 91
5.2.1. Methodology 93
5.2.2. Horizontal Heterogeneity in the Aquifer 94
5.2.3. Alternate Hydraulic Conductivity Fields 99
5.3. Conservative Transport Modeling 99
5.3.1. Transport Through a Well-Connected Aquifer 101
5.3.2. Transport Through a Poorly-Connected Aquifer 104
5.4. Modeling Results and Summary of Calibrated Properties 105
5.4.1. Steady-State Flow Field and Water Budget 106
5.4.2. Transport Modeling Results 109
5.4.3. Summary of Calibrated Properties 115

CHAPTER 6. SENSITIVITY ANALYSES 121
6.1. Introduction 121
6.2. Flow Field 121
6.2.1. The Effect of the Upper Cretaceous Aquitard 123
6.2.2. The Effect of Hydraulic Conductivity in the Upper Dakota Aquifer 123
6.2.3. The Effect of Heterogeneity in the Upper Dakota Aquifer 125
6.3. Chloride Transport 132
6.3.1. Sensitivity Analysis on Simulation C2 135
6.3.2. Sensitivity Analysis on Simulation C3 138
6.4. Summary of Sensitivity Analysis Results 138
CHAPTER 7. EVALUATION OF PUMPING WELLS 142
7.1. Introduction 142
7.2. Transient Calibration from Pumping Test Results 142
7.3. Some Results of Pumping Wells in the Upper Dakota Aquifer 143
CHAPTER 8. SUMMARY AND CONCLUSIONS 149
REFERENCES 152
APPENDIX 1. Gamma-Ray Log Database 155
APPENDIX 2. Stratigraphic Thicknesses from Well Logs 181
APPENDIX 3. Collection of Modeled Directional Semivariograms 205

LIST OF FIGURES

Figure		Page
1.1	Location map of study area in relation to western Kansas	2
1.2	Study area in Ellis County shown by township and range	3
2.1	Topographic map of Ellis County with rivers and township lines	6
2.2	Geologic cross-section through study area	8
2.3	Cross-section of hydrostratigraphy in study area	11
2.4	Extent of Kiowa shale aquitard	13
2.5	Extent of the Upper Cretaceous aquitard	14
2.6	Subcrop of Cedar Hills Sandstone beneath the lower Dakota aquifer	15
2.7	Potentiometric surface map of the Dakota aquifer	17
2.8	Map of water well locations in the study area with head data	18
2.9	Map of Ellis County with sample points shown with chloride concentration listed beside the data points	19
2.10	Generalized contour map of total dissolved solids in the upper Dakota aquifer in the study area	20
2.11	Location map of sample wells from which depth profiles were taken	21
2.12	Depth profiles of chloride concentration in Ellis County	22
2.13a-g	Depth profiles of salinity in Russell County	24 - 30
3.1	Distribution of wells having gamma-ray logs	33
3.2a	Map of Kiowa shale top from gamma-ray logs	35
3.2b	Map of Kiowa shale thickness from gamma-ray logs	36
3.3a	Map of Dakota Formation top from gamma-ray logs	37
3.3b	Map of Dakota Formation thickness from gamma-ray logs	38

3.4 Map of Upper Cretaceous aquitard thickness from gamma-ray logs 39
3.5 Illustration of the three zones of the upper Dakota aquifer 41
3.6a Histogram of aquifer subunit thickness in Zone 1 44
3.6b Histogram of aquifer subunit thickness in Zone 2 45
3.6c Histogram of aquifer subunit thickness in Zone 3 46
3.7 Map showing a blown up area with highly variable thickness values 47
3.8a Map of aquifer subunit thickness of actual data for Zone 1 48
3.8b Map of aquifer subunit thickness of actual data for Zone 2 49
3.8c Map of aquifer subunit thickness of actual data for Zone 3 50
3.9 Illustration of the range and sill of a semivariogram 53
3.10 Illustration of lag and distance tolerance in regular and irregular data sets for semivariograms 54
3.11 Illustration of angle tolerance and bandwidth for semivariograms 56
3.12 Illustration of exponential model fitting to an experimental semivariogram with the nugget effect 57
3.13 Rose plots of zonal anisotropy in each zone 62
3.14a Map showing Kriging results of aquifer subunit thickness for Zone 1 65
3.14b Map showing Kriging results of aquifer subunit thickness for Zone 2 66
3.14c Map showing Kriging results of aquifer subunit thickness for Zone 3 67
3.15 Population distribution of aquifer subunit thickness assigned to the model cells 68
4.1 Illustration of the conceptual flow model 71
4.2 Illustration of the conceptual mass-transport model 73
4.3 Illustration of the seven model layers 77
4.4 Illustration of the leaky aquifer boundary condition and the parameters required by MODFLOW 78
4.5 Illustration of the flow model's boundary conditions 80
4.6 Illustration of the transport model's boundary conditions 82

4.7 Map of potentiometric surface of the Dakota aquifer in the study area..... 85

4.8 Plot of chloride concentration versus total dissolved solids (TDS) concentration 87

5.1 Illustration of high and low aquifer subunit connection and how it could effect transmissivity 96

5.2 Illustration of how the degree of aquifer subunit isolation could effect transmissivity 98

5.3 Contours of chloride concentration in the study area 102

5.4 Map comparing the observed potentiometric surface to that of the modeled surface 107

5.5 Illustration of the flow budget 108

5.6a Map showing the modeled chloride distribution in the well-connected, hydraulic conductivity field..... 110

5.6b Map showing the modeled chloride distribution in the poorly-connected, hydraulic conductivity field..... 111

5.7 Graph of average inflow concentration versus time..... 112

5.8 Graph of the specified concentration gradient in model layer 7..... 113

5.9a Model grid with high and low transmissive regions for Zone 1..... 117

5.9b Model grid with high and low transmissive regions for Zone 2..... 118

5.9c Model grid with high and low transmissive regions for Zone 3..... 119

6.1 Graph of sensitivity analysis on the vertical hydraulic conductivity of Upper Cretaceous aquitard..... 124

6.2 Graph of sensitivity analysis on the horizontal hydraulic conductivity of the upper Dakota aquifer..... 126

6.3 Graph of sensitivity analysis on the vertical hydraulic conductivity of the upper Dakota aquifer..... 127

6.4 Graph of sensitivity analysis on the horizontal anisotropy factor in the upper Dakota aquifer 128

6.5 Graph of sensitivity analysis on the high transmissive regions of the upper Dakota aquifer 130
6.6 Graph of sensitivity analysis on the low transmissive regions of the upper Dakota aquifer 131
6.7 Graph of sensitivity analysis on the sandstone thickness threshold of the upper Dakota aquifer 133
6.8 Graph comparing the heterogeneous model to a homogeneous model..... 134
6.9 Map of the distribution of chloride that develops when the high and low transmissive regions have a contrast in hydraulic conductivity of about two orders of magnitude 137
6.10a Map of the distribution of chloride that develops when the lower boundary has a specified concentration of 2,000 mg/L..... 139
6.10b Map of the distribution of chloride that develops when the lower boundary has a specified concentration of 10,000 mg/L..... 140
7.1 Graph of sensitivity analysis on storativity of the aquifer..... 144
7.2 Map showing the location of pumping wells in layer 3 (Zone 2)..... 145
7.3 Map showing the cone of depression produced by 1 pumping well 147
7.4 Map showing the cones of depression produced by 10 pumping wells..... 148

LIST OF TABLES

Table		Page
2.1	Stratigraphic and hydrostratigraphic names and groupings	7
3.1	Descriptive statistics on aquifer subunit thickness for each zone	43
3.2	Input parameters for semivariogram modeling	59
3.3	Modeled range, sill, and nugget values for each zone	60
5.1	Summary of calibrated model runs for both MODFLOW and MT3D	92
5.2	Summary of flow parameters	116
5.3	Summary of transport parameters	120
6.1	Summary of sensitivity analysis model runs for both MODFLOW and MT3D	122

ACKNOWLEDGMENTS

There are many people who helped make this thesis a success. Their assistance is greatly appreciated, and I will forever be in their debt. First, I would like to thank Dr. P. Allen Macfarlane, Director of the Dakota Project, for his guidance, counsel, and patience throughout the research and writing of this Thesis. I am indebted to the Kansas Geological Survey for its support of this research and the unique opportunity it provided me as a Graduate Research Assistant. Thank you to my committee chair, Dr. G.L. Macpherson, and Dr. D.W. Steeples for their editorial comments and organizational suggestions. The mapping software, WHEAT, developed by Dr. G.W. Pouch of the Kansas Geological Survey was of great assistance in the early and middle stages of this project. Furthermore, valuable assistance was provided by Mark Schoneweis in the final drafting of many of the figures in this Thesis. I am very grateful for his help. Finally, I would like to thank my family and friends for their moral support, especially my wife Elizabeth. I could not have done it without you.

CHAPTER 1. INTRODUCTION

Supplies of surface and ground water are decreasing with time in many areas of central and western Kansas (Macfarlane *et al.*, 1990). The Dakota aquifer is being considered as a potential water resource to replenish the region's dwindling water supplies (Macfarlane *et al.*, 1992). The complexity of the Dakota aquifer makes it difficult to predict the effects of development, especially at the subregional and well field scales. It is highly heterogeneous, being composed of sandstone lenses distributed in a mudstone matrix (Macfarlane *et al.*, 1990). In effect, the regional Dakota aquifer is composed of small scale aquifer and aquitard subunits that may or may not be interconnected. Because the aquifer subunits are much more permeable than the aquitard subunits, ground-water flow occurs primarily through connected aquifer subunits. To further complicate the matter, water quality in the Dakota aquifer is variable, ranging from fresh to highly saline (Macfarlane *et al.*, 1990). The effect development could have on the deterioration of regional water quality in the aquifer is also unknown. It is the purpose of this thesis to further the understanding of the arrangement and occurrence of aquifer subunits and the factors controlling solute movement under natural and pumping conditions in the confined Dakota aquifer.

The study area is located in southwestern Ellis County and is 1,120 km^2 (432 mi^2) in size (Figures 1.1 and 1.2). This investigation concentrates on the Dakota Formation which is hydrostratigraphically equivalent to the upper Dakota aquifer. See Chapter 2 for further explanation on the stratigraphy. This area was chosen for several reasons. The data are relatively abundant including geophysical well logs, water-level measurements, and water-quality information as compared to other areas of the state. The water quality in the upper Dakota aquifer ranges from fresh water ($\leq$ 1,000 mg/L TDS) on the western side of the study area grading into waters of higher salinity ($>$ 5,000 mg/L TDS) on the eastern side (Macfarlane *et al.*, 1990). Lastly, the upper Dakota aquifer is entirely confined, sandwiched between two regional aquitard units.

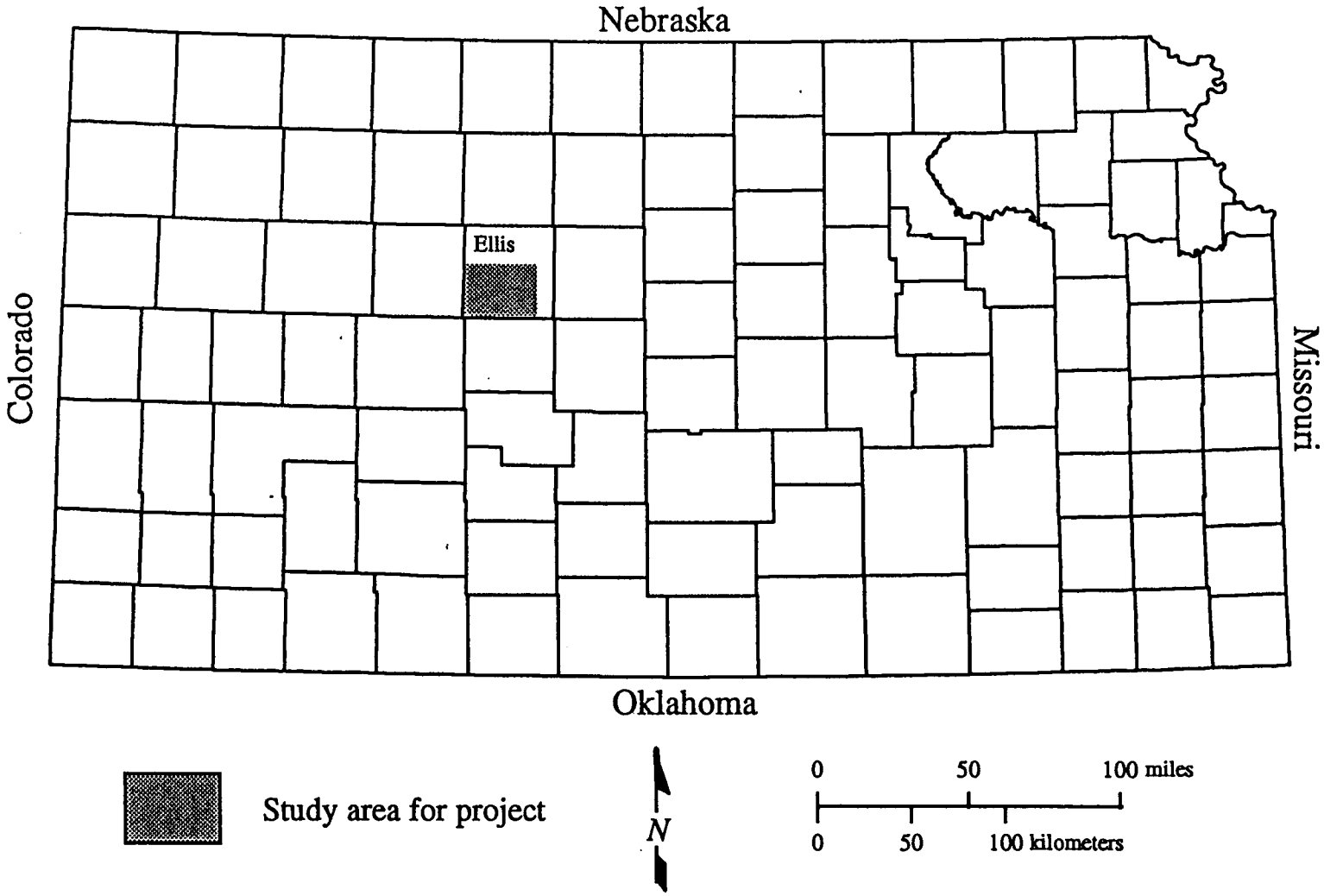

Figure 1.1 Shaded region shows the location of the study area in southwestern Ellis County, Kansas.

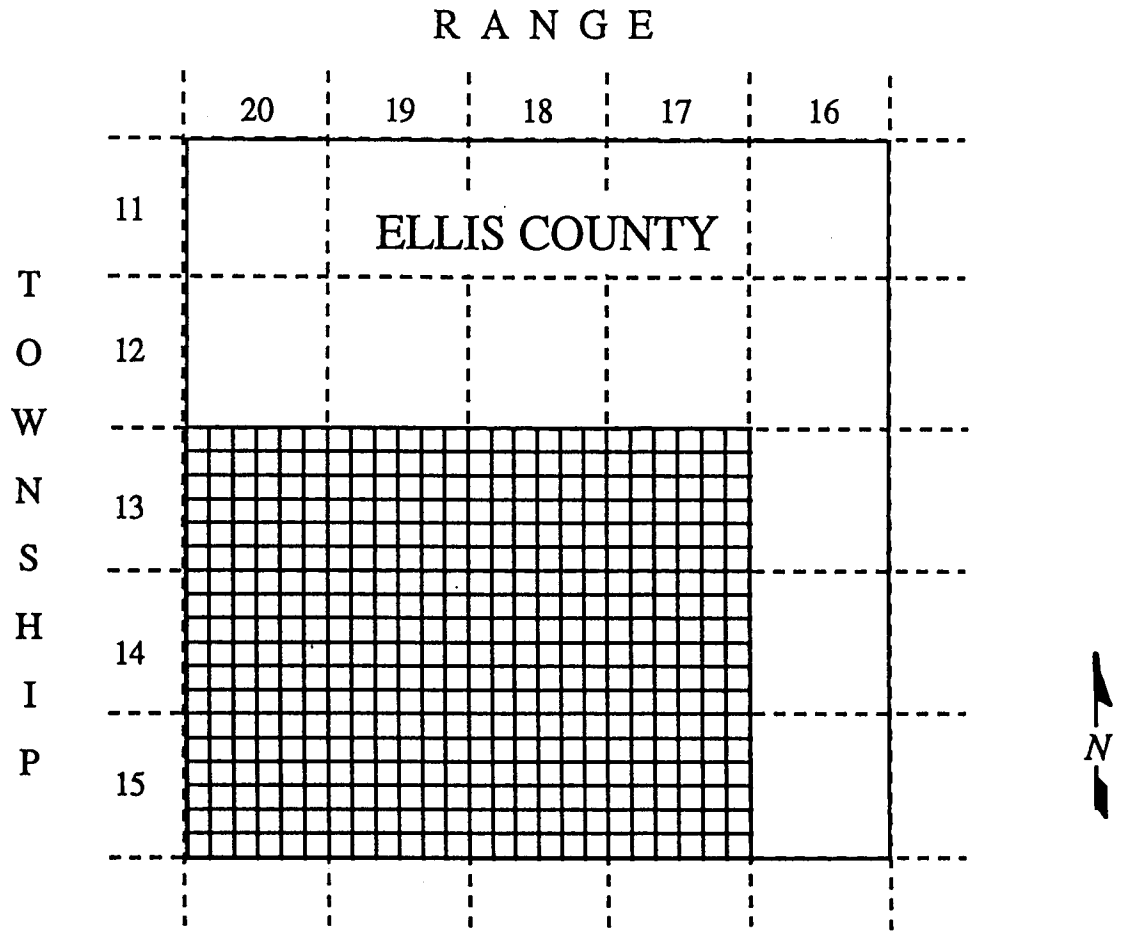

Figure 1.2: The study area includes T. 13 - 15 S. and R. 17 - 20 W. It is approximately 1,120 km^2 (432 mi^2) in area. The section lines are included in the study region. Each section will eventually correspond to a model cell for the flow and transport modeling. One section is 2.6 km^2 (1 mi^2) in area.

This investigation was divided into two major phases. The first phase considered the hydrostratigraphy of the upper Dakota aquifer. Its main goal was to describe the three-dimensional arrangement of aquifer subunits in the upper Dakota aquifer. Geophysical gamma-ray logs were used to determine the geologic framework. The logs were used to identify the top and bottom of the major stratigraphic units and the occurrence of aquifer subunits in the upper Dakota aquifer. Geostatistical techniques were used to describe a quasi three-dimensional arrangement of the distribution of aquifer subunits and then relate this distribution to heterogeneity in the aquifer.

In phase two, the information from phase one was incorporated into a numerical modeling study of the upper Dakota aquifer. The modeling evaluated flow and transport processes in the aquifer under both steady-state and transient conditions. The models simulated both ground-water flow and conservative mass transport in three dimensions. The modeling study consisted of three steps. First, a partially calibrated steady-state model of the flow field was produced. Second, the partially calibrated model was used to simulate the development of the observed salinity distribution throughout the study area and to evaluate hypotheses concerning the processes that produced its distribution. Sensitivity analyses were then carried out on the important parameters controlling flow and transport to understand the limitations of the model results. Finally, the model was used to evaluate the possible effect of development on long range sustainability of the aquifer and its water quality.

CHAPTER 2. HYDROGEOLOGIC SETTING

2.1. Previous Work

There has been an abundant amount of work carried out on the Dakota aquifer system by various investigators. Much of this work has come about as a result of the Kansas Geological Survey's Dakota Aquifer Program and the U.S. Geological Survey's Central Midwest Regional Aquifer Systems Analysis Program. The following is a summary of the research results from these programs.

2.2. Physiography

The study area is located in the High Plains section of the Great Plains physiographic province (Fenneman, 1946). The land surface slopes to the east, ranging in elevation from 700 m (2300 ft) in the west to 580 m (1900 ft) in the east. The Smoky Hill River and Big Creek are the major drainages in the study area and have incised valleys into the Cretaceous bedrock. Significant topographic relief is associated with the incised valleys; with slopes ranging more than 100 m/km (550 ft/mile). Figure 2.1 is a topographic map of the study area.

2.3. Geologic Framework

Table 2.1 is a chart showing the subsurface geologic units pertinent to this study, and Figure 2.2 illustrates schematically their relationship in cross-section. The study area is located on the western flank of the Central Kansas Uplift, reflected in the north-westward dip of the Permian units in the subsurface at an angle of about 0.1°. Cretaceous rocks are separated from the underlying Permian strata in the study area by a regional angular unconformity. Cretaceous units dip to the northeast at an angle of about 0.1°.

Permian strata include the Cedar Hills Sandstone and various undifferentiated rock units. The Cedar Hills Sandstone consists mostly of massively bedded sandstone

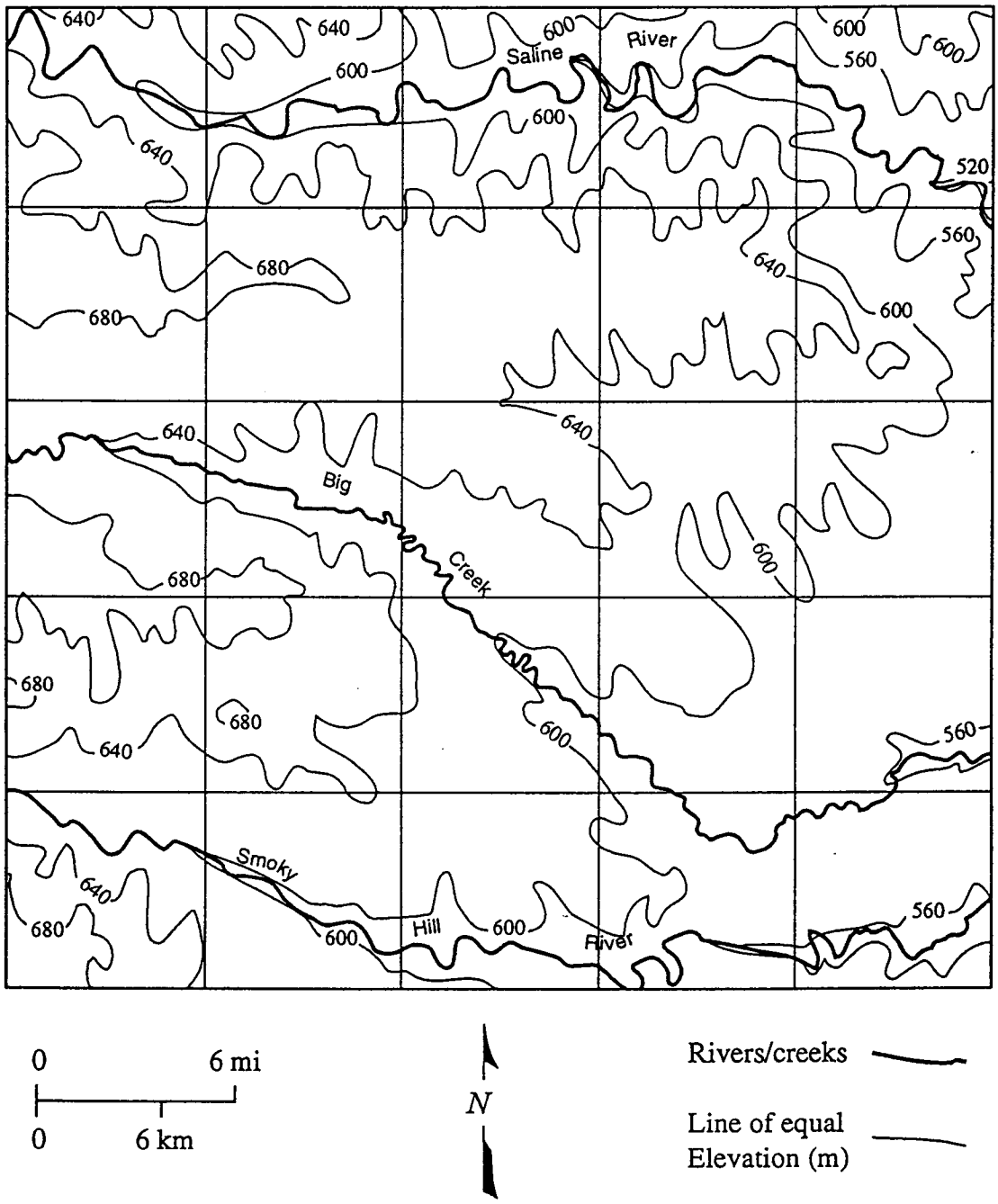

Figure 2.1: Topographic map of Ellis County with major rivers and township lines.

ERA	SYSTEM	ROCK STRATIGRAPHIC UNITS		HYDROSTRATIGRAPHIC UNITS
Cenozoic	Quaternary	Unconsolidated Sediments		Alluvial Valley Aquifers
Mesozoic	Cretaceous	Colorado Group	Niobrara Chalk	Upper Cretaceous Aquitard
			Carlile Shale	
			Greenhorn Limestone	
			Graneros Shale	
		Dakota Fm.		Upper Dakota Aquifer
		Kiowa Fm.	Kiowa Shale	Kiowa Shale Aquitard
			Longford Member	Lower Dakota Aquifer
		Cheyenne Sandstone		
Paleozoic	Permian	Permian Undiff.		Upper Permian Aquitard
		Cedar Hills Sandstone		Cedar Hills Sandstone Aquifer

Table 2.1: Division names of rock stratigraphic and their grouping into hydrostratigraphic units.

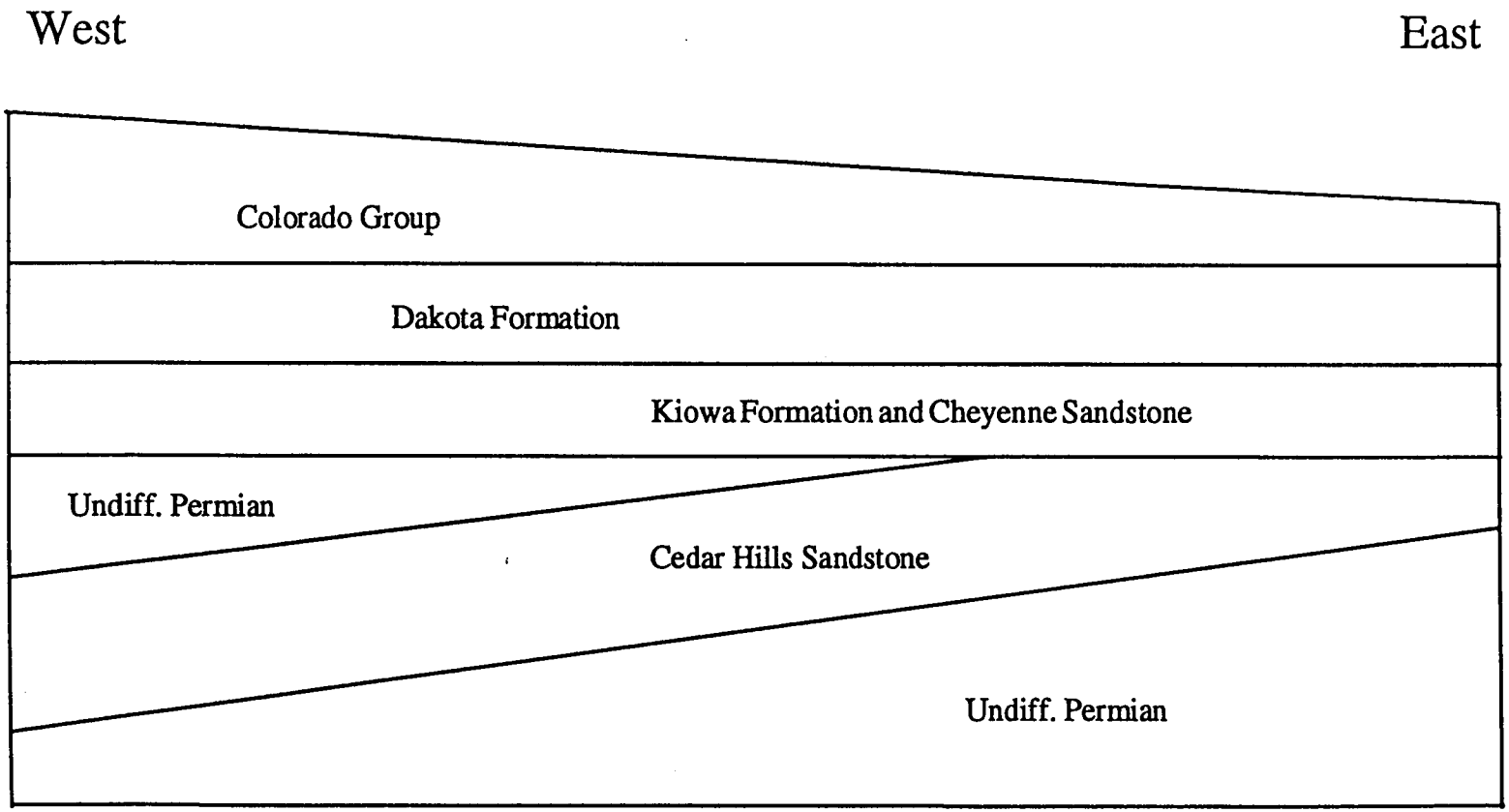

Figure 2.2: Generalized east-west geologic cross-section through the study area.

with clay lenses deposited in a sabhka environment adjacent to an evaporating inland sea (Holdoway, 1978). Thickness ranges up to 75 m (250 ft) downdip of its pinchout in the subsurface. Overlaying the Cedar Hills Sandstone are undifferentiated Permian rocks. The lithology of these rocks includes shales, siltstones, and evaporites (Holdoway, 1978). This unit ranges in thickness up to 100 m (325 ft).

The Cheyenne Sandstone and the Kiowa Formation make up the lower portion of the Cretaceous strata. The alluvial Cheyenne Sandstone was deposited in incised valleys cut into the underlying Permian (Hamilton, 1994; Macfarlane, 1993) and ranges in thickness up to 60 m (200 ft). The Kiowa Formation is a progradational sequence with fluvial to shoreface deposits at the base and primarily marine shale in the upper portion of the formation (Hamilton, 1994). The Kiowa Formation ranges in thickness up to 120 m (400 ft). However, the upper marine shale, ranging in thickness up to 60 m (200 ft), is not present in portions of central Kansas due to non-deposition or erosion (Hamilton, 1989; Macfarlane, 1993; Hamilton, 1994). The basal fluvial and shoreface deposits of the Kiowa Formation are referred to as the Longford Member (Franks, 1966).

The Dakota Formation is separated from the underlying Kiowa Formation by a major regional unconformity and is approximately 90 m (300 ft) thick. The lower two thirds of the formation is alluvial and the upper third has a progressively more marine influence being described as deltaic, coastal plain, and shoreface in origin (Hamilton, 1989; Macfarlane, 1993; Hamilton, 1994). The Dakota Formation consists of a complex arrangement of sandstone lenses embedded in a mudstone matrix. The percentage of sandstone is highly variable at any single location but is approximately 30% on average in Kansas (Keene and Bayne, 1977).

Above the Dakota Formation is the Colorado Group. The Colorado Group in central Kansas includes the Graneros Shale, the Greenhorn Limestone, the Carlile Shale, and the Niobrara Chalk. The contact with the underlying Dakota Formation is gradational with alternating beds of sandy shale, sandstone, and shale (Macfarlane *et*

al., 1990). The upper portion of the Graneros Shale is a medium dark-gray silty shale containing some calcareous sandstone and was deposited in an off-shore, marine environment (Macfarlane *et al.*, 1990). Numerous beds of chalk, chalky limestone, marl, and shale were deposited on top of the Graneros Shale, amounting to a thickness of more than 300 m (1,000 ft) in places. These beds thin to the east and south or have been removed due to erosion. In the study area the Colorado Group ranges in thickness from about 15 m to 120 m (50 ft to 400 ft). In the Smoky Hill River and Big Creek valleys, Quaternary alluvial sediments overlie the Colorado Group. These unconsolidated sediments consist of sand and gravel (Macfarlane *et al.*, 1990) and range in thickness up to approximately 45 m (150 ft).

2.4. Hydrostratigraphy

The various formations discussed in the last section are grouped into regional aquifer and aquitard units (Macfarlane *et al.*, 1990). The grouping of rocks having similar hydraulic properties is known as hydrostratigraphy (Domenico and Schwartz, 1990). A hydrostratigraphic unit can be equivalent to a formation, consist of only a portion of a formation, or be made up of groups of formations (Domenico and Schwartz, 1990). Table 2.1 summarizes the grouping of formations into hydrostratigraphic units. Figure 2.3 shows a generalized cross-section of the hydrostratigraphy through the study area.

For this study, the Cedar Hills Sandstone is considered a regional aquifer unit and called the Cedar Hills Sandstone aquifer. The undifferentiated Permian rocks are grouped together into the Upper Permian aquitard. The Cheyenne Sandstone and the Longford Member of the Kiowa Formation are grouped into the lower Dakota aquifer. The Upper Permian aquitard separates the Cedar Hills Sandstone aquifer from the lower Dakota aquifer in the western part of the study area. The upper marine shale of the Kiowa Formation constitutes the Kiowa shale aquitard. The Dakota Formation is referred to as the upper Dakota aquifer. The Kiowa shale aquitard separates the upper

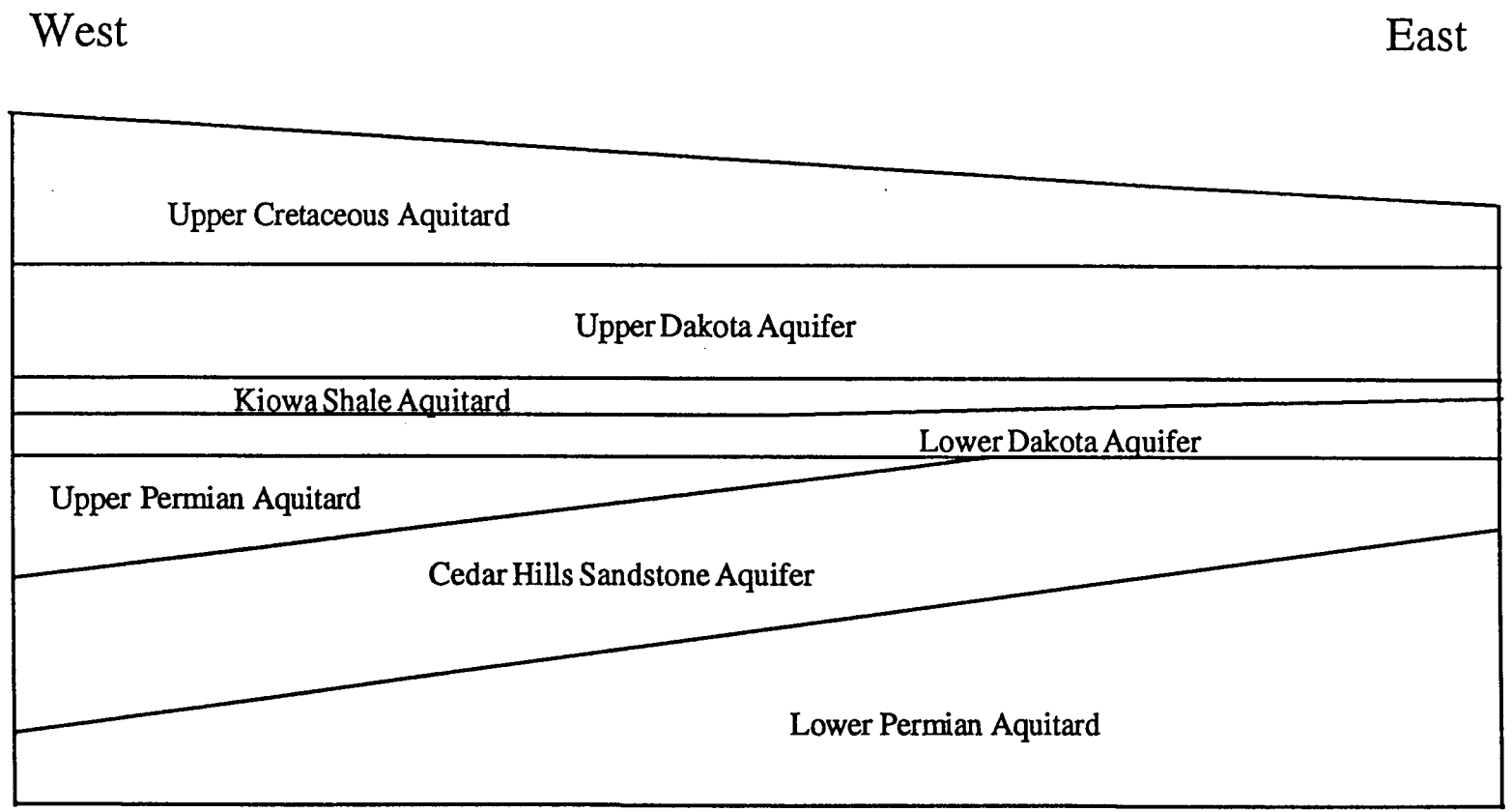

Figure 2.3: Generalized east-west hydrostratigraphic cross-section through the study area.

Dakota aquifer from the lower Dakota aquifer. The Colorado Group is the major confining layer above the upper Dakota aquifer and is referred to as the Upper Cretaceous aquitard. The upper Dakota aquifer is the primary aquifer of interest in this study. Other units that will play an important role in this study include the Upper Cretaceous aquitard, the Kiowa shale aquitard, and the Cedar Hills Sandstone aquifer. The eastern most extents of the Kiowa shale and the Upper Cretaceous aquitards are shown in Figures 2.4 and 2.5. The subcrop area of the Cedar Hills Sandstone beneath the lower Dakota aquifer is illustrated in Figure 2.6.

2.5. Ground-Water Flow in the Upper Dakota Aquifer

The regional recharge area for the upper Dakota aquifer is located in southeastern Colorado, and the regional discharge area of the aquifer is in central Kansas. Macfarlane (1993) demonstrated the importance of regional topography and local relief on the flow system. Three flow regimes were described for the Dakota aquifer system. The study area for this thesis is part of the middle flow regime which consists exclusively of a regional flow system extending from near the Colorado-Kansas border to central Kansas. The flow system is controlled primarily by the regional slope of the land surface. Local relief has little to no influence on the flow system in the confined portion of the aquifer because of the thickness of the Upper Cretaceous aquitard.

The importance of the Upper Cretaceous aquitard as a controlling factor on the flow system of the confined upper Dakota aquifer was also demonstrated by Macfarlane (1993). In the study area, the potentiometric surface of the upper Dakota aquifer can be as much as 60 m (200 ft) below the elevation of the water-table. Macfarlane (1993) reported that although pressure in the upper Dakota aquifer is less than would be expected when compared to the hydrostatic gradient starting at the water-table surface, pressure versus depth within the aquifer parallels the hydrostatic line. This indicates primarily lateral flow within the upper Dakota aquifer. Since the

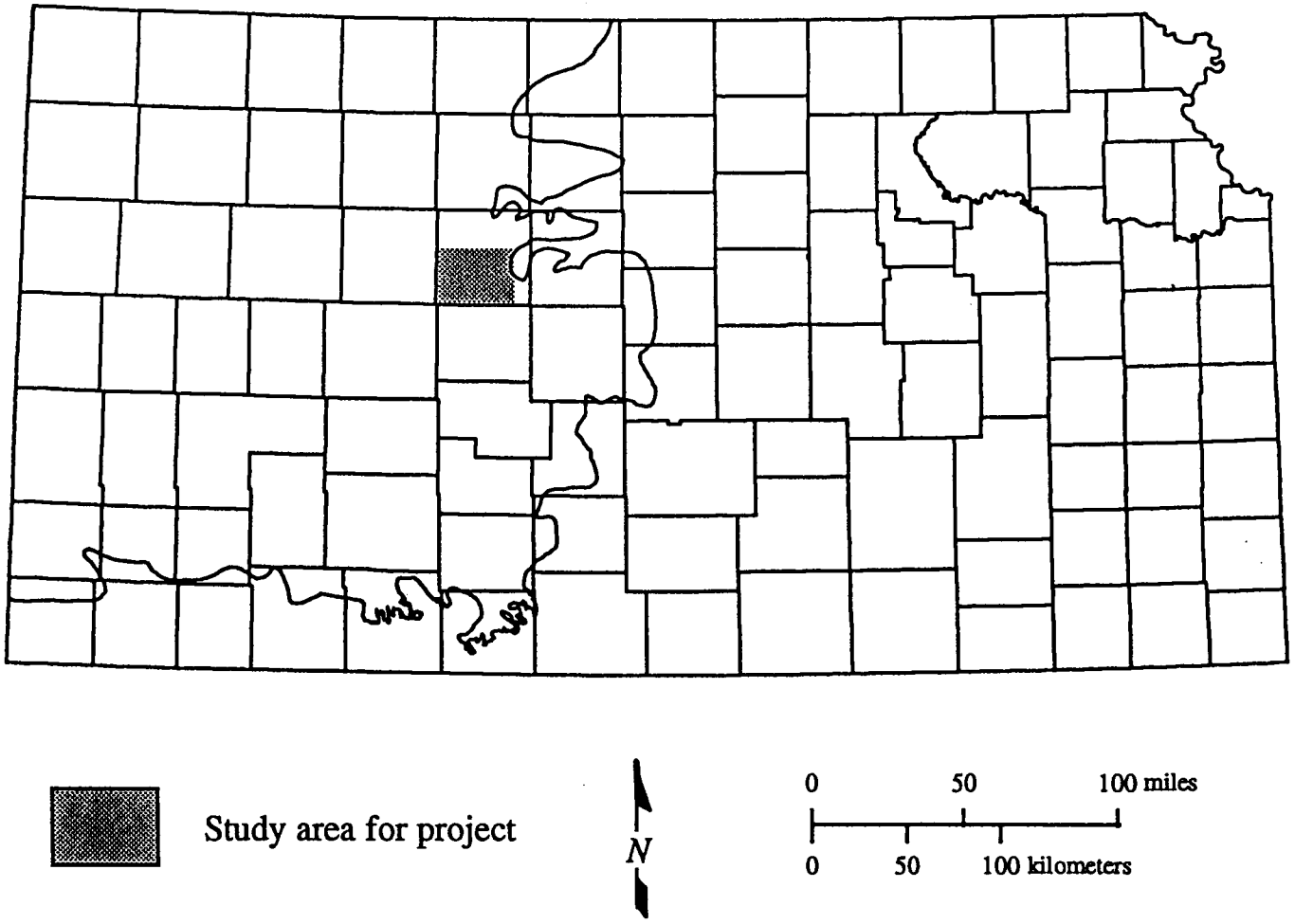

Figure 2.4: Eastern most extent of the Kiowa shale aquitard in western and central Kansas. Shaded area shows the study region.

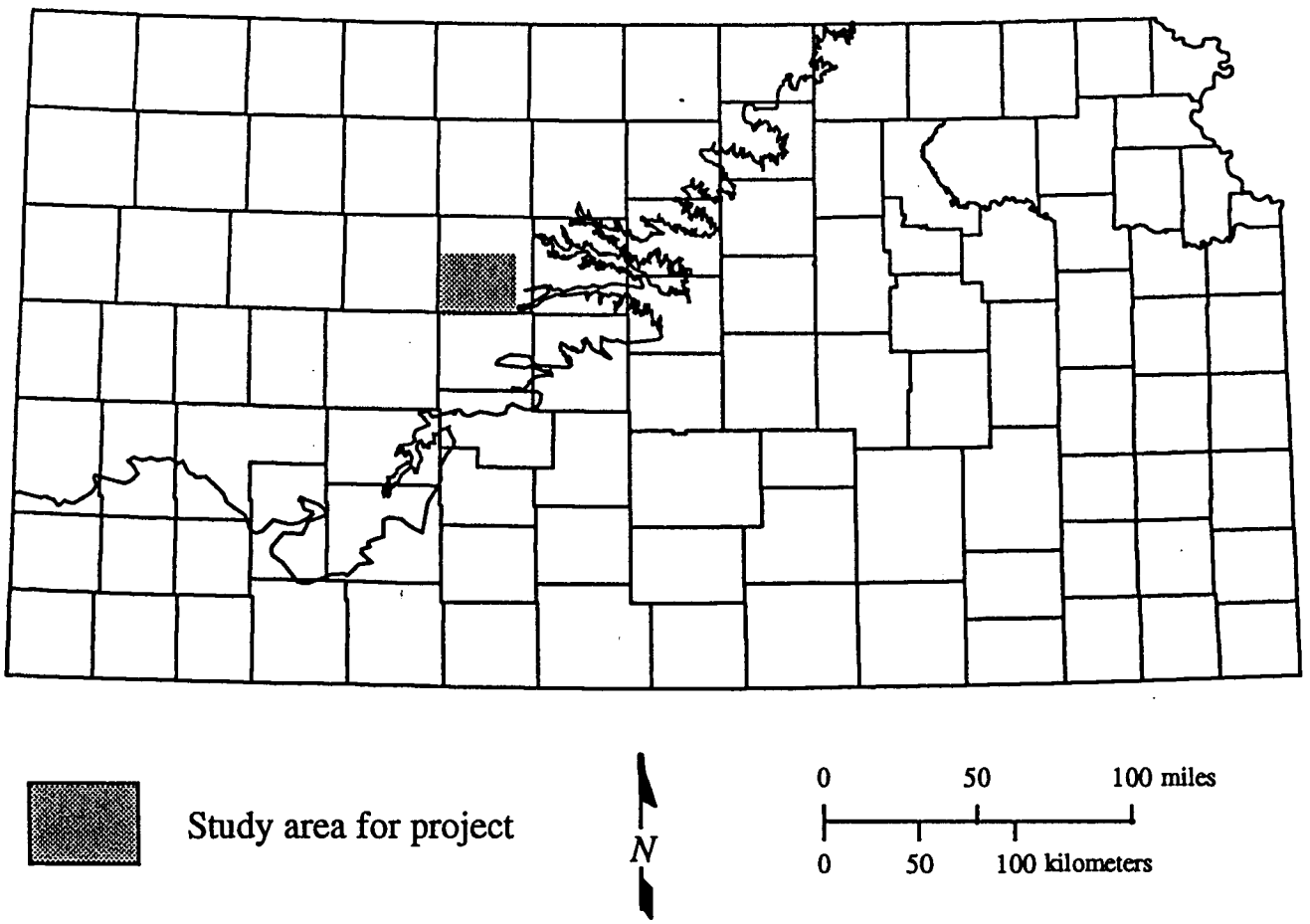

Figure 2.5: Eastern most extent of the Upper Cretaceous aquitard aquitard in western and central Kansas. Shaded area shows the study region.

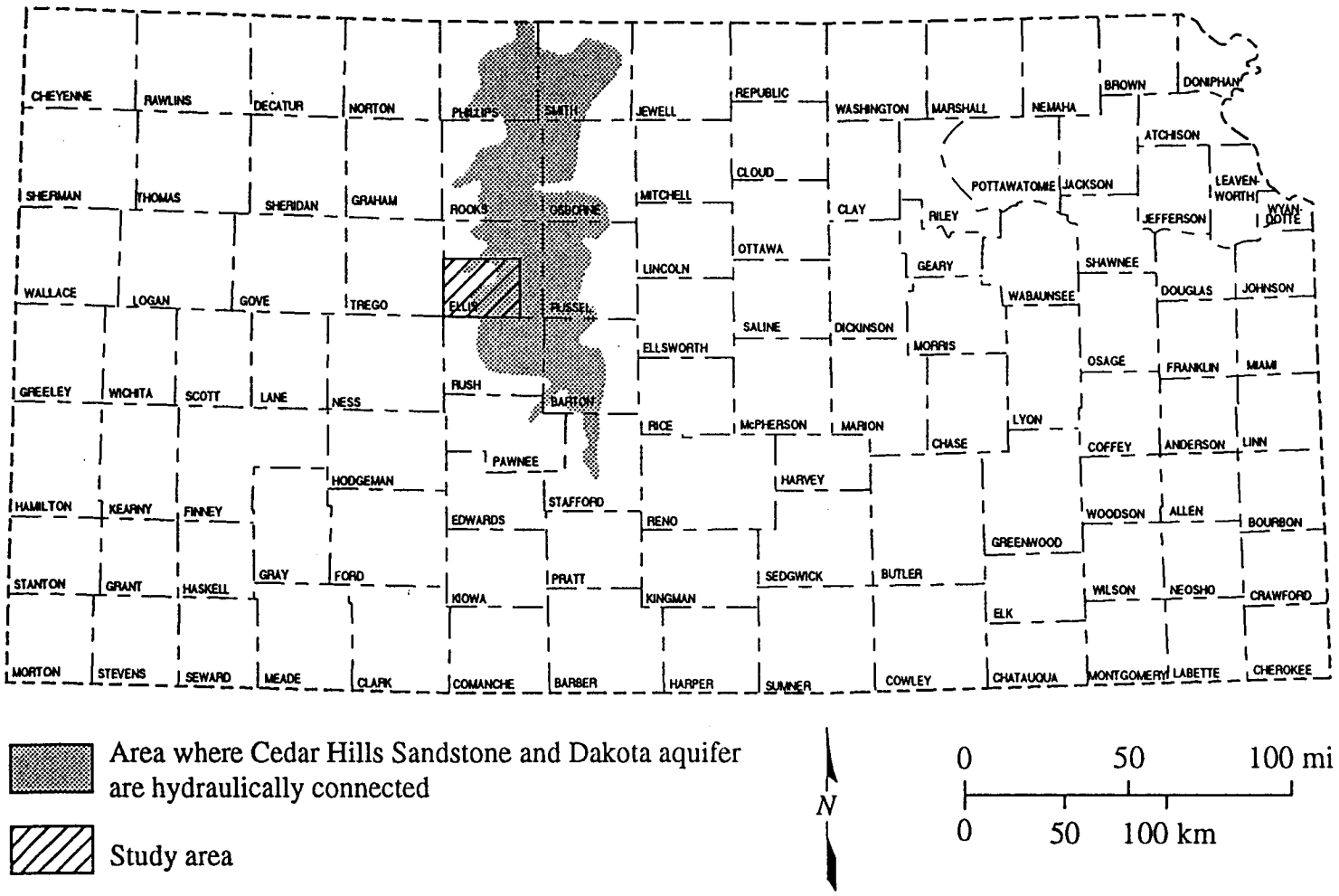

Figure 2.6: Subcrop region of the Cedar Hills Sandstone beneath the Dakota aquifer. Shaded area shows the region where the lower Dakota aquifer and the Cedar Hills Sandstone Aquifers are in contact

pressure versus depth in the upper Dakota aquifer is parallel to but lower than the hydrostatic line, fluid pressures in the aquifer are considered to be subhydrostatic. Macfarlane (1993) demonstrated that subhydrostatic pressures exist because the thick Upper Cretaceous aquitard restricts recharge to the underlying upper Dakota aquifer.

The majority of water-levels for the Dakota aquifer were taken from the upper Dakota aquifer. Figure 2.7 shows a map of the potentiometric surface of the Dakota aquifer. Figure 2.8 is a map of the study area with the actual well locations and their values. It is generally assumed that the potentiometric surfaces of the lower Dakota and the Cedar Hills Sandstone aquifers are nearly equivalent to the heads in the upper Dakota aquifer (Macfarlane, 1993).

2.6 Salinity in the Upper Dakota Aquifer

The presumed distribution of salinity has been mapped in the upper Dakota aquifer (Macfarlane *et al.*, 1990; Whittemore, unpublished). Figure 2.9 is a map of the study area showing the locations of sampled wells and the chloride concentrations of the samples. The data exhibit a large amount of variability. Figure 2.10 is a generalized contour map of Total Dissolved Solids (TDS) concentration in the study area. The TDS isocons of Figure 2.10 mimic the contour pattern of the regional TDS concentration for the state of Kansas as defined by Whittemore (unpublished). Although these contours do not coincide with the observed concentrations shown in Figure 2.9 very well, the regional trend present in central Kansas is depicted (Whittemore, personal communication, 1994). The contour interval was altered from that used by Whittemore (unpublished) to better show the trend across Ellis County.

Because salinity varies both vertically and laterally within the upper Dakota aquifer, a three-dimensional distribution is required. There are few data available to characterize the vertical variability of TDS in the study area. However, to the east of the study region more data exist (Figure 2.11). Figure 2.12 shows the variation in chloride concentration with depth at a site located approximately in the center of the

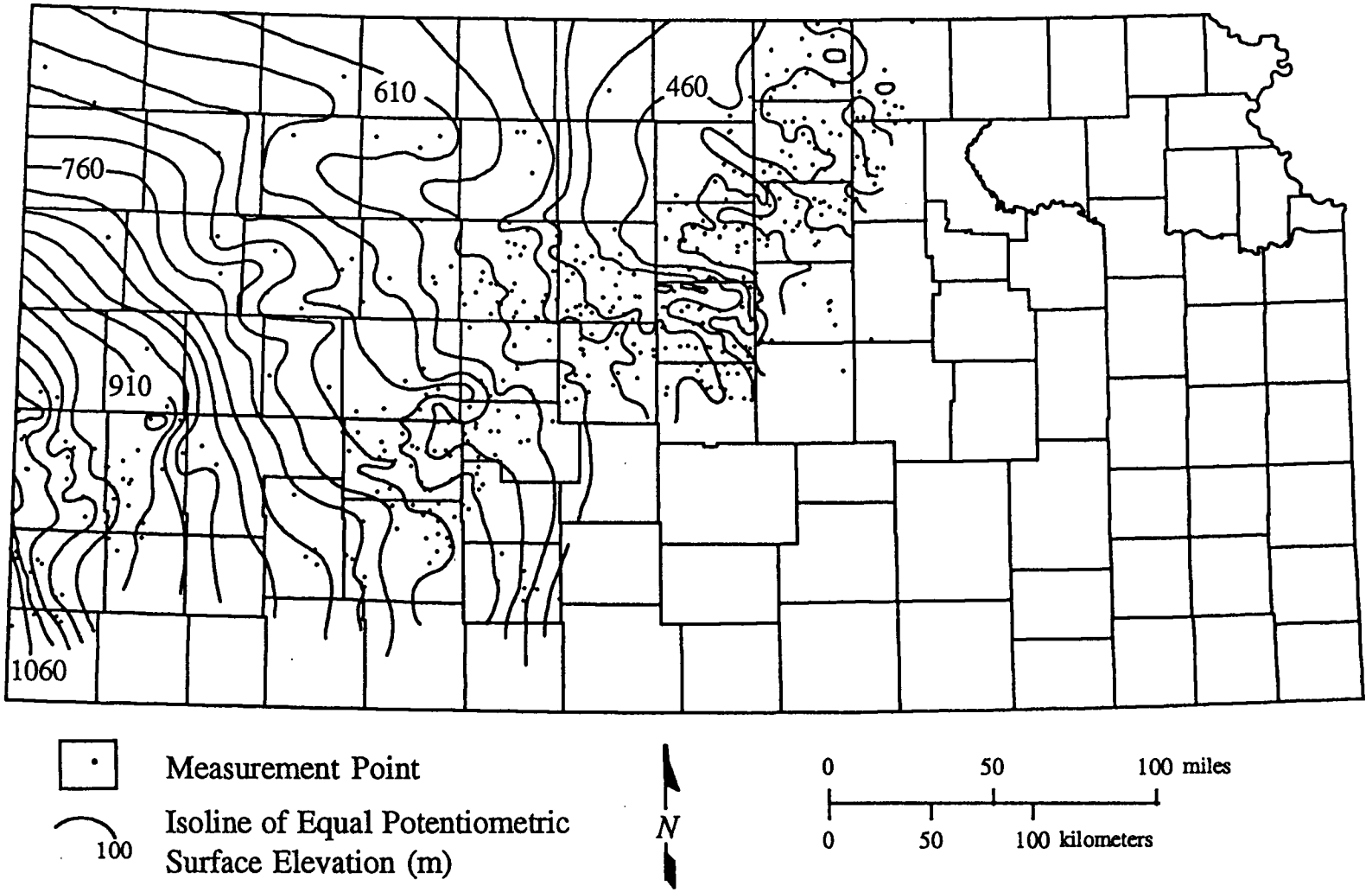

Figure 2.7: Potentiometric surface of the Dakota aquifer with data points shown from Macfarlane (1989). The contour interval is 30 m (100 ft).

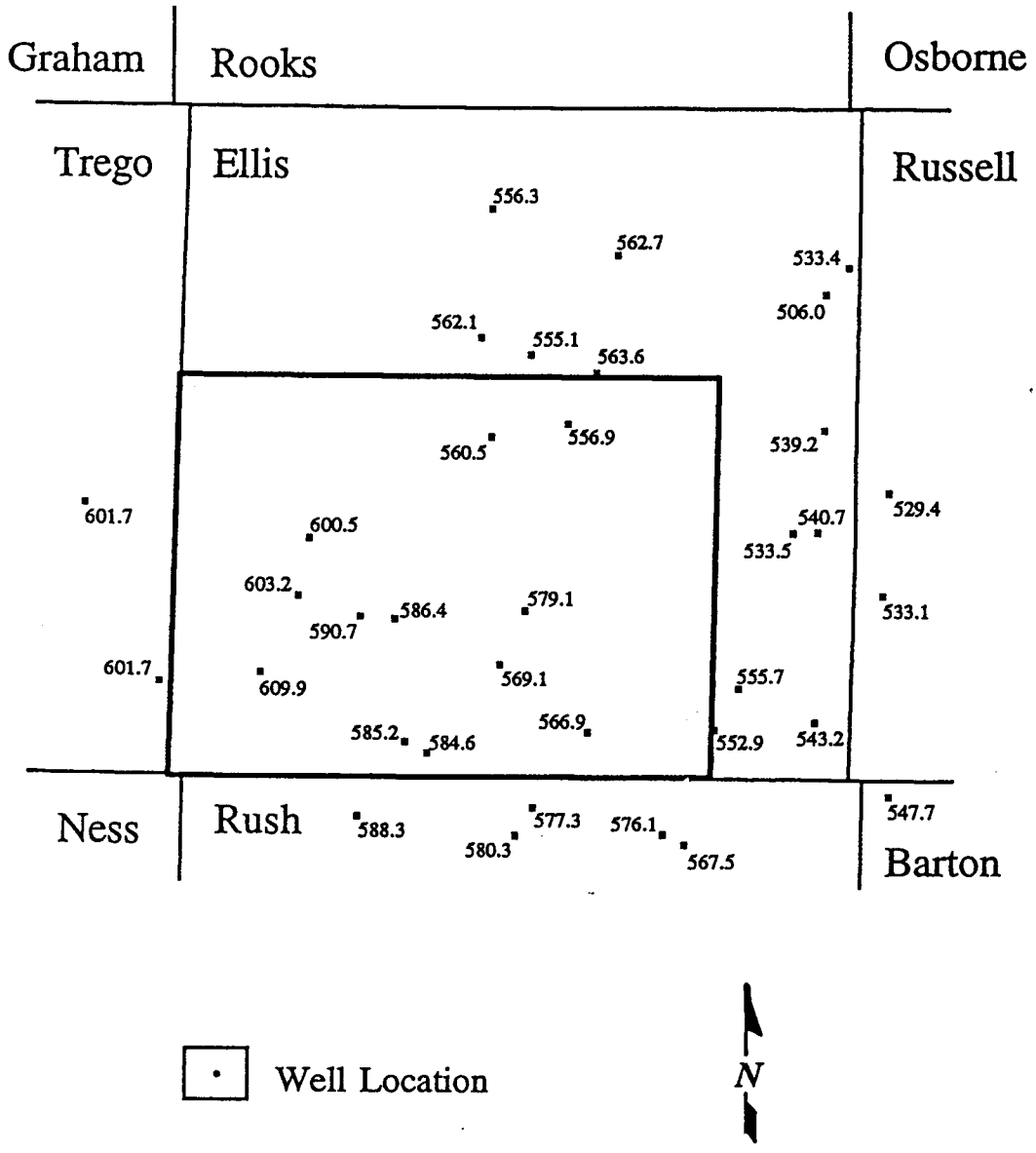

Figure 2.8: Water-level control points for the upper Dakota aquifer in Ellis County measured in meters above sea level. Boxed region shows the study area.

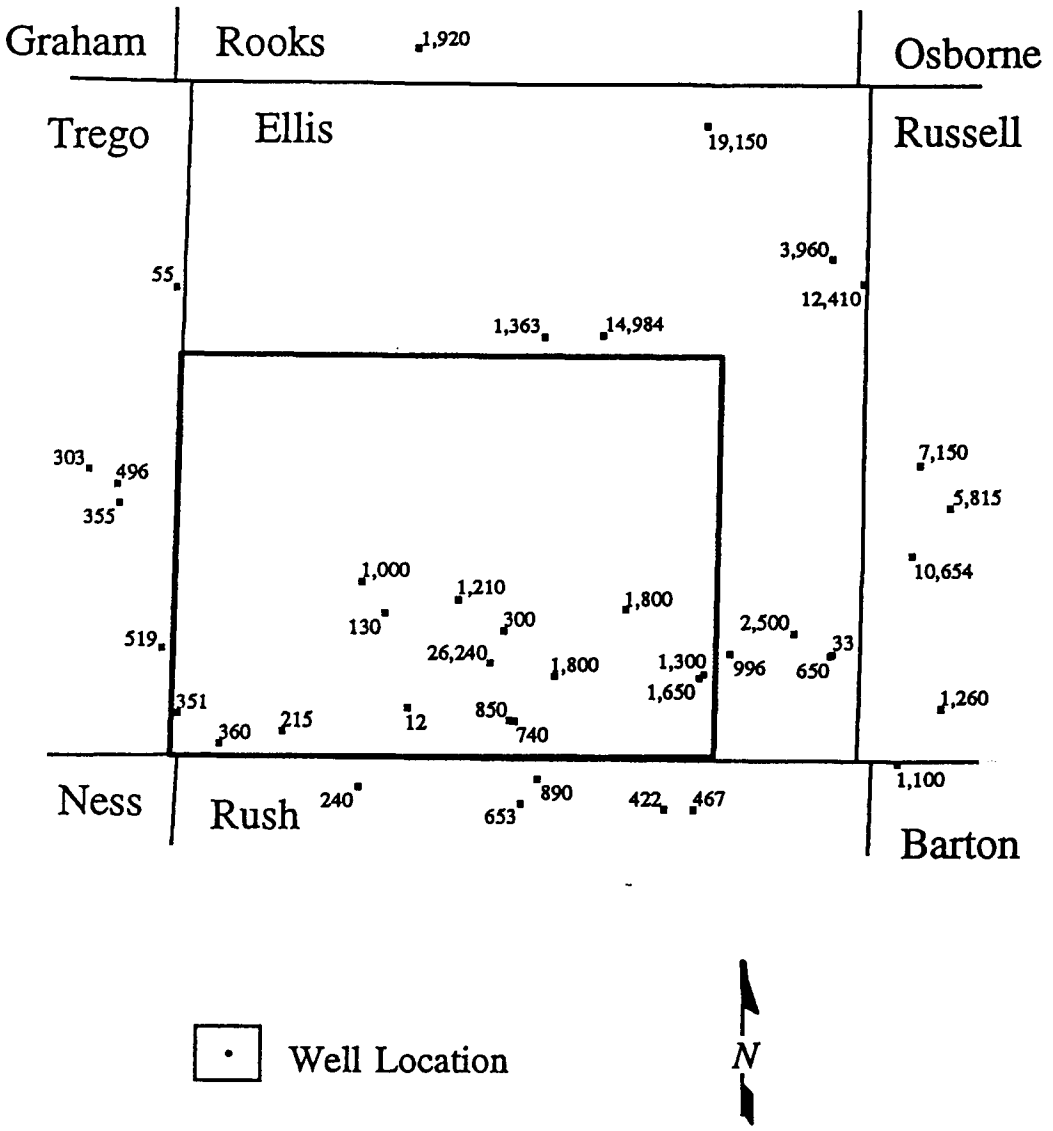

Figure 2.9: Chloride concentration (mg/L) measured from water samples from wells screened in the upper Dakota aquifer. Boxed region shows the study area.

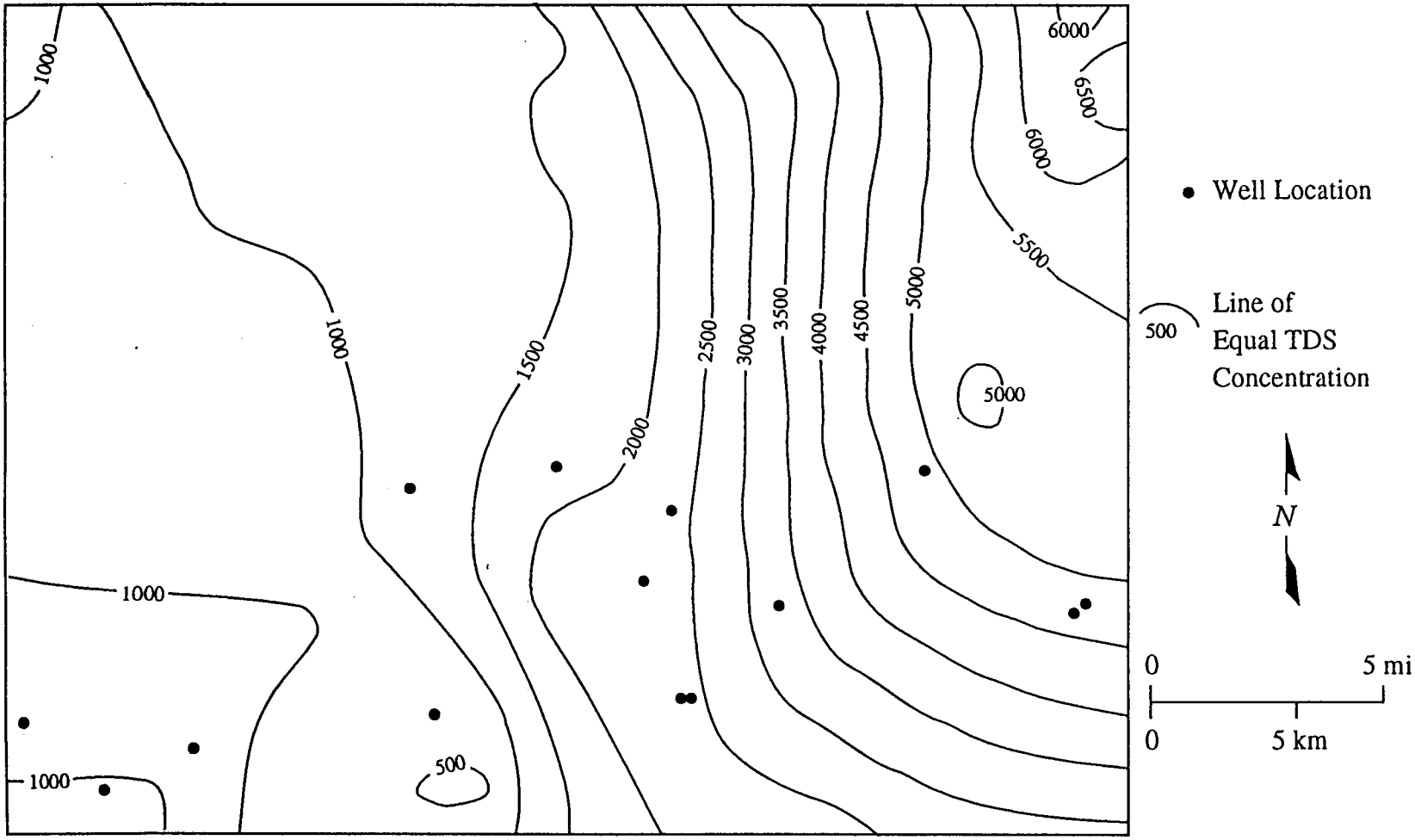

Figure 2.10: Total Dissolved Solids (TDS) isolines measured in mg/L in the study area. A strong concentration gradient is present in the upper Dakota aquifer in the eastern half of the region. This map was produced from data supplied by Whittemore (unpublished) and is meant to show the lowest concentration that one is likely to find in the aquifer regardless of depth (Whittemore, personal communication, 1994).

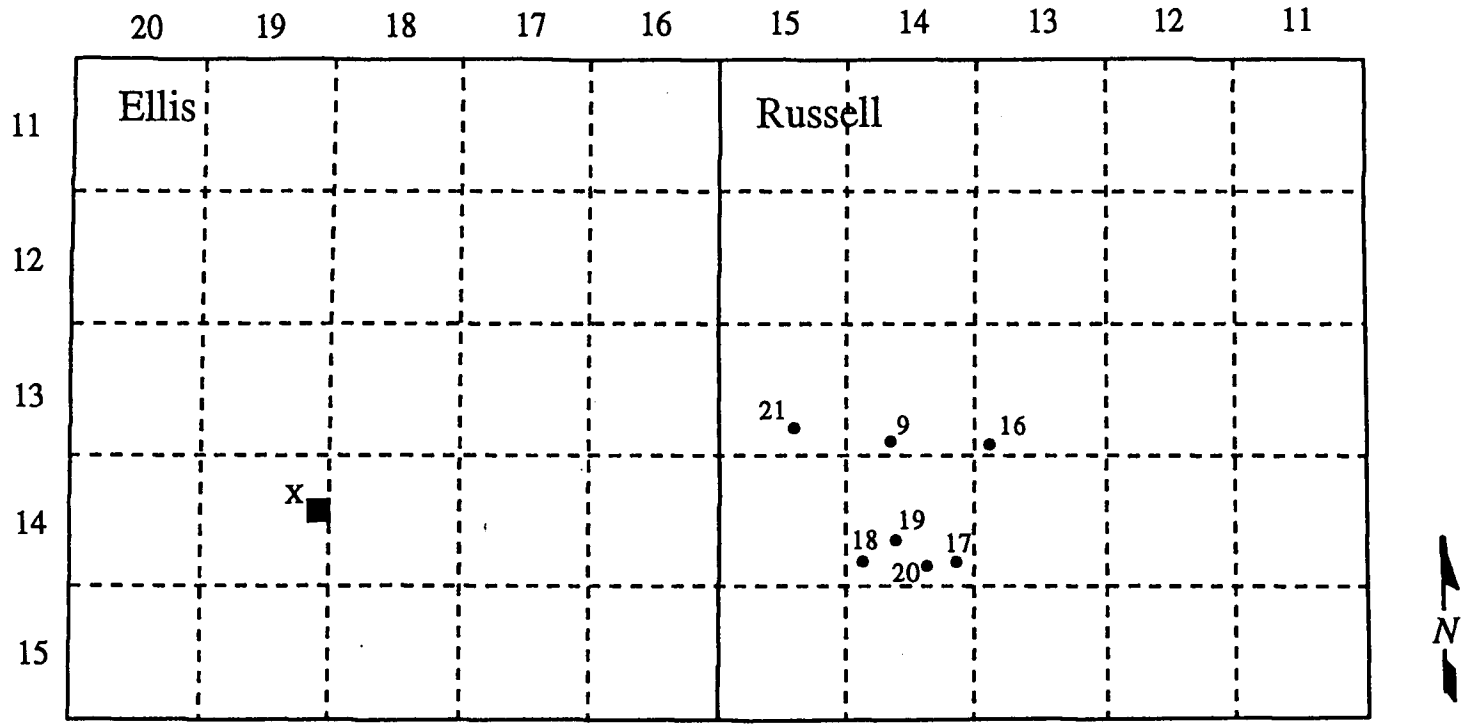

Figure 2.11: Location of sampled wells from which depth profiles of chloride and Total Dissolved Solids (TDS) concentrations were taken. See Figure 2.12 and Figures 2.13a through 2.13g.

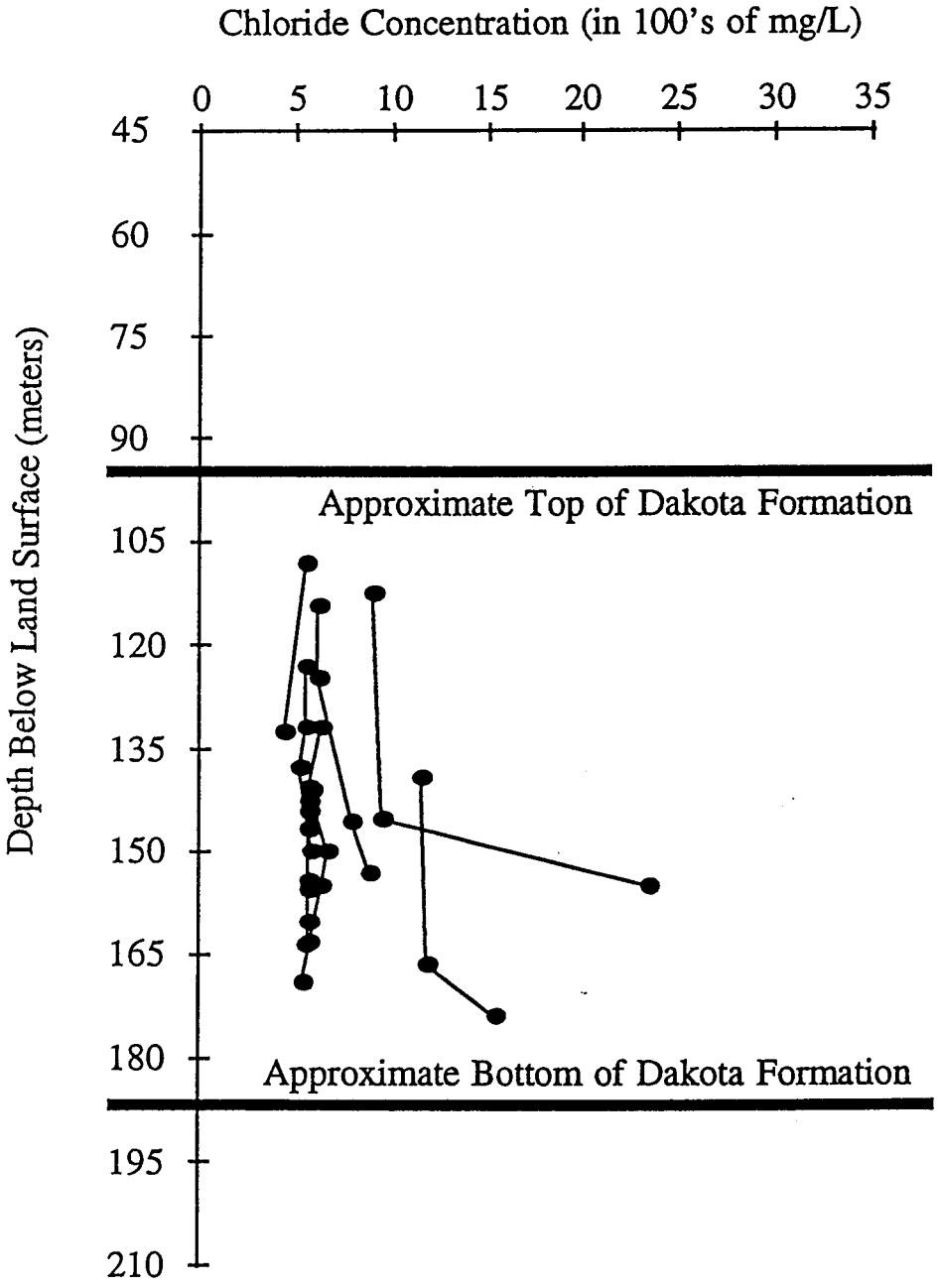

Figure 2.12: Chloride concentration in the upper Dakota aquifer from Ellis County. Data comes from several wells in Sec. 13, T. 14 S., R. 19 W and is marked by an X in Figure 2.11. Lines connect data points taken from individual wells.

study area. Figures 2.13a through 2.13g are depth profiles of TDS in Russell County located to the east of Ellis County. In general, TDS concentrations beneath the upper Dakota aquifer increase eastward due to the thinning of the Upper Permian and Kiowa shale aquitards separating the lower Dakota aquifer from the Cedar Hills Sandstone. Concentrations are greatest in those areas where the Cedar Hills Sandstone subcrops beneath the lower Dakota aquifer. The observed TDS concentrations in units beneath the upper Dakota aquifer increase eastward, ranging from about 2,000 mg/L to 35,000 mg/L. The depth profiles indicate that the lowest TDS concentrations are usually located near the top of the upper Dakota aquifer. However, higher TDS concentrations have been observed above lower concentrations (Whittemore, personal communication, 1994) in the aquifer. This is probably a result of larger sandstone lenses being better flushed of resident saline water because of better connection to the regional flow system.

The salinity in the upper Dakota aquifer has a strong Permian signature indicating that saline water in the aquifer comes from the dissolution of halite and other evaporites in the Permian system and not from remnant sea water trapped in the Dakota aquifer (Whittemore and Fabryka-Martin, 1992). The chemistry suggests that all connate water in the Dakota has been replaced by recharge (Whittemore and Fabryka-Martin, 1992). The higher salinity water of the upper Dakota aquifer and the Cedar Hills Sandstone aquifer is primarily a sodium chloride type (Macfarlane *et al.*, 1990). However, the recharge coming through the Upper Cretaceous aquitard contains calcium sulfate, resulting primarily from the dissolution of gypsum (Macfarlane *et al.*, 1990). In general, the upper portion of the upper Dakota aquifer contains relatively higher concentrations of sulfate than the lower portion of the aquifer (Macfarlane *et al.*, 1990). This indicates mixing of saline waters from below the aquifer with recharge waters from above the aquifer.

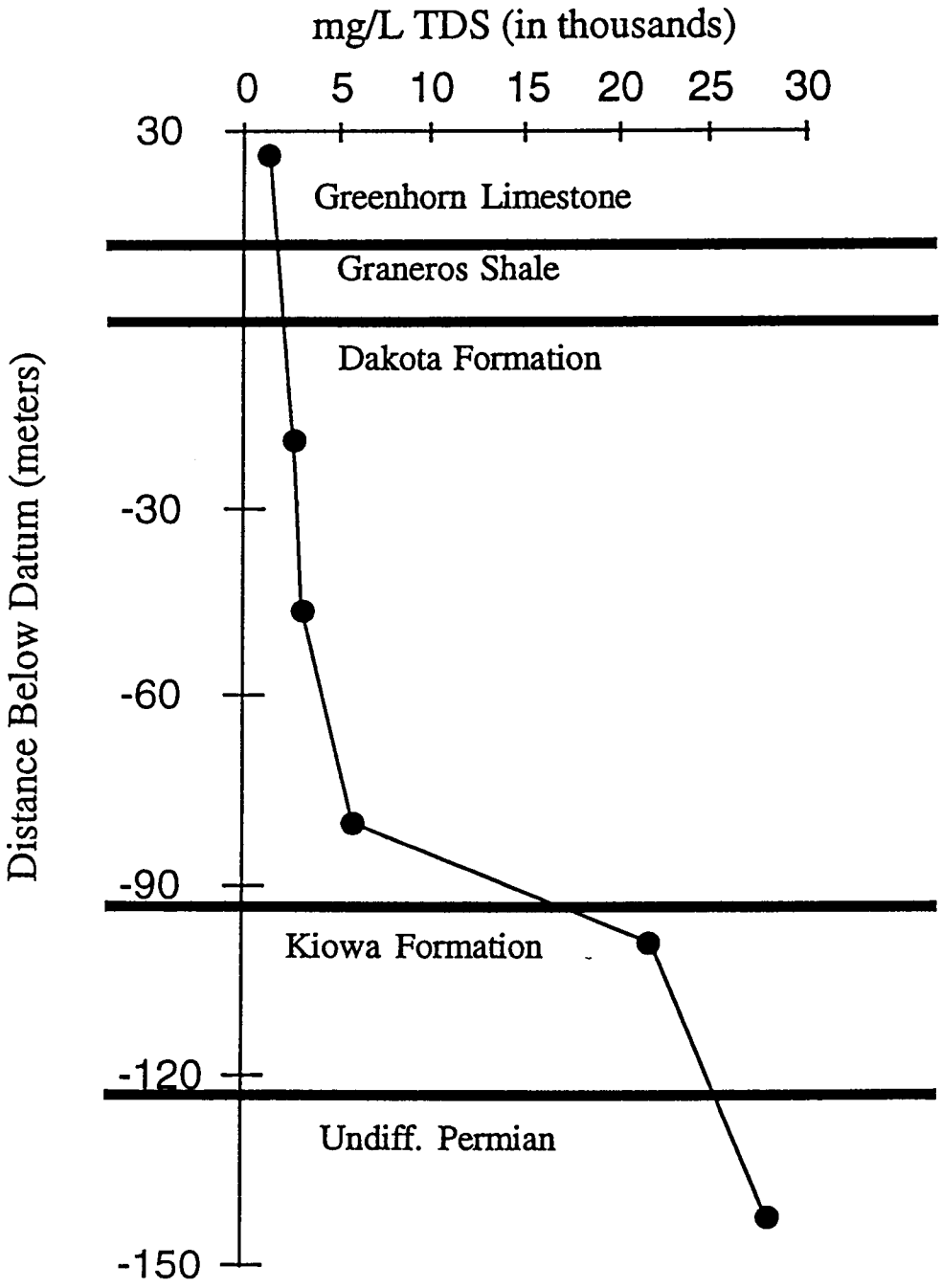

Figure 2.13a: Vertical variation of TDS in the upper Dakota aquifer. Datum is the top of the aquifer. This is well 9, and Figure 2.12 shows the location of the well from which samples were collected. Data comes from Swineford and Williams (1945). Formation tops are approximate. The Cheyenne Sandstone may not be present in this location due to its non-uniform deposition.

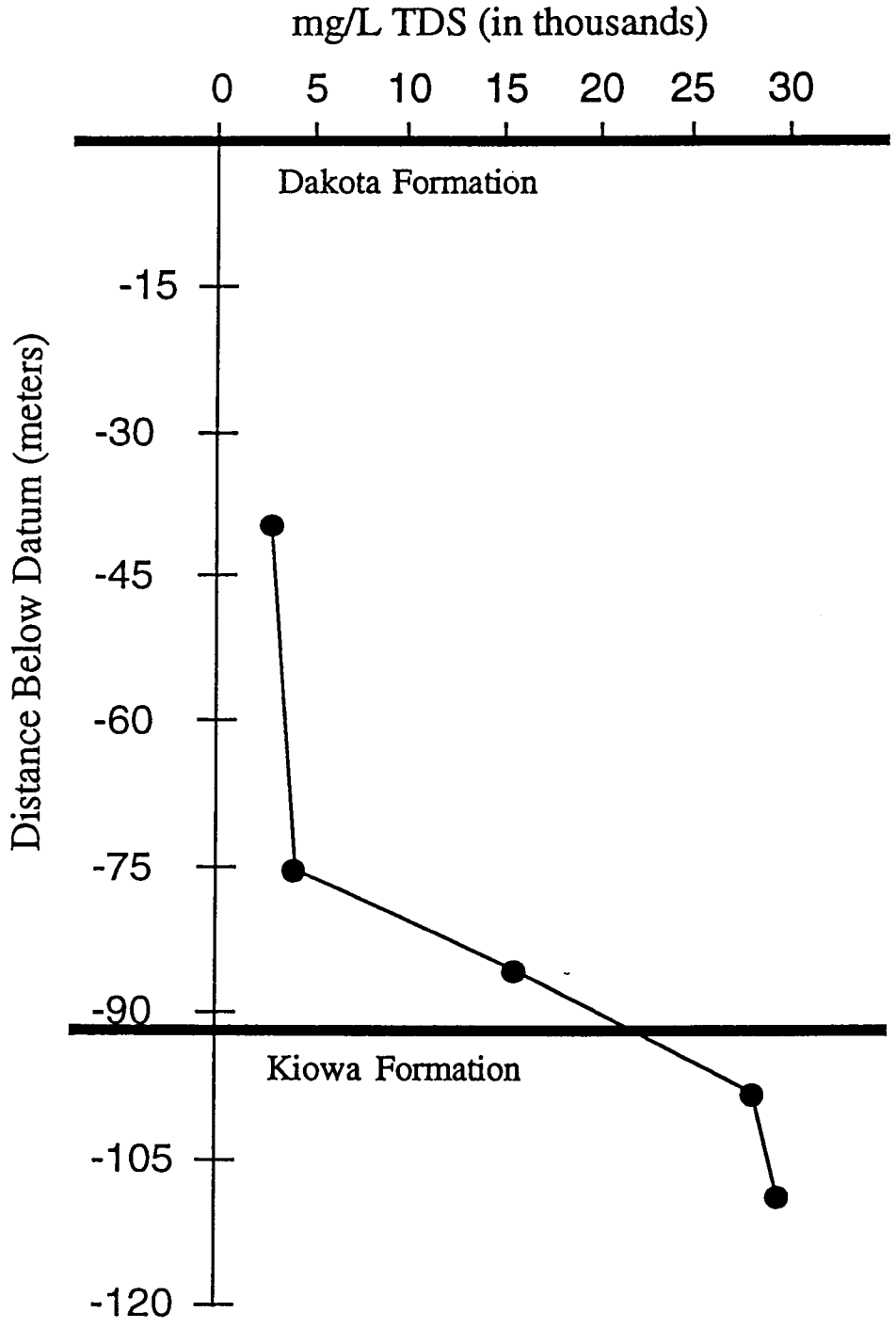

Figure 2.13b: Vertical variation of TDS in the upper Dakota aquifer. Datum is the top of the aquifer. This is well 16, and Figure 2.12 shows the location of the well from which samples were collected. Data comes from Swineford and Williams (1945). Formation tops are approximate.

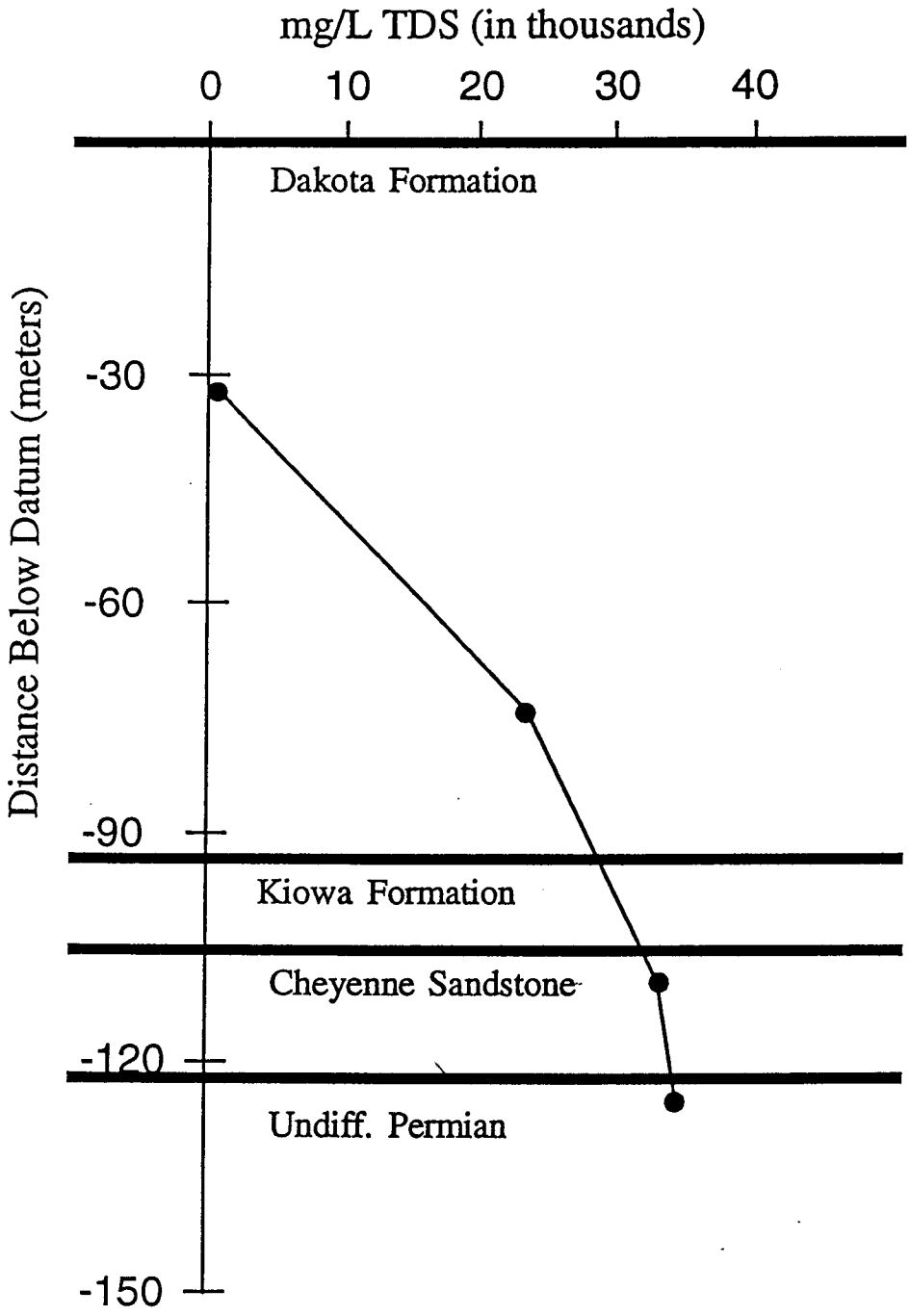

Figure 2.13c: Vertical variation of TDS in the upper Dakota aquifer. Datum is the top of the aquifer. This is well 17, and Figure 2.12 shows the location of the well from which samples were collected. Data comes from Swineford and Williams (1945). Formation tops are approximate.

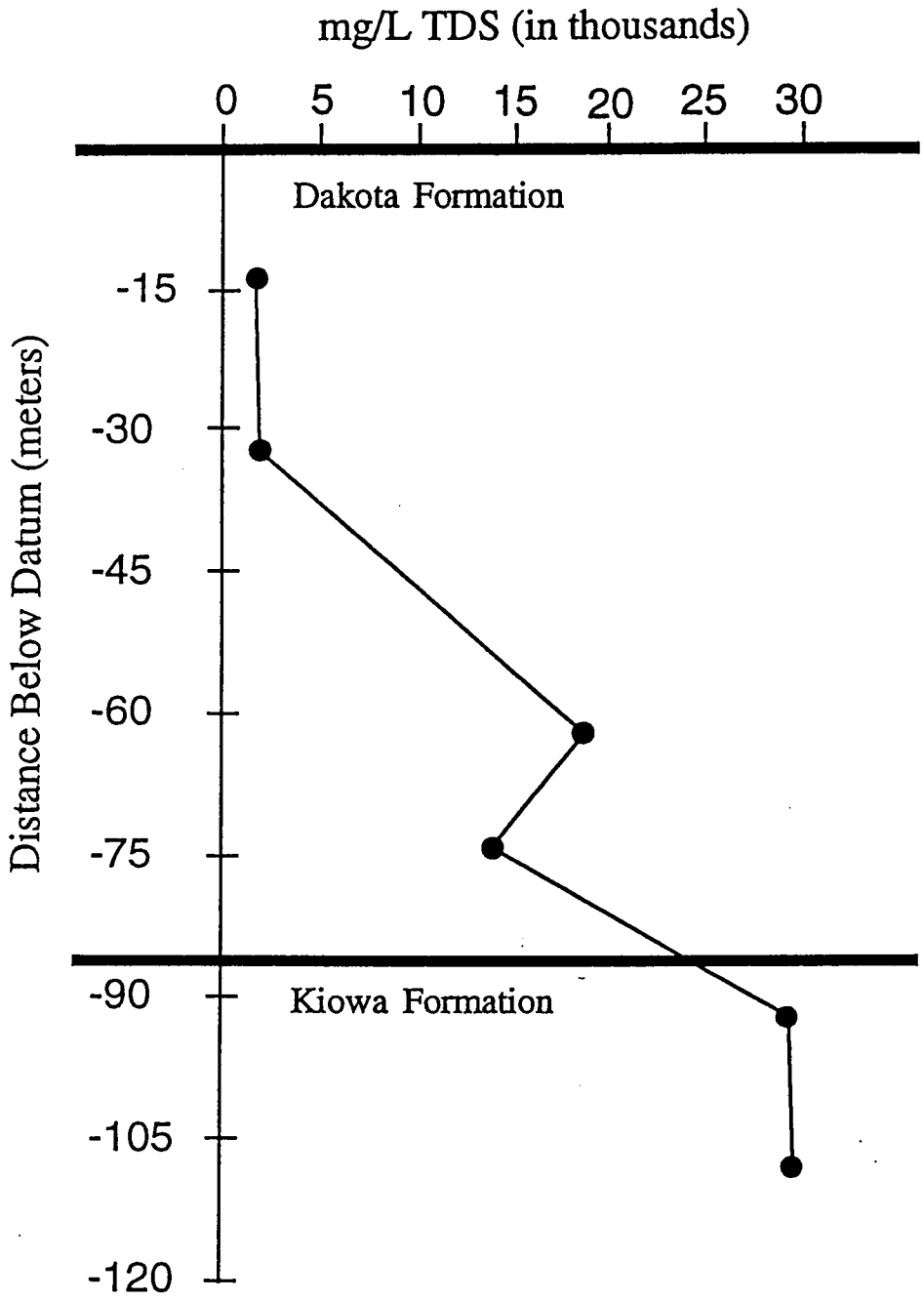

Figure 2.13d: Vertical variation of TDS in the upper Dakota aquifer. Datum is the top of the aquifer. This is well 18, and Figure 2.12 shows the location of the well from which samples were collected. Data comes from Swineford and Williams (1945). Formation tops are approximate.

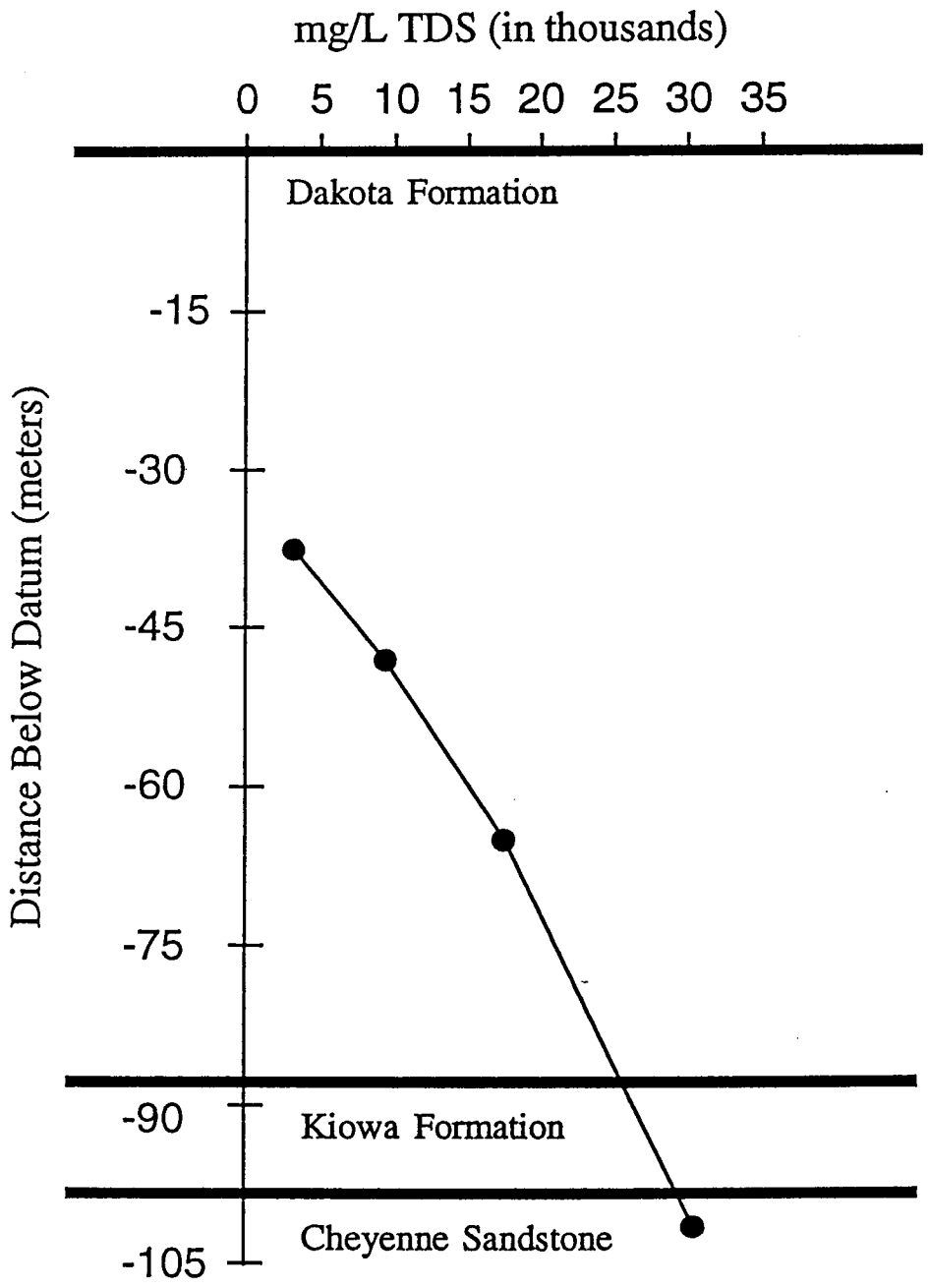

Figure 2.13e: Vertical variation of TDS in the upper Dakota aquifer. Datum is the top of the aquifer. This is well 19, and Figure 2.12 shows the location of the well from which samples were collected. Data comes from Swineford and Williams (1945). Formation tops are approximate.

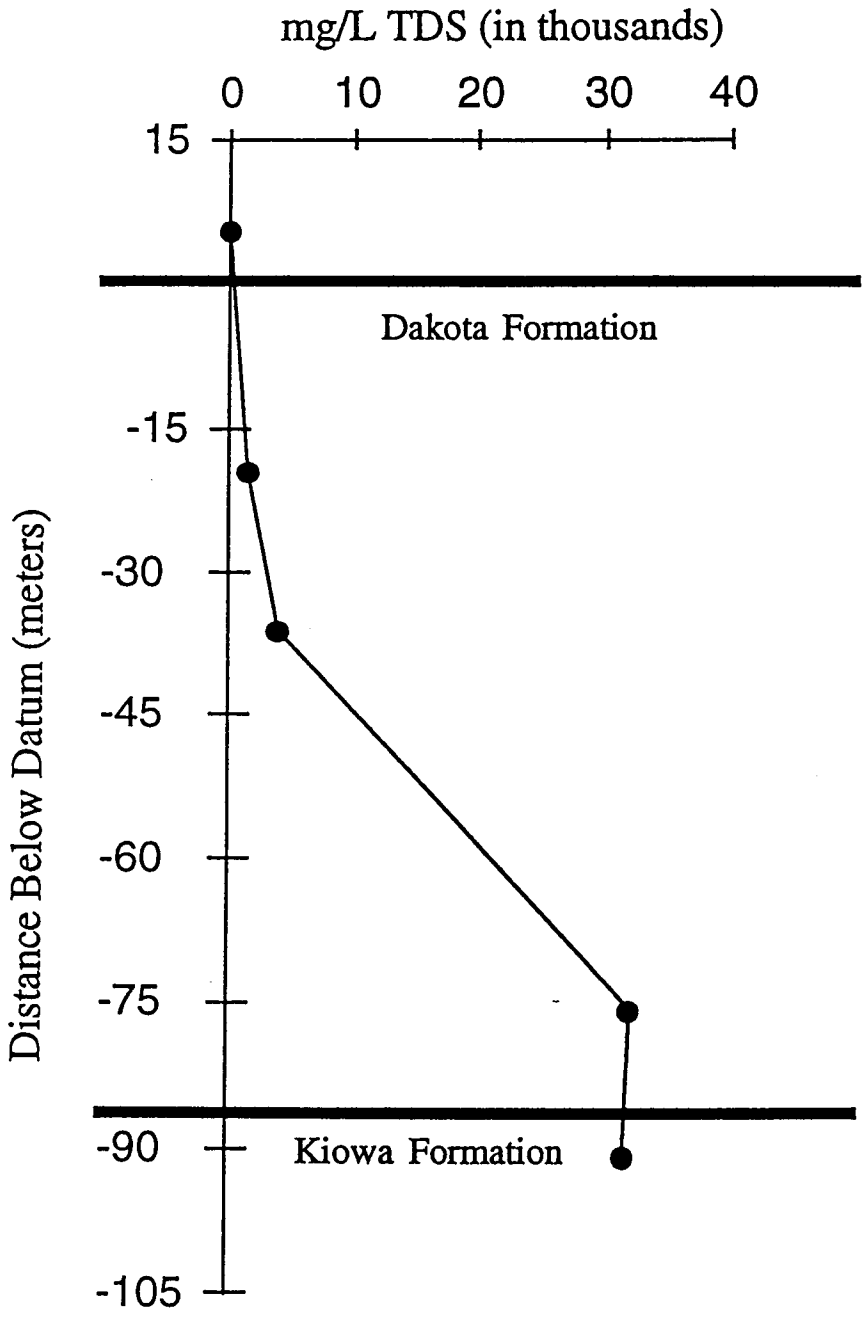

Figure 2.13f: Vertical variation of TDS in the upper Dakota aquifer. Datum is the top of the aquifer. This is well 20, and Figure 2.12 shows the location of the well from which samples were collected. Data comes from Swineford and Williams (1945). Formation tops are approximate.

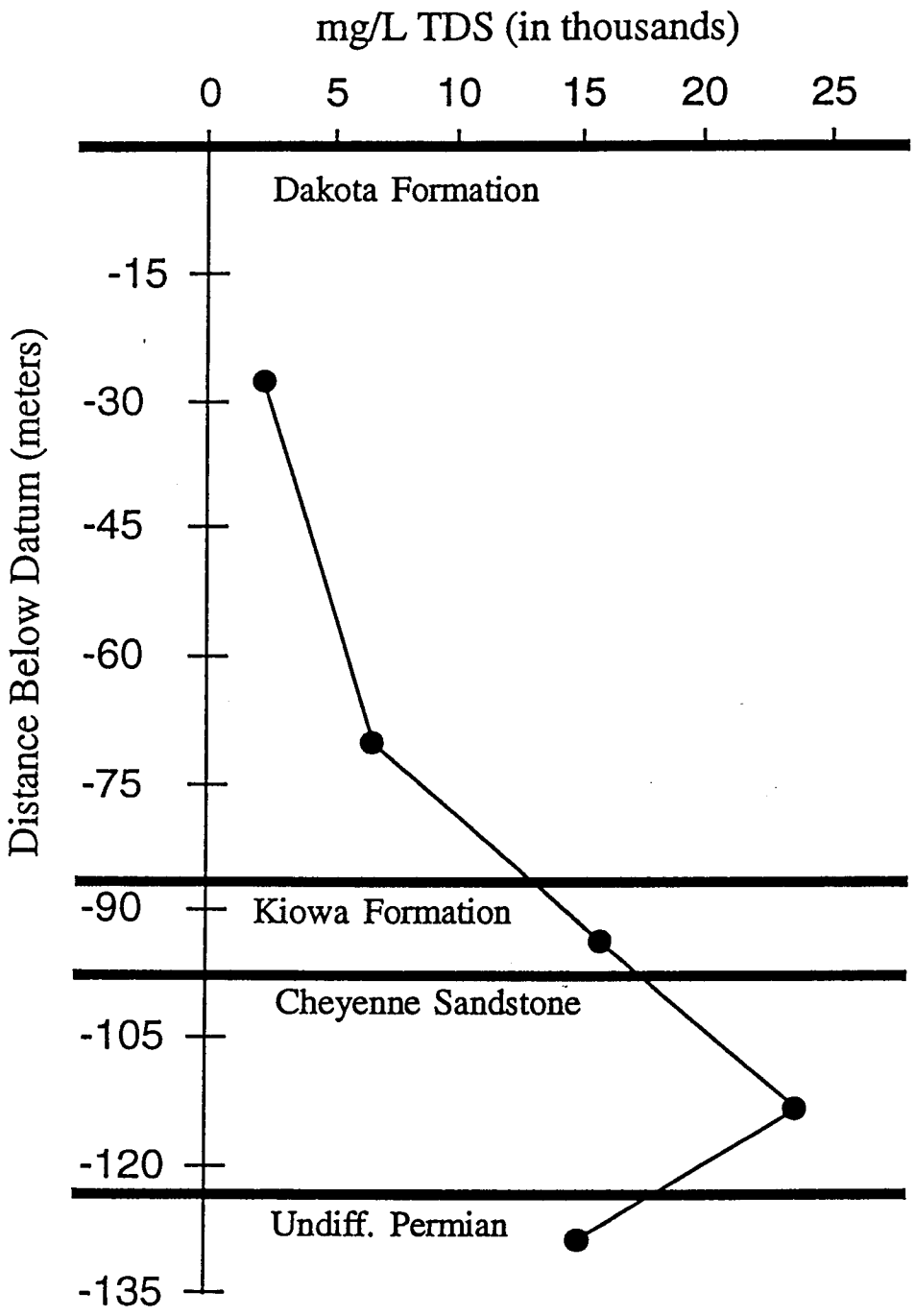

Figure 2.13g: Vertical variation of TDS in the upper Dakota aquifer. Datum is the top of the aquifer. This is well 21, and Figure 2.12 shows the location of the well from which samples were collected. Data comes from Swineford and Williams (1945). Formation tops are approximate.

2.7. Summary of Hydrogeologic Setting

In Summary, the upper Dakota aquifer in the study area is entirely confined and sandwiched between to regional aquitard units. The head within the upper Dakota aquifer is significantly below the water-table elevation resulting in a large potential for recharge to move downward across the Upper Cretaceous aquitard. Because the pressure within the upper Dakota aquifer parallels the hydrostatic gradient with depth there is little potential for vertical flow within the upper Dakota aquifer. Therefore, lateral flow dominates within the aquifer. Furthermore, because the head within the lower Dakota aquifer is nearly equivalent to the head in the within upper Dakota aquifer, the Kiowa Shale aquitard is a very good barrier to flow between the two aquifer units.

TDS is distributed within the upper Dakota aquifer such that there is a relatively uniform concentration distribution in the western half of the study area with a concentration gradient present in the eastern half of the study area. The concentration gradient coincides with the thinning and eventual pinchout of the Upper Permian aquitard. This results in the Cedar Hills Sandstone subcropping beneath the Dakota aquifer system in the eastern half of the study area. The source of salinity in the upper Dakota aquifer is thought to be primarily from the Permian because the salinity within the upper Dakota aquifer has a strong Permian signature. The higher salinity water of the upper Dakota aquifer is primarily a sodium chloride type, with the sodium and chloride ions coming primarily from the dissolution of halite in the Permian. However, the mixing of Dakota water with recharge water moving downward across the Upper Cretaceous aquitard is indicated by elevated sulfate concentrations in the upper portions of the upper Dakota aquifer.

CHAPTER 3. ANALYSIS OF THE DAKOTA AQUIFER FRAMEWORK

3.1. Subsurface Data

Subsurface data were acquired from geophysical logs of wells drilled for oil and gas exploration and production. Gamma-ray logs were used exclusively in this study, because they are useful in distinguishing between shale and sandstone lithologies. Gamma-ray logs record the natural gamma radiation emitted from the rocks. Radiation intensity is usually measured in American Petroleum Institute (API) units; however, older units of measurements such as counts/min or μg Ra-eq/ton have been used. The clays in the mudstone have a higher abundance of minerals containing naturally occurring radioactive isotopes of thorium and potassium than the sandstones. Therefore, a higher activity on the gamma-ray log indicates a mudstone lithology while a lower activity indicates a sandstone lithology (Doveton, 1991). By knowing the various characteristic sections and typical log signatures, one can locate formation boundaries easily.

3.1.1. Gamma-Ray Logs

The Kansas Geological Survey's log library contains 1,131 logs that were used for this study. Appendix 1 lists the company name, well name, and legal location of each well. Figure 3.1 shows the locations of the wells logged in the study area. Additional logs taken from wells located outside the study area were used to eliminate possible edge effects when mapping the elevation and thickness of hydrostratigraphic units and the cumulative thickness of the larger sandstone lenses. The distribution of the wells is non-uniform in the study area. The closest wells are less than 200 m (660 ft) apart, but much larger spacings of up to 6.5 km (4 miles) are present in parts of the study area. The average well density is 2.3 wells per section (one section equals 2.6 km^2 or 1 mi^2).

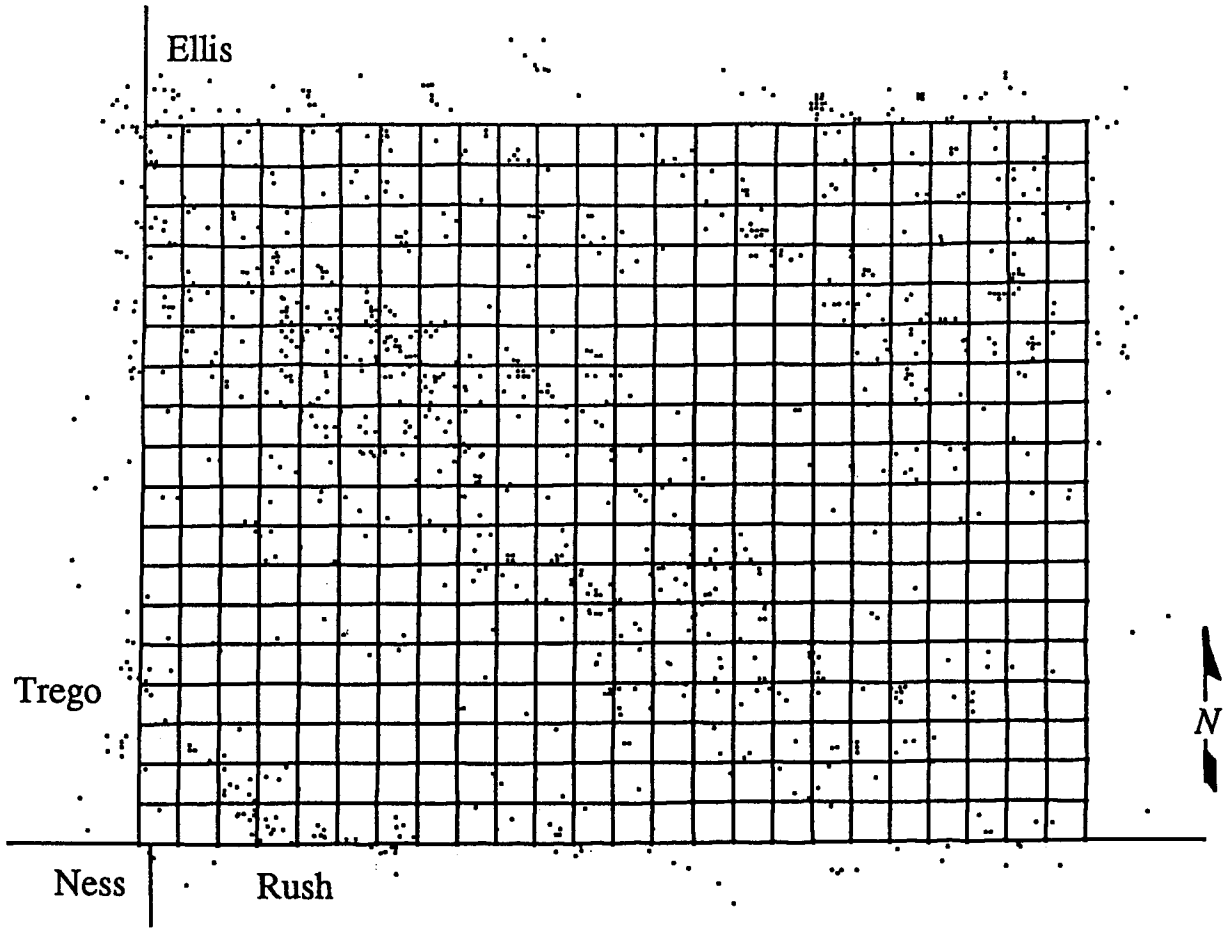

Figure 3.1: Distribution of gamma-ray logs in the study area. Notice that wells are also located outside the study area to eliminate boundary effects within the study area. The study area is defined by the section lines of Ellis County. Each section is one square mile. Other counties containing data are Trego, Ness, and Rush Counties.

3.1.2. Elevation and Thickness of Hydrostratigraphic Units

The thickness and elevation of different hydrostratigraphic units were determined from the gamma-ray logs by subsurface correlation. The definition of the hydrostratigraphic units and the characteristic log signatures separating the units have been presented in work by several authors (Macfarlane *et al.*, 1990; Hamilton, 1989; Macfarlane *et al.*, 1991; and Wade, 1992). Only those logs listing the surface elevation were used. From this information the elevation and thickness of the Upper Cretaceous aquitard, the upper Dakota aquifer, and the Kiowa shale aquitard were entered into a database and mapped within the study area. Figures 3.2a through 3.4 are maps of each unit's elevation and thickness. Appendix 2 contains the thickness data determined from the well logs.

3.2. Subdivision of the Upper Dakota Aquifer

After mapping the elevation and thickness of the various hydrostratigraphic units, the distribution of the larger sandstone lenses, those greater than or equal to 3 m (10 ft), within the Dakota Formation was investigated. The arrangement of the aquifer and aquitard subunits provides for a highly heterogeneous aquifer. Aquifer subunits generally consist of larger sandstone lenses, and aquitard subunits consist of primarily thinly bedded sands, silts, and mudstones. A quasi three-dimensional distribution of the aquifer subunits within the Dakota Formation was investigated. The next few sections describe the procedure used to define the distribution of these subunits in the upper Dakota aquifer.

3.2.1. Three Zones of the Upper Dakota Aquifer

It is commonly observed that aquifer subunits in the Dakota Formation occur in at least two zones, one at the bottom and one at the top. However, aquifer subunits can exist randomly throughout the formation. To better describe the arrangement of these aquifer subunits, the Dakota Formation was divided into three arbitrary zones.

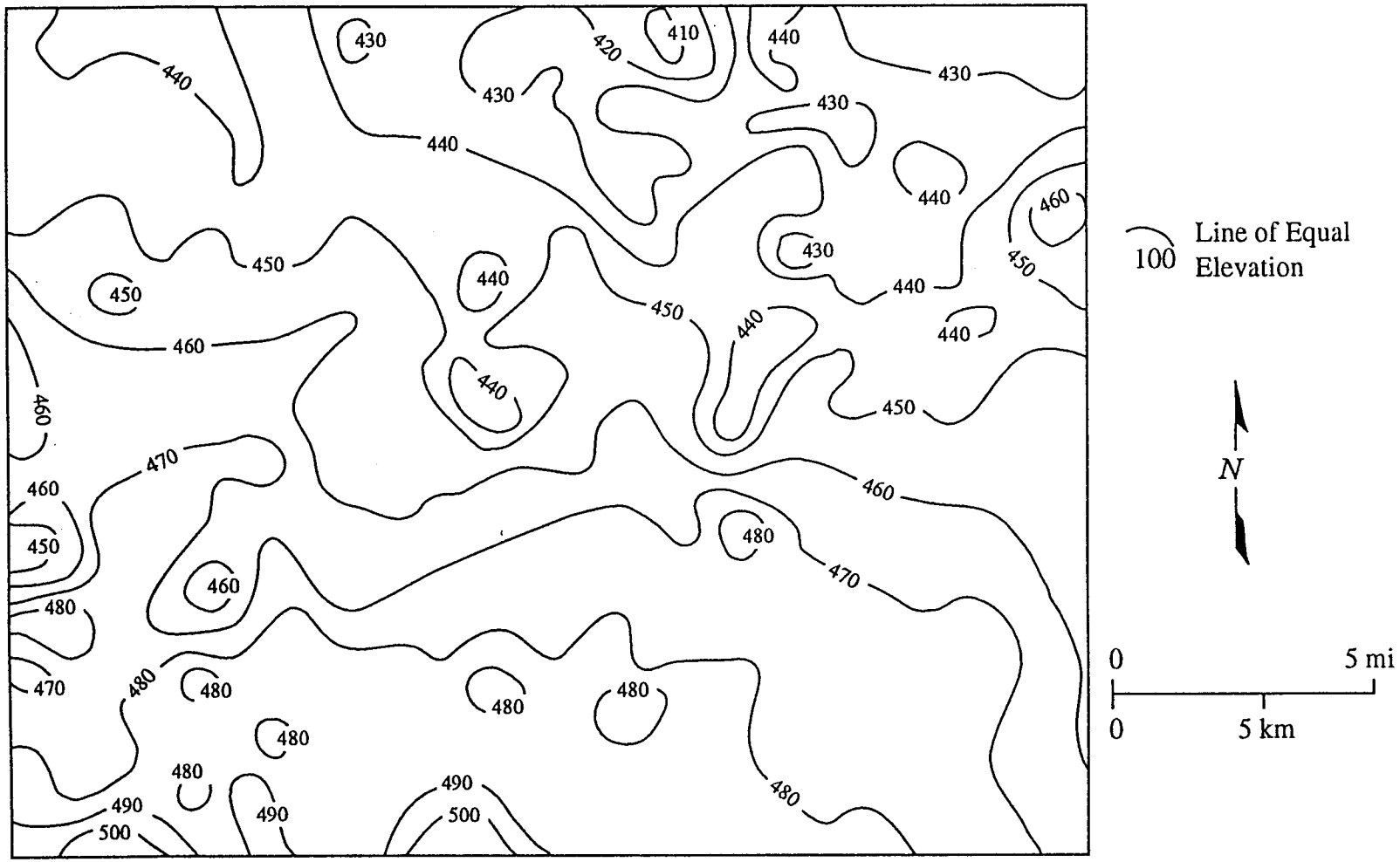

Figure 3.2a: Elevation of the top of the Kiowa shale aquitard in the study area. The contour interval is 10 m (33 ft). The top of the aquitard dips to the north.

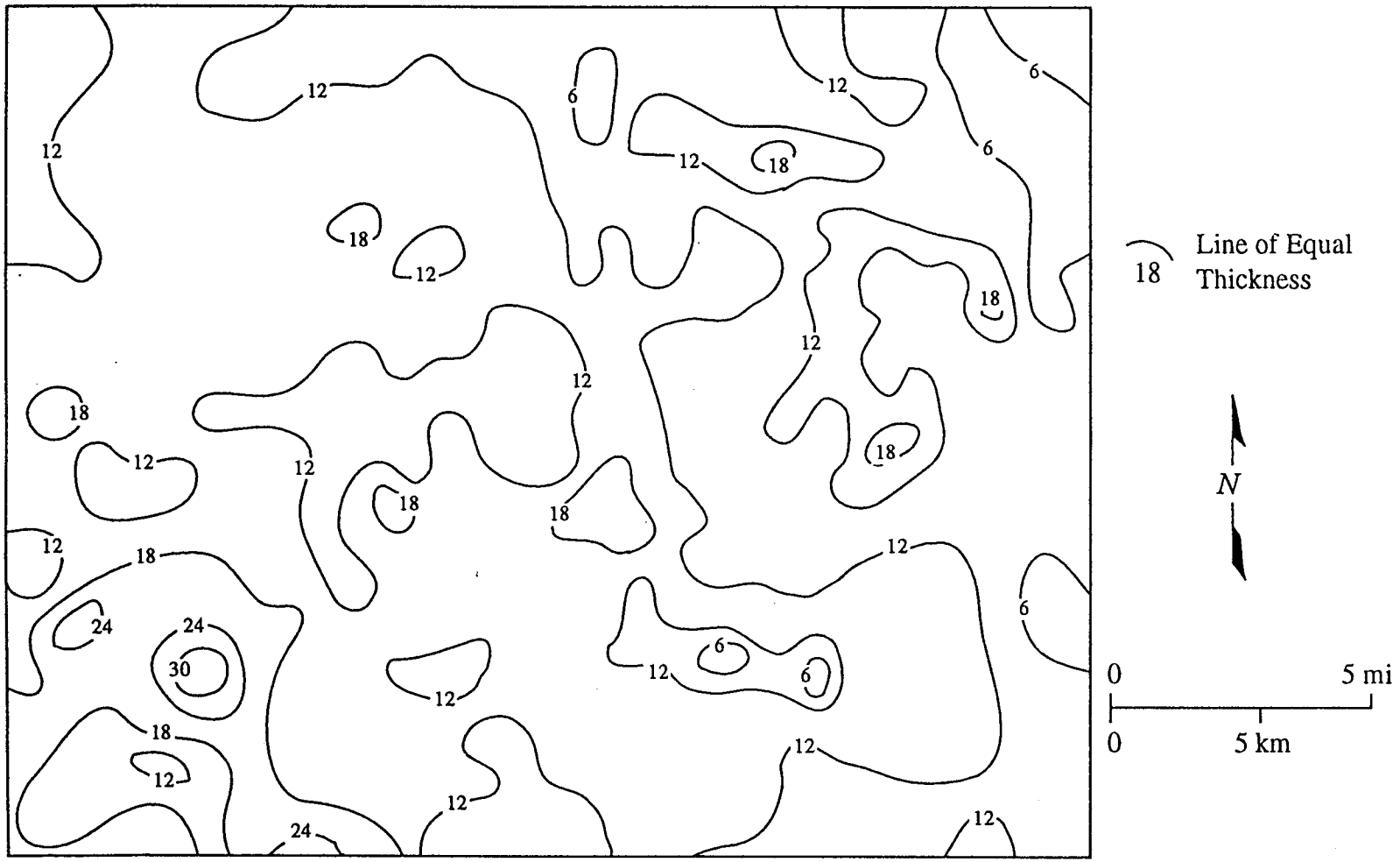

Figure 3.2b: Isopach map of the Kiowa Shale aquitard in the study area. The contour interval is 6 m (20 ft). The aquitard is relatively uniform in thickness with isolated thick and thin areas. The thinnest areas are in the eastern most portion of the study area.

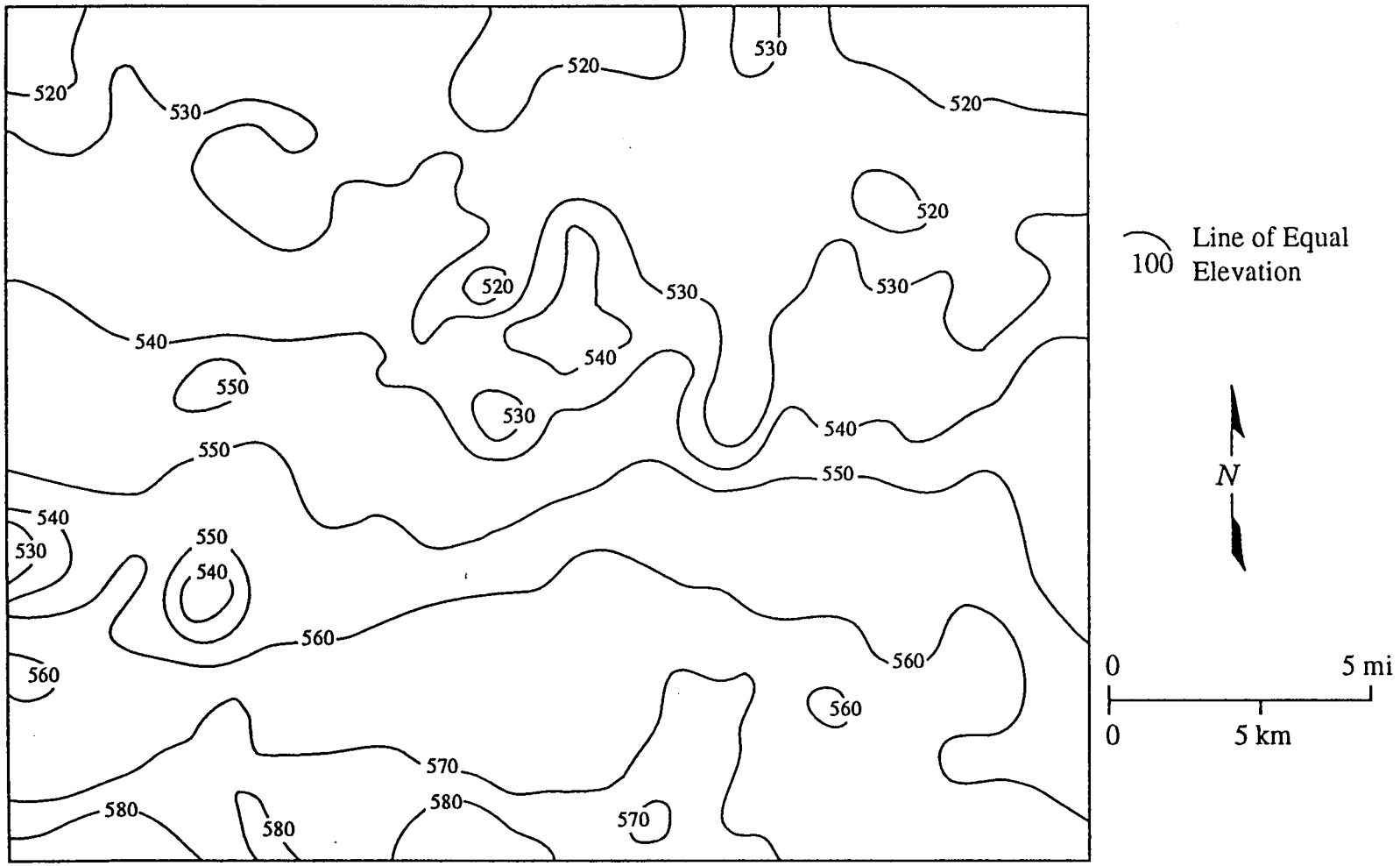

Figure 3.3a: Elevation of the top of the upper Dakota aquifer in the study area. The contour interval is 10 m (33 ft). The top of the aquifer dips to the northeast.

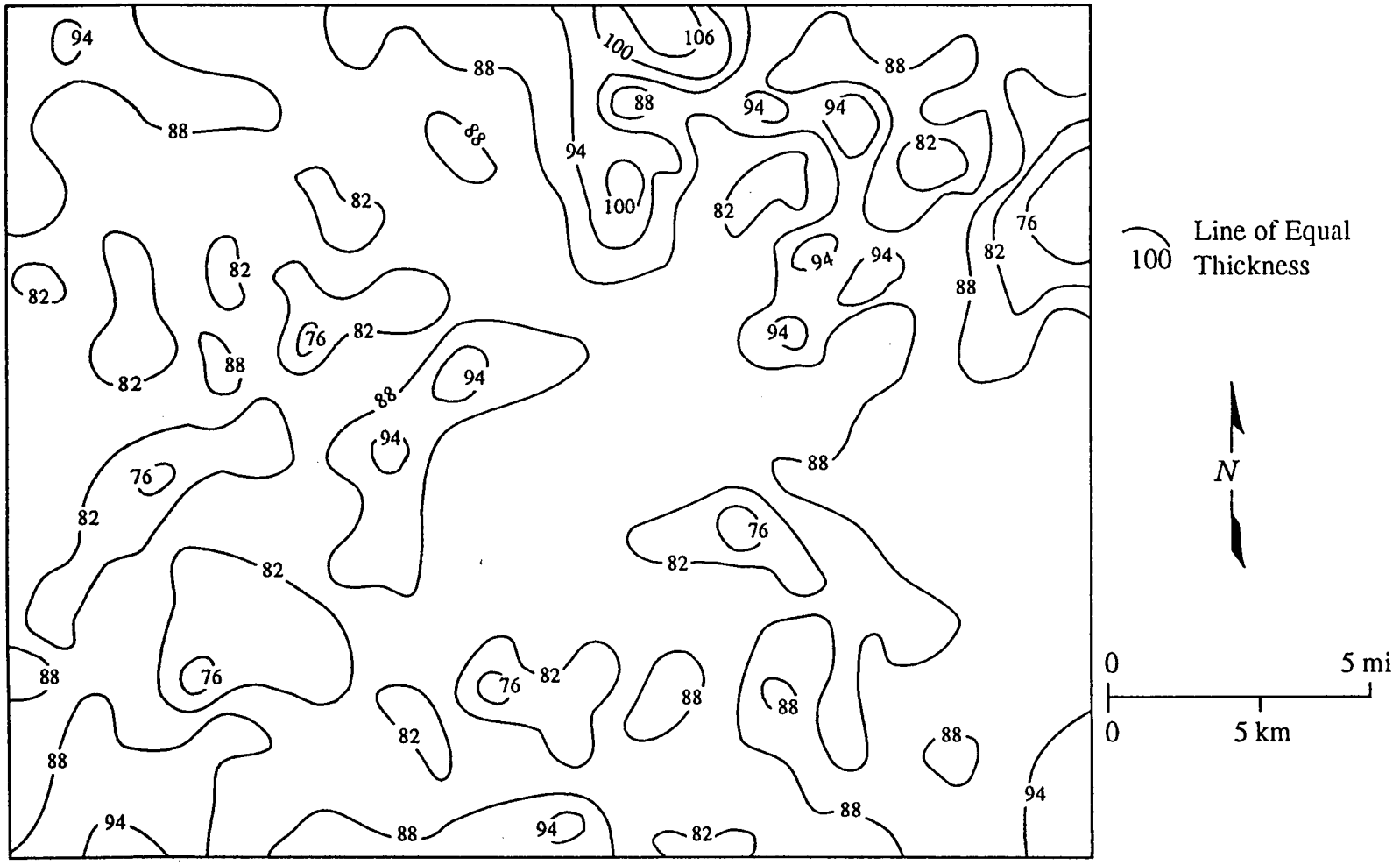

Figure 3.3b: Isopach map of the upper Dakota aquifer in the study area. The contour interval is 6 m (20 ft). The aquifer is relatively uniform in thickness across the study area.

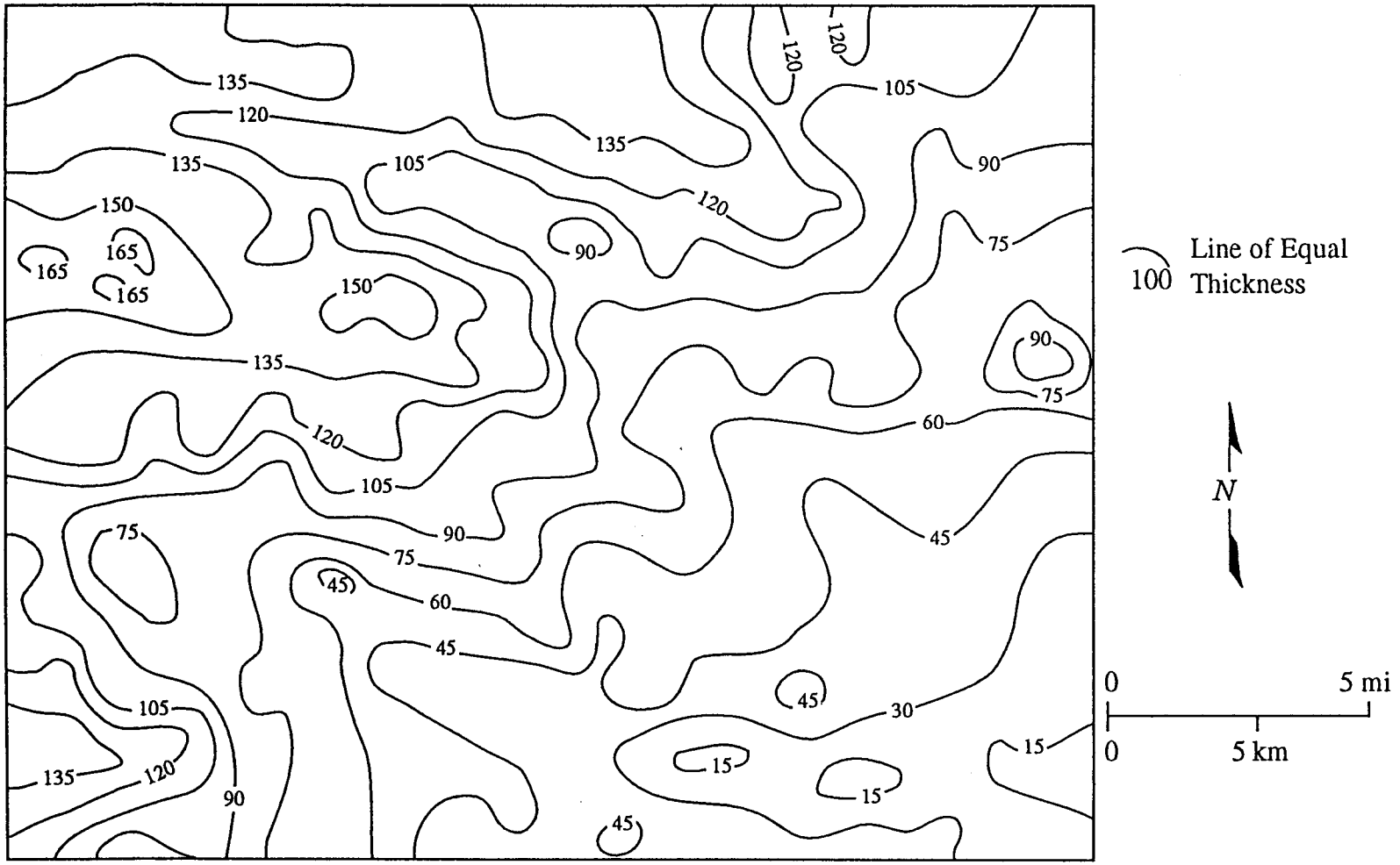

Figure 3.4: Isopach map of the Upper Cretaceous aquitard. The contour interval is 15 m (49 ft). The aquitard is thinnest in the Smoky Hill River and Big Creek valleys.

These zones tend to correspond to different depositional systems within the Dakota Formation. The lower and middle zones are generally thought of as alluvial, while the upper zone is considered to be shoreface or heavily marine influenced (Hamilton, 1989; Hamilton, 1994). However, the zones are arbitrary since there was no attempt to correlate these zones stratigraphically between well logs. It is rare to find three distinct zones of aquifer subunits in any particular well log. However, there are generally several thick aquifer subunits that can be assigned to their appropriate zones.

Correlation of aquifer subunits was determined to be unfeasible because of uncertainties of correlation between well logs. Instead, the following criteria were used to assign zone boundaries: 1) each zone is approximately 30 m (100 ft) thick or approximately one third of the total thickness of the Dakota Formation, 2) boundaries between adjacent zones were adjusted to avoid splitting major aquifer subunits, and 3) the upper shoreface or heavily marine influenced aquifer subunit was assigned to the upper most zone. Many of the logs were sufficiently complex that picking zone boundaries was difficult. In those situations placement of the boundary was done to the best of the author's ability. The most difficult logs were simply divided into thirds. Appendix 2 lists the thickness of aquifer and aquitard subunits by zone for each well log. Figure 3.5 illustrates the concept of the three zones in the Dakota Formation.

3.2.2. Method Used to Distinguish Aquifer and Aquitard Subunits

Although the upper Dakota aquifer is considered a regional aquifer unit, the discontinuity in large sandstone lenses provides for a complex arrangement of local scale aquifer and aquitard subunits within the formation. Therefore, along with dividing the upper Dakota aquifer into zones, an approximate thickness of these local aquifer subunits was determined for each zone. This was done entirely by hand using the 1,131 gamma-ray logs. Once zone boundaries were determined, the cumulative thickness of the aquifer subunits within each zone was estimated to the nearest 10 ft (3 m) interval. A cutoff of 60 API units was used in many instances to distinguish

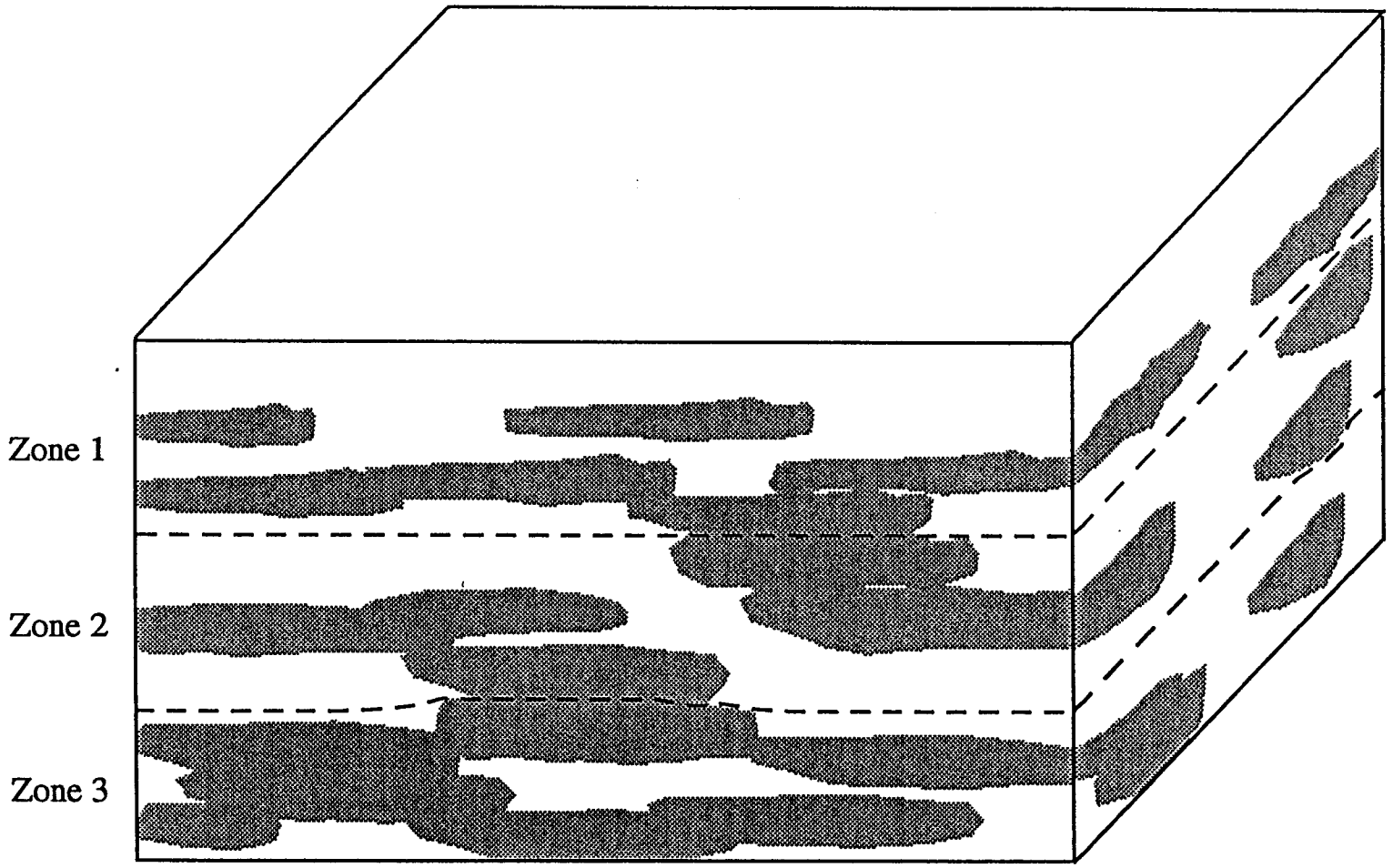

Figure 3.5: Illustration of the three arbitrary zones of the Dakota Formation. Dashed lines indicate the arbitrary zone boundaries, and the shaded areas represent the aquifer subunits of the Dakota Formation. Zone boundaries are adjusted so that major aquifer subunits are not spilt.

between the aquifer and aquitard subunits (Macfarlane *et al.*, 1994). However, the approximate mid-point between high and low gamma-ray readings was used on logs calibrated in other units. The total thickness of aquifer subunits within the Dakota Formation varies laterally, and since the formation was broken vertically into three zones, a quasi three-dimensional distribution of aquifer subunits was determined.

3.2.3. The Percentages of Aquifer Subunits by Zone

The global percentage and average thickness of aquifer subunits were determined for each zone. The Dakota Formation has an average total thickness of 86 m (282 ft) and contains approximately 29% aquifer subunits in the study area. Table 3.1 summarizes the statistical properties of the total aquifer subunit thicknesses and their percentage within each zone. Histograms of the data are shown in Figures 3.6a through 3.6c. The data distribution is highly skewed toward the lower thicknesses because of the large number of logs containing no aquifer subunits in Zones 1 and 2. Zone 3 which has the highest percentage of aquifer subunits is the most symmetrical of the distributions. Very few of the logs are without any Zone 3 aquifer subunits.

It was hoped that when the data were mapped, patterns in the distribution of aquifer subunits would appear; however, this turned out not to be the case due to the high local variability in the data (Figure 3.7). In locations where data are clustered, trends in the data are still difficult to determine. Maps showing the thickness of the aquifer subunits within each zone are shown in Figures 3.8a through 3.8c. Patterns in their distribution develop when all the data are taken into account, although it is still highly variable. However, these maps are inherently generalized because of the automated mapping software used to produce the contours. The final maps were produced by manually editing the contours produced by a computer contouring algorithm.

	Zone 1		Zone 2		Zone 3	
	Meters	Feet	Meters	Feet	Meters	Feet
Mean [L]	8.1	26.6	6.4	21.1	10.6	34.8
Standard Error [L]	0.224	0.735	0.234	0.768	0.185	0.608
Median [L]	6.1	20.0	3.0	10.0	9.1	30.0
Mode [L]	0.0	0.0	0.0	0.0	9.1	30.0
Standard Deviation [L]	7.53	24.7	7.87	25.8	6.23	20.4
Sample Variance [L^2]	56.8	611.0	62.0	667.1	38.8	417.4
Kurtosis	0.583	0.583	3.521	3.521	2.072	2.072
Skewness	1.014	1.014	1.761	1.761	1.091	1.091
Minimum [L]	0	0	0	0	0	0
Maximum [L]	36.6	120	45.7	150	48.8	160
Percent Aquifer Subunits	26	26	21	21	42	42
Average Total Thickness	31	102	30	98	25	82

Table 3.1: Descriptive statistics for 1,131 logs on aquifer subunit thickness. Values are listed in both metric and English units.

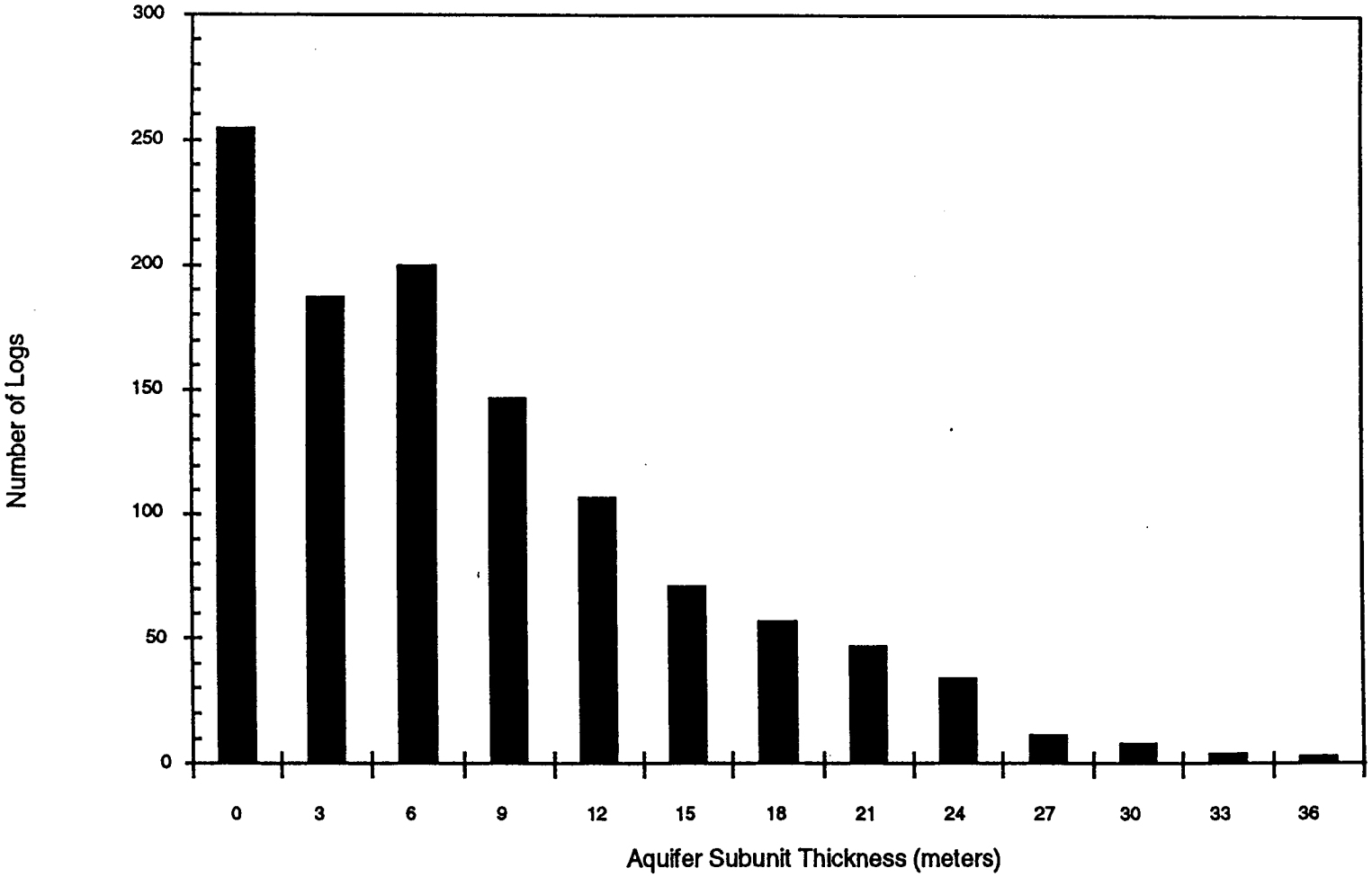

Figure 3.6a: Histogram of aquifer subunit thickness in Zone 1 based on frequency of occurrence in well logs.

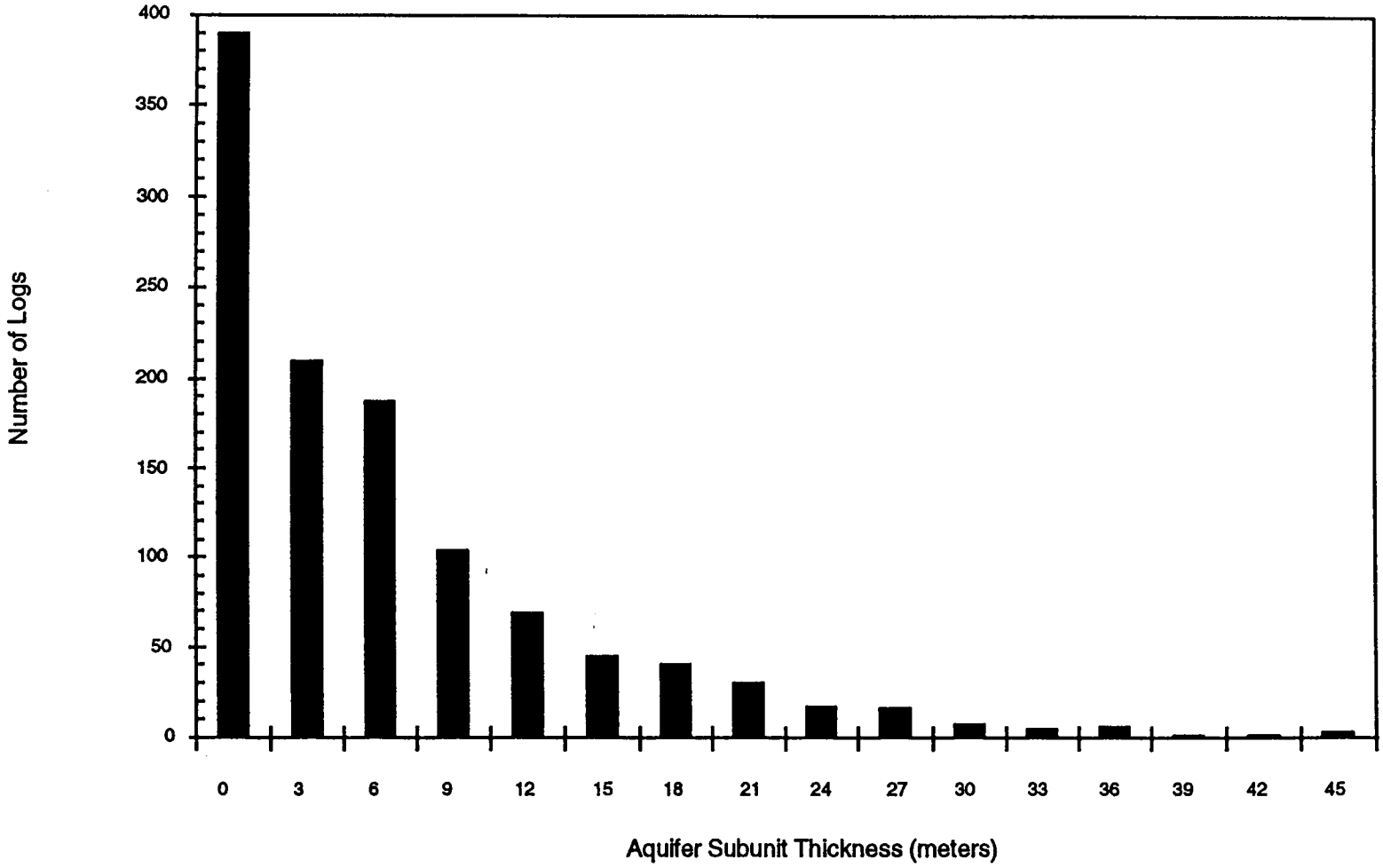

Figure 3.6b: Histogram of aquifer subunit thickness in Zone 2 based on frequency of occurrence in well logs.

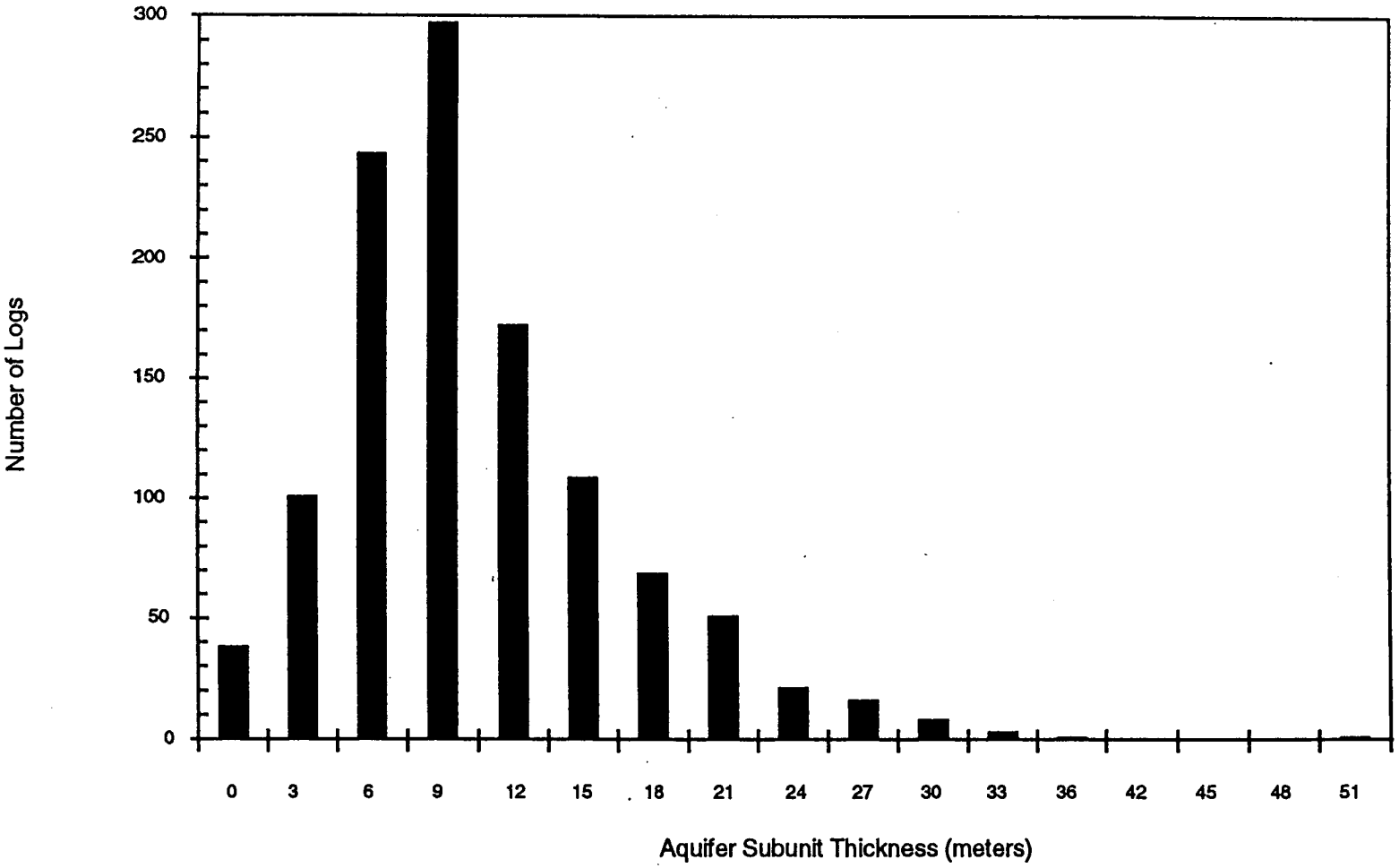

Figure 3.6c: Histogram of aquifer subunit thickness in Zone 3 based on frequency of occurrence in well logs.

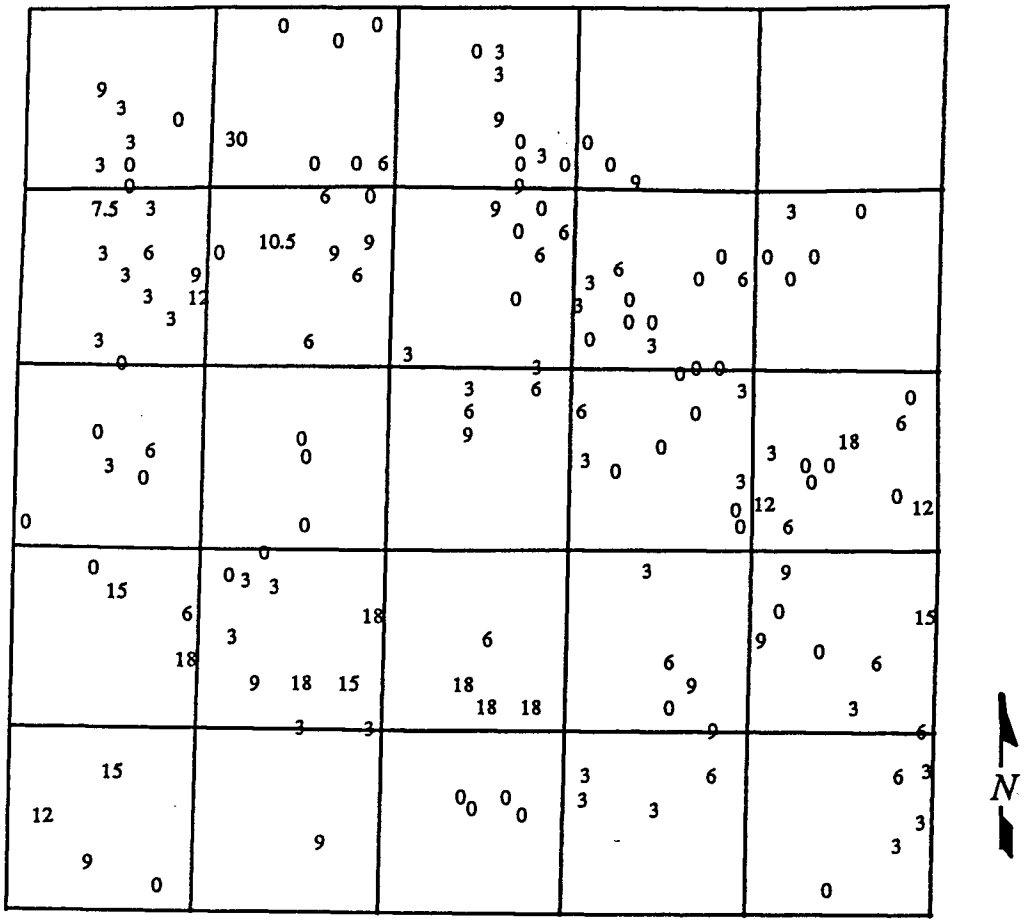

Figure 3.7: Map showing the typical degree of variability in aquifer subunit thickness in Zone 2. Each square is one section (2.6 km^2). Notice the extreme variability of thicknesses and the seemingly erratic distribution even in locations very close to one another. In some places there are hints of a pattern but there is no regional trend that can effectively be picked out.

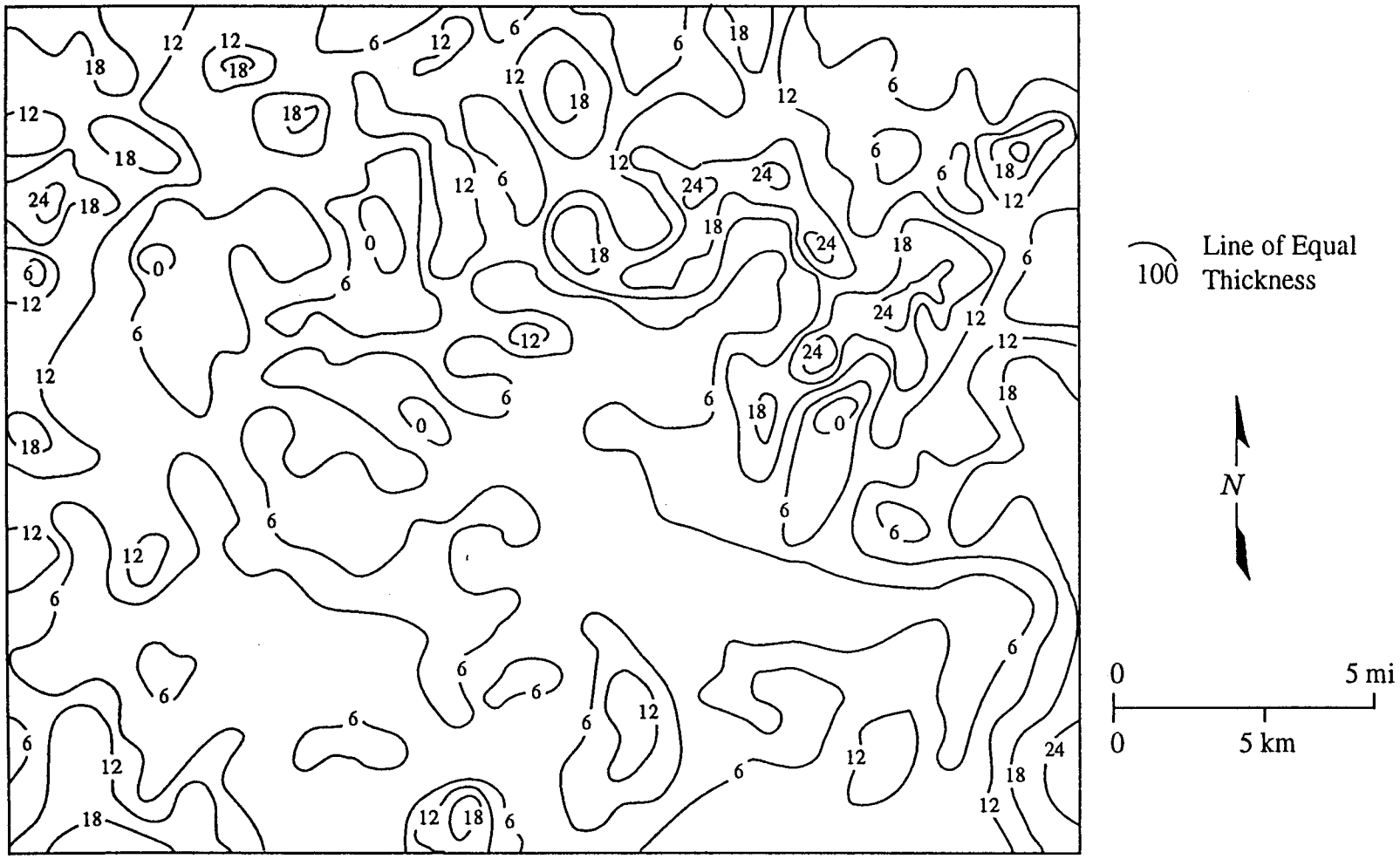

Figure 3.8a: Isopach map of cumulative aquifer subunits for Zone 1. The contour interval is 6 m (20 ft).

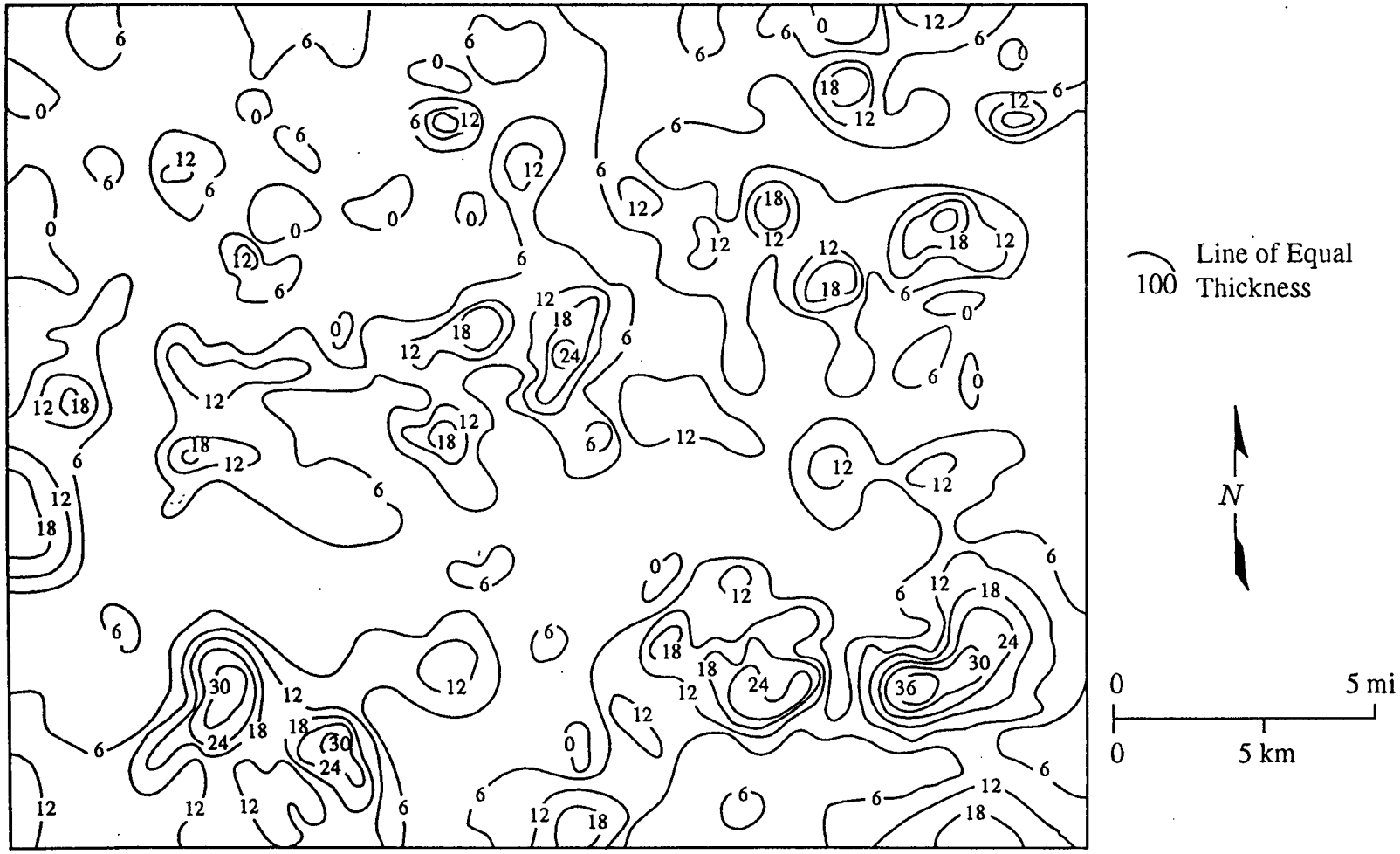

Figure 3.8b: Isopach map of cumulative aquifer subunits for Zone 2. The contour interval is 6 m (20 ft).

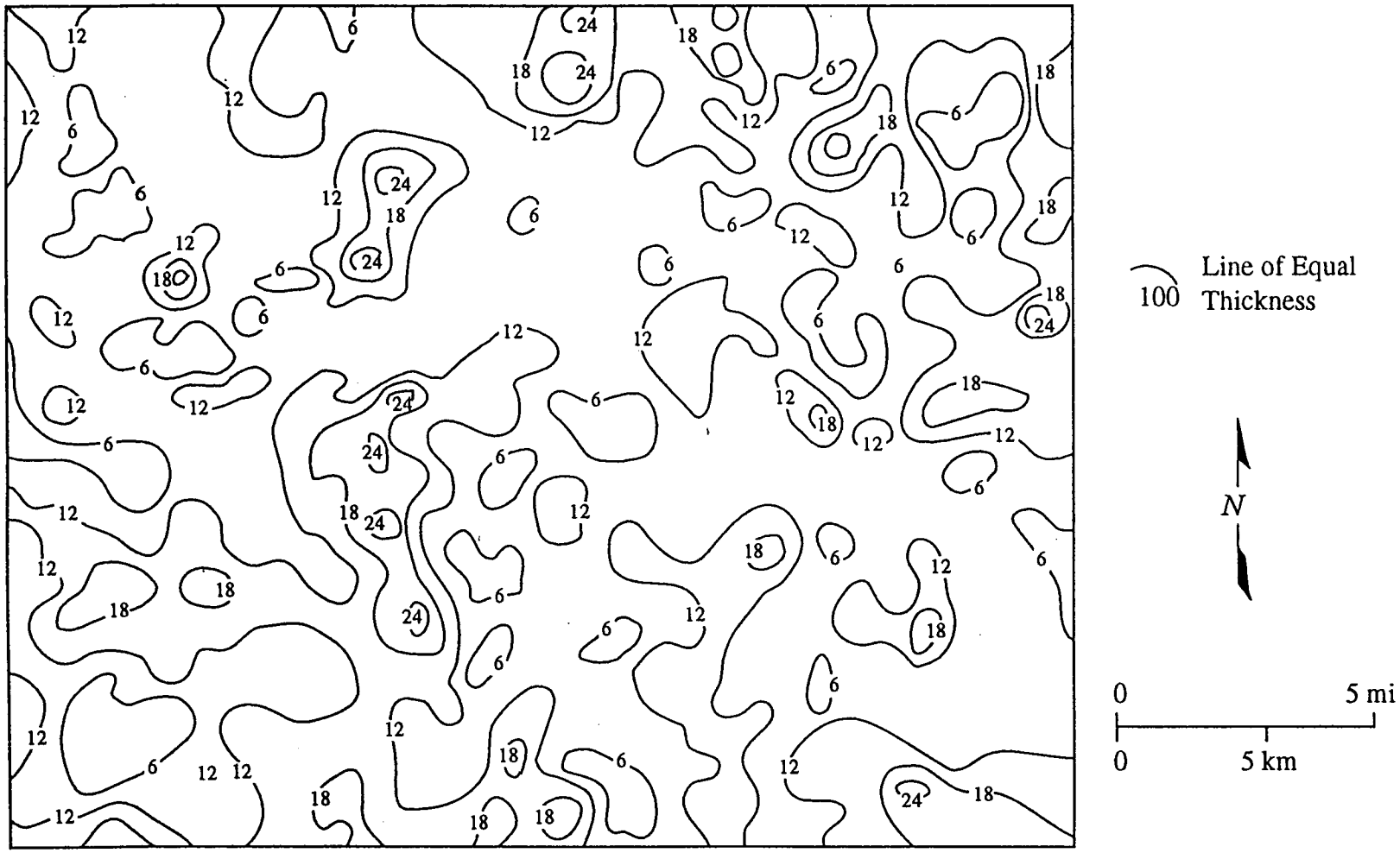

Figure 3.8c: Isopach map of cumulative aquifer subunits for Zone 3. The contour interval is 6 m (20 ft).

3.3. Geostatistics

As a means of analyzing the thickness data in a more objective manner, geostatistical methods were used. Geostatistical analysis is a useful means for evaluating the spatial distribution of a measured variable. This method can often highlight patterns and provide other information on spatially distributed data that cannot be achieved from more traditional methods of analysis. Geostatistical methods were used to evaluate patterns in aquifer subunit thickness for each zone. Geostatistics assumes the existence of a regionalized variable (Davis, 1986). This variable is both deterministic and random in its properties and has continuity over an unknown distance. However, the changes in the variable with distance cannot be adequately described by a deterministic function (Davis, 1986). Therefore, the regionalized variable is random with some sort of spatial relationship and can only truly be known through sampling. In this study, the cumulative thickness of the aquifer subunits in each zone is assumed to be a regionalized variable. This study used semivariograms and kriging to analyze each data set using the geostatistical software package GSLIB: Geostatistical Software Library (Deutsch and Journel, 1992).

3.3.1. Background

The semivariance is a statistical measure of the degree of spatial dependence between sample points (Davis, 1986). The equation for semivariance is,

$$\gamma_h = \sum_{i}^{n-h} (X_i - X_{i+h})^2 / 2n \qquad \text{eq. 3.1,}$$

where γ_h is the semivariance; n is the number of measurement points; h is the separation distance between measurement points; X_i refers to the measurement point at location i; and X_{i+h} refers to another measurement point taken h distance away from i. A plot of the semivariance vs. distance, known as the semivariogram, describes the spatial dependence of the regionalized variable. In many cases the semivariance increases with distance. This indicates that data points closer to one another are more

likely to be related than data points further away. A semivariogram is a mirror image of a plot of the covariance (Davis, 1986).

It is common for the semivariance to increase with distance up to a certain value and then level off to a value equal to the variance of the data set. The distance beyond which the semivariance becomes constant is termed the range of the semivariogram or the range of correlation of the data set. The range of correlation refers to the distance around which values of the variable of interest are statistically related to each other (Davis, 1986). The value of the semivariance at the range is termed the sill of the semivariogram. Figure 3.9 illustrates these different parts of a semivariogram.

In an irregularly spaced, two-dimensional data set, such as was used in this study, several other parameters require definition before one can proceed with a discussion of the geostatistical analyses. The variable h from equation 3.1 is usually considered to be constant. Points selected for the semivariance equation are therefore multiples of h away from X_i. Each multiple of h is known as a lag. In regularly spaced data there is always a data point present at each lag, however in irregularly spaced data, data points are rarely a constant distance from each other. This is why a distance tolerance is introduced as a parameter. Instead of rigidly selecting only those data points present at each lag, measurement points can also be selected if they are within a given tolerance from the lag (Deutsch and Journel, 1992). As a result, all data points can be used in the analysis. Figure 3.10 illustrates the idea of a lag and a distance tolerance in a regular and an irregular data set. A distance tolerance is not required in a regularly spaced data set.

Both the range and sill values can be dependent upon direction (Deutsch and Journel, 1992). This directional dependence is known as anisotropy. In order to bring out this anisotropy one must be selective about which data points are used when calculating the semivariance. Anisotropy is evaluated by including only those points found along a certain direction. The resulting semivariogram is known as a directional

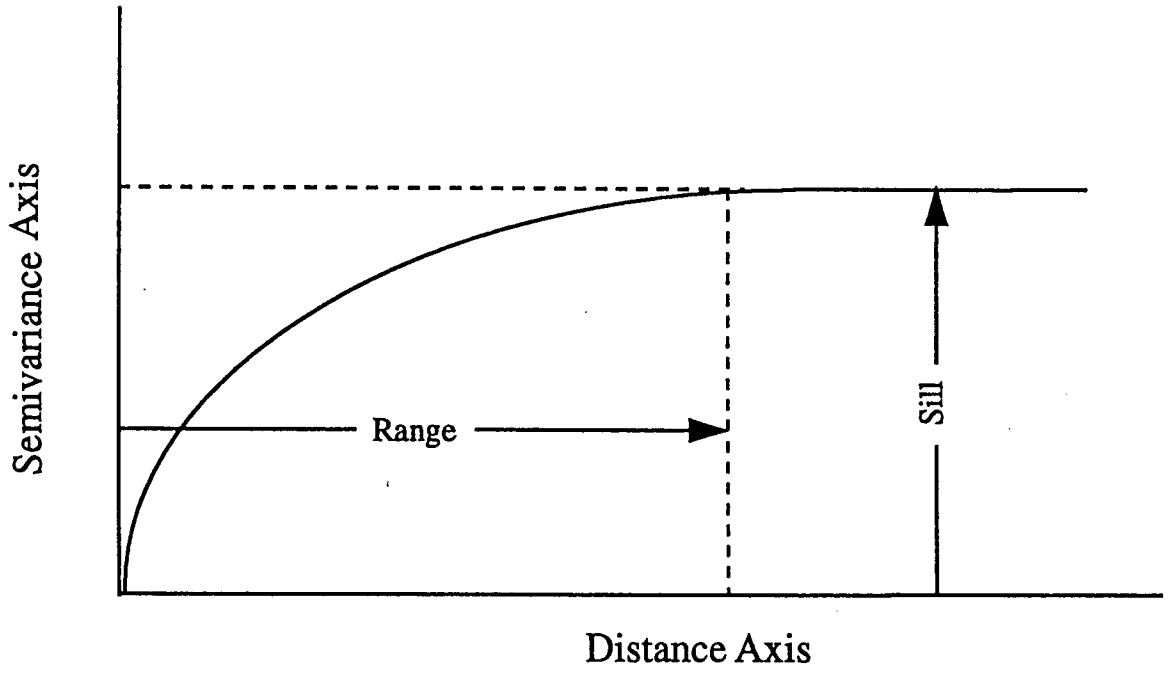

Figure 3.9: Illustration of the range and sill in a semivariogram. The sill is measured on the semivariance axis and the range is measured on the distance axis.

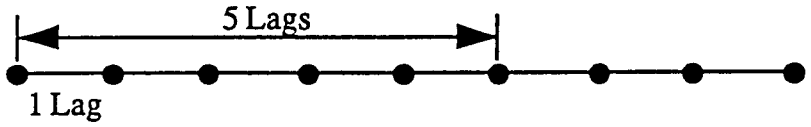

Regular Data Set

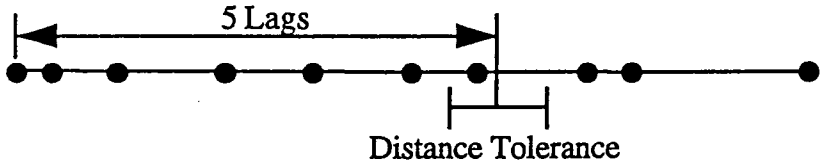

Irregular Data Set

Figure 3.10: Illustration of the difference between a regular data set and an irregular data set. For an irregular data set both a lag and the distance tolerance are used to calculate semivariance.

semivariogram. For example, if a north-south direction is chosen, then only those points north and south from X_i are selected and used in equation 3.1. It is common to have an angle tolerance and bandwidth (Deutsch and Journel, 1992) about the chosen direction (Figure 3.11). The angle tolerance is similar to the distance tolerance mentioned previously, and the bandwidth restricts the linear distance selected sample points can be from the direction vector.

A semivariogram is produced by plotting the semivariance against the distance between measurement points. The resulting plot is referred to as an experimental or sample semivariogram (Davis, 1986). However, in order to quantitatively describe the spatial correlation of the variable of interest, a mathematical model must be fitted through the data points usually by inspection. There are many mathematical models of spatial correlation available, and it is common to try several to achieve the best looking fit. An exponential model was used for this study, since it gave good results and was fairly easy to use (Figure 3.12). The equation for the exponential model is,

$$\gamma_h = \sigma_o^2 (1 - e^{-h/a}) \qquad \text{eq. 3.2,}$$

where a is the range; h is the lag distance; and σ_o^2 is the sill.

As a final complication, nested structures can be represented in the experimental semivariogram (Davis, 1986), and sometimes it is necessary to model these structures. Nested models consist of two or more superimposed simple semivariogram models. A commonly found nested model is termed a hole effect (Isaaks and Srivastava, 1989). A hole effect basically is an oscillatory function indicating periodicity in the measured variable. Many of the semivariograms in this study exhibit this oscillation. The interpretation of nested models is often complicated and is generally beyond the scope of this work.

Another nested structure relevant to this study is known as a nugget effect (Davis, 1986). The nugget effect is a non-zero starting point of the semivariogram on the semivariance axis (Figure 3.12). The semivariograms discussed in the following section all have pronounced nugget effects. The nugget effect is generally interpreted

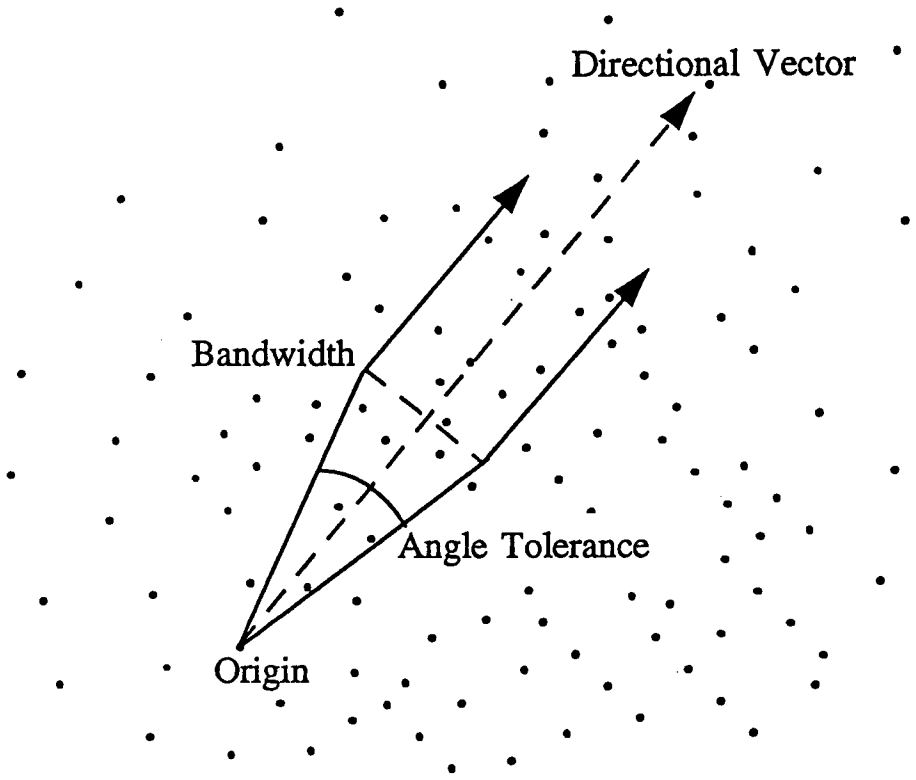

Figure 3.11: Illustration of the angle tolerance used for a directional semivariorgam in a two-dimensional irregular data set. The dashed arrow represents the directional vector chosen as for the variogram. An angle tolerance is defined about the vector and then a bandwidth of maximum linear distance is defined. The bandwidth is the maximum distance the points can be away from the vector. This would also extend in the opposite direction from the point, i.e. 180 degrees.

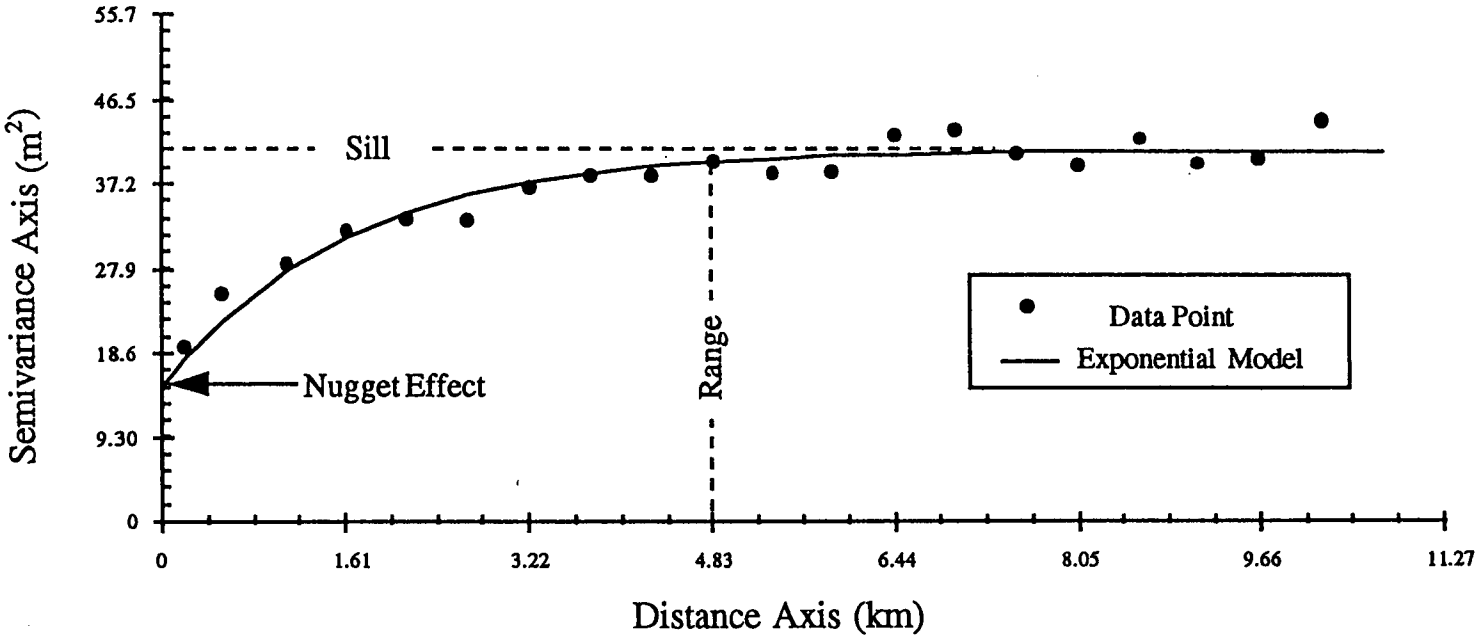

Figure 3.12: A directional semivariogram with an exponential model fitted through the experimental semivariogram. The sill equals 40.9 m^2 (440 ft^2), the range is 4.8 km (3.0 miles), and the nugget effect is 14.9 m^2 (160 ft^2). This semivariogram is for Zone 1 in the east-west direction. The range in an exponential model is defined as 95% of the sill value.

as a randomness in the data set or can represent variability in the measured variable at a scale less than the distance of the sample interval (Isaaks and Srivastava, 1989).

3.3.2. Results of Semivariograms

Directional semivariograms of aquifer subunit thicknesses were produced for each zone at 22.5° intervals. Table 3.2 contains the semivariogram input parameters used in the GSLIB program. Output from the GSLIB program was imported into a spreadsheet program where it was analyzed. Semivariogram modeling was performed interactively using available graphing functions and referenced cells containing appropriate parameter values. Fitting of the exponential model to the experimental data was done by eye on a trial and error basis.

All of the semivariograms were modeled using an exponential model with good results. However, some of them exhibit pronounced hole effects. The hole effects were modeled by superimposing sine or cosine functions onto the exponential model. The hole effects were modeled along with the simple exponential model in order to better evaluate the sill and range values in the experimental semivariogram. The collection of modeled directional semivariograms is shown in Appendix 3. Table 3.3 summarizes the sill, range, and nugget effect of the semivariogram modeling for each zone.

All of the semivariograms have pronounced nugget effects. In some cases the nugget effect is over half the final sill value. The value of the nugget effect is usually compared to the sill by reporting it as a percentage of the sill value (Table 3.3). Since the sill value represents the variance in the entire data set, the percentage of the overall variance due to the nugget effect is an important parameter. A high percentage is indicative of the high degree of variability in the thickness of the measured variable at a scale of less than the lag spacing (535 m).

The range and sill values of each semivariogram varied with direction for each zone. The directional dependence of the sill is known as zonal anisotropy and the

	Lag Distance	Lag Tolerance	Angle Tolerance	Bandwidth
Zone 1	536 m	268 m	45 degrees	8050 m
Zone 2	536 m	268 m	45 degrees	8050 m
Zone 3	536 m	268 m	45 degrees	8050 m

Table 3.2: Semivariogram input parameters used for GSLIB for each zone. Directional semivariograms were determined at increments of 22.5 degrees. The parameters were uniform for all analyses to maintain consistency.

Zone	Range (km)			Sill (m^2)			Nugget (m^2)			% Nugget		
1	11.25	10.5	8.0	46.5	46.5	43.7	25.5	23.2	22.3	55	50	51
	7.25	4.75	5.5	43.7	40.9	40.9	16.7	14.9	18.6	38	36	45
	11.25	12.0		44.6	46.5		23.2	24.2		52	52	
2	1.5	4.0	4.75	53.4	53.9	52.0	23.2	23.2	23.2	43	43	45
	6.5	6.5	4.75	54.8	55.7	55.7	21.4	23.2	23.2	39	42	42
	4.25	3.25		56.7	54.8		23.2	91.4		41	51	
3	6.5	6.5	5.0	37.6	37.2	35.3	25.1	23.2	23.2	67	63	66
	5.0	6.5	5.0	36.2	36.2	36.2	18.6	230	23.2	51	59	64
	5.0	5.0		37.6	37.2		23.2	25.1		62	68	

Table 3.3: Summary of the range, sill, and nugget values for the three zones from the directional semivariogram analysis. Eight values are given for each item. Each represents one of the eight directions in which the semivariograms where done. The directions running across rows are 0°, 22.5°, 45°, 67.5°, 90°, 112.5°, 135°, and 157.5° respectively. The ninth square is intentionally left blank.

directional dependence of the range is known as geometric anisotropy (Deutsch and Journel, 1992). Figure 3.13 shows rose plots of the zonal anisotropy of each zone. Their character can indicate features about the arrangement and continuity of aquifer subunits. The maximum ranges of the two fluvial zones are similar but smaller than the maximum range in Zone 1 which has a more marine influence. The larger range observed in Zone 1 is indicative of the broad sheet sands that would be deposited adjacent to a shoreline. The north-south direction of the long axis in the anisotropy is likely due to the possible elongation of sandstone bodies parallel to the shoreline at the time of deposition (Hamilton, 1989; Hamilton, 1994). The smaller ranges found in Zones 2 and 3 represent the more sinuous sand-body geometry expected in alluvial deposits. Zone 2 has its long axis of anisotropy in an east-west direction. This suggests an elongation of sandstone lenses parallel to the depositional dip. The range in Zone 3 fluctuates with no distinct trend and is therefore considered to be isotropic. However, the experimental semivariogram may only appear isotropic because the undulating character of the anisotropy could not be sorted out (Isaaks and Srivastava, 1989).

Since Zone 3 is alluvial, it is promising that it has a similar maximum range as that of Zone 2 which is also alluvial. The isotropic range would not be expected, but it is possible that an abundance of aquifer subunits could mask any trend in their geometry. Furthermore, Zone 3 has a much greater average thickness than the other zones and is more evenly distributed making any trend in the thickness of aquifer subunits difficult to determine. Wade (1992) observed a greater degree of continuity in the aquifer subunits at the bottom of the Dakota Formation and stated that it was probably the dominant conduit of flow through the aquifer in his study area. It is likely that the basal aquifer subunits are relatively continuous in this region as well. The semivariograms of Zones 2 and 3 also had pronounced hole effects. This could indicate a large scale periodicity in aquifer subunit thickness. It is unknown what this

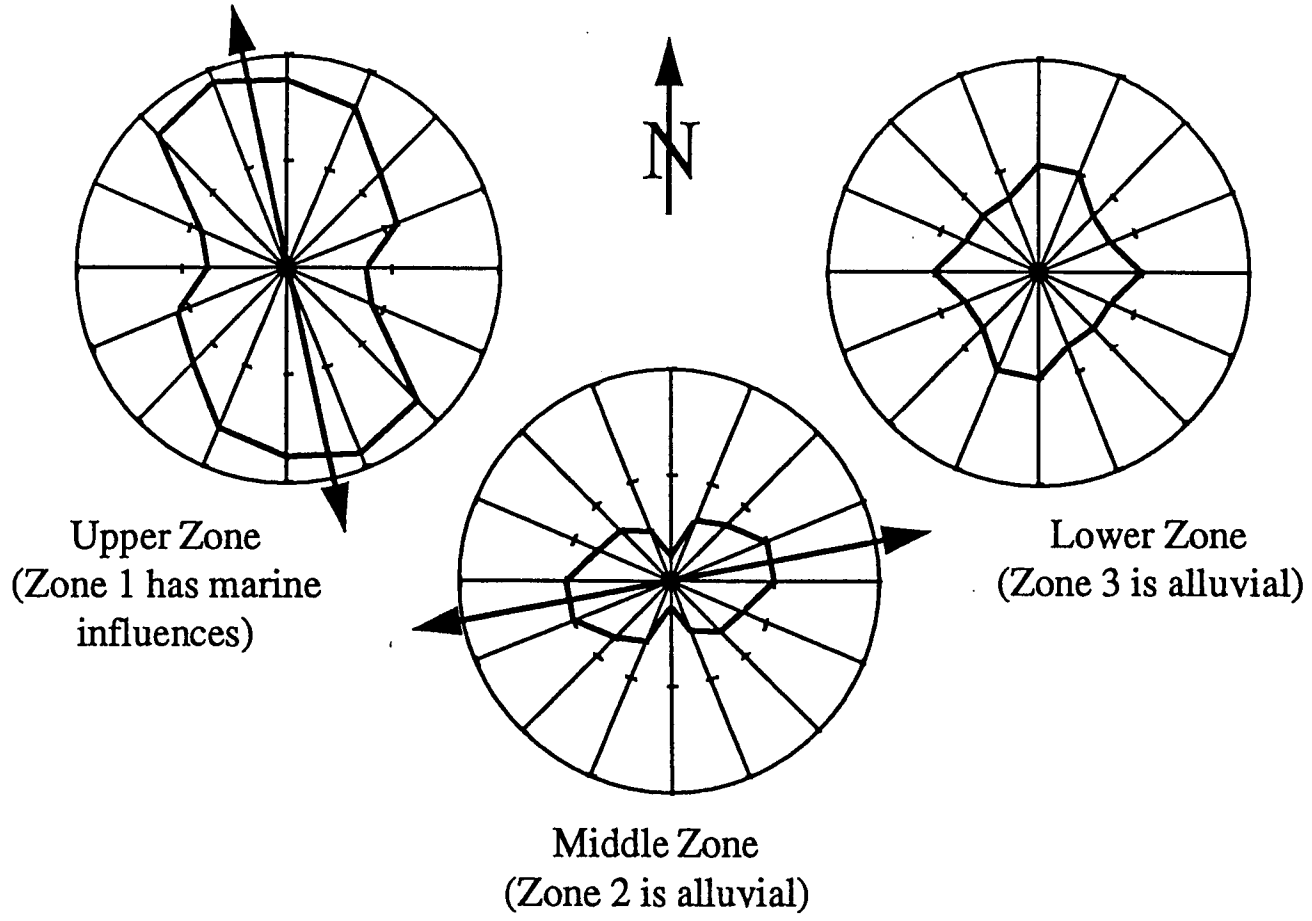

Figure 3.13: Rose plots of the range from the directional semivariograms. The upper and middle zones show axes of anisotropy while the lower zone does not. The alluvial zones both have smaller maximum ranges when compared to the range of the upper zone with more of a marine influence. Each circle is 12.88 km (8 mi) in radius with the inner tic marks being half the radius.

periodicity could represent, but possibilities include the meandering and sinuous nature of alluvial deposits or valley occurrence.

3.3.3. Kriging

Kriging is an interpolation technique that utilizes information from the semivariograms to estimate a grid of values from the original data set. It produces an unbiased best estimate of the variable of interest at unsampled locations while honoring the original data. The procedure uses a weighting function with parameters coming from the semivariogram analysis (Deutsch and Journel, 1992). An evaluation of the error or reliability of the kriging estimates also comes from the kriging procedure. In this thesis, it is used as an objective way of assigning average aquifer subunit thickness values to the model grid discussed in the next chapter.

The equation for kriging is,

$$Z(u) = \sum_{\alpha=1}^{n} \lambda_\alpha(u)\, Z(u_\alpha) + \left[1 - \sum_{\alpha=1}^{n} \lambda_\alpha(u) \right] m \qquad \text{eq. 3.3,}$$

where u is a measured data point; Z(u) is the value at the estimation point; $\lambda(u)$ is a weighting function; and m is the mean of the data set (Deutsch and Journel, 1992). The weighting function is determined by minimizing the kriging variance. The equation for the kriging variance is,

$$\sigma^2(u) = C(0) - \sum_{\alpha=1}^{n} \lambda_\alpha(u)\, C(u - u_\alpha) \qquad \text{eq. 3.4,}$$

where $\sigma^2(u)$ is the kriging variance; C(0) is the stationary variance; and $C(u - u_\alpha)$ is a covariance function (Deutsch and Journel, 1992).

The type of kriging used in this study is known as block kriging. Block kriging is used to estimate values for specified areas or blocks rather than estimating point values (Deutsch and Journel, 1992). Its advantage is that an average value can be assigned to a region of interest, in this case the model cell. Since kriging estimates values to grid blocks, it has been designed to coincide with the nodes in the model grid

discussed later. Values assigned to the nodes of the model should be representative of the entire cell region. Block kriging allows just such an estimation. The disadvantage of kriging is the same as would be expected with any other estimation technique. The estimated values are only as good as the data used for the estimation, and the number of control points used in the estimation procedure.

The areal averaging also serves to filter out highs and lows in the values of thickness found very close to one another. As an example, assume that there are five data points all relatively close to one another, and four of those data points are over 15.25 m (50 ft) while one has the value of zero. Next assume that the zero value is extremely close to the intended point of estimation. Point kriging respects the closest point and produces a value very close to zero at the estimation point. However, block kriging would produce a value of 15.25 m (50 ft). This still respects the data but is an average value for the block area instead. For the purpose of this study, the value of 15.25 m (50 ft) would be the more desirable estimation because it better represents the aquifer subunits thickness within the cell. Average values of aquifer subunit thickness were assigned to a model grid of the study area with the block kriging method. Figures 3.14a through 3.14c are contour maps of the average thickness of the aquifer subunits for each zone. Figure 3.15 is a graph showing the distribution of aquifer subunit thickness assigned to the model cells.

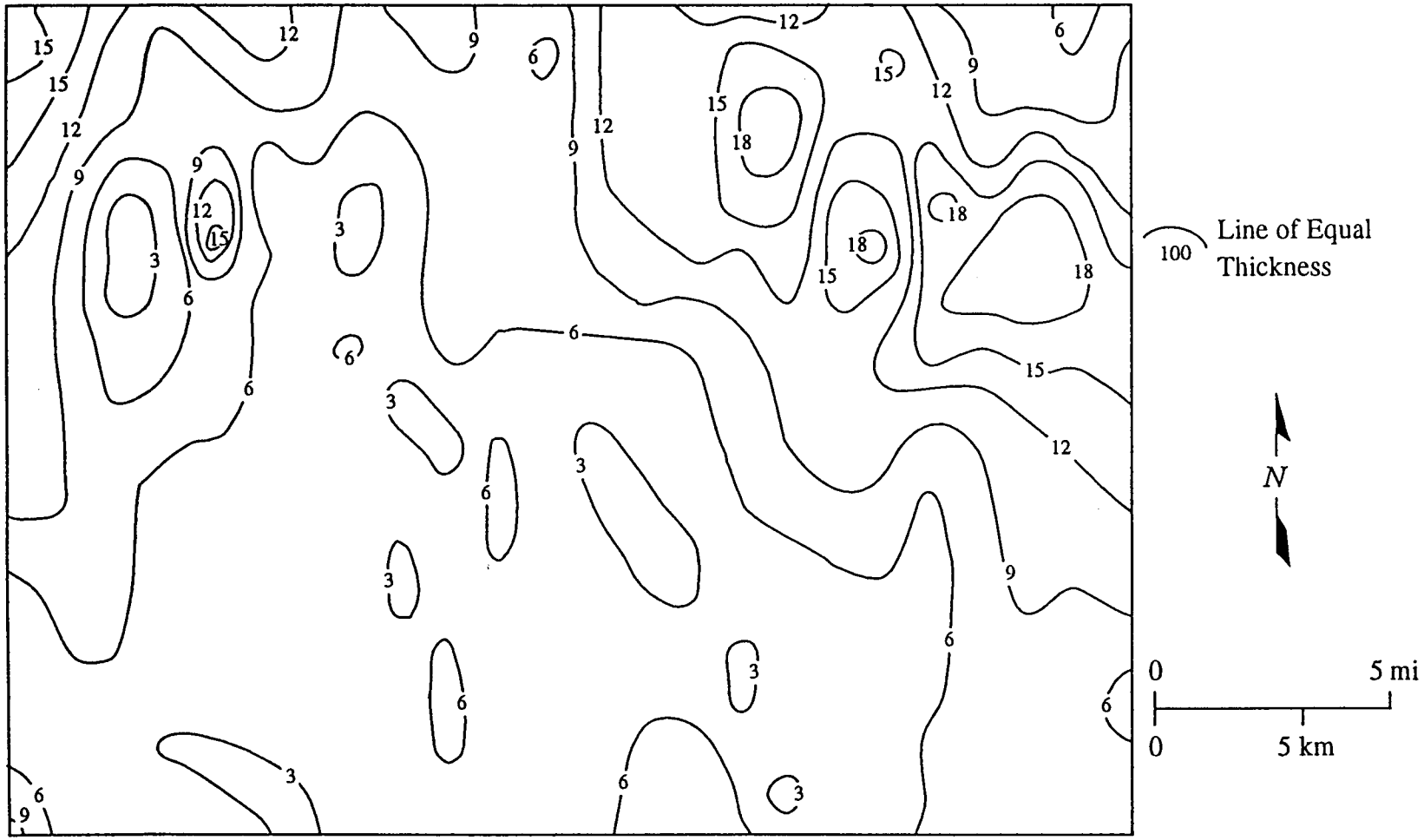

Figure 3.14a: Isopach of average aquifer subunit thickness in Zone 1. The contour interval is 3 m (10 ft). the thickest aquifer subunits occur in the northern portion of the study area. The 6 m (20 ft) line seperates the high from the low transmissive regions.

Figure 3.14b: Isopach of average aquifer subunit thickness in Zone 2. The contour interval is 3 m (10 ft). The thickness of the aquifer subunits trends in an east-west direction. The 6 m (20 ft) line seperates the high from the low transmissive regions.

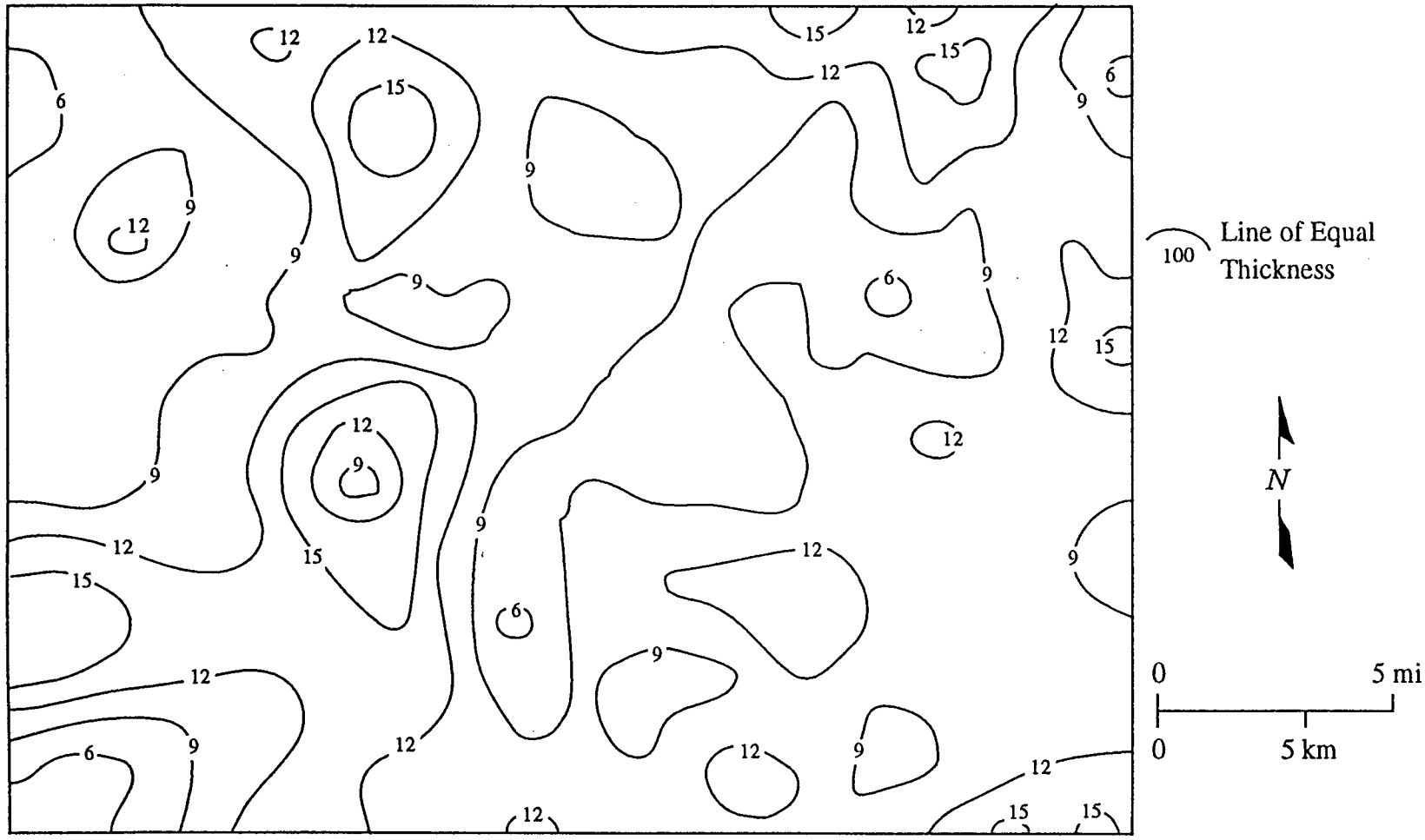

Figure 3.14c: Isopach of average aquifer subunit thickness in Zone 3. The contour interval is 3 m (10 ft). The distribution of the aquifer subunits are more even, and they have a greater cumulative thckness than found in Zones 1 and 2. The 6 m (20 ft) line seperates the high from the low transmissive regions.

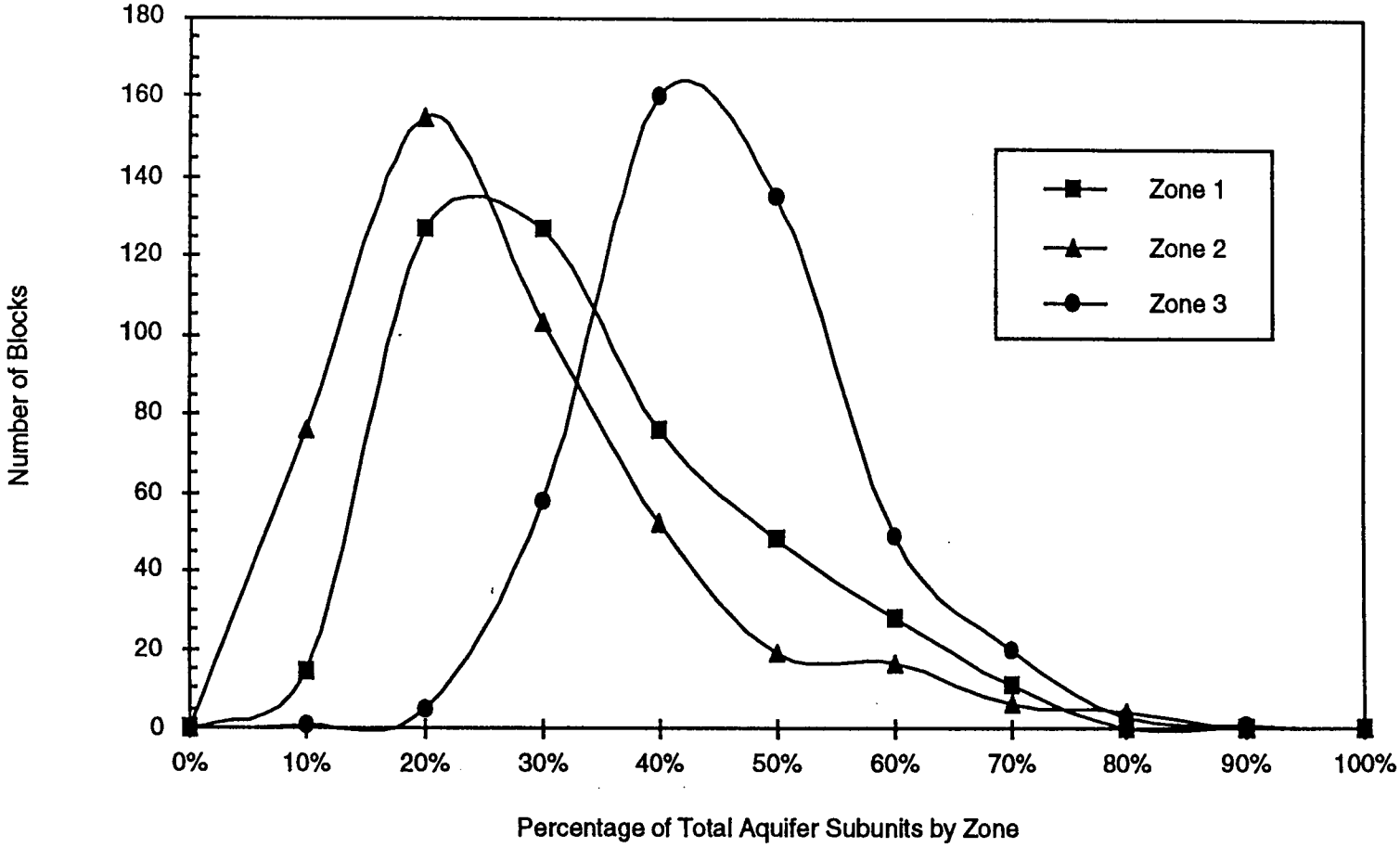

Figure 3.15: Average aquifer subunit percentage by zone as assigned to the model grid using block kriging. The graph is read in the following manner. The data point at the 20% mark on the Zone 2 curve represents about 155 blocks with between 10% and 20% aquifer subunits.

CHAPTER 4. MODEL DESCRIPTION AND INPUT PARAMETERS

4.1. Conceptual Model of Ground-Water Flow and Mass Transport

Before discussing the input parameters and the modeling programs chosen for this project, a conceptualization of the ground-water flow and mass transport processes is presented here. Conceptualization of the flow and transport processes provides guidance about boundary conditions, model domain, and limitations of the modeling study. The modeling phase of this project was used for hypothesis testing to better understand the factors controlling ground-water flow and mass transport in the upper Dakota aquifer. Conceptualization also helps in the selection of the numerical modeling programs required for the modeling project, since the programs must be able to handle the modeling objectives.

The study region was chosen so that the flow field could be described in fairly simple terms. The upper Dakota aquifer is sandwiched between two regional aquitards. Each aquitard restricts flow into or out of the aquifer. The upper aquitard restricts recharge to the aquifer. Water-level data show that the potentiometric surface of the Dakota aquifer is significantly less than the elevation of the water-table, therefore flow should move downward across the Upper Cretaceous aquitard into the upper Dakota aquifer. However, the considerable thickness and very low hydraulic conductivity reduces the amount of recharge contributed to the aquifer, as compared to the total flux. Likewise, the lower aquitard restricts the movement of water between the upper and lower Dakota aquifers. Since the head difference across the Kiowa shale aquitard is believed to be small, the flow between the upper and lower Dakota aquifers is small (Macfarlane, 1993). As a result, most of the flow in the upper Dakota aquifer is assumed to be lateral, moving down the hydraulic gradient. This is consistent with the subhydrostatic pressure gradient observed in the aquifer (Macfarlane, 1993).

The presence of both aquifer and aquitard subunits in the Dakota Formation suggests a dual distribution of hydraulic conductivity in the aquifer. The aquifer subunits should have a relatively high hydraulic conductivity in comparison to the aquitard subunits. As a result, it is believed that most of the flow takes place in the large sandstone lenses making up the aquifer subunits of the Dakota Formation. However, this assumes that the aquifer subunits are sufficiently connected to provide regional conduits for ground-water flow. The problems associated with describing the connection of aquifer subunits and its impact on ground-water flow and mass transport are a major focus of this modeling study. Figure 4.1 summarizes the conceptual flow model.

In the conceptual model for mass transport, various sources of salinity contribute to its distribution in the upper Dakota aquifer. The recharge moving across the Upper Cretaceous aquitard is relatively low in salinity. Lateral flow transports some upgradient salinity in the aquifer into the study area. However, the source of most of the salinity is believed to be from the Permian. Salinity from the Permian moves into the aquifer most likely by diffusion. This is supported by the lack of vertical flow in the aquifer and the small amount of water passing through the Kiowa shale aquitard. Determining the relative contributions of these different sources to the total salinity is one of the goals of the transport modeling.

To add to the conceptual understanding of the transport processes, time is also a factor in the mass transport process in the upper Dakota aquifer. It is likely that the salinity of the aquifer was rather high in the past due to the presence of remnant sea water and water from dissolution of Permian salt. As time progressed, the salinity has gradually been reduced due to flushing of the aquifer with water originating in the primary recharge area in southeast Colorado (Whittemore and Fabryka-Martin, 1992) due to the periods of uplift and erosion associated with tectonic activity in the Rocky Mountains. The majority of the flushing would have taken place in the interconnected aquifer subunits. However, the isolated aquifer subunits and many of the aquitard

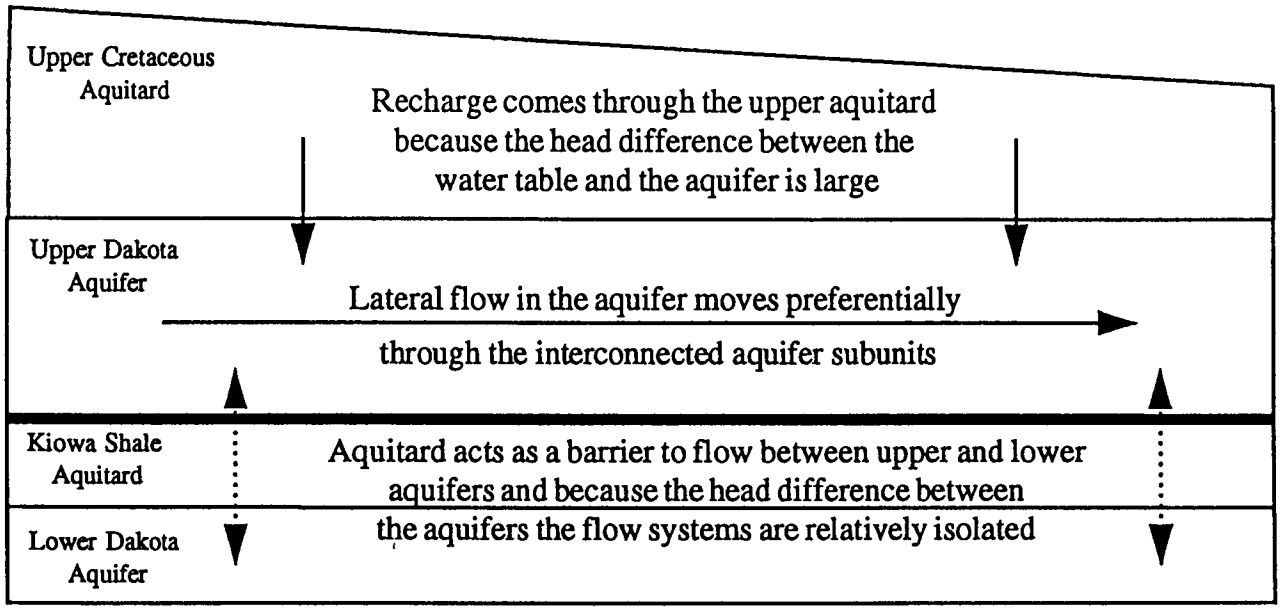

Figure 4.1: Illustration of conceptual flow model. Lateral flow in the aquifer moves primarily through interconnected aquifer subunits. The aquifer receives a small amount of recharge coming through the upper aquitard due to the difference in head between the water table and the aquifer. The Kiowa Shale aquitard restricts flow between the upper and lower aquifers and because there is not much of a head difference between the aquifers.

subunits would not have been directly affected by the flushing because of the much lower hydraulic conductivity of the aquitard subunits. The interconnection and arrangement of the aquifer subunits then become important in interpreting the observed distribution of salinity in the aquifer. Figure 4.2 summarizes the conceptual transport model.

4.2. Description of Numerical Modeling Programs

The modeling programs used for this project were selected on the basis of their ability to simulate the hydrologic phenomena presented in the previous section, their relative ease of use and accessibility, and the numerical method used to simulate mass transport. Two modeling programs were used to simulate ground-water flow and mass transport. MODFLOW (McDonald and Harbaugh, 1988) was used to simulate ground-water flow, while MT3D (Zheng, 1990) was used to simulate solute transport.

MODFLOW is a well tested and widely used ground-water flow modeling package for the simulation of ground-water flow in three dimensions under both steady-state and transient conditions. MODFLOW uses an implicit block-centered finite-difference solution technique to solve the flow equation in three dimensions,

$$\partial(K_{xx}(\partial h/\partial x))/\partial x+\partial(K_{yy}(\partial h/\partial y))/\partial y+\partial(K_{zz}(\partial h/\partial z))/\partial z-W=S_s(\partial h/\partial t) \quad \text{eq. 4.1,}$$

where K is hydraulic conductivity; x, y, and z are Cartesian coordinates along the major axes of hydraulic conductivity; h is the potentiometric head; W is a volumetric flux per unit volume representing sources and/or sinks; S_s is the specific storage; and t is time (McDonald and Harbaugh, 1988).

MODFLOW is a modular program and is structured such that a main program calls upon other subprograms to handle a variety of hydrologic stresses and boundary conditions. The design of the program allows for the inclusion or removal of various sources and sinks. Furthermore, changes in the type of boundary conditions can be accomplished with minimal difficulty. The various sources and sinks are handled by

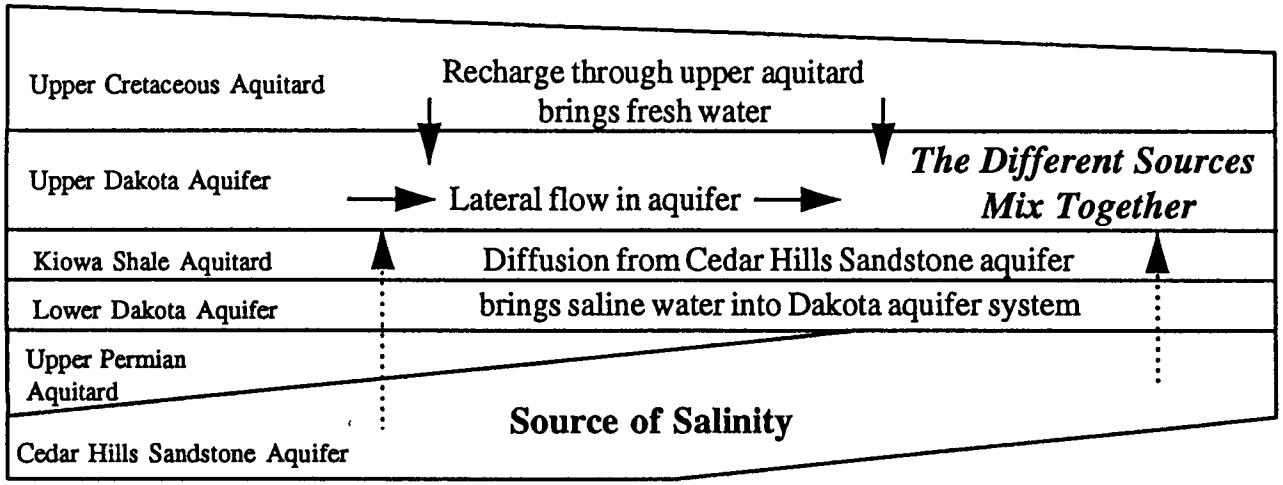

Figure 4.2: Illustration of conceptual mass transport model of chloride Three sources contribute salinity to the aquifer 1) diffusion of chloride from the Permian, 2) recharge of fresh water, and 2) upgradient salinity within the upper Dakota aquifer. These three sources then mix together in the upper Dakota aquifer resulting in the current salinity distribution.

different packages which are actually subprograms called by the main program (McDonald and Harbaugh, 1988). The packages were used to simulate wells and recharge in this modeling project.

MT3D requires the input of hydraulic heads and flux rates from a previously run flow model to simulate mass transport and therefore, is not a stand alone modeling package (Zheng, 1990). Any block-centered, finite-difference flow modeling software package can provide this information, but MT3D was designed to accept input from MODFLOW fairly easily (Zheng, 1990). Since the flow and transport processes are essentially uncoupled, MT3D assumes that dissolved mass has no effect upon the flow field. Therefore, the possible effects that changes in density and viscosity may have on the flow field cannot be taken into account. This is a limitation, but it is one that should not significantly impact model results since the changes are very small.

MT3D models mass transport by solving the advective-dispersive-reactive equation in three dimensions,

$$\partial(D_{ij}(\partial C / \partial x_j)) / \partial x_i - \partial(v_i C) / \partial x_i + (q_s / \theta)C_s + \sum R_k = \partial C / \partial t \quad \text{eq. 4.2,}$$

where C is the concentration of the contaminant dissolved in the ground-water; t is time; x_i is the distance along the respective axis; D_{ij} is the hydrodynamic dispersion coefficient; v_i is the linear pore velocity; q_s is the volumetric flux of water per unit volume of aquifer representing sources and/or sinks; C_s is the concentration at the sources and/or sinks; θ is the effective porosity of the porous medium; and ΣR_k is a chemical reaction term (Zheng, 1990). The transport equation is linked to the flow equation by the following relationship,

$$v_i = (K_{ii} / \theta)(\partial h / \partial x_i) \qquad \text{eq. 4.3,}$$

where K_{ii} is the principal component of the hydraulic conductivity tensor (Zheng, 1990). It is assumed that the principal components of the hydraulic conductivity tensor coincide with the north-south, east-west, and vertical coordinates.

MT3D was chosen because of the numerical method used to solve the mass-transport equation. The simulation of mass transport in three dimensions is considered to be many times more difficult than the simulation of ground-water flow. This is because transport modeling is much more vulnerable to numerical errors such as numerical dispersion and artificial oscillation (Zheng, 1990). MT3D uses a mixed Eulerian-Lagrangian approach in solving the three-dimensional, advective-dispersive-reactive equation. This approach can eliminate the numerical errors mentioned previously. MT3D can use either the method of characteristics (MOC), the modified method of characteristics (MMOC), or a hybrid of the two methods (HMOC) to solve the transport equation (Zheng, 1990). These solution techniques are required because of the large area being modeled and the size of the model cells. If the model were to solve the transport equation by standard finite-difference techniques, numerical errors would occur making model results suspect or even meaningless.

4.3. Model Domain and Boundary Conditions

The model domain was chosen to achieve as much simplicity as possible. The horizontal area covered by the model includes all of the study area shown previously in Figure 1.2. The model includes only the upper Dakota aquifer and the Kiowa shale aquitard. The effects that other units such as the Upper Cretaceous aquitard have on the flow and transport systems are incorporated into the boundary conditions.

4.3.1. Model Grid and Layers

The model is an 18 row by 24 column grid corresponding to the legal sections of Ellis County, thus each model cell is 2.6 km^2 (1 mi^2) in area with 432 cells per model layer. The model was divided into 6 layers for the ground-water flow modeling and then a seventh layer was added for the transport modeling. Reasons for this are discussed in the following sections. The six model layers represent the upper Dakota aquifer and result from dividing each of the three zones of the Dakota Formation into

two layers (Figure 4.3). Therefore, model layers 1 and 2 are equivalent to Zone 1. This was done to provide more vertical discretization of the aquifer. It also serves to dampen the influence that the lower and upper boundary conditions have upon the interior of the model. The seventh layer, added later, represents the Kiowa shale aquitard.

4.3.2. Boundary Conditions for the Flow Model

The model domain is rectangular requiring boundary conditions on all six sides. The upper boundary was considered to be leaky and allows recharge to move downward across the Upper Cretaceous aquitard into the upper part of the Dakota aquifer. The general head boundary package available in MODFLOW was used to simulate this boundary. Two terms are required by the package (McDonald and Harbaugh, 1988). The first is a conductance term, and the second is the elevation of the boundary head located outside the aquifer. In this case the boundary head is the elevation of the water-table. It is assumed that the water-table elevation remains relatively constant and is not affected by minor changes within the upper Dakota aquifer at the scale of this model. The conductance term is a lumped parameter required by MODFLOW defined by the equation,

$$C = K\,A/L \qquad \text{eq. 4.4,}$$

where C [L^2/T] is the conductance term; K [L/T] is the hydraulic conductivity of the material outside the model domain; A [L^2] is the area through which the conductance term passes; and L [L] is the length over which the conductance term is applied (McDonald and Harbaugh, 1988). For this modeling project K is the vertical hydraulic conductivity of the Upper Cretaceous aquitard; A is the area of the model cell (2.6 km^2 or 1 mi^2); and L is the thickness of the Upper Cretaceous aquitard (Figure 4.4).

For the initial flow simulation, the lower boundary was designated no-flow. This is consistent with the assumption that the head in the Kiowa Formation and the underlying units is nearly equivalent to the head in the upper Dakota aquifer. If the

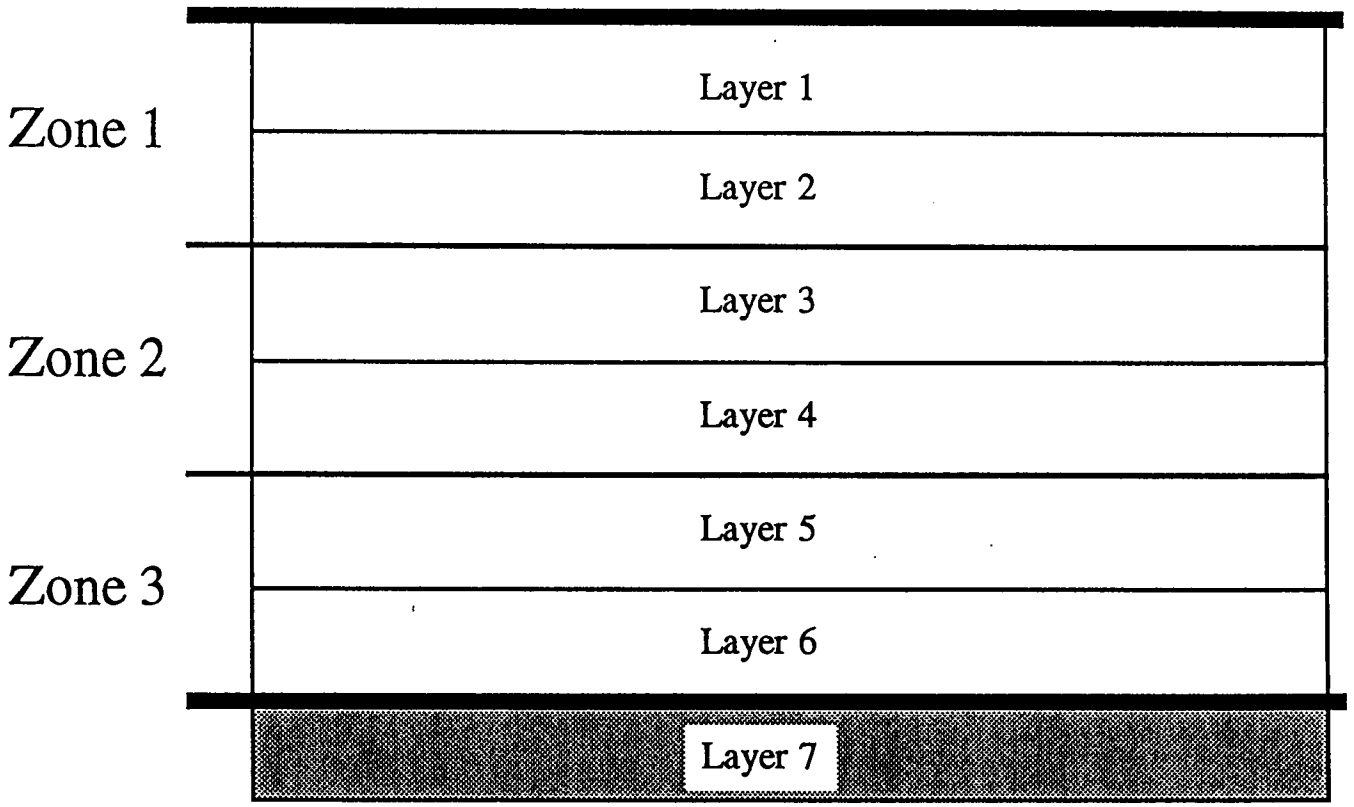

Figure 4.3: Illustration of the seven model layers. Layers 1 through 6 are in the Upper Dakota aquifer while Layer 7 represents the Kiowa Shale aquitard. Only Layers 1 through 6 were used in the original flow model. Layer 7 was added later for the transport model. It serves as a reservoir for chloride to diffuse up into the aquifer.

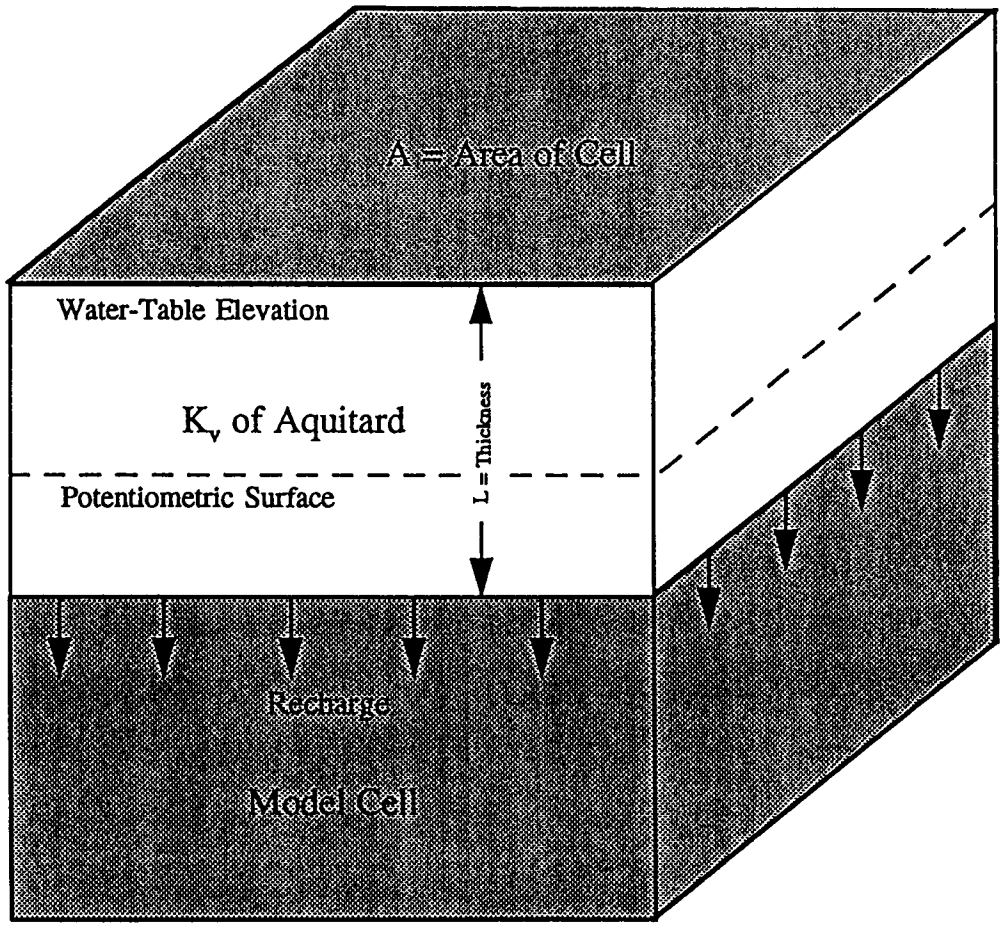

Figure 4.4 Illustration of leaky aquifer boundary. Parameters driving the conductivity term are L, A, and K_v. The other term needed by MODFLOW is the boundary head outside the model. In this case it equals the water-table elevation. The difference in head between the potentiometric surface of the aquifer and the water-table elevation in the aquitard drives recharge into the model domain.

heads are nearly equivalent, then there should be no significant flow across this aquitard, thus justifying the no-flow boundary. However, during the transport simulations the lower boundary was changed to specified head, equaling the calibrated heads from the initial flow simulations. A seventh layer representing the Kiowa shale aquitard was added and contained the specified-head boundary (Figure 4.5). Reasons for the addition of this seventh layer and the change in boundary type will be explained in Section 4.3.3.

Within the upper Dakota aquifer there are no natural hydrogeologic boundaries in the study area such as a lake or a ground-water divide. As was mentioned previously, this portion of the upper Dakota aquifer is actually part of a very large regional flow system. If one were to define physical or hydrologic boundary conditions, the recharge area in southeastern Colorado would have to be included in the model region. This is not practical since the purpose of this study is to investigate the confined Dakota aquifer on a much smaller scale. Therefore, the boundary conditions on the four lateral sides must be specified in order to allow lateral flow of water into and out of the model domain and maintain the head in the aquifer. Defining the sides of the model as specified-head boundaries satisfies these conditions providing there are no outside stresses placed on the boundaries. For instance, if wells withdrew water near the edges of the model, the specified-head boundaries would tend to overestimate the amount of water flowing into the model.

An assumption that the head within the aquifer is known around the edges of the model must therefore be made. The head around the edges of the aquifer was defined from a map of the potentiometric surface in the study area. This map was constructed from head measurements taken from wells screened in the upper Dakota aquifer. The potentiometric surface in the area is discussed in more detail in Section 4.3.1. By specifying the head around the edges of the model, the flexibility of the model to adjust the head in the aquifer is limited. However, this is a trade off that must be made in order to model at this scale.

a) Plan View for Simulations C1, C2, and C3

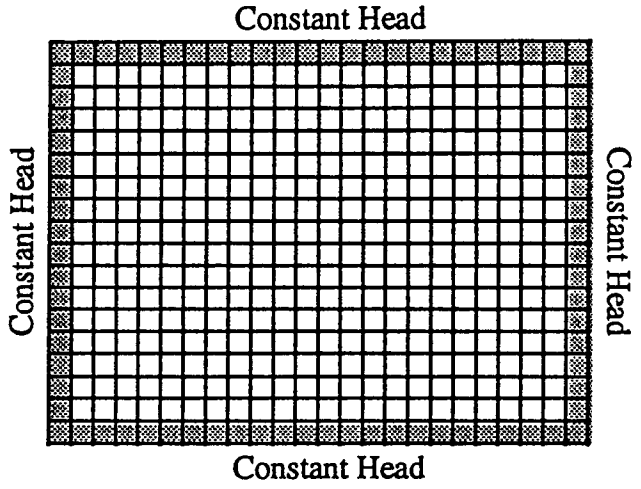

b) X-Section View for Simulation C1

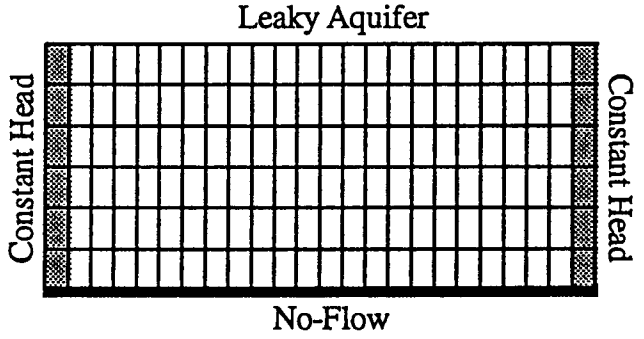

c) X-Section View for Simulations C2 and C3

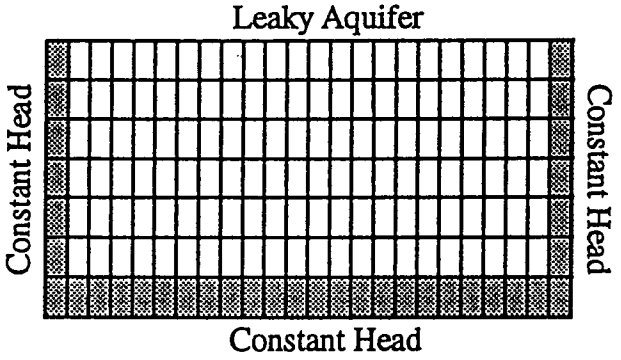

Figure 4.5: Boundary conditions for MODFLOW a)plan view of model grid with shaded cells indicating constant head cells, b) cross-section of boundary conditions for six layer model, c) cross-section of boundary conditions for seven layer model.

4.3.3. Boundary Conditions for the Transport Model

MT3D makes two boundary conditions available for the mass boundary conditions (Zheng, 1990). The first is a constant-concentration boundary condition. This boundary condition is similar to a constant-head boundary condition in that the concentration specified will not change during the simulation. It acts as a continuous source and never decreases or increases in concentration. The second boundary condition is a specified-mass-flux boundary. As water moves into the model due to the pre-determined flow field, the concentration of the water flowing into the model must be specified. This boundary condition can exist at specified-head, leaky-aquifer, and specified-flux boundaries. The specified-mass-flux boundary condition is used for the top and the four sides of the model domain.

In the previous section it was mentioned that a seventh layer was added for the transport modeling. This was done because, although the lower aquitard has no significant influence in the flow modeling, it is likely to have a large influence on the transport modeling. It is hypothesized that diffusion from the Permian contributes to the salinity of the aquifer (Whittemore and Fabryka-Martin, 1992). With MT3D the only way to incorporate diffusion is to include the source as a physical part of the model. Therefore, the Kiowa shale aquitard is added as a seventh layer, serving as a reservoir for the salinity to diffuse up into the aquifer. As a simplifying assumption, the boundary condition specified within the aquitard is a constant-concentration boundary. This assumes that the Kiowa shale acts as a constant source of salinity remaining constant in concentration over time. Figure 4.6 summarizes the mass-transport boundary conditions.

4.4. Model Input Data

Input data for the modeling are divided into four types: 1) geologic framework, 2) water-level data, 3) solute-concentration data, and 4) hydrologic properties. The geologic framework includes the spatial arrangement of layers in the

a) Plan View for Simulations C2 and C3

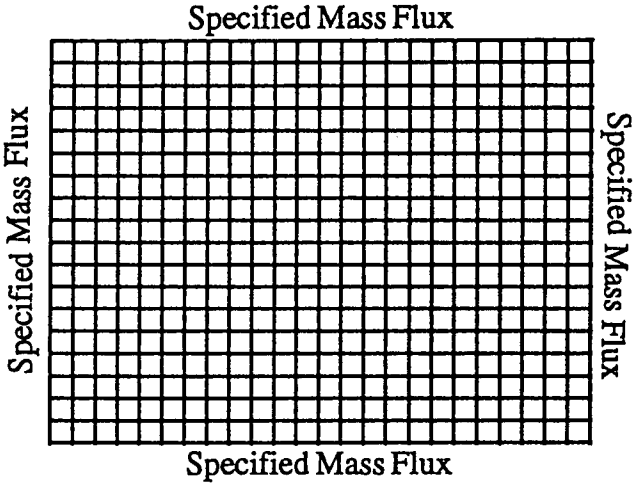

b) X-Section View for Simulations C2 and C3

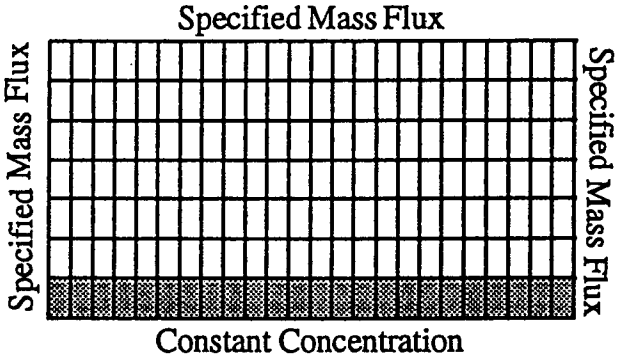

Figure 4.6: Boundary conditions for MT3D a) Plan view of model grid. All exterior cells have their inflow concentration specified. b) Cross-section of model grid. Bottom cells are constant concentration while all other exterior cells have their inflow concentration specified.

subsurface. These data came from analysis of the gamma-ray logs discussed previously in Chapter 3. The data obtained included the thickness of the Upper Cretaceous aquitard, the upper Dakota aquifer and its zones, and the Kiowa shale aquitard. Also required by the model is the elevation of the land surface and the top of the Dakota Formation. The thickness of aquifer subunits determined for each zone will be used in constructing the hydraulic conductivity field of the upper Dakota aquifer. The method used to determine the heterogeneity of the aquifer will be discussed in Section 4.4.3a on hydraulic conductivities. The different data types and sources are discussed in the following sections.

4.4.1. Water-Level Data

The elevation of the water-table and the potentiometric surfaces of the upper Dakota aquifer and units below the upper Dakota aquifer are required as input for the flow model. However, water-level data are fairly sparse in the region of interest. Only data for the upper Dakota aquifer exist. Data are virtually non-existent for the water-table, thus some assumptions were made. The first assumption is that the water-table elevation is equal to the elevation of the land surface. For the scale of interest this is probably an adequate representation of the water-table because the top of the saturated zone is likely to be a subdued reflection of the land surface (Domenico and Schwartz, 1990). The actual configuration of the water-table is lacking in this area because shallow aquifers are present only in the Smoky Hill River and Big Creek valleys.

The regional potentiometric surface of the Dakota aquifer was shown previously in Figure 2.7. Data for this map came from water supply wells and observation wells screened in the upper Dakota aquifer (Macfarlane *et al.*, 1990). To better represent the potentiometric surface of the upper Dakota aquifer in the study area, a subset of the data points within the region of interest was selected. These data points were then hand-contoured at a 6 m (20 ft) contour interval giving a more

detailed look at the potentiometric surface in this area (Figure 4.7). It is assumed that there is no significant vertical flow in the upper Dakota aquifer. Therefore, the head at the top of the upper Dakota aquifer must be approximately equal to the head at the bottom of the aquifer (Macfarlane, 1993). It is also assumed that the head in the units below the upper Dakota aquifer is equal to the head in the upper Dakota aquifer (Macfarlane, 1993).

4.4.2. Water Quality Data

A three-dimensional concentration distribution in the aquifer is required as input into the model. However, little is known about this distribution. From data presented in Chapter 2, the high degree of variability in the chloride concentrations throughout the aquifer were observed (Figure 2.9). The distribution of salinity in the study area was shown previously in Figure 2.10, but this is a highly generalized map. Furthermore, this map only shows the horizontal distribution of TDS and its lowest concentration regardless of depth in the Dakota. Ultimately, assumptions need to be made. The first assumption is that the concentration of chloride increases with depth. Although this is not always the case, the trend of increased salinity with depth exists (Figure 2.12 and Figures 2.13a through 2.13g). Therefore, the salinity map shown in Figure 2.10 is assumed to be representative of the salinity in the upper portion of the upper Dakota aquifer. The problem now becomes one of describing the change in salinity with depth.

Figures 2.12 and 2.13a through 2.13g showed depth profiles of either chloride or TDS concentrations in Ellis and nearby Russell Counties. From these graphs several generalizations can be made. First, they show that the concentration of TDS is relatively constant with increasing depth down to a certain point and then increases abruptly near the bottom of the aquifer. Concentration levels vary beneath the Dakota Formation. The TDS beneath the aquifer is probably around 2,000 mg/L in the western half of the study area and around 35,000 mg/L in the eastern half. This is due

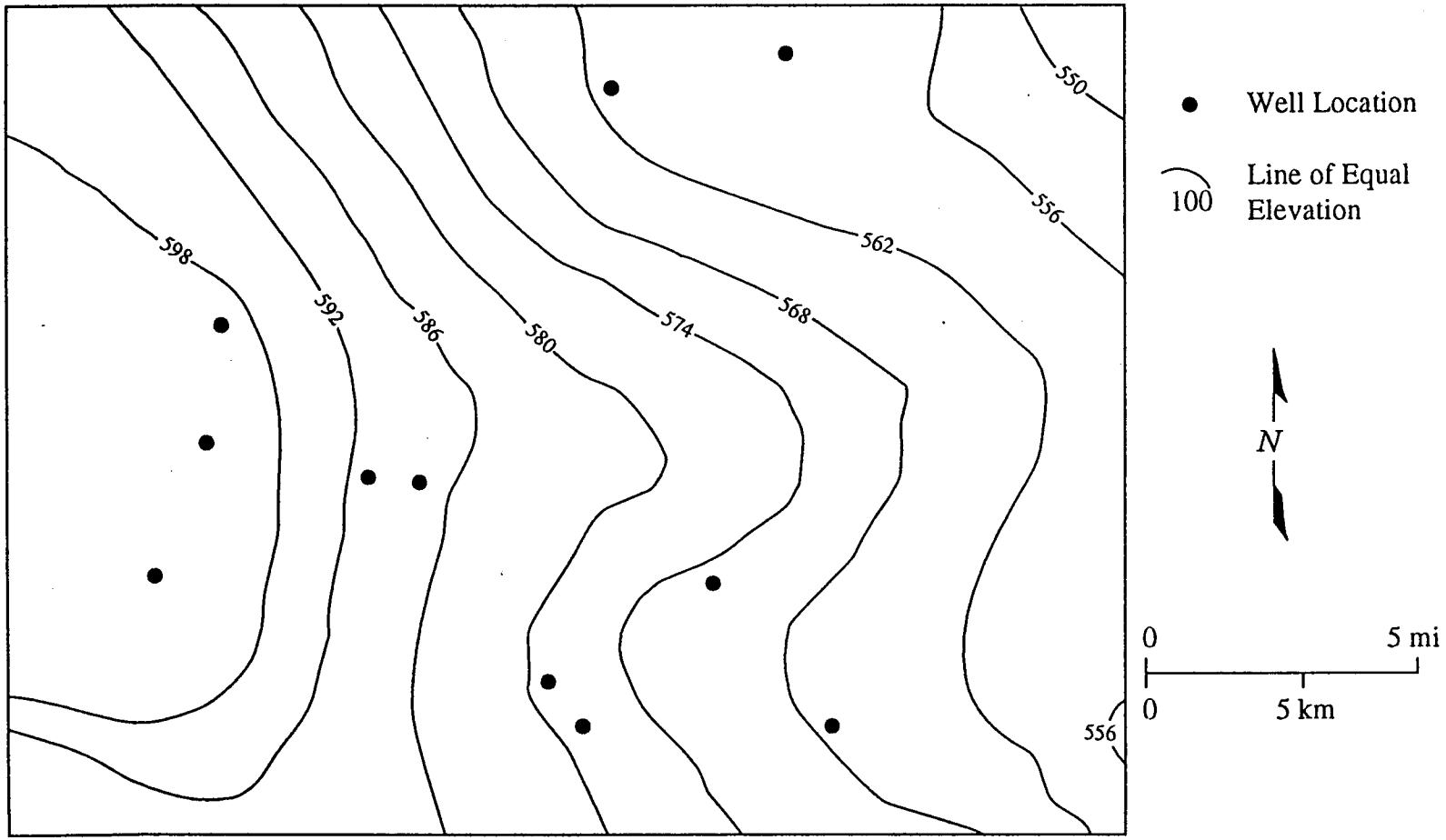

Figure 4.7: Pre-development potentiometric surface of the upper Dakota aquifer in the study area. Contour interval is 6 m (20 ft). Data points within the study area are shown. There were points located outside the study area (not shown) that were used to better define the surface in the study area.

to the pinchout of the Upper Permian aquitard separating the Dakota from the Cedar Hills Sandstone in the study area. It is assumed that TDS concentrations in the lower portion of the upper Dakota aquifer range from about 2,000 to 30,000 mg/L. Furthermore, the concentration distribution in the lower portion of the aquifer mimics the distribution observed in the upper portion of the aquifer. Finally, it is assumed that TDS concentrations increase with depth, gradually in the upper and middle portions of the aquifer and then at a much greater rate towards the bottom.

MT3D is capable of simulating only a single constituent. Since the ground water is primarily a sodium chloride type, chloride is used as the constituent of interest. The use of chloride also simplifies the mass-transport equation by neglecting the reactive term. This can be done because chloride is generally considered a conservative tracer. Therefore, a method for determining chloride concentration from TDS is needed. An empirical relationship relating TDS to chloride concentration has been developed for the Dakota aquifer (Whittemore, personal communication, 1994). Figure 4.8 shows a best fit line through field data. This line consists of two equations,

$$Cl^- = 0.382\ TDS - 163 \quad [TDS \geq 1350\ mg/L] \quad \text{eq. 4.5a,}$$

$$Cl^- = 0.544\ TDS - 381 \quad [TDS < 1350\ mg/L] \quad \text{eq. 4.5b.}$$

These equations were used to convert the TDS map and the other TDS concentrations into chloride concentrations.

4.4.3. Hydrogeologic Properties

Each modeling program requires different types of hydrogeologic properties. MODFLOW requires hydraulic conductivities in both the horizontal and vertical directions. Storativities are required to run transient simulations. MT3D indirectly uses the storativity and hydraulic conductivity of the aquifer and aquitard units. The transport properties required by MT3D include porosity, diffusion parameters, and dispersion coefficients. Parameter estimates for this project vary in origin from those

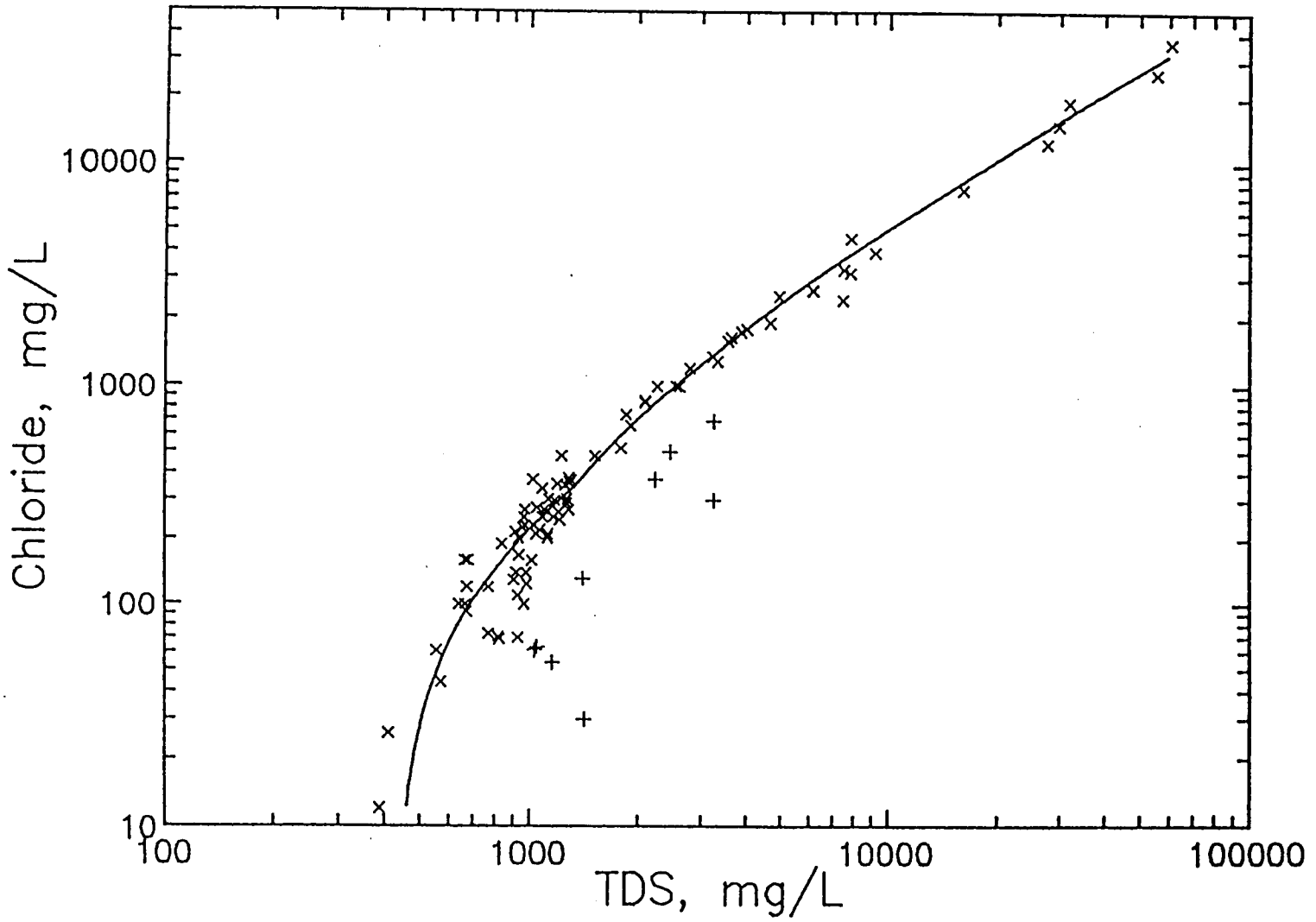

Figure 4.8: Plot of chloride concentration versus total dissolved solids concentration.

reported in the literature to those based on field data. The following sections discuss the sources of the data and the reasons for choosing the values.

4.4.3a. Hydraulic Conductivities

Hydraulic conductivity data are needed for the Upper Cretaceous aquitard, the upper Dakota aquifer, and the Kiowa shale aquitard. However, only the vertical hydraulic conductivity of the aquitards is needed because their effects are simulated in the boundary conditions. Data for the two aquitards are minimal with the best values for the parameters coming from other modeling studies. Macfarlane (1993) used values ranging from 10^{-5} to 10^{-8} m/day (10^{-4} to 10^{-7} ft/day) for the Upper Cretaceous aquitard and found a value of 10^{-7} m/day (10^{-6} ft/day) adequate for the Kiowa shale aquitard. Values similar to these were used in this modeling study.

Past modeling studies have considered the upper Dakota aquifer to be fairly homogeneous often lumping it into one model layer. However, because one of the goals of this thesis was to incorporate heterogeneity into the modeling of the aquifer, a distribution of parameters is considered. Core permeameter tests indicate that the sandstones in the Dakota Formation have hydraulic conductivities on the order of a meter (a few feet) per day to tens of meters (hundreds of feet) per day while the mudstones are most likely less than 10^{-5} m (10^{-4} ft) per day (Macfarlane *et al.*, 1994). Permeameter tests also indicated that conductivities of Dakota sandstones vary somewhat with depositional environment (Macfarlane *et al.*, 1994). There is a tendency for alluvial sandstones to have higher average conductivities than marine and shoreface sandstones (Macfarlane *et al.*, 1994).

Pumping and slug test data indicate that hydraulic conductivities of the Dakota sandstones are about equal to the average values observed from the lab permeameter test cores (Macfarlane *et al.*, 1994). All these data were considered when assigning conductivities to model layers. The sandstone data are considered to be representative of the aquifer subunits and the mudstone data are considered to be representative of

aquitard subunits of the upper Dakota aquifer. The conductivities assigned to the model grid will not only vary by layer but also within each layer, thus incorporating heterogeneity into the model. Conductivities were based on the thickness of the aquifer subunits previously determined for the three zones of the Dakota Formation. This will be discussed further in Section 5.2.2.

4.4.3b. Storativities

Storativities are required for transient simulations. Data for this parameter come from pumping test results. Macfarlane (personal communication, 1994) found storativities to vary from between 10^{-3} to 10^{-5} from pumping tests in the upper Dakota aquifer in the study region. These values represent the aquifer subunits of the upper Dakota aquifer since pumping wells primarily extract water from the high hydraulic conductivity material during the aquifer tests. The aquitard subunits probably have slightly higher values than the aquifer subunits since they are primarily composed of mudstone (Freeze and Cherry, 1979) and likely range from 10^{-2} to 10^{-4}.

4.4.3c. Transport Properties

Transport properties required by MT3D include effective porosities, dispersivities, and diffusion coefficients. Porosity in the Dakota sandstones ranges from 20% to 30% (Macfarlane, personal communication, 1994), but good field data for the other parameters do not exist. Common values cited in the literature were used for lack of a better source. A value between 5% to 10% will be used for the effective porosity of the mudstones (Domenico and Schwartz, 1990). Dispersion is both a mechanical and a chemical process (Freeze and Cherry, 1979). Mechanical dispersion results from the deviation of the velocity at the microscopic scale from the average velocity field used in the modeling. In reality the velocity field is highly variable, following a tortuous path between sand grains and flowing through rock of variable

hydraulic conductivity on the smallest of scales. This results in the spreading and mixing of water as it flows through the porous medium.

Dispersion is dependent upon direction and has six components. MT3D calculates these six components from the longitudinal, horizontal transverse, and vertical transverse dispersivities supplied by the user (Zheng, 1990). Values from the literature are used for the three dispersivities. For the scale of this model values for the longitudinal dispersivities ranging from a few tens of meters to a few hundred meters could be appropriate (Domenico and Schwartz, 1990). The transverse dispersivities in the horizontal and vertical directions are assumed to be on the order of 10^0 meters and 10^{-1} meters respectively.

Diffusion or chemical diffusion refers to the driving force moving a constituent from regions of higher concentration to regions of lower concentration. Diffusion of chloride is given as 20.3×10^{-6} cm^2/sec or 1.75×10^{-4} m^2/day (Domenico and Schwartz, 1990). This value is for chloride in water, but in an aquifer the matrix lowers the diffusion coefficient. For this reason an effective diffusion coefficient is defined based on the porosity and the tortuousity of the porous medium. This tends to lower the diffusion coefficient by about an order of magnitude resulting in a value of 1.75×10^{-5} m^2/day (Domenico and Schwartz, 1990).

CHAPTER 5. MODEL CALIBRATION AND RESULTS

5.1. Introduction

The partial calibration of the flow and transport models is discussed in this chapter. As mentioned in Chapter 1, the numerical modeling was divided into three parts. The first part resulted in a partially calibrated, steady-state flow field. The second part simulated the flushing of salinity from the aquifer and the processes that produced the present salinity distribution. The final part looked at the possible effect water-resources development could have on the long-range sustainability of the aquifer's water quality. The steady-state flow and transient, mass-transport model calibration and results are discussed in this chapter, while the third phase of the modeling study is discussed separately in Chapter 7. For reasons discussed in the following sections, there were several partially calibrated models developed. Table 5.1 summarizes these different model simulations.

5.2. Calibration of the Steady-State Flow Field

Using MODFLOW, a steady-state flow field for the upper Dakota aquifer was calculated. Results provided flux rates from which a flow budget was determined, as well as a hydraulic conductivity field for the aquifer. Aquifer heterogeneity was the primary focus in the calibration of the flow model. Assumptions on the interconnection of aquifer subunits played a large role in the definition of aquifer heterogeneity. Two flow models were ultimately developed each representing end-members of the hydraulic conductivity in the upper Dakota aquifer. Reasons for this will be presented in the discussion on flow model calibration and then further in the sections on mass-transport modeling. The development and partial calibration of a steady-state flow field is discussed in the following two sections. This corresponds to simulation C1 in Table 5.1.

Simulation Number	Models Used	Simulation Purpose	Methods Used
C1	MODFLOW	Establish a calibrated steady-state flow field with a regional K_h of 1 m/day.	Various flow parameters were adjusted including an arbitrary thickness threshold until an RMS error below 6 m (20 ft) was achieved.
C2	MODFLOW & MT3D	Evaluate the steady-state flow field during mass-transport.	Recalibrated flow model based on transport simulations by reducing K_v of Upper Cretaceous aquitard until a concentration gradient developed throughout the model.
		Evaluate transport in a well-connected aquifer with a high regional K_h.	Used a high regional hydraulic conductivity of about 1 m/day. This is representative of the interconnected aquifer subunits.
C3	MODFLOW & MT3D	Evaluate transport in a poorly-connected aquifer with a low regional K_h.	Reduced all hydraulic conductivities by three orders of magnitude resulting in a low regional hydraulic conductivity of about 1×10^{-3} m/day. This is representative of the aquitard subunits of the Dakota Formation.

Table 5.1: Summary of partially calibrated model runs for both MODFLOW and MT3D.

5.2.1. Methodology

The ground-water flow field in the upper Dakota aquifer was considered to be at steady-state before development of the aquifer began (Macfarlane, 1993). The flow model was calibrated by matching as close as possible simulated heads to the observed heads, generally considered to be from pre-development times. The root mean square (RMS) error was used to access the progress of the calibration. Heads from the model output were interpolated back to the coordinates of the observed values, and then compared using the following equation for RMS error,

$$\text{RMS error} = [\ 1/n \ \sum_{i=1}^{n} \ (h_m - h_s)_i^2\ ]^{0.5} \qquad \text{eq. 5.1,}$$

where h_m is the measured head; h_s is the simulated head; and n is the number of calibration values (Anderson and Woessner, 1992). An RMS error value less than 6 m (20 ft) was considered adequate because of errors in the head and elevation data.

Parameters used in the partial calibration of the flow field included the vertical hydraulic conductivity (K_v) of the Upper Cretaceous aquitard and the hydraulic conductivity of the upper Dakota aquifer. Macfarlane (1993) demonstrated that the head in the confined Dakota aquifer is most sensitive to the K_v of the Upper Cretaceous aquitard. The head is secondarily sensitive to the hydraulic conductivity of the upper Dakota aquifer. Therefore, model calibration began by adjusting the K_v of the Upper Cretaceous aquitard until a low in the RMS error was observed assuming a uniform K_v.

The hydraulic conductivity of the upper Dakota aquifer was adjusted next. In calibrating the hydraulic conductivity of the aquifer, three separate parameters were available for adjustment (McDonald and Harbaugh, 1988). The horizontal and vertical hydraulic conductivity of the aquifer along with an anisotropy ratio of the horizontal hydraulic conductivity were used. The anisotropy ratio is equal to the hydraulic conductivity parallel to the rows divided the hydraulic conductivity parallel to the columns in the model grid. One value is supplied for each model layer.

Since it was the purpose of this thesis to investigate heterogeneity of the aquifer all three parameters were used. First the horizontal hydraulic conductivity (K_h) of the aquifer was adjusted. Then the K_v of the aquifer and the anisotropy ratio were used. In practice all three parameters including the K_v of the Upper Cretaceous aquitard were adjusted in combination until a low in RMS error was achieved. As a result of adjusting these parameters, one possible combination of parameter values representing the heterogeneity between layers and the anisotropy within layers were determined. The distribution of heterogeneity within each model layer was also investigated. It was based upon the thickness of aquifer subunits interpolated to the model grid using the block kriging, and it is the topic of the next section.

5.2.2. Horizontal Heterogeneity in the Aquifer

In Chapter 3 the distribution of aquifer subunit thicknesses in the upper Dakota aquifer was described. The aquifer was divided into three zones and the total thickness of the aquifer subunits within each zone was recorded. Then, through the use of block kriging, an average areal total thickness of the aquifer subunits was assigned to each model cell. The distribution of total thickness values was used to guide the assignment of hydraulic conductivities to model layers. An equivalent hydraulic conductivity using the thickness of the aquifer subunits can be calculated using following equation (Domenico and Schwartz, 1990),

$$K_{x(eq)} = \Sigma (m_i K_{xi}) / \Sigma m_i \qquad \text{eq. 5.2,}$$

where $K_{x(eq)}$ is the equivalent horizontal hydraulic conductivity; K_{xi} is the homogeneous hydraulic conductivity of a unit; and m_i is the thickness of the unit. In this case a bimodal distribution of homogeneous hydraulic conductivities would exist, one representing the aquifer subunits and the other representing the aquitard subunits. Due to the large differences in conductivities between the aquifer and aquitard subunits, the conductivity of the aquifer subunits dominates $K_{x(eq)}$. If equation 5.2 is used, most of the equivalent hydraulic conductivities would range within a few factors of the chosen

hydraulic conductivity for the aquifer subunits. Given that the error involved in choosing a particular hydraulic conductivity is greater than the range of values that would result from this equation, it was not the method of choice.

Another approach is necessary in order to make use of these data. It is hypothesized that the interconnection of aquifer subunits controls the movement of fluid through the aquifer. Regions of relatively high connection are more transmissive than regions of relatively low connection (Van De Graaff and Ealey, 1989; Figure 5.1). A thickness threshold is assumed to exist dividing regions where aquifer subunits are well connected from regions where they are relatively isolated and the aquitard subunits dominate the regional hydraulic conductivity. Model cells with an average aquifer subunit thickness above this threshold are designated relatively high transmissive regions. Model cells below this threshold are designated relatively low transmissive regions. Therefore, the average aquifer subunits thickness distribution was used to define high and low transmissive regions within the model layers.

An arbitrary value is selected to discriminate between the high and low transmissive regions. This value then becomes another parameter for calibration. Since it is known from other modeling studies that the Dakota has a regional hydraulic conductivity of about 1 m/day (Belitz, 1985; Macfarlane, 1993; Helgeson *et al.*, 1993), it was assumed that the high transmissive regions are close to this value. It would be appropriate to assume a slightly higher value, since the low transmissive regions will tend to lower the overall regional hydraulic conductivity of the aquifer. Although the actual interconnection of aquifer subunits is unknown, it is hypothesized that if there is to be a significant amount of regional flow then there must be a network of interconnected aquifer subunits extending from southeast Colorado to central Kansas.

It is more difficult to say what the low transmissive regions should be. It would likely depend upon the degree of aquifer subunit isolation, i.e. partial or total isolation of the aquifer subunits. If the aquifer subunits are entirely isolated, the regional hydraulic conductivity could be as low as 10^{-5} m/day (10^{-4} ft/day), the

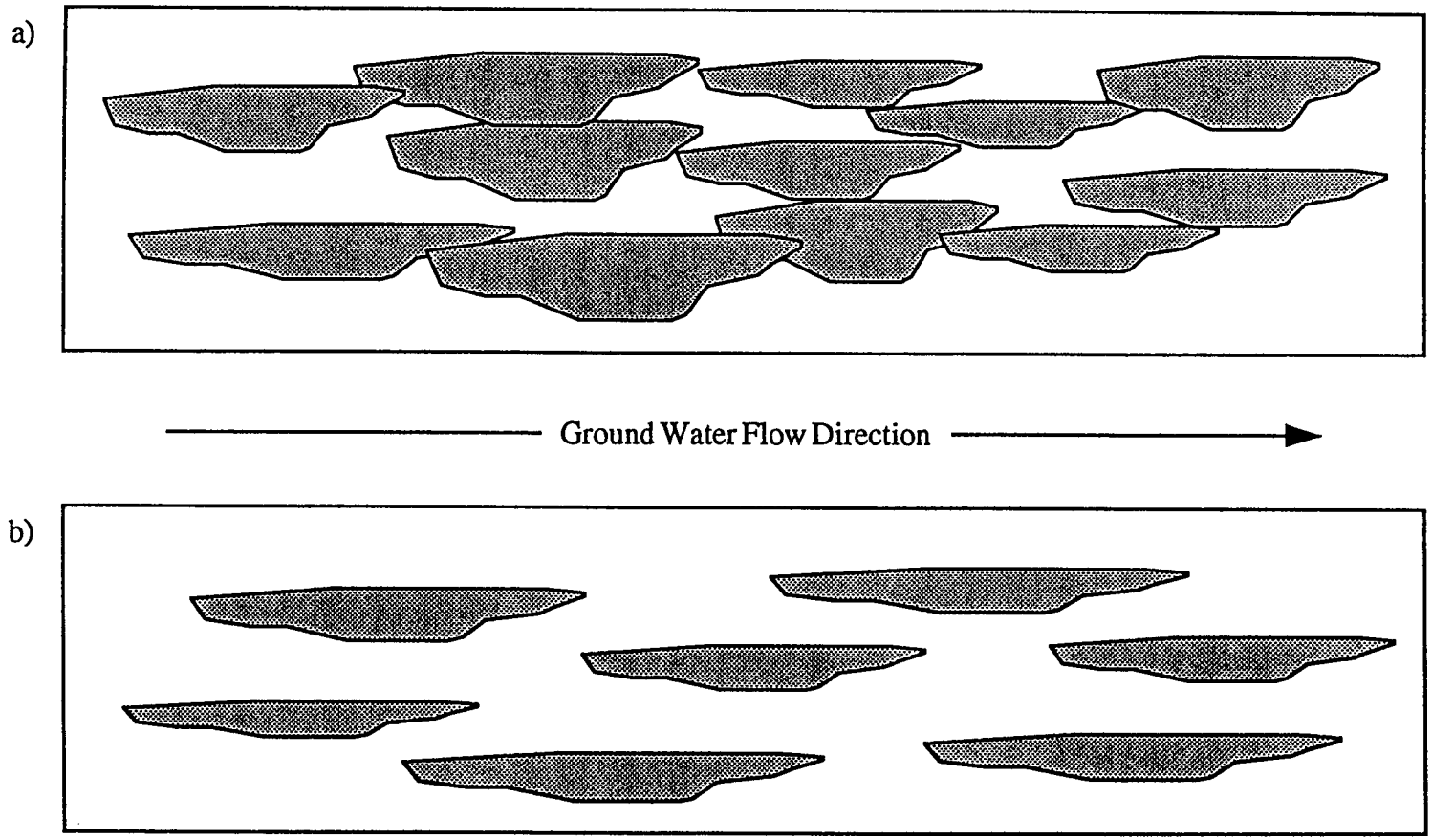

Figure 5.1: Illustration of aquifer subunit connection in the Dakota and its effect on the regional hydraulic conductivity of the aquifer, a) high connection would result in greater transmissivity since the aquifer subunits would dominate the horizontal hydraulic conductivity, b) isolated aquifer subunits would result in lower transmissivity since the aquitard subunits would dominate the horizontal hydraulic conductivity.

hydraulic conductivity of the mudstone. This is due to the fact that the mudstone would control the hydraulic conductivity in these regions. However, if they are only partially isolated, it would be expected that the effective hydraulic conductivity would be between that of the high transmissive regions and the assumed low of 10^{-5} m/day (Figure 5.2). This was tested for during model calibration. Results of the partially calibrated flow model are discussed in Section 5.4.1.

Fogg (1989) investigated the interconnection of alluvial and deltaic sand-bodies in the Wilcox Group of eastern Texas using stochastic methods. His results indicated several important points significant in understanding the likelihood of sand-body interconnection. First, the probability that sand-bodies or aquifer subunits will be interconnected increases with increasing sand fraction. Furthermore, a threshold value seems to exist beyond which there is a high degree of interconnection. Finally, the threshold value necessary for a high probability of interconnection decreases with an increasing value in the range of the semivariogram produced from the data set. He found that for a range of 21,000 ft (6.4 km) a sand fraction greater than 0.2 was necessary to provide for a high probability of sand-body interconnection.

Allen (1978) investigated the interconnection of alluvial sand-bodies in a two-dimensional cross-section perpendicular to a hypothetical alluvial valley, along the depositional strike. He found that as the sandstone content dropped below about 50% sand-body interconnection decreased rapidly. The depositional strike during the Cretaceous was for the most part in a north-south direction in the study area. From the gamma-ray logs it is known that the percentage of the total thickness taken up by the aquifer subunits in Zones 2 and 3 are 21% and 42%, respectively. It is therefore likely that the interconnection of aquifer subunits in the north-south direction is low. This will be important in the discussion on horizontal anisotropy in the following sections.

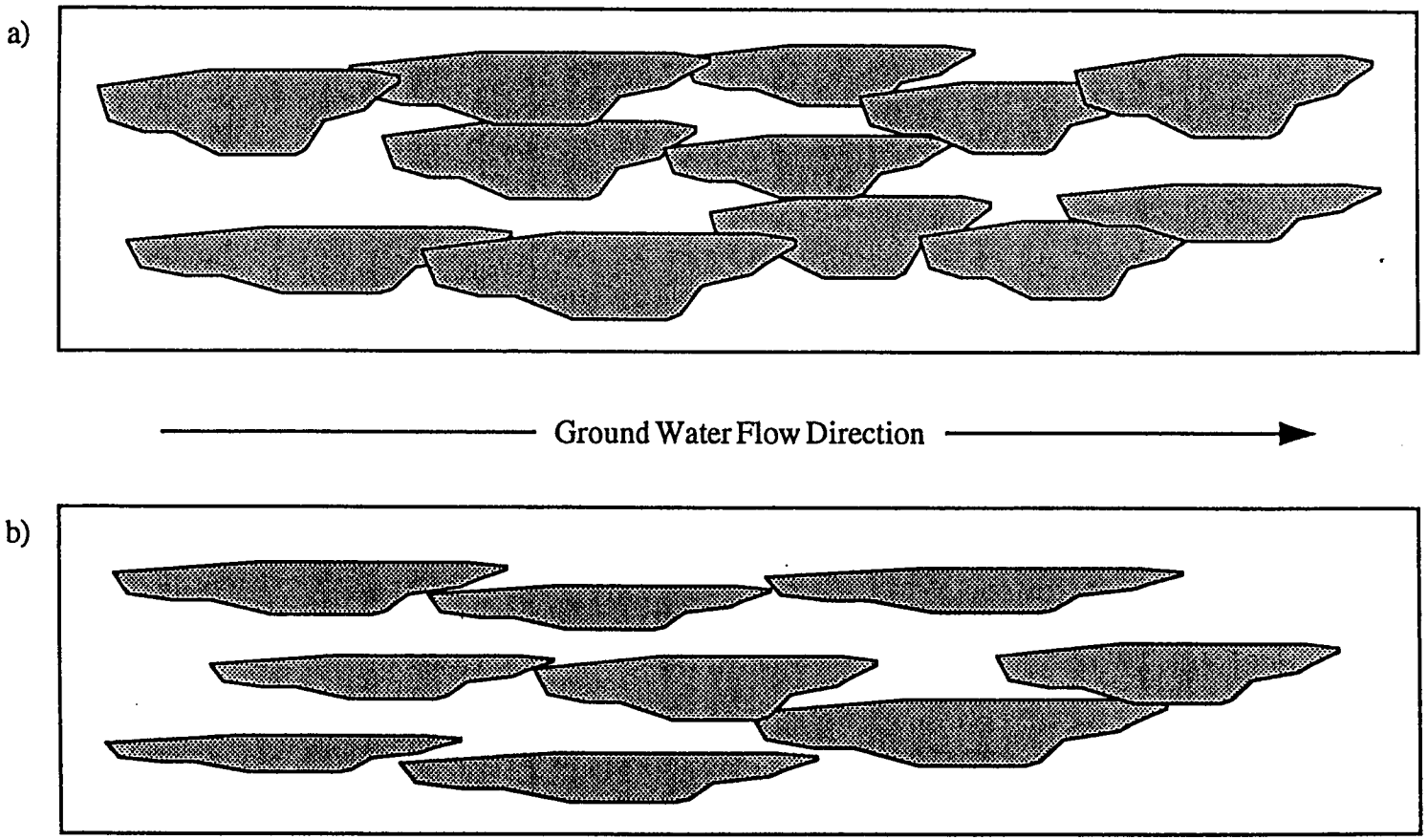

Figure 5.2: Illustration of the degree of aquifer subunit connection in the Dakota and its effect on its regional hydraulic conductivity, a) a high degree of connection would result in high transmissivity, b) partially isolated aquifer subunits would result in a lower transmissivity than the scenario shown in figure a but would have a higher transmissivity than entirely isolated aquifer subunits.

5.2.3. Alternate Hydraulic Conductivity Fields

During model calibration, a hydraulic conductivity field was developed (Simulation C1 in Table 5.1). However, because there were at least five parameters used in the calibration, it can only be considered a near-optimal, hydraulic conductivity field. It is more than likely that other hydraulic conductivity fields would give similar results with entirely different values for the calibration parameters. The sensitivity analysis in Chapter 6 will demonstrate this. It can only be said that the final hydraulic conductivity field is consistent with other regional modeling studies since an overall, regional hydraulic conductivity of around 1 m/day was used (Belitz, 1985; Macfarlane, 1993; Helgeson *et al.*, 1993). Furthermore, because the only information used to calibrate the flow model involved head matching, flux rates were ignored. It is possible to achieve the exact same head distribution as was produced with the original hydraulic conductivity field by reducing all hydraulic conductivity parameters in the model by an equal factor. Therefore, there could actually be an endless number of hydraulic conductivity fields established with identical results.

To demonstrate this non-uniqueness, all hydraulic conductivities were reduced by three orders of magnitude. The resulting distribution of heads was identical to the distribution produced by the original hydraulic conductivity field. The only difference in the results between the two hydraulic conductivity fields was that the flux rate through the model was also reduced by three orders of magnitude. Since a particular flux rate cannot be targeted for the aquifer, there is no way to know which hydraulic conductivity field is correct. It can only be stated that the hydraulic conductivity field from simulation C1 (Table 5.1) is in agreement with other modeling projects on the Dakota aquifer system (Belitz, 1985; Macfarlane, 1993; Helgeson *et al.*, 1993).

5.3. Conservative Transport Modeling

As a result of the flow simulations conducted using MODFLOW a near-optimal hydraulic conductivity field for the upper Dakota aquifer and a vertical

hydraulic conductivity for the Upper Cretaceous aquitard were developed. An additional seventh layer representing the Kiowa shale aquitard was then added for reasons discussed previously. This layer was designated a specified-head and mass boundary with the assigned head equaling the final head in the aquifer after running the steady-state model with the lower boundary designated no-flow. The resulting head and flux data were then used as input into MT3D. Upon modeling the mass transport, it was discovered that information obtained from the transport model helped to better calibrate the flow model. This was because the transport model provided additional information on aquifer dynamics. This new model configuration was designated Simulation C2 (Table 5.1).

During the transport simulations it was decided that two entirely different hydraulic conductivity fields would be used to properly investigate mass transport in the aquifer. The first hydraulic conductivity field was equivalent to the hydraulic conductivity field in Simulation C2 (Table 5.1). The second hydraulic conductivity field was equivalent to that of Simulation C2 except all hydraulic conductivities were reduced by three orders of magnitude. This new model configuration was designated Simulation C3 (Table 5.1). This was done primarily for two reasons. First, Simulation C3 was used to check the assumptions about the interconnection of the aquifer subunits. The greater the connection the greater the regional hydraulic conductivity, therefore Simulation C2 represents a well-connected regional aquifer and Simulation C3 represents a poorly-connected regional aquifer. The second reason was to observe the transport processes separately in the aquifer and aquitard subunits of the upper Dakota aquifer. The regional hydraulic conductivity of Simulation C2 is more representative of the aquifer subunits, while the regional hydraulic conductivity of Simulation C3 is more representative of the aquitard subunits.

5.3.1. Transport Through a Well-Connected Aquifer

In a well-connected regional aquifer, it is assumed that the aquifer subunits of the Dakota Formation are connected and provide regional conduits for ground-water flow. This is consistent with other modeling projects on the Dakota aquifer system. By assigning an average hydraulic conductivity to the model cells, the transport modeling is biased towards representing the interconnected aquifer subunits rather than the aquitard subunits. This is because most of the ground-water flow will occur through the most permeable part of the system. With the bias of the hydraulic conductivity field of Simulation C2 in mind, the transport modeling was conducted using MT3D.

The first goal of the transport modeling was to reproduce the general character of the chloride distribution observed in the study area. Contours of chloride concentration in the study region are shown in Figure 5.3. From these contours a generalized pattern of chloride distribution can be made. A relatively constant chloride concentration exists in the western half of the study area with a steep concentration gradient present in the eastern half coinciding with the subcrop of the Cedar Hills Sandstone beneath the Dakota aquifer system. Vertically, the concentration was assumed to increase with depth as was mentioned in Section 4.4.2. Before beginning the simulations, the initial conditions of chloride concentration throughout the model region were required. An arbitrary starting chloride concentration of 7,000 mg/L was assumed so that the flushing of chloride from the aquifer could be observed. The model was then executed in an attempt to reproduce the major characteristics of the current chloride distribution in the study area.

The results quickly indicated that an imbalance in the input sources existed. The recharge flux rate was too high which had the overwhelming effect of reducing the chloride concentration throughout the model too quickly. More importantly, it was impossible to develop a concentration gradient horizontally across the model. The incoming surface recharge was in effect flushing the aquifer of chloride, since this

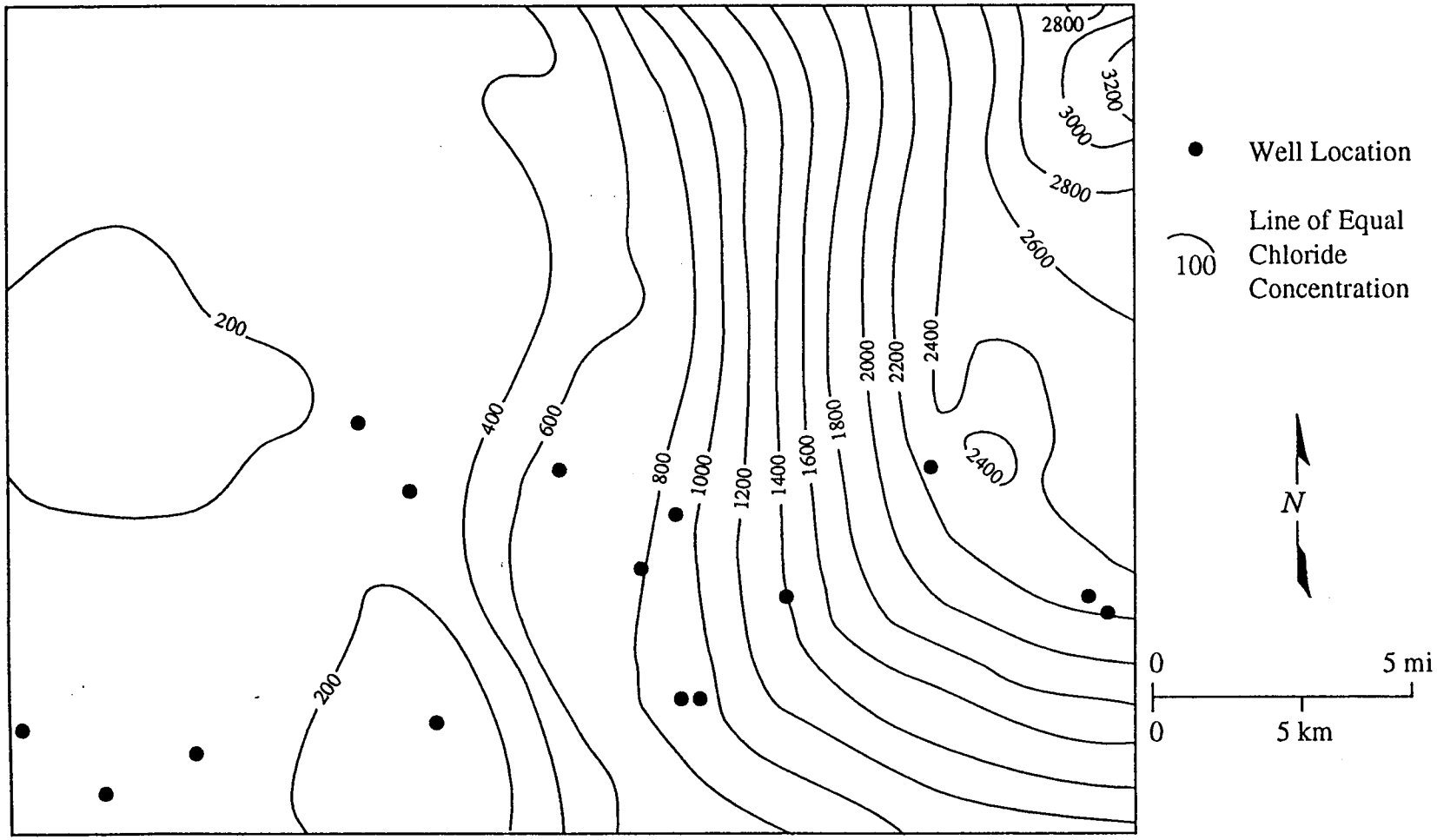

Figure 5.3: Contours chloride concentration in mg/L in the study area. There is a strong concentration gradient in the eastern half of the region. This map was produced from data supplied by Whittemore (unpublished), the TDS map was coverted into chloride concentration using the equations shown in Figure 4.6.

recharge had a very low chloride concentration. It was concluded that the K_v of the Upper Cretaceous aquitard was too high and allowed too much recharge into the upper Dakota aquifer. Therefore, the K_v of the aquitard was lowered until recharge no longer overwhelmed the concentration throughout the model domain and a concentration gradient developed. This posed a problem because the flow had already been calibrated. However, the RMS error of this newly calibrated flow model was only slightly higher than the original RMS error, indicating that the flow model is not sensitive to a lowering of the K_v. This will be confirmed by a sensitivity analysis presented in Chapter 6. However, it is concluded that the transport model is very sensitive to the amount of recharge coming into the model domain. Therefore, information from the transport modeling helped to further calibrate the flow model.

Once the recharge rate was lowered, the model produced regions of high and low concentration as was originally expected. However, the gradient between the regions was sharp. Furthermore, it was discovered that transport in this simulation was advectively dominated, i.e. the lateral flow through the western boundary controlled the concentration throughout the model. As an initial try, the inflow concentration through this boundary was set equal to the chloride concentration observed today. However, it is most likely incorrect to assume that it will be that low when the model domain started at a relatively high concentration. It is more realistic to assume that the incoming concentration will begin at the same level as the model's starting concentration. Then, as time progresses the inflow concentration will decrease until it is at the current levels observed today.

The observed concentration field was reproduced gradually by lowering the inflow concentration over time. At first, the inflow concentration equaled the starting concentration used in the model domain. The inflow concentration was then lowered incrementally until it reached the current chloride concentration levels. At no point was the inflow concentration reduced below the concentration levels observed today. Both the concentration level and the time step for that particular concentration level

were adjusted by trial and error until the major characteristics of the observed chloride distribution were reproduced. This suggests that in this simulation lateral flow and therefore advection controls the chloride distribution.

The final step in the reproduction of the chloride distribution included the adjustment of the effective porosity in the upper Dakota aquifer. The effective porosity was assumed to be higher in the high transmissive regions and lower in the low transmissive regions. It was adjusted until the simulated concentration gradient closely matched the observed gradient.

5.3.2. Transport Through a Poorly-Connected Aquifer

The hydraulic conductivity field of Simulation C3 is used in the second portion of the transport simulation. This simulation was more representative of the aquitard subunits and the regions of isolated aquifer subunits because of the low regional hydraulic conductivity of the aquifer. Therefore, it provided a means to investigate transport processes in areas isolated from the regional flow system. This simulation also provides a means to check the assumption about the interconnection of aquifer subunits. Simulation C2 assumed that the aquifer subunits were interconnected providing a relatively high regional hydraulic conductivity. If this assumption is incorrect and the aquifer subunits are not interconnected at all, then the aquitard subunits should dominate resulting in a very low regional hydraulic conductivity.

As was mentioned previously, the hydraulic conductivity field of Simulation C3 was three orders of magnitude lower than the one used in Simulation C2. Hydraulic conductivities were on the order of 10^{-3} to 10^{-4} m/day. One of the goals of this portion of the transport modeling was to determine if the process of diffusion will have more of an impact on the distribution of chloride in the aquifer. Since the previous transport model was advectively dominated, it might be expected that as the advective velocity decreases diffusion will play more of a significant role. Thus the lower, specified-mass

boundary would have a larger role in controlling the observed distribution of chloride than in Simulation C2.

Upon running Simulation C3, it was discovered that velocities had decreased to the point where the lower boundary now played a major role in the distribution of chloride in the model domain. Diffusion was more of a factor in the chloride transport. Furthermore, the chloride distribution was no longer dependent on a progressive lowering of the inflow concentration. Instead, the specified concentration gradient along the lower boundary controlled the chloride distribution in the model domain. However, the time needed to develop the chloride distribution took much too long, about 2.6×10^9 years. The time should be closer to 65 million years, around the beginning of the Laramide Orogeny (Macfarlane, 1993). This would suggest that a poorly-connected aquifer dominated entirely by diffusive transport is not reasonable due to the unrealistic amount of time required to develop the chloride distribution. However, Simulations C2 and C3 demonstrate the likelihood that two competing mechanisms exist with diffusion dominating in the aquitard subunits and advection in the interconnected aquifer subunits. Therefore, it is hypothesized that the presence of both aquifer and aquitard subunits must modify each other's chloride content producing the observed distribution of chloride. Unfortunately, it is impossible to properly investigate their interaction in detail at this scale.

5.4. Modeling Results and Summary of Calibrated Properties

The following three sections discuss the results from Simulations C1, C2, and C3. It should be kept in mind that the primary purpose of this modeling project was to test hypotheses concerning flow and mass transport. It was not meant to be used for predictive purposes. Many of the parameter values are estimated or represent lumped or averaged values. Items discussed in the following section include the final steady-state flow field and water budget for the flow model. The boundary conditions and the mixing of chloride sources along with the development of the chloride distributions are

also discussed. Finally, the parameter values from the calibrated models are summarized. Discussion on the limitations of the modeling parameters and the major controlling factors on the flow and transport processes are presented in the next chapter through a presentation of sensitivity analyses.

5.4.1. Steady-State Flow Field and Water Budget

Simulation C2 was calibrated to an RMS error of approximately 5.5 m (18 ft) which is well within the error of water-level measurements and the accuracy of the other data used in the model. The potentiometric surface from the model closely matches the observed surface (Figure 5.4). The flow budget for the aquifer shows that 92.7% of the flow moving through the aquifer is lateral flow. Recharge accounts for 7% of the total flow and 0.3% comes through the lower boundary (Figure 5.5). Flow through the lower boundary results from the interaction between the lower aquitard and the aquifer. This interaction allows a very small amount of flux to move from the aquitard into the aquifer. The average recharge rate through the Upper Cretaceous aquitard is 3.2×10^{-2} mm/yr (1.25×10^{-3} in/yr). This recharge rate is for Simulation C2. The recharge rate in Simulation C3 is three orders of magnitude lower.

The flow budget presented in the previous paragraph was for Simulation C2 and resulted from the recalibration of Simulation C1 using information from the transport model. The flow field in Simulation C1 had an RMS error of about 0.5 m (1.5 ft) lower than Simulation C2. Furthermore, Simulation C1 had a flow budget of only 61% lateral flow with 39% of the flow resulting from surface recharge. This is obviously too much recharge as was indicated by the transport modeling. A recharge rate of less than 10% of the total flow is much more appropriate given the highly confined conditions of the upper Dakota aquifer and is consistent with the recharge rates reported in Macfarlane (1993).

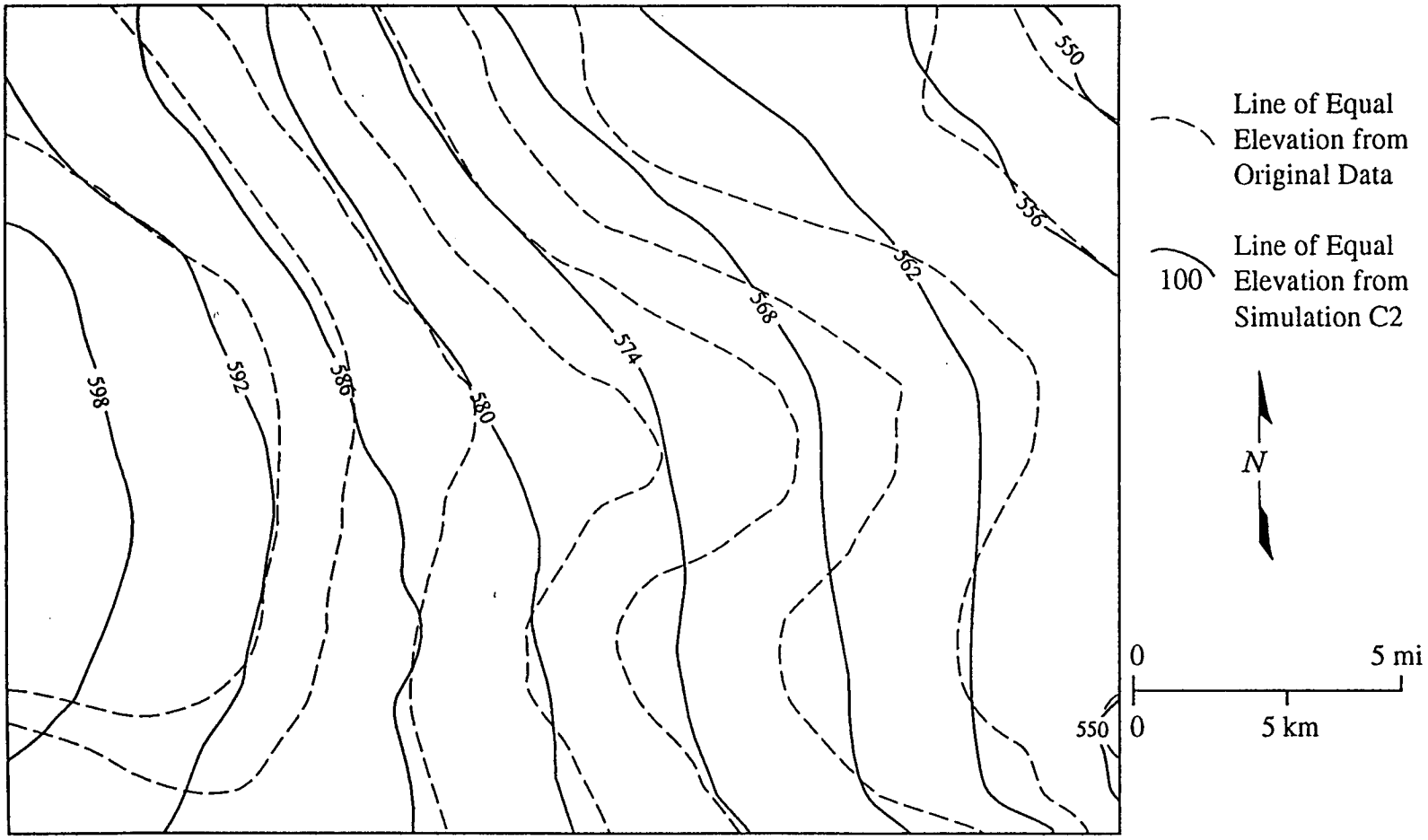

Figure 5.4: Comparison of the pre-development surface in the upper Dakota aquifer to the modeled potentiometric surface. The Root Mean Squared (RMS) error of the simulated heads are within acceptable limits when compare to the actual data points.

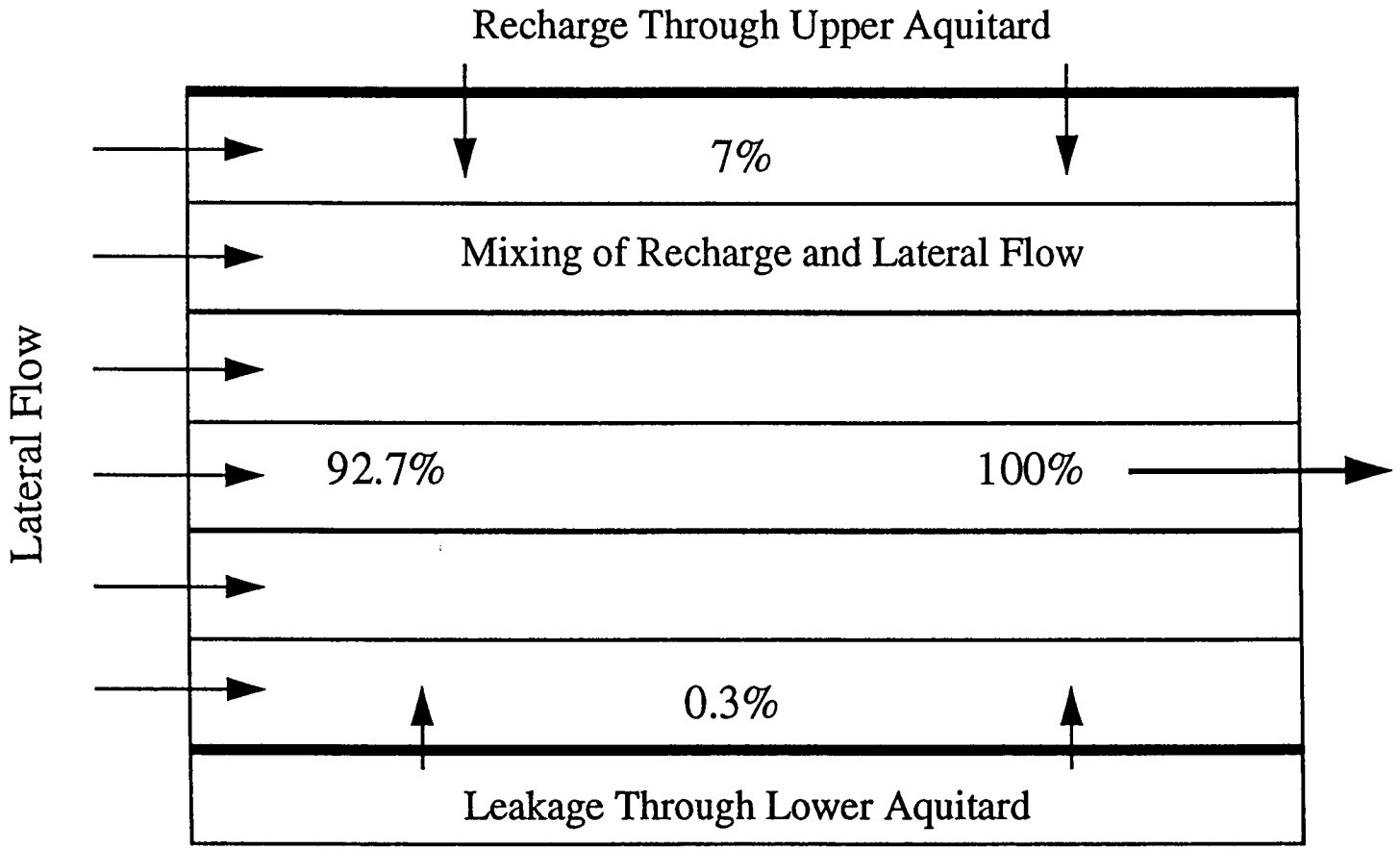

Figure 5.5 Illustration of calibrated water budget in the upper Dakota aquifer. Lateral flow dominates flow in the aquifer.

5.4.2. Transport Modeling Results

Two different hydraulic conductivity fields were used during the transport modeling. Simulation C2 simulated mass transport in a well-connected, high hydraulic conductivity aquifer and was biased towards the aquifer subunits of the Dakota Formation. Simulation C3 simulated mass transport in a poorly-connected, low hydraulic conductivity aquifer and was biased towards the aquitard subunits of the Dakota Formation. Figure 5.6a shows the simulated chloride distribution from Simulation C2, while Figure 5.6b shows the simulated chloride distribution from Simulation C3. The final chloride distributions produced by MT3D were chosen strictly by visual comparison of observed and simulated concentration distributions, therefore there was no measure of overall fit.

The mass-transport simulations were used to test hypotheses about the processes that produced the current chloride distribution in the study area. As was stated previously, advection dominated mass transport in Simulation C2, and diffusion dominated mass transport in Simulation C3. In Simulation C2, the concentration of the lateral inflow controlled the distribution of chloride in the model domain. It was necessary to gradually reduce the concentration of the lateral inflow over time (Figure 5.7). This is representative of mass transport in the interconnected aquifer subunits. On the other hand, a specified chloride concentration gradient in the bottom layer controlled the chloride distribution in Simulation C3 (Figure 5.8). This is representative of mass transport in the aquitard subunits and those areas isolated from the regional flow system.

The pattern in the chloride distribution differed in Figures 5.6a and 5.6b. Local highs and lows in the chloride concentration are observed in Figure 5.6a, while the contours in Figure 5.6b are regular and well behaved. This is because advection dominates mass transport in Simulation C2. As a result heterogeneity within the model layers greatly influence mass transport. The areas lowest in concentration correspond to the high transmissive regions (Figures 5.6a and 5.9a). However,

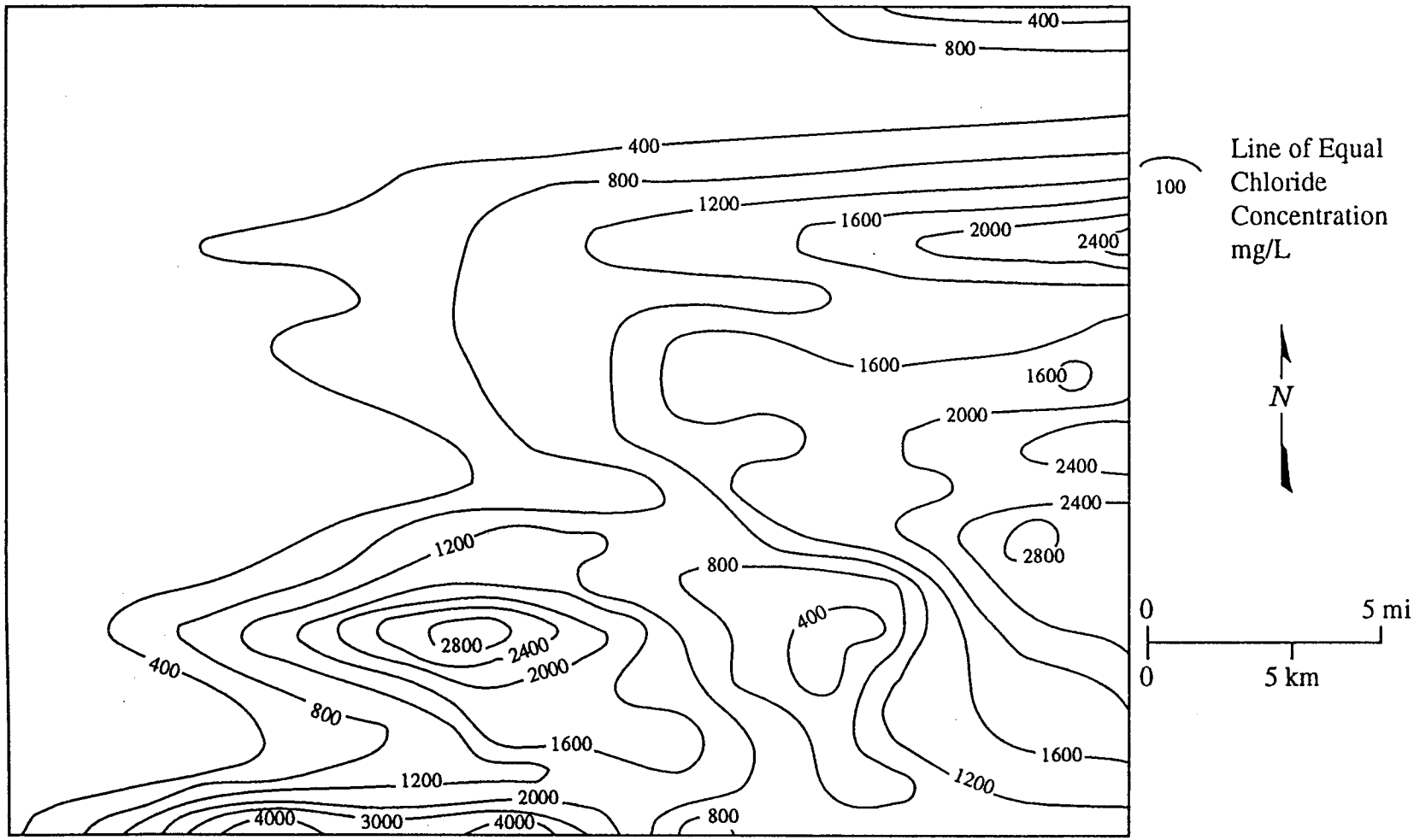

Figure 5.6a: Map showing the resulting chloride distribution from Simulation C2 (Table 5.1). Transport is dominated by lateral flow from the west.

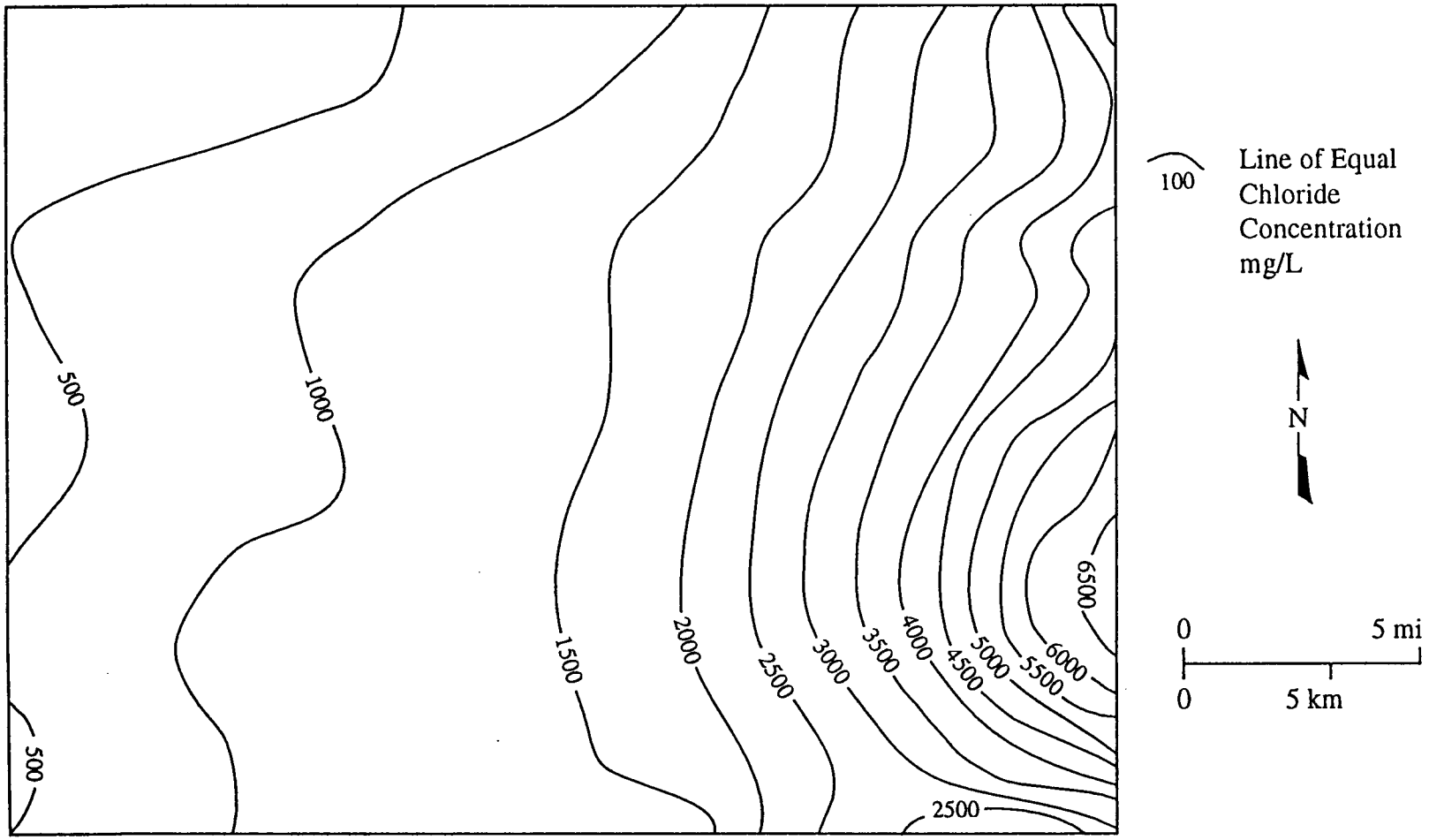

Figure 5.6b: Map showing the resulting chloride distribution from Simulation C3 (Table 5.1). Chloride distribution results from a mixture of lateral flow greatly influenced by the diffusion of chloride from beneath the aquifer.

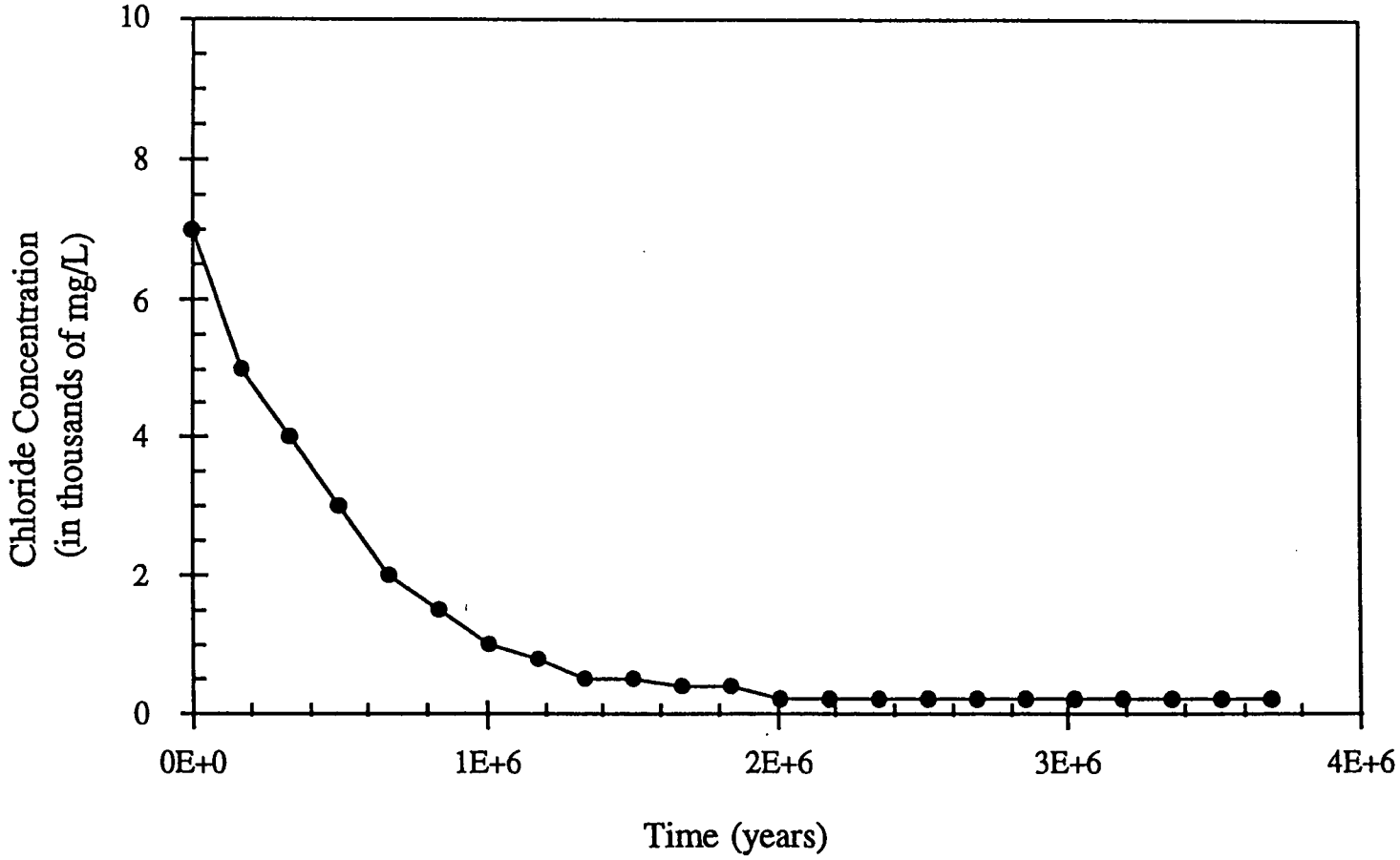

Figure 5.7: Average inflow concentration through the western edge of layer 1 in Simulation C2 (Table 5.1). The decrease in concentration of the lateral flow causes the concentration gradient to develop. The period of constant concentration causes a region of relatively uniform concentration to exist in the western half of the model.

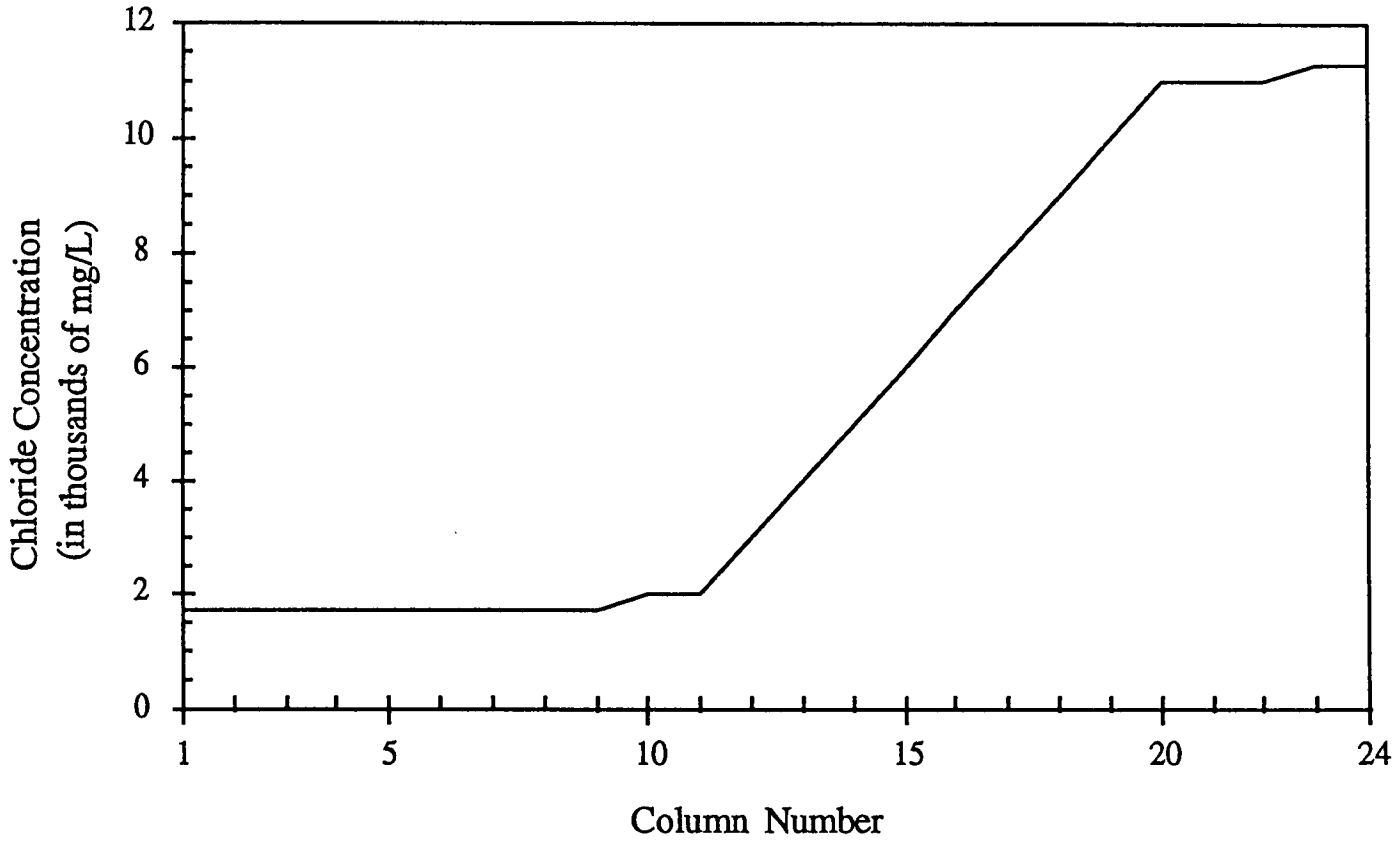

Figure 5.8: Graph showing the concentration assigned to layer seven of the model. The specified concentration along the bottom layer controls the distribution of chloride in the model domain because diffusion has a major role in Simulation C3 (Table 5.1).

because diffusion dominates in Simulation C3, heterogeneity has little impact on the distribution of chloride. Instead, chemical diffusion evenly spreads the chloride throughout the model domain with the lower boundary controlling the chloride concentration gradient in the aquifer.

However, the actual data suggested that concentrations are much more variable than either hydraulic conductivity field could produce (Figure 2.9). A large degree of variability should not be surprising considering that aquifer and aquitard subunits are interspersed among each other. The interaction between the aquifer and aquitard subunits at the appropriate scale could not be incorporated into the numerical model. It is very likely that the chloride in the aquitard subunits interacts with the interconnected aquifer subunits to modify each other's chloride content. However, the results from Simulations C2 and C3 can be considered end-members, as far as the mass-transport processes are concerned.

Finally, the unrealistic amount of time required to develop the chloride distribution in Simulation C3 suggests that diffusion cannot be the only means of chloride transport. There must be interconnected aquifer subunits providing regional conduits for ground-water flow which serve to flush the aquifer of chloride. The large variability in the concentration data also supports the idea that certain areas have been better flushed than others. Furthermore, because it took about 4 million years to develop the current distribution of chloride with a regional hydraulic conductivity of about 1 m/day, the regional hydraulic conductivity cannot be less than about 0.06 m/day (0.2 ft/day) assuming the assumptions about the model are correct. This is because the time to flush the aquifer of chloride seems to be inversely dependent upon the regional hydraulic conductivity of the aquifer and assumes that the maximum allowable time is about 65 million years, the beginning of the Laramide Orogeny.

5.4.3. Summary of Calibrated Properties

Table 5.2 summarizes the partially calibrated values used in MODFLOW for Simulation C2. The flow model required hydraulic conductivity values for the aquifer and the aquitards. The aquifer was considered to be heterogeneous and was assigned high and low transmissive regions defined by the average thickness of the aquifer subunits. Each zone had its own partially calibrated value for its high transmissive regions. The average thickness of the aquifer subunits used as a cutoff for differentiating the relatively high transmissive regions from the relatively low transmissive regions was also a calibration parameter. The same value was used for all three zones to maintain consistency (Figures 5.9a through 5.9c). The anisotropy ratio was the final calibration parameter used in the model.

Table 5.3 summarizes the different parameters used to run MT3D. Dispersion and diffusion coefficients were constant throughout the model. Storativity values were required by MODFLOW in order to run MT3D in transient simulation. However, it was determined that they did not have any effect on either the flow field or the transport process since there were no sources or sinks such as pumping wells. Storativity values were therefore simply selected to fall within a common range. The effective porosity was the last parameter used. Two values were used one representing the relatively high transmissive regions and another representing the relatively low transmissive regions.

		Metric units (m/day or meters)			English units (ft/day or feet)		
K_v of the Upper Cretaceous aquitard		1.524×10^{-7}			5.0×10^{-7}		
K_v of the Upper Dakota aquifer		3.05×10^{-5}			10^{-4}		
K_h of the Upper Dakota aquifer	High Transmissive	0.91	0.61	1.22	3.0	2.0	4.0
	Low Transmissive	0.0305	0.0305	0.0305	0.1	0.1	0.1
Thickness threshold		6.1	6.1	6.1	20	20	20
Anisotropy Factor		0.01	0.01	0.01	0.01	0.01	0.01
K_v of the Kiowa Shale aquitard		3.05×10^{-7}			10^{-6}		

Table 5.2: Summary of final flow parameters used in MODFLOW for Simulation C2 (Table 5.1). Both metric and English units are given. If three values are given, they correspond to separate values assigned to each of the three zones of the aquifer with Zone 1 on the left and Zone 3 on the right.

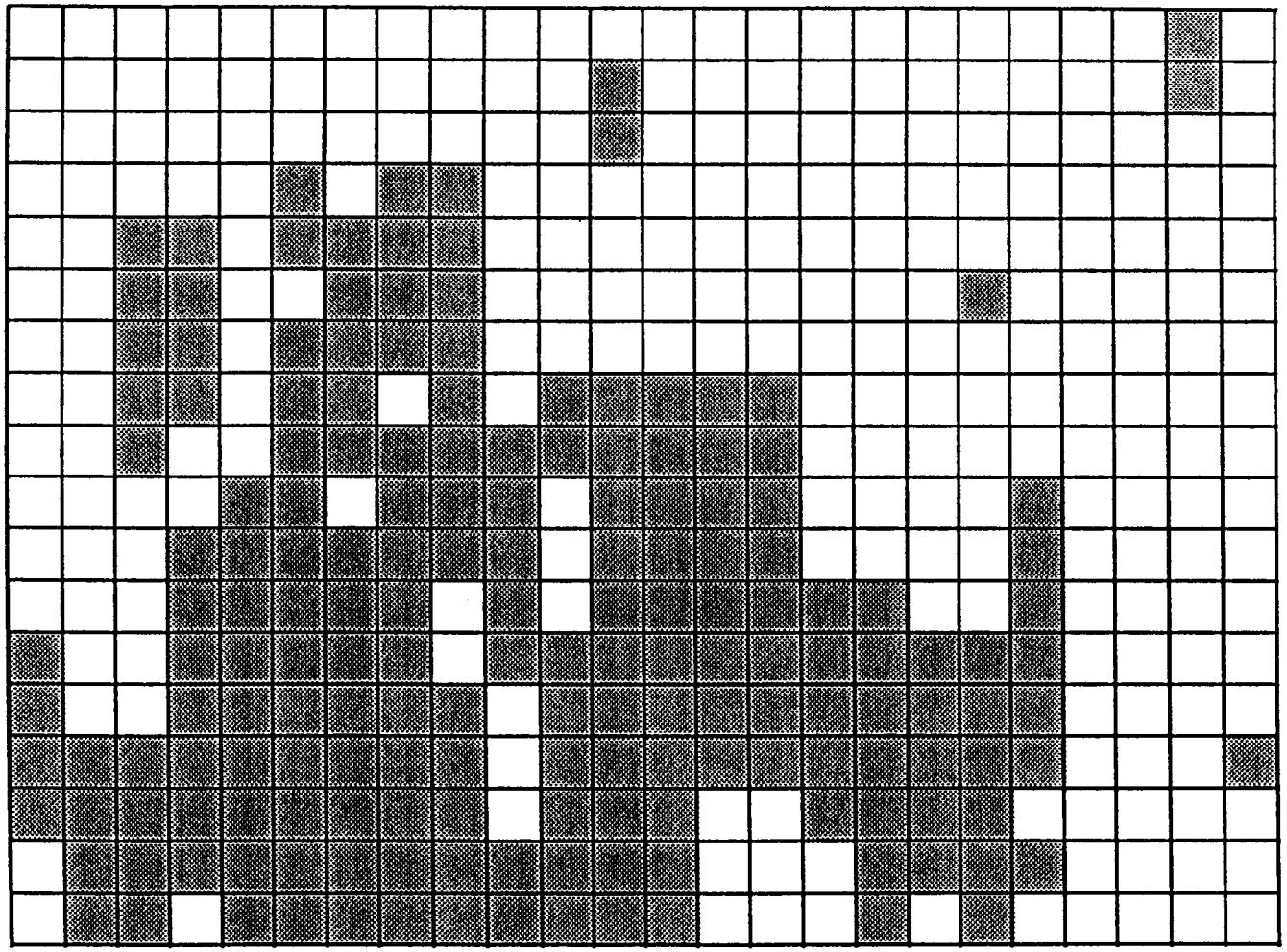

Figure 5.9a: Illustration of the high and low transmissive regions from zone 1. Darker regions indicate lower transmissive regions. This distribution was used for model layers 1 and 2.

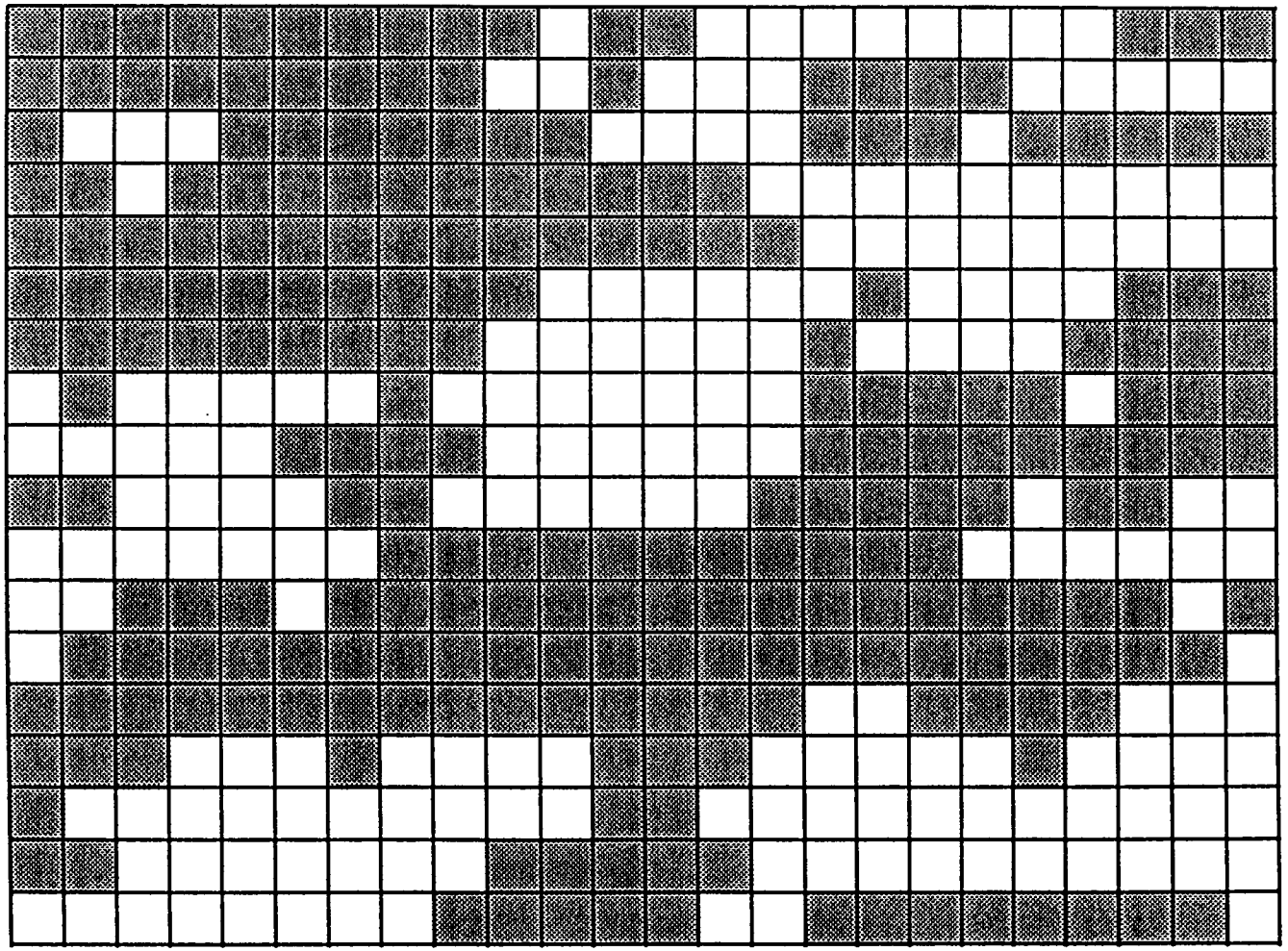

Figure 5.9b: Illustration of the high and low transmissive regions from zone 2. Darker regions indicate lower transmissive regions. This distribution was used for model layers 3 and 4.

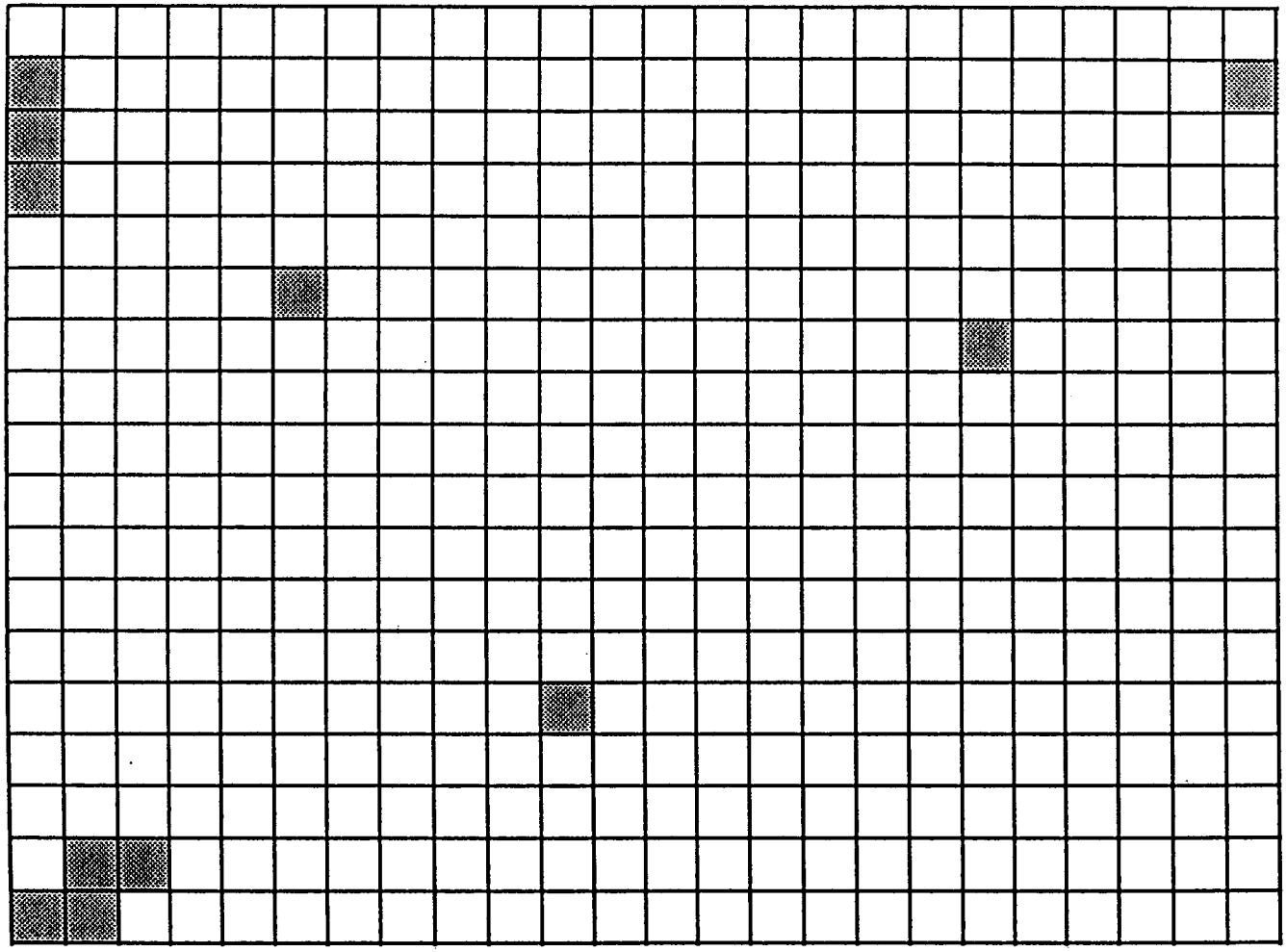

Figure 5.9c: Illustration of the high and low transmissive regions from zone 3. Darker regions indicate lower transmissive regions. This distribution was used for model layers 5 and 6.

		Metric units			English units		
Storativity	High Transmissive	1×10^{-4}			1×10^{-4}		
	Low Transmissive	1×10^{-3}			1×10^{-3}		
Effective Porosity	High Transmissive	0.2	0.2	0.2	0.2	0.2	0.2
	Low Transmissive	0.08	0.08	0.08	0.08	0.08	0.08
Dispersion Coefficients		100 m	1 m	0.1 m	328 ft	3.28 ft	0.328 ft
Diffusion Coefficient		1.75×10^{-5} m^2/day			1.88×10^{-4} ft^2/day		

Table 5.3: Summary of parameters used in MT3D and MODFLOW for the transport modeling. Both metric and English units are given. The three values list for the effective porosity correspond to separate values assigned to each of the three zones of the aquifer with Zone 1 on the left and Zone 3 on the right. The three dispersion coefficients listed are the longitudinal (left), horizontal transverse (middle), and vertical transverse (right) dispersion coefficients respectively. The same parameters were used in both Simulations C2 and C3 (Table 5.1).

CHAPTER 6. SENSITIVITY ANALYSES

6.1. Introduction

The purpose of a sensitivity analysis is to quantify the uncertainty in the parameters of the calibrated model (Anderson and Woessner, 1992). The influence of certain parameters on the flow and transport processes will also be discussed. The lack of sufficient data makes modeling results inherently uncertain. Therefore, sensitivity analyses were performed on both the flow and transport models. The parameters used in the flow model were evaluated individually by adjusting a parameter incrementally both higher and lower than its calibrated value. The effect of the parameter change was then measured by the resulting RMS error in the model. There is no sensitivity analysis performed on the boundary conditions of the flow model because they are assumed to be appropriate. The parameters used in the transport model were also evaluated for their effect on chloride transport. However, only the general effects of the parameter adjustments are presented since there was no measure of the overall fit to the observed chloride distribution. Assumptions about the boundary conditions in the transport model were evaluated for their effect on the chloride distribution. Table 6.1 lists the different sensitivity analysis tests.

6.2. Flow Field

Sensitivity analyses were performed on the K_v of Upper Cretaceous aquitard and the hydraulic conductivity of the upper Dakota aquifer. Various parameters were investigated to determine their degree of influence on the flow system in the aquifer and the degree of uncertainty in the calibrated values. The effect of the Upper Cretaceous aquitard on the flow field of the upper Dakota aquifer has already been investigated by Macfarlane (1993), and the results presented here are not significantly different. Most of the sensitivity analyses focus on aquifer heterogeneity because this has not been investigated previously and is one of the main concerns of this thesis.

Simulation Number	Simulation Tested	Process Being Evaluated	Parameter Tested or Other Adjustment to the Models
S1	C2	Flow	K_v of the Upper Cretaceous Aquitard
S2	C2	Flow	K_h of the Upper Dakota Aquifer
S3	C2	Flow	K_v of the Upper Dakota Aquifer
S4	C2	Flow	Anisotropy Factor of the Upper Dakota Aquifer
S5	C2	Flow	High Transmissive Regions in the Upper Dakota Aquifer
S6	C2	Flow	Low Transmissive Regions in the Upper Dakota Aquifer
S7	C2	Flow	Threshold Thickness from Block Kriging
S8	C2	Flow	Homogeneous Hydraulic Conductivity Field
S9	C2	Transport	Decreased the K_h of the Low Transmissive Regions
S10	C3	Transport	Uniform Specified Concentration of 2,000 mg/L
S11	C3	Transport	Uniform Specified Concentration of 10,000 mg/L

Table 6.1: Summary of sensitivity analysis model runs for both MODFLOW and MT3D.

Anisotropy in the horizontal and vertical directions is discussed in addition to heterogeneity in the horizontal conductivity of the aquifer. The thickness threshold defined in Chapter 5 is also investigated because it is the main parameter defining heterogeneity in the aquifer. Finally, the heterogeneous hydraulic conductivity field is compared to a homogeneous hydraulic conductivity field, to support the incorporation of heterogeneity in the modeling. The sensitivity of model parameters are generally evaluated by increasing and decreasing the parameter either over several orders of magnitude or by several factors from the calibrated value. The RMS error is then observed and plotted against the multiplier of the calibrated value.

6.2.1. The Effect of the Upper Cretaceous Aquitard

The impact of vertical hydraulic conductivity (K_v) of the Upper Cretaceous aquitard on the flow system was evaluated first (Simulation S1 in Table 6.1). Figure 6.1 shows the resulting RMS error due to changes in the parameter value over several orders of magnitude. Values greater than the calibrated value by about an order of magnitude cause the RMS error to increase rapidly. However, values less than the calibrated value have little impact on the RMS error. This is because there is so little recharge to the aquifer that any reduction in K_v has little impact on the overall water budget of the aquifer. However, increases in the parameter dramatically increase the recharge and cause a significant impact on the water budget of the aquifer. From this it can be interpreted that an upper limit to the recharge rate can be established but a lower limit is more difficult to ascertain without additional data. The mass-transport simulations helped to establish the final calibrated value as less than the point where the RMS error begins to increase significantly, but an exact value is still unknown.

6.2.2. The Effect of Hydraulic Conductivity in the Upper Dakota Aquifer

This section evaluates the influence of the overall horizontal hydraulic conductivity (K_h), the vertical hydraulic conductivity (K_v), and the horizontal

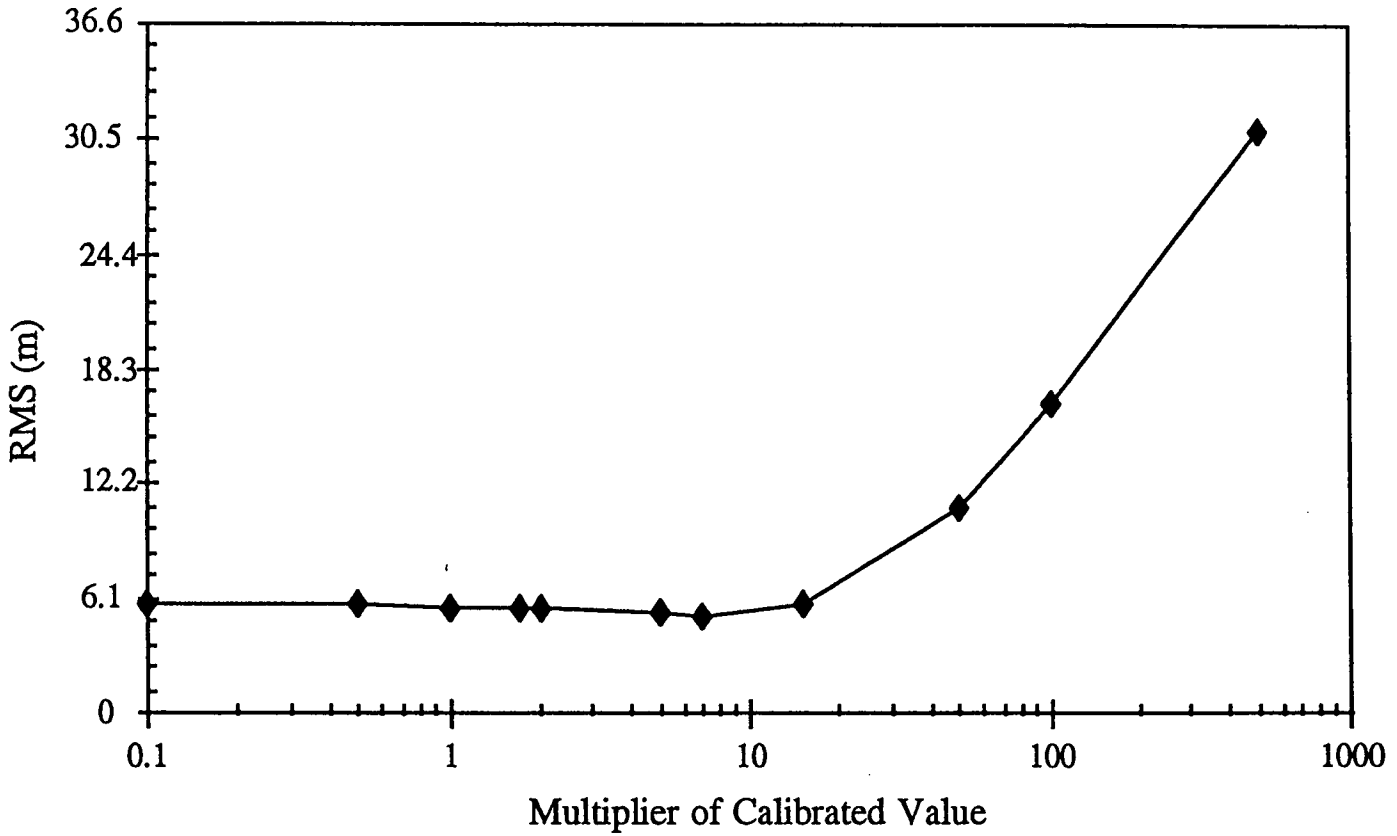

Figure 6.1: Sensitivity analysis on the vertical hydraulic conductivity of the Upper Cretaceous aquitard (Simulation S1 in Table 5.1).

anisotropy on the flow system in the aquifer. A discussion on the effect of the heterogeneity within each layer is reserved for the next section. First the overall K_h of the aquifer is evaluated by incrementally changing the entire hydraulic conductivity field using a multiplier (Simulation S2 in Table 6.1). As a result it was discovered that decreasing K_h had a greater impact on the RMS error than increasing it (Figure 6.2). In fact, there is not a significant change in the RMS error until K_h is reduced 1.5 orders of magnitude from the calibrated value. In contrast, changes to K_v of the aquifer has very little influence on the RMS error (Figure 6.3) because of the primarily horizontal flow in the aquifer (Simulation S3 in Table 6.1). This implies that K_v of the aquifer is not an important parameter in the flow field.

The horizontal anisotropy of the aquifer was evaluated by both increasing and decreasing the anisotropy factor over several orders of magnitude from the calibrated value (Simulation S4 in Table 6.1). The anisotropy factor is equal to the hydraulic conductivity parallel to the columns divided by the hydraulic conductivity parallel to the rows. If the factor equals one, then K_h is isotropic. However, values less than one lowers K_h in the north-south direction and values greater one lowers K_h in the east-west direction. Figure 6.4 shows the change in RMS error with different anisotropy factors. The lowest RMS error occurs when the anisotropy factor is 0.01. This suggests that the K_h in the upper Dakota aquifer is 100 times lower in the north-south direction than in the east-west direction.

6.2.3. The Effect of Heterogeneity in the Upper Dakota Aquifer

Because a heterogeneous hydraulic conductivity field is important in defining the velocity field of the aquifer, heterogeneity in the upper Dakota aquifer was investigated. The heterogeneity of the aquifer was determined for the model grid based on the average thickness of the aquifer subunits from block kriging. A thickness threshold was defined to distinguish high and low transmissive regions in the aquifer for each of the three zones of the Dakota Formation. A sensitivity analysis was

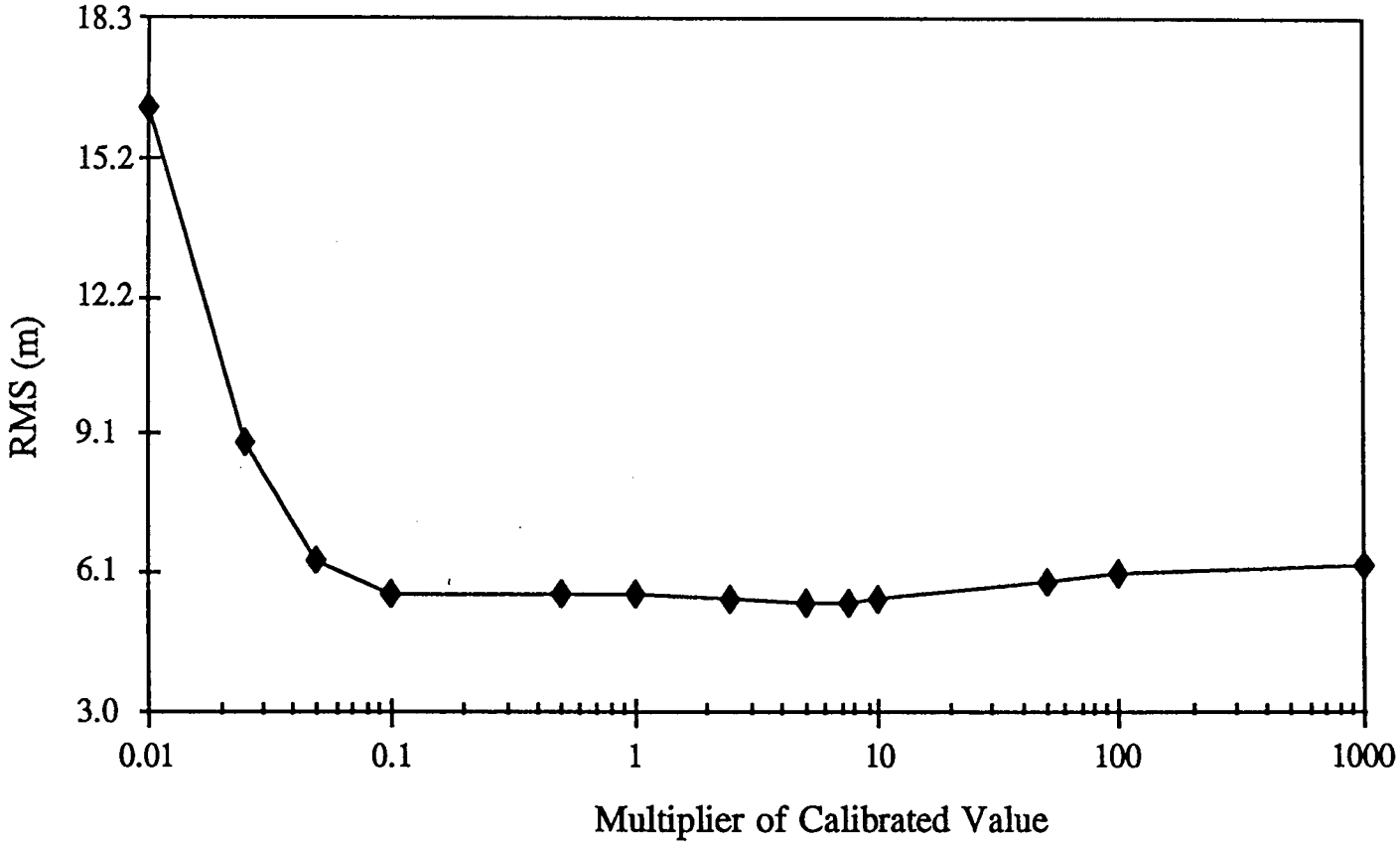

Figure 6.2: Sensitivity analysis on the horizontal hydraulic conductivity of the upper Dakota aquifer (Simulation S2 in Table 5.1).

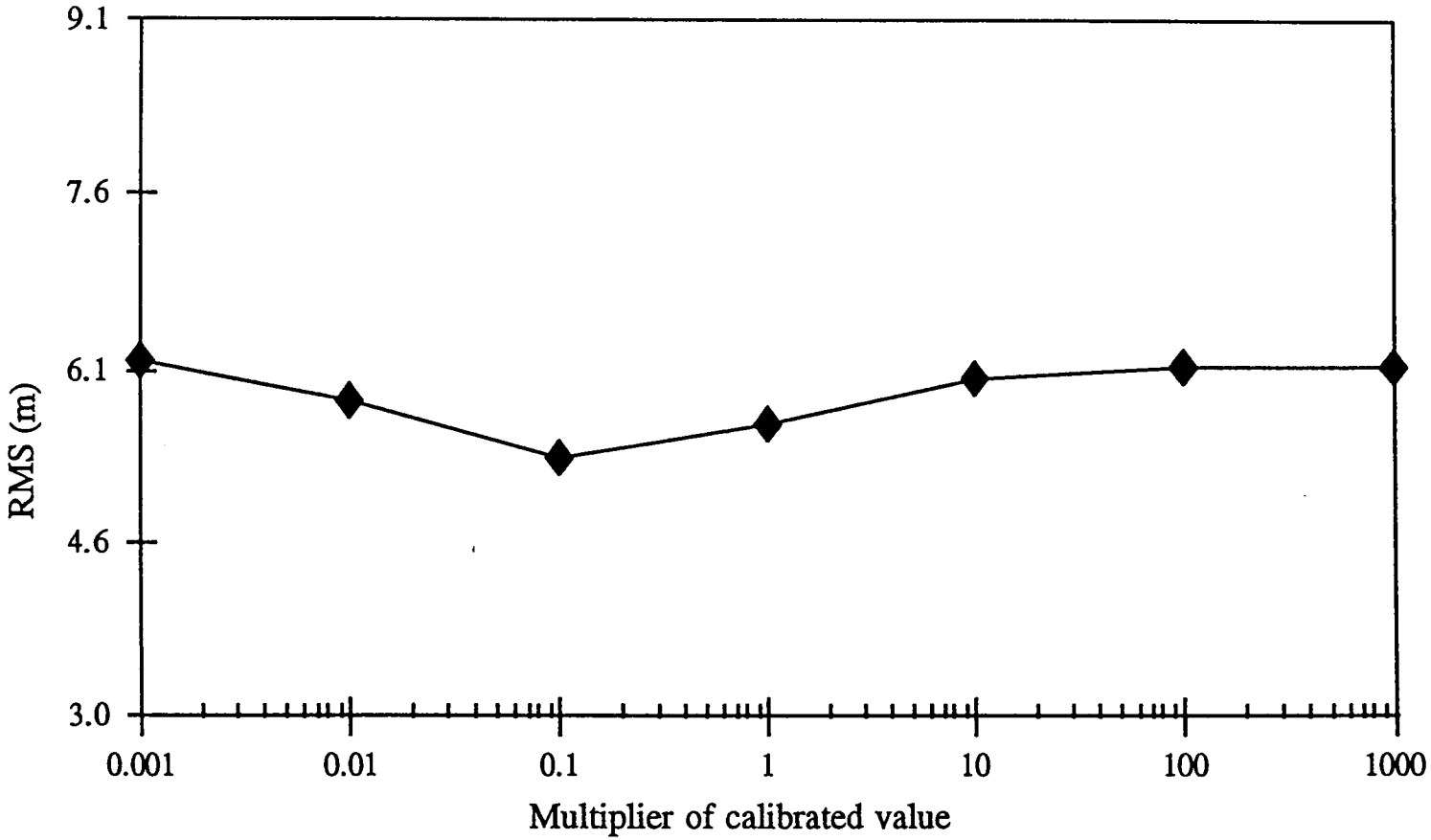

Figure 6.3: Sensitivity analysis on the vertical hydraulic conductivity of the upper Dakota aquifer (Simulation S3 in Table 5.1).

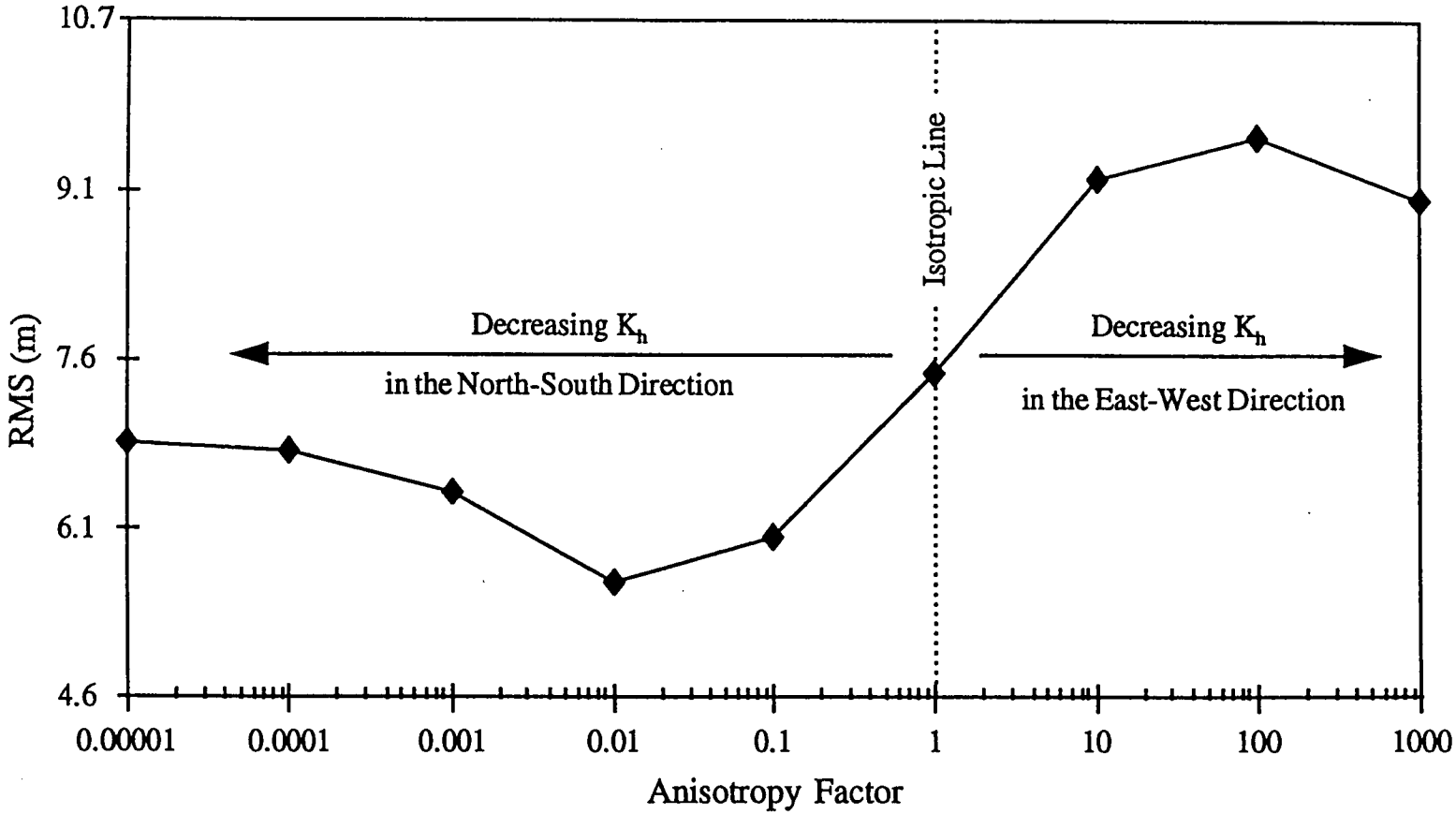

Figure 6.4: Sensitivity analysis on the horizontal anisotropy factor of the upper Dakota aquifer (Simulation S4 in Table 5.1). The anisotropy factor is equal to the hydraulic conductivity perpendicular to the columns divided by the hydraulic conductivity perpendicular to the rows. Therefore, a factor less than 1 represents decreasing K_h in the north-south direction. A factor of 1 represents an isotropic horizontal hydraulic conductivity in the model.

performed to determine the effect of the assigned values of K_h in the high and low transmissive regions on the flow system. Next, the value used for the thickness threshold was evaluated. Finally, the heterogeneous aquifer is compared to a homogeneous aquifer in order to evaluate the effectiveness of incorporating heterogeneity into the modeling.

Figure 6.5 shows the impact of varying only the hydraulic conductivity within the high transmissive regions on the RMS error (Simulation S5 in Table 6.1). This figure shows that values less than an order of magnitude below the calibrated value cause the RMS error to increase significantly. Figure 6.6 shows the impact of varying the hydraulic conductivity just within the low transmissive regions on the RMS error (Simulation S6 in Table 6.1). This figure shows that increases in the value have a greater impact on the RMS error than decreases; however, the overall impact on the RMS error is less than that observed in Simulation S5.

A comparison between Figures 6.5 and 6.6 suggests that there is a tendency for the high transmissive regions to be higher in value and the low transmissive regions to be lower in value, as indicated by their trends in RMS error. However, although this provides for a better model fit to the head data, there were two reasons for using the chosen hydraulic conductivities. The first reason was to have an overall hydraulic conductivity of 1 m/day consistent with other model investigations (Belitz, 1985; Macfarlane, 1993; Helgeson *et al.*, 1993). Secondly, an order of magnitude difference between the high and low transmissive regions was maintained for better results in the transport model. The effect of a larger difference between the high and low transmissive regions on chloride transport will be presented during the sensitivity analysis of the mass-transport model.

The final parameter that was evaluated was the thickness threshold separating the high and low transmissive regions (Simulation S7 in Table 6.1). To test this arbitrary parameter, the areal distribution of the two regions was adjusted by changing the thickness threshold in increments of 1.5 m (5 ft). An increase in the threshold

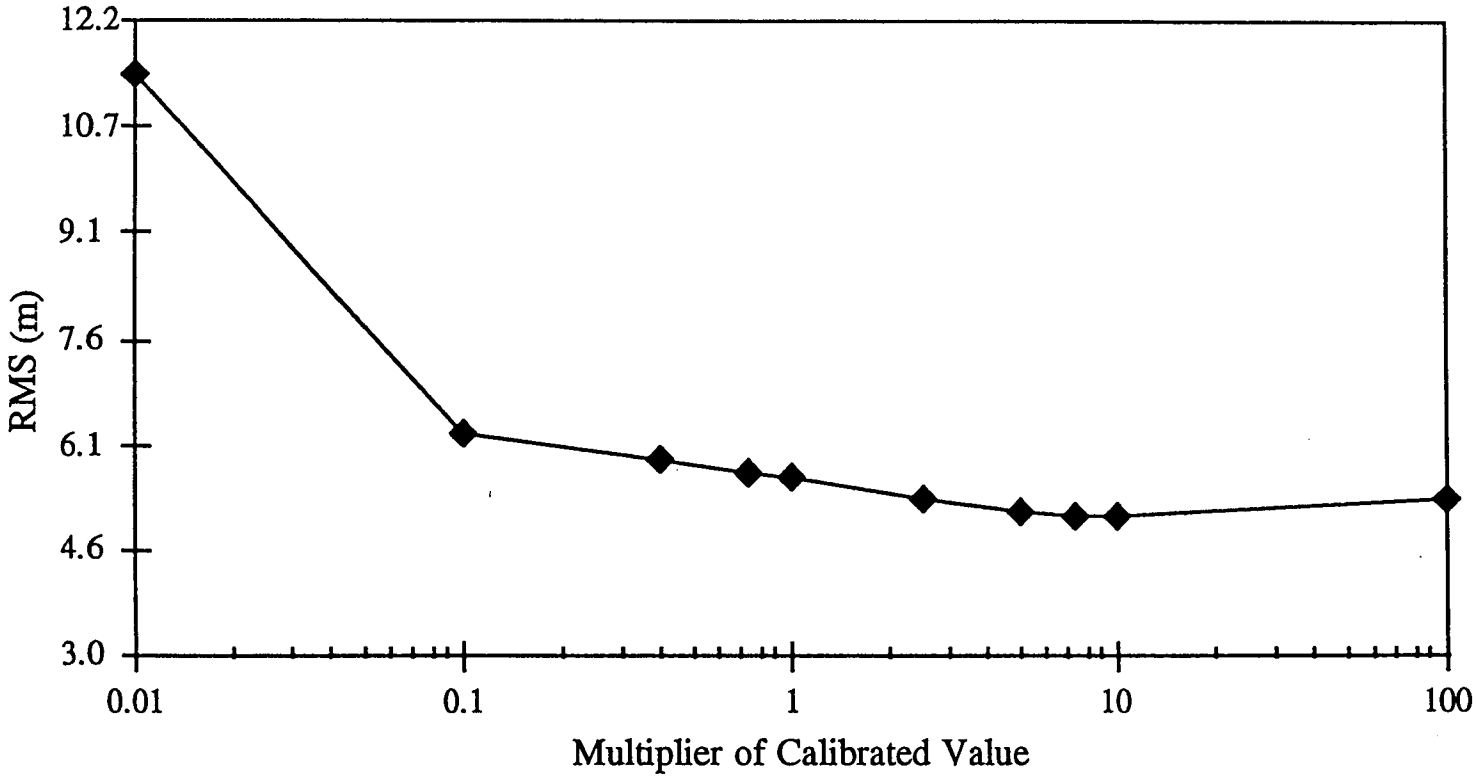

Figure 6.5: Sensitivity analysis on the high transmissive regions in the upper Dakota aquifer (Simulation S5 in Table 5.1).

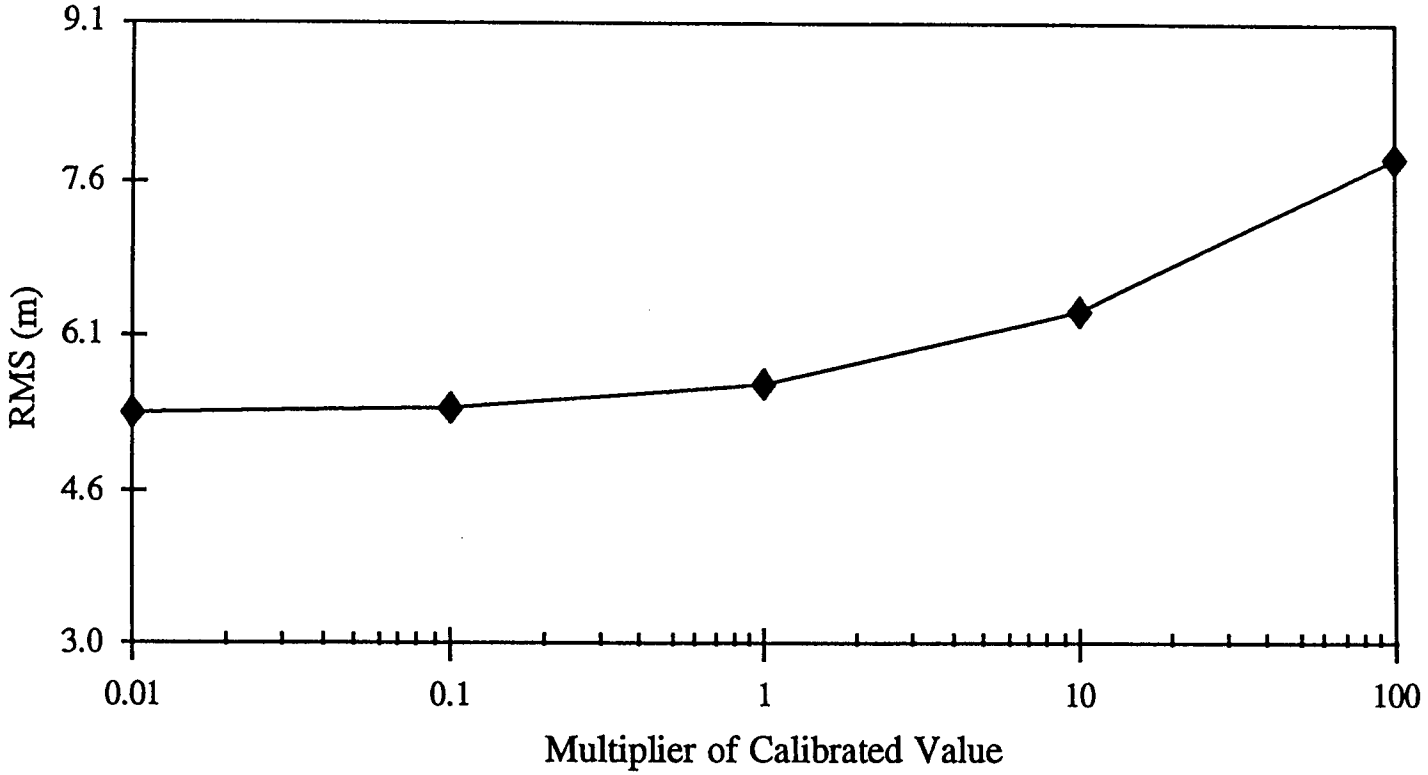

Figure 6.6: Sensitivity analysis on the low transmissive regions in the upper Dakota aquifer (Simulation S6 in Table 5.1).

thickness decreases the area of the high transmissive regions. Figure 6.7 shows the results of this sensitivity analysis test. There is no apparent trend seen in the graph. The lowest error occurs at a value of 6 m (20 ft) and was chosen as the threshold separating the high and low transmissive regions. However, this is strictly an empirical value that seems to work for this modeling project. A more detailed investigation of the sandstone and mudstone distributions should be done to better determine an appropriate threshold. Although the thickness threshold is seemingly an empirical value only appropriate for this model, the 6 m (20 ft) value is consistent with the work by Fogg (1989) because the approximate sand fraction is 0.2 and the ranges of correlation in the east-west direction were on the order of 6.5 km (4 mi).

To evaluate the influence of heterogeneity on the model results, the heterogeneous aquifer was compared to a homogeneous aquifer (Simulation S8 in Table 6.1). A homogeneous aquifer was produced by assigning one horizontal conductivity value to all layers within the aquifer, keeping everything else the same. This model was than calibrated by adjusting its hydraulic conductivity until the lowest possible RMS error was achieved. The final hydraulic conductivity of the homogeneous aquifer was 0.2 m/day (0.65 ft/day). Figure 6.8 compares the calibrated homogeneous aquifer to the heterogeneous aquifer. The heterogeneous model has an RMS error almost 1.5 m (5 ft) lower than the homogeneous model. This suggests that characterizing the aquifer as heterogeneous was appropriate and was a more accurate representation of the aquifer's hydraulic conductivity field.

6.3. Chloride Transport

A sensitivity analysis on the mass transport was handled differently than the sensitivity analysis on the flow field because there was no measure of overall fit between the observed and simulated chloride distributions. Therefore, the "calibrated" chloride distribution was visually compared to the distribution produced by a particular sensitivity analysis run. Moreover, many of the sensitivity analyses showed little to no

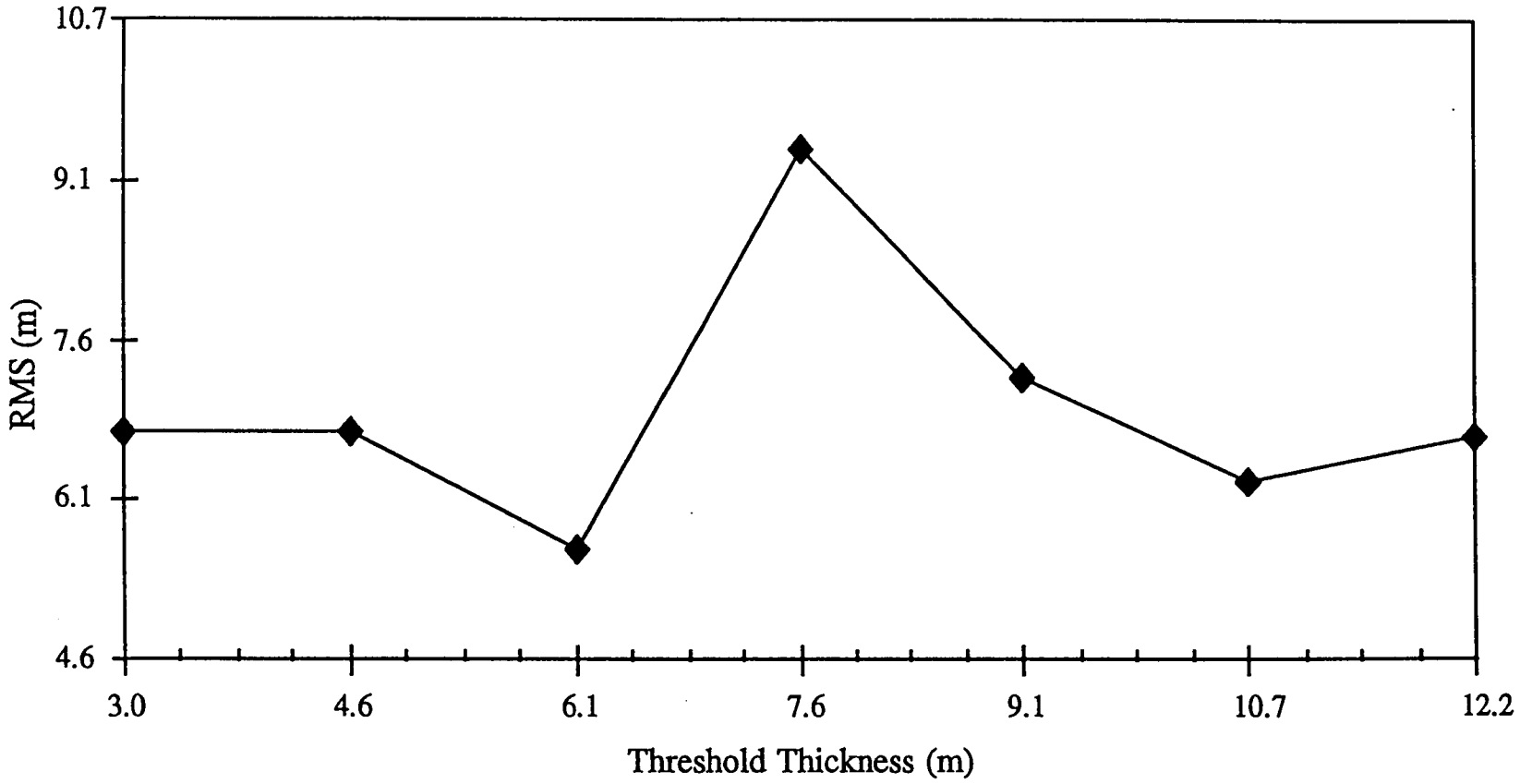

Figure 6.7: Sensitivity analysis on the thickness threshold used to distinguish high and low transmissive regions in the upper Dakota aquifer (Simulation S7 in Table 5.1). Increasing the threshold thickness has the effect of decreasing the high transmissive regions.

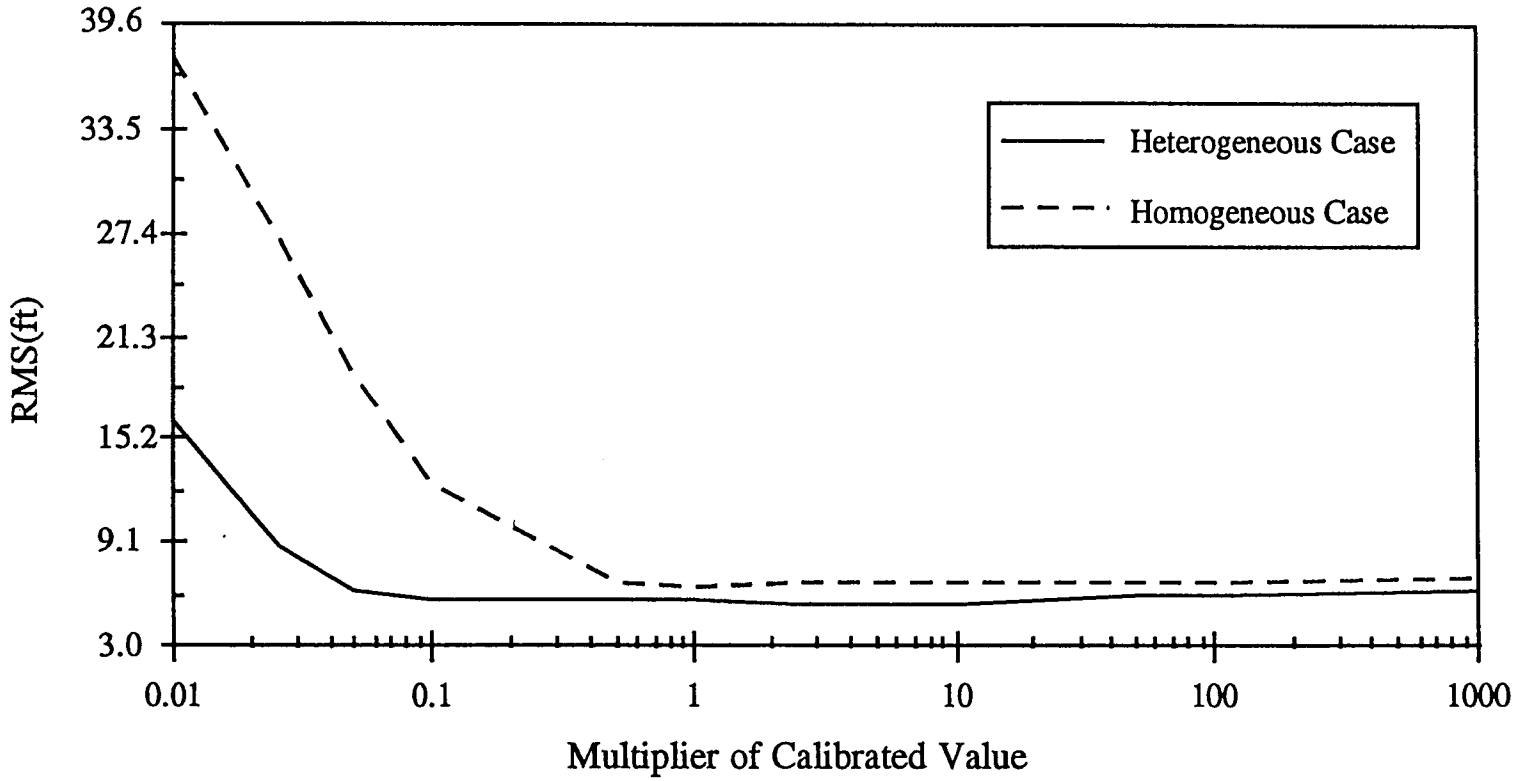

Figure 6.8: Comparison of the heterogeneous and a homogeneous hydraulic conductivity fields. Shown are the sensitivity analyses on the horizontal hydraulic conductivity of the upper Dakota aquifer (Simulations S2 and S8 in Table 5.1). The dashed line is the homogeneous case, and the solid line is the heterogeneous case.

effect on the chloride distribution indicating that the model was not sensitive to those parameters. In general, the sensitivity analyses included the impact of changing the porosity, hydraulic conductivity, dispersion coefficients, diffusion coefficient, and the different boundary conditions.

Since two different configurations of the hydraulic conductivity field were used during the transport modeling (Table 5.1), each was evaluated separately. It has already been determined that the transport processes in Simulations C2 and C3 were quite different. Therefore, the sensitivity of each simulation to different parameters would be expected. The advective transport of Simulation C2 and the diffusive transport of Simulation C3 have already been discussed in Chapter 5. It was determined that the impact of decreasing the overall hydraulic conductivity of the aquifer was to decrease the velocity of the flow field, as was expected. As a result, the residence time of mass in the aquifer increased. A secondary effect was that as the velocity decreased, diffusion began to have more of an impact on mass transport. An average hydraulic conductivity of 10^{-3} m/day results in diffusion playing a significant role in mass transport. However, an average hydraulic conductivity of one order of magnitude higher results in advection again dominating mass transport and diffusion being insignificant.

6.3.1. Sensitivity Analysis on Simulation C2

When the average hydraulic conductivity of the aquifer is relatively high (order of 1 m/day), advection dominates mass transport. It has been determined that the concentration specified for the lower boundary has no influence on the distribution of chloride in this model. Furthermore, the recharge coming into the aquifer through the Upper Cretaceous aquitard decreases the chloride concentration in the aquifer by a very small amount but has only a slight effect on its distribution. If the recharge coming through the Upper Cretaceous aquitard is reduced to zero, concentrations in the aquifer increase by a very small amount.

Heterogeneity has a pronounced effect on the transport of chloride. Specifically, the contrast in hydraulic conductivity between the high and low transmissive regions provides for a non-uniform velocity field which in turn impacts the distribution of chloride. As a result, chloride does not flow at a uniform rate through all parts of the aquifer (Figure 5.6a). In Simulation C2, the contrast was about an order of magnitude. However, if the contrast is two orders of magnitude or greater, then high concentrations of chloride persist in the low transmissive regions (Simulation S9 in Table 6.1). At the same time, chloride is flushed through the high transmissive regions of the model domain (Figure 6.9). This further illustrates the advective nature of transport in Simulation C2.

Because mass transport is advectively dominated, the flow system is also sensitive to the effective porosity assigned to the aquifer. With a uniform effective porosity, the water flux is greater in the northeast, since the high transmissive regions are generally in the northern half of the model (Figures 5.9a and 5.9b). By assigning lower values for the effective porosity to the low transmissive regions, the pore velocity increases. This has the effect of increasing the velocity in the southern portion of the model allowing for a more even distribution of chloride in the model over time.

Lastly, the impact of the diffusion and dispersion coefficients on the chloride distribution were evaluated. It was determined that the diffusion coefficient had no impact on the chloride distribution since mass transport was dominated by advection. Increases of 2 to 3 orders of magnitude in the transverse dispersivities had no impact on the distribution of chloride indicating that the model is also insensitive to these parameters. Decreasing the longitudinal dispersivity also had no impact on the distribution of chloride; however, increasing the parameter to 10,000 m did. The effect was to broaden the concentration gradient throughout the model. However, the spreading was still not enough to account for the observed distribution of chloride in the aquifer.

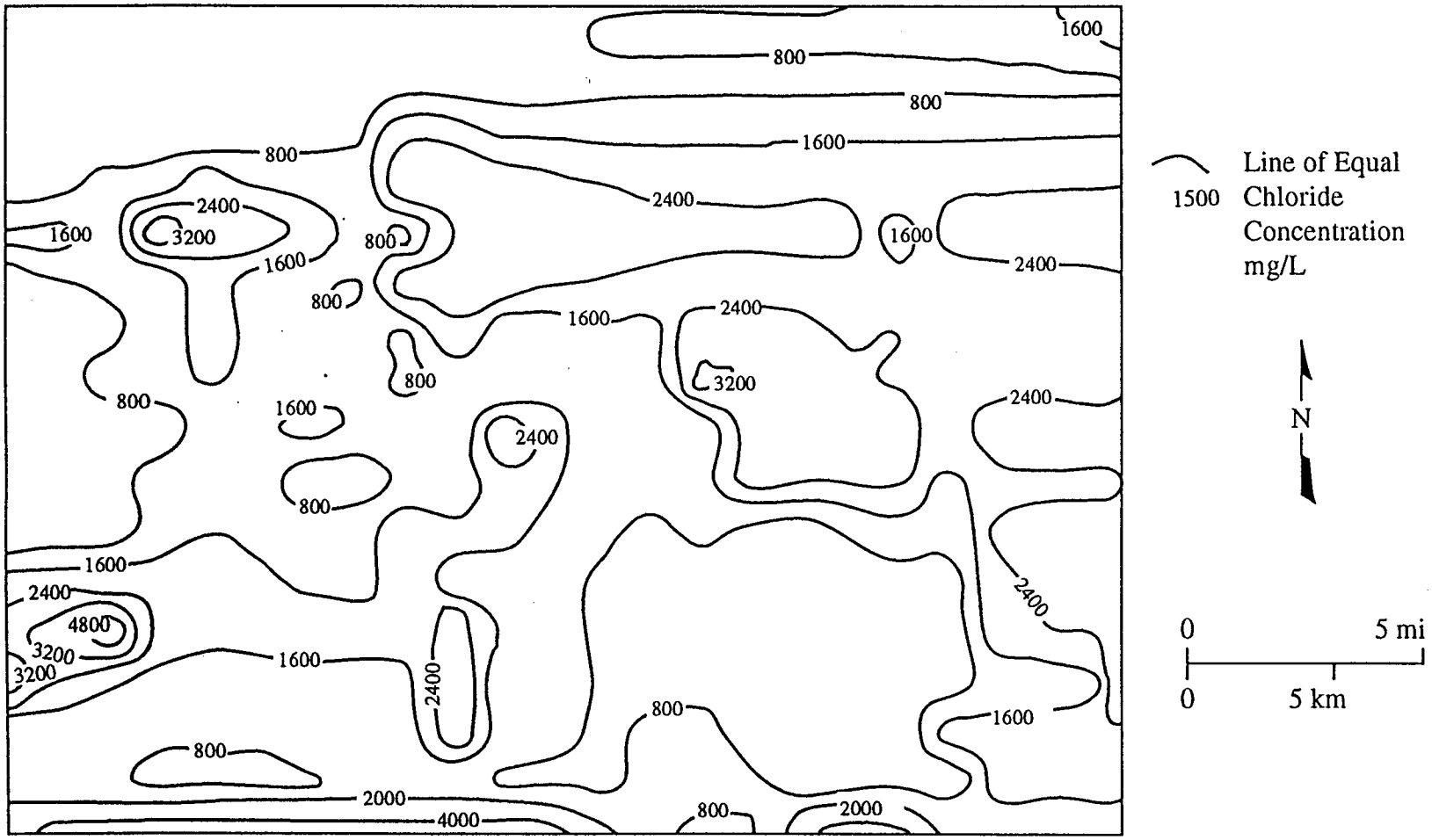

Figure 6.9: Map showing the chloride distribution from the model. The contrast between the high and low transmissive regions is about two orders of magnitude. As a result the local highs and lows in the concentration are greater (Simulation S9 in Table 5.1).

6.3.2. Sensitivity Analysis on Simulation C3

When the average hydraulic conductivity is around 10^{-3} m/day, diffusion of chloride from the lower boundary controls the chloride distribution in the aquifer. Figures 5.8 and 5.6b show the concentration gradient in the lower boundary and the resulting chloride distribution in the aquifer. In order to test the influence of the concentration assigned to the lower boundary, MT3D was run first with a uniform chloride concentration of 2,000 mg/L assigned to the lower boundary (Simulation S10 in Table 6.1) and then with a uniform chloride concentration 10,000 mg/L (Simulation S11 in Table 6.1). The resulting chloride distributions are shown in Figures 6.10a and 6.10b. These figures accentuate the control that the lower boundary has on the distribution of chloride in the aquifer. The concentration of the lateral flow coming into the model through the western edge has only a minor effect on the distribution of chloride. A reduction in the K_v of the Upper Cretaceous aquitard had an insignificant effect on the chloride distribution, but an increase in the value had a similar effect as was seen in Simulation C2, i.e. the aquifer was flushed of chloride. Dispersion and porosity have little impact on the distribution of chloride in the aquifer, since these parameters influence advective transport.

6.4. Summary of Sensitivity Analysis Results

This section summarizes the sensitivity of the flow and transport processes to changes in the aquifer properties used in the flow and transport models. Macfarlane (1993) stated that the flow system of the upper Dakota aquifer is most sensitive to increases in the K_v of the Upper Cretaceous aquitard and secondarily sensitive to the horizontal hydraulic conductivity of the aquifer. However, a modification of this statement, at least at the subregional scale, should be that the flow model is most sensitive to the balancing of the lateral flow in the model with the recharge coming though the Upper Cretaceous aquitard. If the percentage of recharge to the total flow in the aquifer exceeds a certain threshold, the RMS error increases dramatically. This

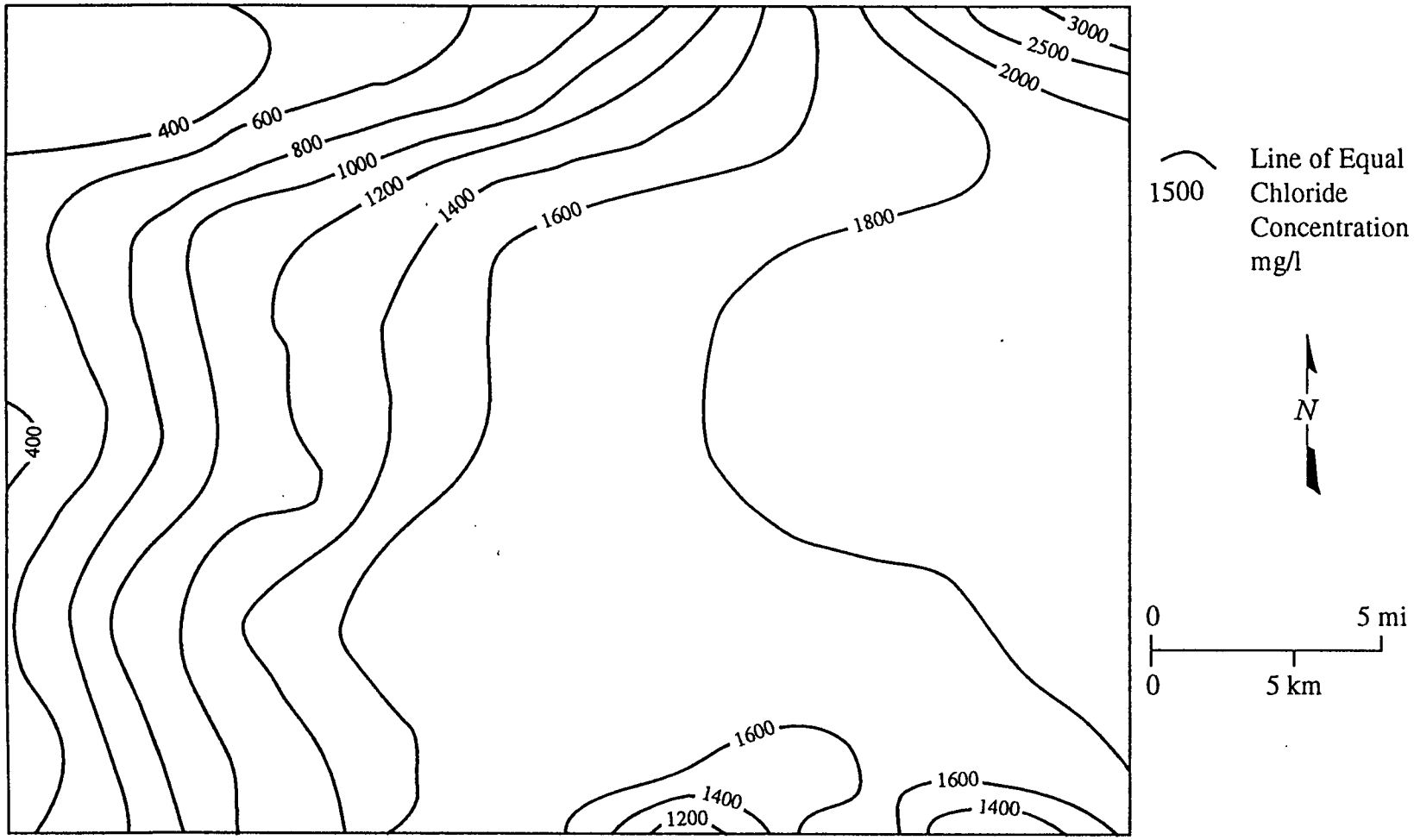

Figure 6.10a: Map showing the resulting chloride distribution from the model (Simulation S10 in Table 5.1). The regional hydraulic conductivity is 0.001 m/day. The bottom layer has a constant concentration of 2000 mg/L.

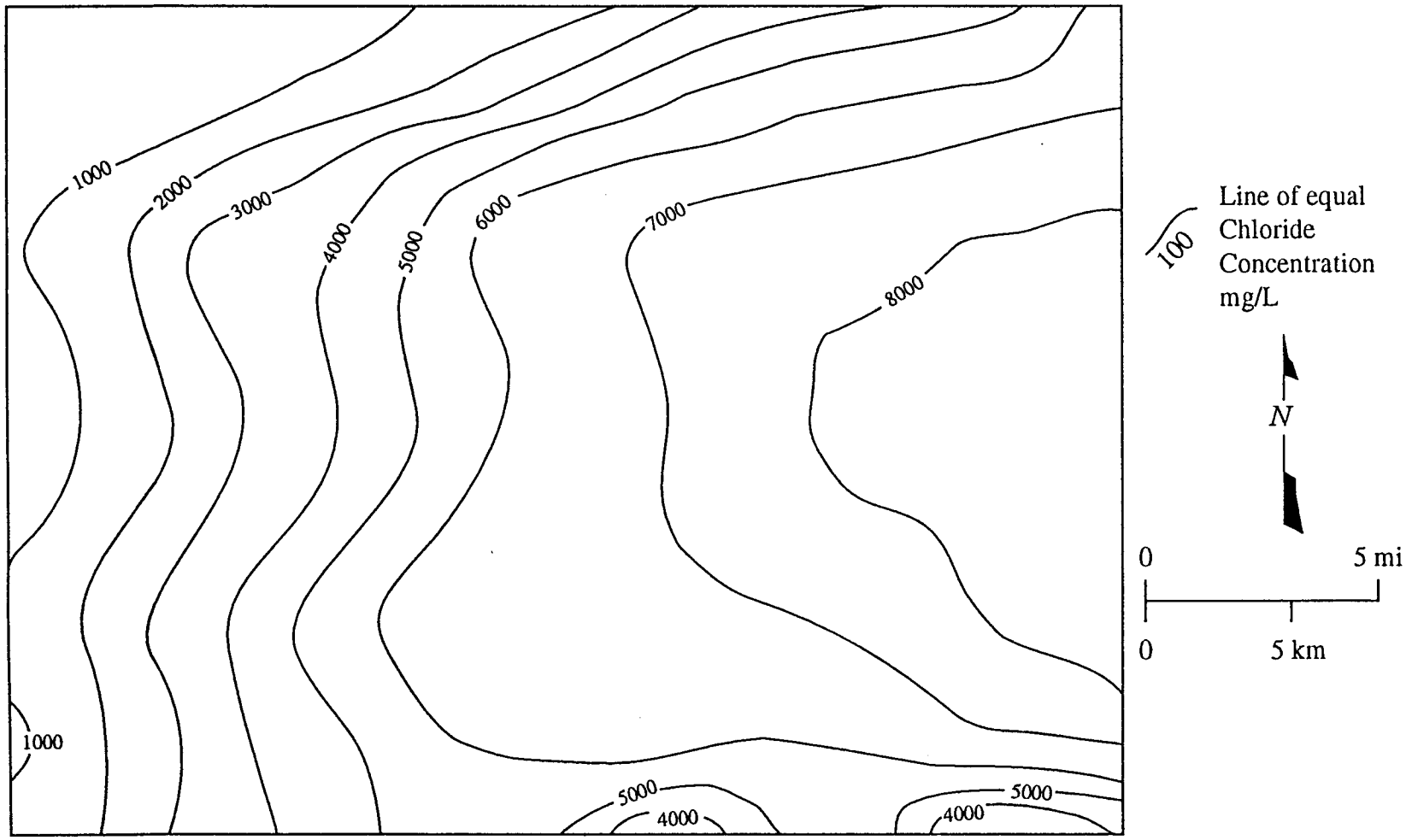

Figure 6.10b: Map showing the resulting chloride distribution from the model (Simulation S11 in Table 5.1). The regional hydraulic conductivity is 0.001 m/day. The bottom layer has a constant concentration of 10,000 mg/L.

can be seen in Figures 6.1 and 6.2. Increasing the K_v of the Upper Cretaceous aquitard has the same general effect as decreasing the K_h of the aquifer. Anisotropy is the next major parameter to which the flow model has a large degree of sensitivity (Figure 6.4). Heterogeneity has only a small effect on the flow field (Figures 6.7 and 6.8) as does the K_v of the aquifer (Figure 6.3).

The transport simulations were most sensitive to increases in the percentage of recharge coming through the Upper Cretaceous aquitard relative to the total flow. If the percentage of recharge was too great, then the aquifer was flushed of chloride (see Section 5.3.1). The regional hydraulic conductivity of the aquifer controlled the time involved for the overall flushing of chloride through the aquifer. However, the processes controlling the distribution of chloride in the aquifer depended on the average regional velocity of the ground-water flow field. Advective transport dominated at higher velocities (Simulation C2 in Table 5.1) and diffusive transport at lower velocities (Simulation C3 in Table 5.1). The heterogeneity of the aquifer was only significant for the higher velocity field. At a high regional hydraulic conductivity (Simulation C2 in Table 5.1), chloride distribution was greatly effected by the heterogeneity of the aquifer. At a low regional hydraulic conductivity (Simulation C3 in Table 5.1), the specified chloride concentration for the lower boundary had the greatest control on the distribution of chloride in the model domain (Figures 6.10a and 6.10b). Effective porosity was only important in Simulation C2 because it served to modify the velocity field of the aquifer thus having an impact on the distribution of chloride throughout the model. Dispersion parameters had only a minor to negligible effect on the transport of chloride.

CHAPTER 7. EVALUATION OF PUMPING WELLS

7.1. Introduction

As was mentioned in Chapter 1, the Dakota aquifer is being considered as a potential water resource to replenish dwindling water supplies of central and western Kansas. However, there are several problems associated with developing the Dakota aquifer as a water resource. A major complicating factor is the difficulty in finding aquifer subunits large enough to accommodate high capacity pumping wells, especially considering the amount of local variability in the aquifer subunits. In Ellis County another concern is the possible effect the pumping of wells could have on the regional water quality of the aquifer. This is because of the existence of higher salinity waters in the eastern half of the county. The concern is that heavy development could cause the encroachment of the transition zone between fresh and saline water. Therefore, the model developed for this thesis was used to determine the possible effect pumping wells could have on the distribution of chloride in the aquifer.

7.2. Transient Calibration from Pumping Test Results

Under pumping conditions the storativity of the aquifer becomes an important parameter. Therefore the flow model was first calibrated for storativity before different pumping scenarios are investigated. As was mentioned in Section 4.4.3b, data from pumping tests indicate that the storativity of the aquifer should range between 10^{-3} and 10^{-5} for the sandstones. Data from pumping tests showed average drawdowns to range between 15 and 18 m (50 and 60 ft) over a three day period when the well was pumped at a rate of 12.6 L/sec (200 gal/min; Macfarlane, personal communication, 1994).

The pumping test discussed in the above paragraph was simulated to calibrate the model for the storativity parameter. A pumping well was placed in row 9 column 12 of layer 3 in the model. Because the model layers were partitioned into high and

low transmissive regions it was assumed that the storativity differs between regions. An order of magnitude difference in the storativity was assumed to exist between the high and low transmissive regions because of the difference in the content of mudstone. It was determined that a storativity of around 7×10^{-3} (Figure 7.1) is representative for the high transmissive regions. Therefore, a value of 7×10^{-2} was assumed for the low transmissive regions. This model was then used to determine the effects, if any, that development could have on the regional water quality in the aquifer.

7.3. Some Results of Pumping Wells in the Upper Dakota Aquifer

Once the flow model was calibrated for the pumping well, pumping was simulated for the purpose of determining whether withdrawals would have an impact on the water quality in the region. To begin the pumping scenarios a single well was pumped continuously at a rate of 12.6 L/sec (200 gal/min; Figure 7.2). The model results indicate that there is no effect on the chloride distribution in the aquifer after ten years of pumping. It was also determined that the pumping of many wells also had little impact on the regional water quality of the aquifer.

Two reasons are offered as explanation for why there is no impact on the regional water quality in the aquifer due to the pumping of wells. The maximum pumping rate in the aquifer is a limiting factor. Rates of only 5 to 10 L/sec (80 to 150 gal/min) can be maintained in the confined Dakota aquifer because of the low hydraulic conductivity and recharge rates of the aquifer. Low pumping rates also reduce the amount of mixing of waters and are not sufficient to transport higher salinity water to pumping wells over the 10 year period of simulation. Velocities are less than 100 m/yr (325 ft/yr), and the higher salinity water is on the order of many kilometers from the area where wells are likely to be pumped.

Several points on the effect pumping wells have on the flow system can be made. First, the source of water flowing to the well during pumping comes entirely

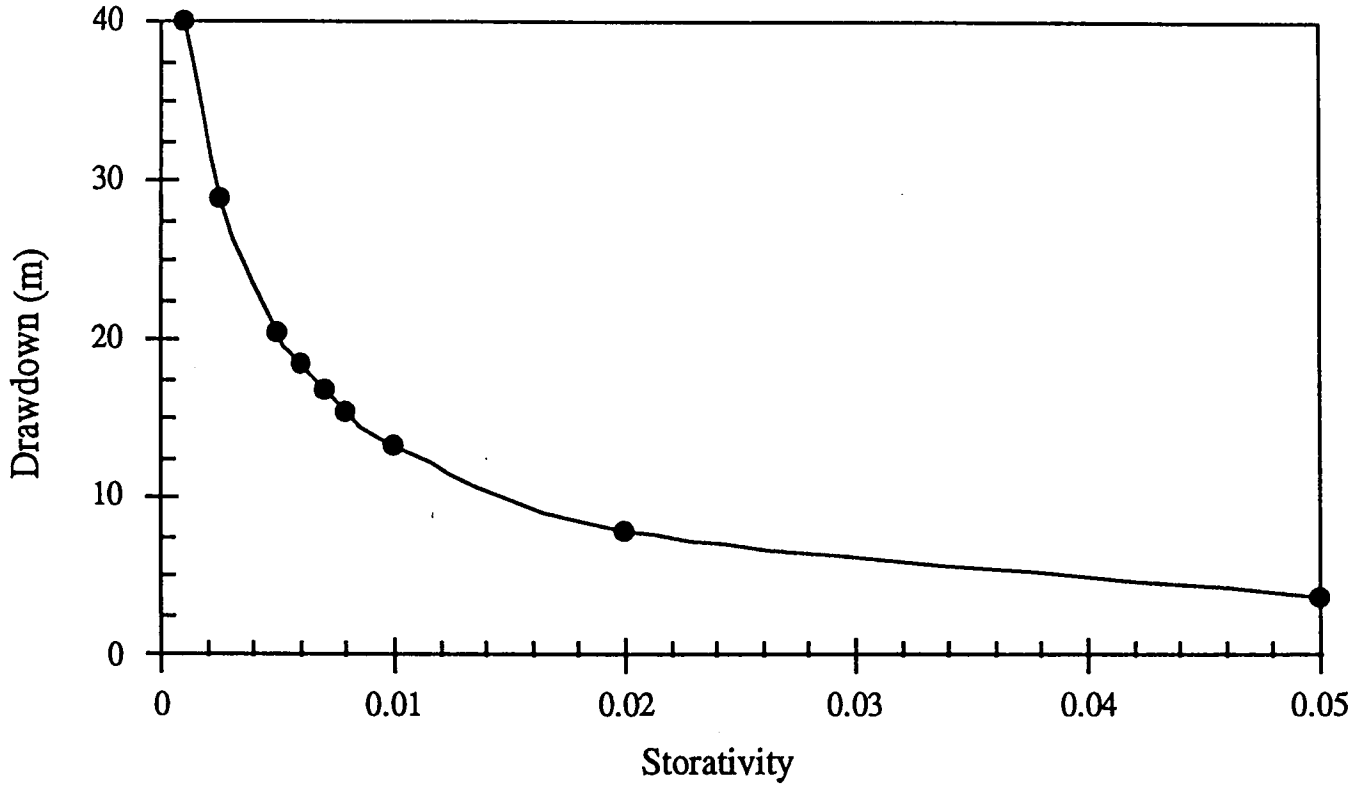

Figure 7.1: Graph of drawdown versus the storativity parameter. In a three day pumping test at 12.6 L/sec (200 gal/min) the drawdown was between 15 and 18 meters, therefore the storativity of the model is about 7×10^{-3}.

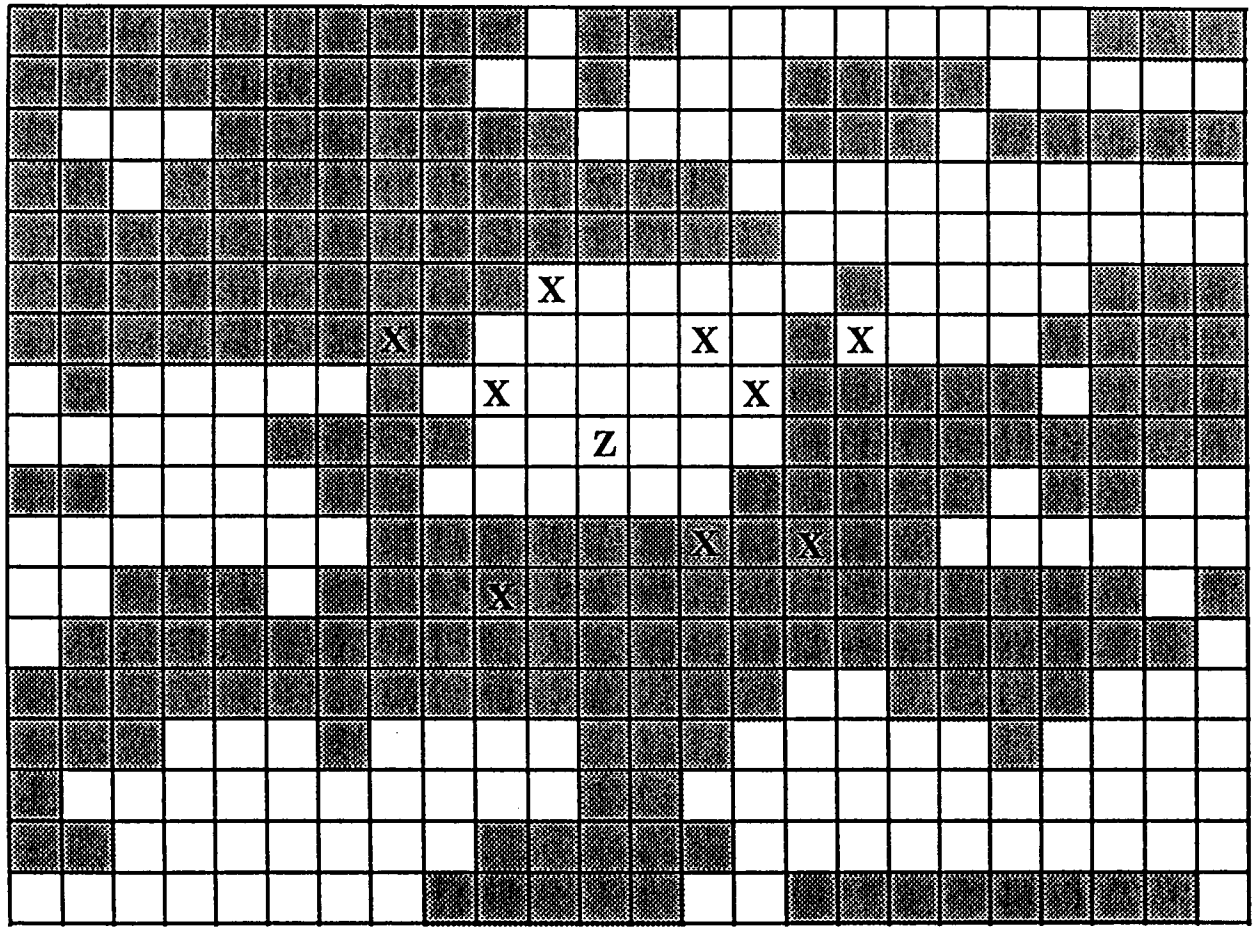

Figure 7.2: Map of the model grid with the high and low transmissive regions in Zone 2 shown. The low transmissive regions are shaded gray. The location of the pumping wells are marked by a Z or an X. The Z marks the location of the single pumping well used to calibrate the model and in the first pumping scenario. The ten pumping wells used in the second pumping scenario are marked by the X's along with the well located in the cell marked with the Z.

from storage. If the well is pumped for a short period (less than a month), storage is released equaling the pumping rate, and induced recharge is insignificant. This occurs until the cone of depression reaches the boundaries of the model, then the amount of water coming from storage decreases while lateral flow from the constant head boundaries increase. However, since this boundary is unrealistic being used only as a matter of convenience, it is more accurate to assume that water will continue to come from storage thus depleting the aquifer of water over the long term.

The cone of depression made by the same pumping well that was used in the previous paragraph is shown in Figure 7.3. The elliptical shape is due to the strong anisotropy of the model. The shape of the cone of depression has an impact on the possible spacing of wells in the upper Dakota aquifer. Well spacing should be at least 32 km (20 miles) along an east-west trend and 8 km (5 miles) along a north-south trend to prevent the overlap of cones of depression. However, the east-west spacing may need to be greater if the cone of depression continues to grow during pumping past the boundaries of the study area. Overlapping cones of depression result in increasing drawdowns at the pumping wells and cause over development of the aquifer. To demonstrate the effect that wells could have on each other 10 wells were pumped at a rate of 6.3 L/sec (100 gal/min) for 10 years (Figure 7.2). A map of the drawdown produced by the model is shown in Figure 7.4.

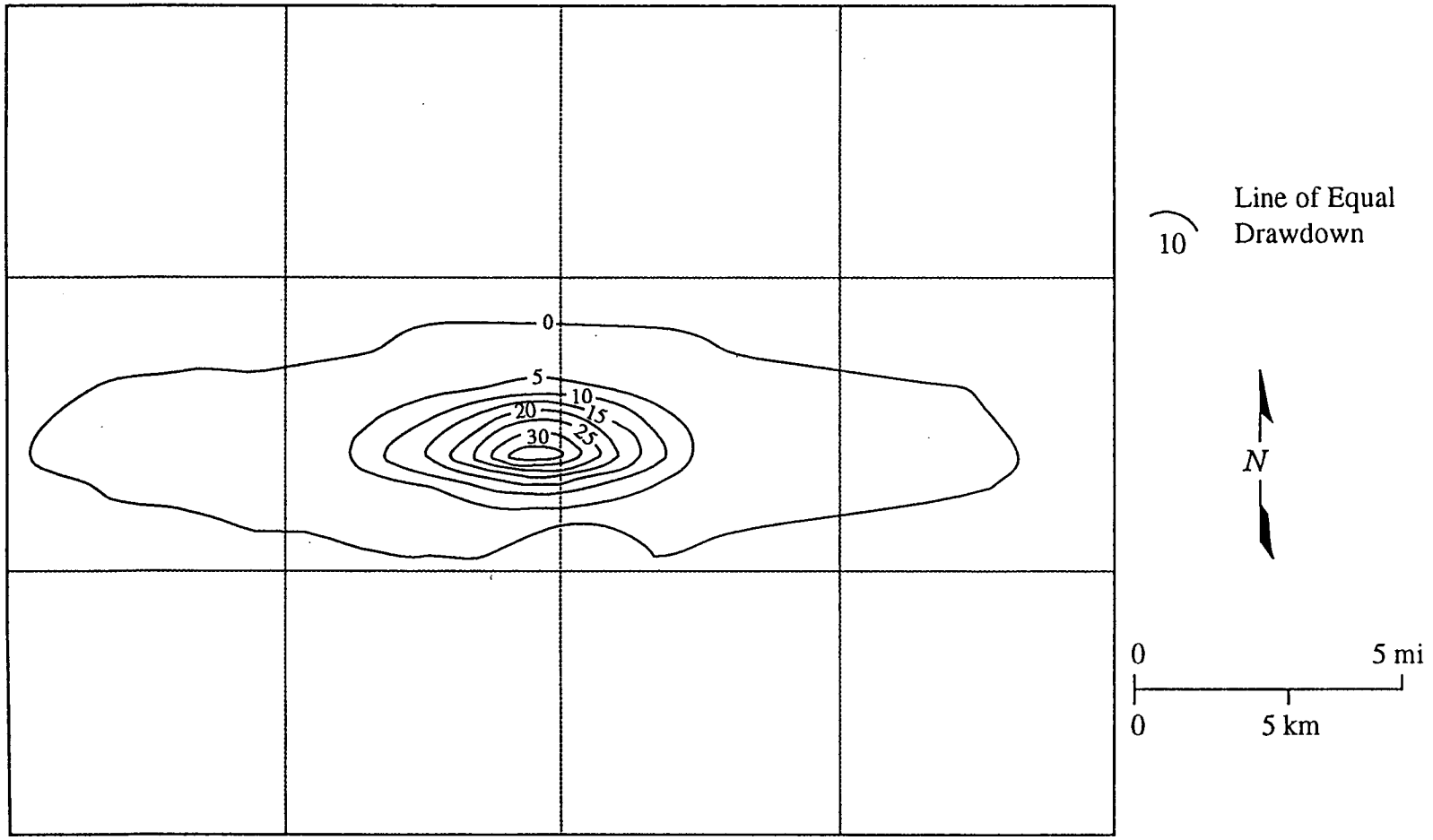

Figure 7.3: Contours of drawdown due to one pumping well. The anisotropy in the aquifer forces the cone of depression to be elliptical. This would imply that wells should be placed farther away from each other in an east-west direction and could be closer to one another in a north-south direction. For scale, the township lines are shown. One township is 6 by 6 miles (6 miles = 9.656 km). Contour interval is 5 m (16.4 ft).

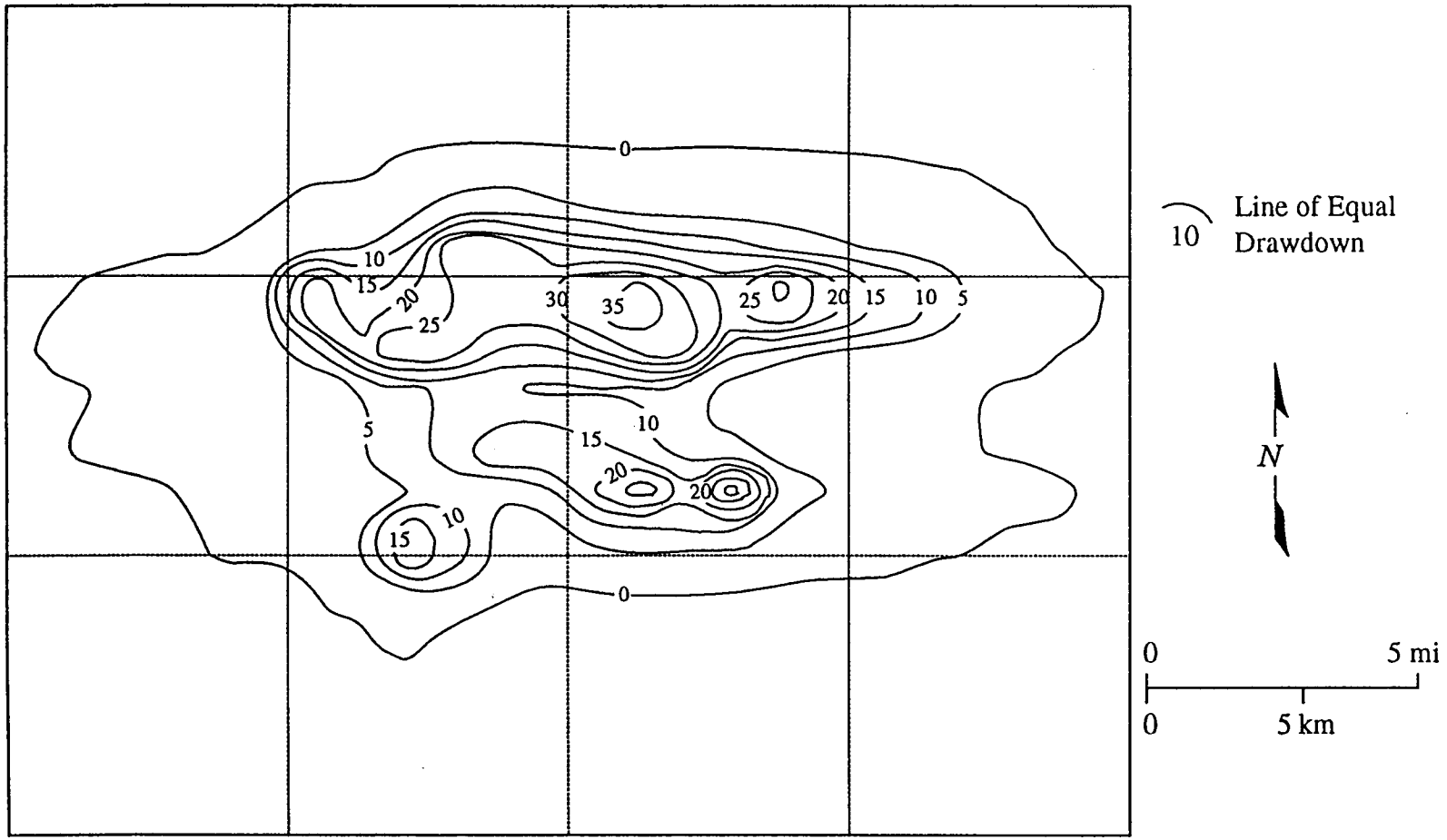

Figure 7.4: Contours of drawdown due to ten pumping wells. The anisotropy in the aquifer forces the cones of depression to be elliptical. For scale the township lines are shown. One township is 6 by 6 miles (6 miles = 9.656 km). The wells located in the low transmissive regions of the layer have more drawdown associated with the pumping well. Contour interval is 5 m (16.4 ft).

CHAPTER 8. SUMMARY AND CONCLUSIONS

The objectives of this thesis were to: 1) describe the arrangement and occurrence of aquifer subunits in the upper Dakota aquifer (Dakota Formation), 2) characterize aquifer subunit heterogeneity, 3) determine the effects of heterogeneity on ground-water flow and mass transport, 4) describe the various factors influencing the distribution of chloride in the study area, and 5) assess the potential effects of development on the regional ground-water flow and quality. These objectives were accomplished in two phases. The first phase described the geologic framework and aquifer subunit distribution, and the second phase included flow and transport modeling of the upper Dakota aquifer. Information gained from phase one helped describe the heterogeneity of the aquifer assisting the flow and transport modeling during the second phase.

Gamma-ray logs of the subsurface were used to describe the geologic framework and aquifer subunit distribution within the Dakota Formation. The Dakota Formation was divided into three zones approximating the depositional systems represented in the formation. The strata of the upper zone are strongly marine influenced, while the middle and lower zones are alluvial. Directional semivariograms were used to determine the range of correlation of the aquifer subunits along specific orientations. Each of the three zones is distinctly different from the others. The range of correlation is greatest in the upper zone with the major axis of anisotropy trending north-south (parallel to depositional strike). The middle zone is also anisotropic with the major axis of anisotropy trending east-west (perpendicular to depositional strike). The lower zone had the greatest overall thicknesses but was isotropic. The analysis emphasized the high degree of local variability in thickness values less than the lag spacing of 535 m (1760 ft). This was shown by the extreme nugget effects observed in the semivariograms, from 40% to 60% of the sill value. But at the same time, there is some degree of correlation at a scale of several kilometers.

Block kriging was then used to assign an average thickness of the aquifer subunits to a grid. This grid corresponded to the one used for ground-water flow and single-constituent, conservative, mass-transport modeling. High and low transmissive regions were determined using a thickness threshold of 6 m (20 ft) to separate the two regions. The model layers corresponding to the lowest zone of the Dakota Formation were determined to be the most transmissive. The horizontal anisotropy in the flow model was determined to be large with the hydraulic conductivity 100 times lower in the north-south direction as compared to the east-west direction. However, only a near-optimal flow model could be calibrated due to the uncertainty in model parameters and the lack of sufficient data for further calibration. Therefore, it was determined that various hydraulic conductivity fields were possible.

Because of bias in the flow parameters and the uncertainty in model calibration, two end-member hydraulic conductivity fields were used to investigate mass transport. The first was considered representative of the aquifer subunits and was assumed to consist of well-connected aquifer subunits producing high regional continuity. The second was considered representative of the aquitard subunits and was assumed to consist of poorly-connected aquifer subunits producing low regional continuity. Processes of mass transport were determined to be quite different in the two hydraulic conductivity fields. Advection dominates the first hydraulic conductivity field, (regional K_h = 1 m/day) and lateral flow from the west controls the distribution of chloride in the model. However, diffusion dominates the mass transport process in the second hydraulic conductivity field (regional $K_h = 1 \times 10^{-3}$ m/day), and the specified concentration in the lower aquitard controls the chloride concentration in the model.

Because the time required to reproduce the observed chloride distribution in the second hydraulic conductivity field was unreasonably long (order of 10^9 years), it was determined that the aquifer subunits must be sufficiently interconnected to provide regional conduits for ground-water flow. Furthermore, it is hypothesized that the presence of both aquifer and aquitard subunits must modify each other's chloride

content to account for the observed distribution of chloride. However, the simulation of this process was not possible with the model design used in this investigation. The degree of interconnection is one of the major questions that was not easily answered by this project and is an area that will require much more work. A better description of the interconnection of the aquifer subunits throughout the Dakota Formation will be critical in understanding the dynamics of the aquifer.

Finally, the model was used to simulate the effects of pumping wells in the confined upper Dakota aquifer. The model results demonstrate that there should be no significant regional deterioration in water quality in the aquifer due to pumping wells over at least a ten year period. This is because pumping rates are too low (5 to 10 L/sec) and induced velocities (less than 100 m/yr) in the aquifer are not sufficient to transport saline water from the eastern half of the county to the pumping well over the ten year period that was simulated. It was determined that water flowing to a single pumping well comes primarily from the depletion of storage in the aquifer, and induced recharge is insignificant. Due to the extreme anisotropy in the horizontal hydraulic conductivity, the pumping of a single well produces an elliptical cone of depression, elongated in an east-west direction. Therefore, the spacing of wells in the upper Dakota aquifer should be longer in the east-west direction than in the north-south direction to avoid overlapping cones of depression.

However, the major question on the local effects of development still remains. This question could possibility be answered by a model constructed at a very local scale, i.e. several square kilometers. However, a model of this type will likely have to be a hypothetical case. This is due to the lack of data available to define in detail the geologic framework of the aquifer at that scale. Even in areas with the greatest well control, it is difficult to say with any degree of certainty the three-dimensional arrangement of aquifer and aquitard subunits. It is precisely this arrangement that will be critical in understanding aquifer dynamics at the local scale.

REFERENCES

Allen, J.R.L., 1978, Studies in fluviatile sedimentation: an exploratory quantitative model for the architecture of avulsion-controlled alluvial suites: Sedimentary Geology, Vol. 21, p. 129-147.

Anderson, M.P., and Woessner, W.W., 1992, Applied groundwater modeling simulation of flow and transport: Academic Press, 381 p.

Belitz, K.,1985, Hydrodynamics of the Denver basin: an explanation of subnormal fluid pressures (Ph.D. dissertation): Stanford University, 194 p.

Davis, J.C., 1986, Statistics and data analysis in geology, 2nd edition: John Wiley & Sons, Inc., 646 p.

Deutsch, C.V., and Journel, A.G., 1992, GSLIB: Geostatistical Software Library and User's Guide (version 1.2): Oxford University Press, 314 p.

Domenico, P.A., and Schwartz, F.W., 1990, Physical and chemical hydrogeology: John Wiley and Sons, 842 p.

Doveton, J.H., 1991, Reading the rocks from wireline logs: Kansas Geological Society Short Course, 104 p.

Fenneman, N.M., 1946, Physical subdivisions of the United States (Map): United States Geological Survey, 1:700,000, 1 sheet.

Fogg, G.E., 1989, Stochastic analysis of aquifer interconnectedness: Wilcox Group, Trawick area, east Texas: Bureau of Economic Geology, Report of Investigations No. 189, 68 p.

Franks, P.C., 1966, Petrology and stratigraphy of the Kiowa and Dakota Formations (basal Cretaceous), north-central Kansas (Ph.D. dissertation): University of Kansas, 2 volumes, 312 p.

Freeze, R.A., and Cherry, J.A., 1979, Groundwater: Prentice-Hall, Inc., 604 p.

Hamilton, V.J., 1989, Stratigraphic sequences and hydrostratigraphic units in lower Cretaceous strata in Kansas (M.S. thesis): Colorado School of Mines, 165 p.

Hamilton, V.J., 1994, Sequence stratigraphy of Cretaceous Albian and Cenomanian strata in Kansas: *in* Shurr, G.W., Ludvigson, G.A., and Hammond, R.H., eds., Perspectives on the Eastern Margin of the Cretaceous Western Interior Basin: Boulder, Colorado, Geological Society of America Special Paper 287, p. 79-95.

Helgeson, J.O., Leonard, R.B., and Wolf, R.J., 1993, Hydrology of the Great Plains aquifer system in Nebraska, Colorado, Kansas, and adjacent areas: United States Geological Survey Professional Paper 1414-E, 80 p.

Holdoway, K., 1978, Deposition of evaporites and red beds in the Nippewalla Group, Permian, Western Kansas: Kansas Geological Survey Bulletin 215, 43 p.

Isaaks, E.H., and Srivastava, R.M., 1989, An introduction to applied geostatistics: Oxford University Press, 561 p.

Keene, K.M., and Bayne, C.K., 1977, Ground Water in Cretaceous rocks in Kansas: Kansas Geological Survey Chemical Quality Series 5, 18 p.

Macfarlane, P.A., Whittemore, D.O., Townsend, M.A., Doveton, J.H., Hamilton, V.J., Coyle, W.G., Wade, A., Macpherson, G.L., and Black, R.D., 1990, The Dakota Aquifer Program: Annual Report, FY89: Kansas Geological Survey Open-File Report 90-27 (report and map plates addendum), 301 p.

Macfarlane, P.A., Wade, A., Doveton, J.H., and Hamilton, V.J., 1991, Revised stratigraphic interpretation and implications for pre-Graneros paleogeography from test-hole drilling in central Kansas: Kansas Geological Survey Open-File Report 91-1A, 73 p.

Macfarlane, P.A., Whittemore, D.O., Chu, T., Butler, J.J., Jr., Wade, A., Coleman, J., Doveton, J.H., Mitchell, J., and Kay, S., 1992, The Dakota Aquifer Program: Annual Report, FY91: Kansas Geological Survey Open-File Report 92-1, 93 p.

Macfarlane, P.A., 1993, The effect of topographic relief and hydrostratigraphy on the upper part of the regional ground-water flow system in southeastern Colorado and western and central Kansas, with emphasis on the Dakota aquifer (Ph.D. dissertation): University of Kansas, 197 p.

Macfarlane, P.A., Doveton, J.H., Feldman, H.R., Butler, J.J., Jr., Comes, J.M., and Collins, D.R., 1994, Aquifer/aquitard units of the Dakota aquifer system in Kansas: methods of delineation and sedimentary architecture effects on ground-water flow and flow properties: Journal of Sedimentary Research, Vol. B64, No. 4, p. 464-480.

Macfarlane, P.A., 1994, personal communication.

McDonald, M.G., and Harbaugh, A.W., 1988, A modular three-dimensional finite-difference ground-water flow model: Techniques of Water-Resources Investigations of the United States Geological Survey, Book 6, Chapter A1, 528 p.

Swineford, A., and Williams, H.L., 1945, The Cheyenne Sandstone and adjacent formations of a part of Russell County, Kansas: Kansas Geological Survey Bulletin 60 part 4, p. 101-168.

Van De Graaff, W.J.E., and Ealey, P.J., 1989, Geological Modeling for Simulation Studies: The American Association of Petroleum Geologists Bulletin, Vol. 73, No. 11, p. 1436-1444.

Wade, A., 1992, Ground-water flow systems and the water-resources potential of the Dakota aquifer in a two-county area in north-central Kansas (M.S. Thesis): University of Kansas, 158 p.

Whittemore, D.O., and Fabryka-Martin, J., 1992, Halogen geochemistry of Cretaceous sandstone aquifers of North America: *in* Kharaka, Y.K., and Maest, A.S. eds., Proceedings of the 7th International Symposium on Water-Rock Interaction, Rotterdam, Netherlands, A.A. Balkema Publishers, p. 855-858.

Whittemore, D.O., 1994, TDS contours for upper Dakota aquifer (Map): work is unpublished.

Whittemore, D.O., 1994, personal communication.

Zheng, C., 1990, A modular three-dimensional transport model for simulation of advection, dispersion and chemical reactions of contaminants in groundwater systems: S.S. Papadopulos & Associates, Inc., prepared for the United States Environmental Protection Agency, Robert S. Kerr Environmental Research Laboratory, 72 p.

Appendix 1: Gamma-Ray Log Database

The following table contains the well logs used for this thesis. The location, company name, well name, and the elevation listed on the log are given. All townships are south and all ranges are west. The ID# is the catalogue number assigned by the author for the purpose of handling the information in an electronic database. It is also the reference number used in Appendix 2 where the unit thicknesses and formation tops are listed. Every effort was made to reduce errors to a minimum; however, the following list is not guaranteed to be free from errors. The elevation is given in feet above sea level since that is the way it was listed on the log (1 foot = 0.3048 m).

ID	T	R	Sec. Loc.	Company Name	Wel Name	Elevation
1	12	16	31ADD	Leben, etal	Miller #1	2015
2	12	17	31ADC	Brooks Hall Oil Corp.	Karlin #1	2084
3	12	17	31DDDC	Messman & Rinehart Oil Co.	Karlin #3	2076
4	12	17	32DBC	Beacon Resources Corp.	Staab #1	2096
5	12	17	32DBB	Beacon Resources Corp.	Staab #2	2121
6	12	17	32DBD	Beacon Resources Corp.	Staab #3	2081
7	12	17	32DBA	Beacon Resources Corp.	Staab #4	2095
8	12	17	33DACB	Petroleum, Inc.	Schmidt #1-A-C	2056
9	12	17	34AAC	Clinton Oil Co.	Schmeidler #1-V	2063
10	12	17	34AAB	Clinton Oil Co.	Schmeidler #2-D	2073
11	12	17	34ADD	H.A. Horwitz	Schmeidler #1	2085
12	12	17	34CAB	K & E Drilling, Inc.	Schmidt #1	2046
13	12	17	34CBD	Pentagon Corp.	Schmidt #1	2067
14	12	17	35CAB	Staab Oil Co.	Leikan #2 SWD	------
15	12	18	28DCC	Bergman Oil Co.	Dumler #1	2144
16	12	18	29ABB	Rains & Williamson Oil Co.	Joy #1	------
17	12	18	34CBBB	Dreiling, LTD of Colorado	Marintzer #1	2126
18	12	18	34DAB	Raymond Oil Co.	Jensen #1	2089
19	12	18	34ACCA	The National Oil Co., Inc.	Lueke #1	2096
20	12	18	35DDD	The Texas Co.	A. Jensen #1	2083
21	12	18	35DDA	The Texas Co.	A. Jensen #2	2089
22	12	18	35DDC	The Texas Co.	A. Jensen #3	2091
23	12	18	35DAD	The Texas Co.	A. Jensen #5	2087
24	12	18	35DAA	The Texas Co.	A. Jensen #6	2093
25	12	18	35DDB	The Texas Co.	Jensen #4	2095
26	12	18	36CDC	Sierra Petroleum Co.	Walters #1 SWD	2055
27	12	18	36CCC	Trans-Era Petroleum, Inc.	Schmidt #1	2081
28	12	18	36CCB	Trans-Era Petroleum, Inc.	Schmidt #2	------
29	12	18	36CBC	Trans-Era Petroleum, Inc.	Schmidt #3	2078
30	12	18	36CBB	Trans-Era Petroleum, Inc.	Schmidt #4	2081
31	12	18	36CCAB	Trans-Era Petroleum, Inc.	Schmidt #5	------
32	12	19	26BBC	Kern Drilling Co.	Johnson #1	2172
33	12	19	26CCD	Raymond Oil Co.	Ubert #2	2170
34	12	19	26CCCA	Raymond Oil Co., Inc.	Ubert #1	2159
35	12	19	27DBB	Graybol Oil Corp.	Drieling #1	2166
36	12	19	27DDDB	Raymond Oil Co.	Dreiling #2	2142

ID	T	R	Sec. Loc.	Company Name	Wel Name	Elevation
37	12	19	27DDB	Raymond Oil Co., Inc.	Dreiling #1	2146
38	12	19	27BBD	Smokey Hill Exploration	Denning #1	2156
39	12	19	31ADA	Martin & Keller	Schoenthaler #2	2146
40	12	19	32DCD	Dalco Exploration Co.	Bahl #1-A	2156
41	12	19	32BCA	Martin & Keller	Amerine #2	2125
42	12	19	32BCB	Martin & Keller	Amrein #1	2130
43	12	19	32CBD	Martin & Keller	Bahl #1	2136
44	12	19	32CBA	Martin & Keller	Bahl #2	2149
45	12	19	32CDB	Martin & Keller	Bahl #3	2152
46	12	19	35DAA	Raymond Oil Co.	Wolf #1	------
47	12	20	31CDD	Murfin Drilling Co.	Bittel #7-A	2198
48	12	20	31BC	Sunray DX Oil Co.	Huber #6-A	2197
49	12	20	31DABB	Sunray Mid-Continent Oil Co.	Bittle #6-A	2178
50	12	20	31BDDB	Sunray Mid-Continent Oil Co.	Huber #2-A	2181
51	12	20	31BAB	Sunray Mid-Continent Oil Co.	Huber #5-A	2199
52	12	20	31???	Sunray Oil Corp.	Huber #1-B	2182
53	12	20	31DBAC	Sunray Oil Corp.	Huber #1-B	2182
54	12	20	31ACDB	Sunray Oil Corp.	Huber #2-B	------
55	12	20	32CCDB	J.B. Collins	Huber #1	2169
56	12	20	32DDC	Lions Oil Co.	Schubert #1	2159
57	12	20	32ABC	Murfin Drilling Co.	Huber #1	2190
58	12	20	33CDC	C & G Drilling Co.	Erbert #1	2170
59	12	20	34ADD	Frontier Oil Co.	Schneller #1	2183
60	12	20	34DCC	Lion Oil Co.	Lee #1	2163
61	12	20	34BCA	Petroleum, Inc.	Schmeidler #1-H	2150
62	12	20	35CCA	Petroleum, Inc.	King #1-K	2199
63	12	20	35CCB	Petroleum, Inc.	King #2-K	2202
64	12	20	35CBB	Petroleum, Inc.	King #3-K	2197
65	12	20	35BCC	Rupe-Stoskopf & Glasco	King #1	2189
66	12	20	36BAAC	Winwell 1968 Exploration Co.	Schwagel #1	2156
67	12	21	36BDA	Cooperative Refining Assoc.	Gugler #4-A	2222
68	12	21	36CBDB	Murfin Drlg & Patton Oil Co.	Gugler #12-A	2194
69	12	21	36CDAC	Murfin Drilling Co.	Gugler #2	2198
70	12	21	36CCBB	Murfin Drilling Co.	Gugler #3	2206
72	13	16	6ACA	J.L. King Oil Co.	Windholz #2 SWD	2016
73	13	16	6BDD	Lion Oil Co.	Brungardt #1	2000
74	13	16	6BBD	San Juan Oil/Sterling Drlg	Hammerschmidt #1	2009
75	13	16	7CBC	L.J. Dreiling Oil Co.	Sanders #1	2017
79	13	16	18BAA	Alpine Oil & Royalty Co., Inc.	Windholtz #1	2006
80	13	16	18CCC	Murphy Oil Co.	Pfeifer #1	1997
81	13	16	18ACB	Petroleum, Inc.	Von Lintel #1-B	1995
82	13	16	19ACC	Artnell Co.	Rome #1-A	1992
84	13	16	30AAB	Gulf Oil Corp.	Theodore Gore #3	1982
85	13	16	30DDC	Jay Kornfeld	Sanders #3	1931
86	13	16	31ADA	Artnell Co.	Brungardt #1	1962
87	13	16	31CCA	Dreiling, LTD	Braun #1	1979
88	13	16	31DDCA	Range Oil Co.	Peter Braun #1	1968
89	13	16	31CBA	V. Francis Weigel	Braun #1-A	1990
90	13	16	32BBDB	R.P. Nixon	P. Brown #3 SWD	1929

ID	T	R	Sec. Loc.	Company Name	Wel Name	Elevation
91	13	17	2ABC	Gear Petroleum Co.	Staab #1-2	2062
92	13	17	3ACC	Earl F. Wakefield	Schmidt #1-B	2031
93	13	17	3ADA	Earl F. Wakefield	Schmidt #5-B	2053
94	13	17	3DCC	Hi-Kat Petroleum	Walter #1 SWD	2009
95	13	17	3BAD	Raymond Oil Co., Inc.	Schmidt #1	2032
96	13	17	4CDD	G.M.R. Oil Co.	Wolf #1-A	2060
97	13	17	4DCC	Isis Operating Co.	Walters #2-A	2054
98	13	17	4BAC	The Texas Co.	M. Wolf #5	2079
99	13	17	4BAD	W.L. Hartman	Wolf #1	------
100	13	17	5BBD	Rains & Williamson Oil Co.	Scheneidler #1	2037
101	13	17	6BBC	Colorado Oil & Gas Corp.	Polifka #3	2074
102	13	17	6AAB	Tenneco Oil Co.	Alois Schmidt etal #1	2070
103	13	17	6ACB	Vicorp Energy, Inc.	A. Lang #1	2066
104	13	17	7BDD	Continental Oil Co.	R. Staab #1	2052
105	13	17	7BDB	Continental Oil Co.	R. Staab #2	2041
106	13	17	7BDA	Continental Oil Co.	Staab #3	2036
107	13	17	8BAA	Francis Polifka	Polifka #1-F	2040
108	13	17	8ACA	Petroleum, Inc.	Polifka #1	2021
109	13	17	9BAA	G.M.R. Oil Co.	Schmidt #1	2056
110	13	17	10DBD	Kewanee Oil Co.	Giebler #8-B	2004
111	13	17	11DCD	Alpine Oil & Royalty Co., Inc.	Rome #1	2032
112	13	17	11BCC	Cities Service Oil Co.	Anderson #1-C	2016
113	13	17	11AAC	Petroleum, Inc.	Rome #1	2028
114	13	17	11ACC	Sierra Petroleum Co., Inc.	Rome #2	2037
115	13	17	11CBC	Wilkinson Drilling, Inc.	Dreiling #1	2018
116	13	17	12AAA	D Oil Operations	Von Lintel #1	2017
117	13	17	13BDD	Francis Oil & Gas, Inc.	Walters #1	2000
118	13	17	14BAB	Anderson Prichard Oil Corp.	Schuetz #2	2023
119	13	17	14CBD	K & E Drilling Co.	Kuhn #3-A	1989
120	13	17	14DAB	Petroleum, Inc.	Karlin #1-B	2015
121	13	17	15ADD	A.F. Schmidt	Dorzweiler #1	1981
122	13	17	15DAD	K & E Drilling, Inc.	Von Lintel #1	1992
123	13	17	16ABAC	Mallonee Drilling Co.	Catherene #1-A	2020
124	13	17	16AABB	Tomlinson Oil Co., Inc.	Catherene #2-A SWD	------
125	13	17	17AACC	A. Scott Ritchie	Staab #3-A	2019
126	13	17	17ABB	A. Scott Ritchie	Staab #4-A	2032
127	13	17	17AADB	A. Scott Ritchie	Staab #5-A	2007
128	13	17	17CCDD	Derby Oil Co.	Miller #4	2140
129	13	17	17AAB	Scott Ritchie	Staab #2-A	2010
130	13	17	18DAC	W.J. Coppinger Drilling Co.	Polifka #3	2125
131	13	17	19CCD	Clinton Oil Co.	Madden #1-A	2123
132	13	17	19CDC	Raymond Oil Co.	Madden #1	2100
133	13	17	20BAD	W.J. Coppinger	Younger #5	2133
134	13	17	21BCA	Petroleum, Inc.	Hammerschmidt #1-B	2031
135	13	17	21BBD	Petroleum, Inc.	Hammerschmidt #2-B	2004
136	13	17	21BBAC	Petroleum, Inc.	Hammerschmidt #3-B	2018
137	13	17	22???	H.G. Kaiser Oil Operations	Von Lintel #5 SWD	1988
138	13	17	23BAD	Alpine Oil & Royalty Co.	A.M. Kuhn #1	1993
139	13	17	23A	Alpine Oil & Royalty Co.	Dinkie #1	1998

ID	T	R	Sec. Loc.	Company Name	Wel Name	Elevation
140	13	17	23ABC	Alpine Oil & Royalty Co.	Dinkie #2	1996
141	13	17	23CCD	Murfin Drilling Co.	Rome #11-A	1967
142	13	17	23CBB	Murfin Drilling Co.	Rome #5	1967
143	13	17	24ACA	The Texas Co.	J.J. Dinkel #1	1970
144	13	17	25CCB	McNames & Patterson	Braun #1	1978
145	13	17	26CBB	Bell Brothers	Von Lintel #1	1986
146	13	17	26BCD	Bell Brothers	Von Lintel #2	1976
147	13	17	26BBB	Bell Brothers	Von Lintel #3	1974
148	13	17	26BBC	Bell Brothers	Von Lintel #4	1959
149	13	17	26BBA	Bell Brothers	Von Lintel #5	1960
150	13	17	26BAB	Murfin Drilling Co.	Von Lintel #2	1970
151	13	17	27DBD	Gulf Oil Corp.	A.B. Weber #6	1984
152	13	17	27DBB	Gulf Oil Corp.	Ann Weber #9	1987
153	13	17	27CAA	Gulf Oil Corp.	Weber #2	1988
154	13	17	27DBA	Gulf Oil Corp.	Weber #5	1988
155	13	17	27DAB	Gulf Oil Corp.	Weber #7	1989
156	13	17	27DADC	Gulf Oil Corp.	Weber #8	1988
157	13	17	27AAD	Murfin Drilling Co.	Rome #10-A	1986
158	13	17	27AAA	Murfin Drilling Co.	Rome #9-A	1979
159	13	17	29CAC	Chief Drilling Co.	A.J. Lang #1	2050
160	13	17	29CAA	K & E Drilling, Inc.	Lang #1-B	2065
161	13	17	29CAA	Kennedy & Mitchell, Inc.	Lang #43-587	2064
162	13	17	30CCB	Clinton Oil Co.	Dinkel #2-X	2079
163	13	17	30BAA	D.R. Lauck Oil Co.	Brungardt #1	2099
164	13	17	30BBA	Raymond Oil Co.	Brungardt #2	2123
165	13	17	30CAB	Raymond Oil Co.	Dinkel #1	2038
166	13	17	31BCAD	Energy Reserves Group, Inc.	Braun #1-C	2060
167	13	17	31ABD	Raymond Oil Co.	Weisner #2	2041
168	13	17	31DDC	Rosen Oil Co.	Weisner #1	2014
169	13	17	31DACC	TGT Petroleum, Corp.	Weisner #1-A	2025
170	13	17	32CAA	Brack Oil Co.	Hoffman #1	2038
171	13	17	32BDD	Energy Reserves Group, Inc.	Lang #1	2045
172	13	17	32???	H.G. Kaiser Oil Operations	Von Lintel #5 SWD	2030
173	13	17	32ABD	Murfin Drlg/Whitestone Petro	Lang #1	2050
174	13	17	32D	Okmar Oil Co.	Dinkel SWD #?-B	------
175	13	17	32AAB	Victor Drilling Co.	Lang #1	2043
176	13	17	33DACC	Allison & Black	Braun #1-C	2010
177	13	17	33DAC	Allison & Black	Braun #3-C	2004
178	13	17	33DDCD	L & H Oil Operations	Brown #1	1963
179	13	17	33BBD	Patton Oil Co./Murfin Drlg Co.	Weber #2-A	2031
180	13	17	33BAC	Petroleum Management	Weber #1	2007
181	13	17	33ABC	Petroleum, Inc.	Braun #1-A	1997
182	13	17	34DCB	American Petroleum	Braun #8-A	1975
183	13	17	34CAD	Champlin Refining Co.	Dreiling #1	1952
184	13	17	35DBC	Birmingham-Bartlett	Braun #1-A	1936
185	13	17	35CDA	Birmingham-Bartlett	Sanders #2-A	1959
186	13	17	35DCB	Sunray Mid-Continent Oil Co.	Braun #1	1938
187	13	17	35DCC	Sunray Mid-Continent Oil Co.	Braun #2	1932
188	13	17	35DCA	Sunray Mid-Continent Oil Co.	Braun #3	1949

ID	T	R	Sec. Loc.	Company Name	Wel Name	Elevation
189	13	17	36BBB	Anschultz Drilling Co.	Lang #1	1955
190	13	17	36CBB	Tennessee Gas Trans. Co.	Margaret Kuhn #1	1952
191	13	18	1AAB	Colorado Oil & Gas Corp.	Staab #2	2080
192	13	18	1???	Harms & Knight	Urert #1	2052
193	13	18	1ABBD	Karst Brothers Oil Co.	Staab #1 SWD	2062
194	13	18	1CBAB	National Development	Crissman SWD	2135
195	13	18	1AAD	Raymond Oil Co.	Staab #1	2084
196	13	18	2AAD	Alpine Oil & Royalty Co.	Crissman #1-B	2081
197	13	18	2AAA	Alpine Oil & Royalty Co.	Crissman #2-B	2082
198	13	18	3BDB	Jones-Gebert & Clinton Oil	Saunders #1	2146
199	13	18	5DDC	TXO Production Corp.	Arnhold #1	2172
200	13	18	6DBB	Gear Production Co.	Schmeidler #1-6	2172
201	13	18	7ACB	Frontier Oil Co.	Farmers State Bank #1	2173
202	13	18	8ABCD	Dreiling Resources	Polifka #2	2175
203	13	18	8BBCD	Dreiling Resources	Polieka #2	2175
204	13	18	8BA	Dreiling Resources, Inc.	Polifka #4	2149
205	13	18	8DBB	John O. Farmer, Inc.	Polifka #1	2169
206	13	18	9BDC	Dreiling Resources, Inc.	Dreiling #2-D	2166
207	13	18	10CCD	Shields Oil Producers	Fellers #1-A	2158
208	13	18	10CCC	Shields Oil Producers, Inc.	Fellers #2-A	2134
209	13	18	10CBC	Zenith Drilling Co.	Fellers #1	2169
210	13	18	11AAA	Thornton E. Anderson	Dreiling #1	2150
211	13	18	12ABD	Don Pratt	Ubert #2-A	2081
212	13	18	12CDD	Dreiling Resources	Stephen-Ellis #2	2147
213	13	18	12CDBA	Ernest & Steinlf Oil Operations	M. Staab #3	------
214	13	18	13BBAC	Ernest & Steinlf Oil Operations	M. Staab #1-C	2160
215	13	18	15CDD	Clinton Oil Co.	Braun #1-A-V	2087
216	13	18	15CDC	Clinton Oil Co.	Braun #2-A-D	2083
217	13	18	15DCC	Clinton Oil Co.	P. Pfeifer #1-V	2123
218	13	18	15CDBB	Energy Reserves Group	Braun #5-A	2098
219	13	18	15DCD	Energy Reserves Group, Inc.	P. Pfeifer #2	2142
220	13	18	15ACC	Energy Reserves Group, Inc.	Pete Pfeifer #1-A	2134
221	13	18	15CCC	Petroleum, Inc.	Braun #1-G	2126
222	13	18	15BBA	Shields Oil Producers, Inc.	Braun #2	2159
223	13	18	16BBD	Clinton Oil Co.	Nickolson #1	2124
224	13	18	16CCDB	F & M Oil Co.	Dreiling #1	2123
225	13	18	16DBB	Fleming & Woodman Drlg	Leiker #1	2129
226	13	18	18CCC	PETX Petroleum Corp.	Roth-Hassett #1	2083
227	13	18	19CAD	Abercrombie Drilling, Inc.	Brull #1	2083
228	13	18	19CCC	Virginia Drilling Co.	Brull #1	2022
229	13	18	20BC	Graybol Oil Corp.	Brull #1	2064
230	13	18	22DDB	Betorm A Oil Co.	Stackhouse #1	2075
231	13	18	22BBA	Clinton Oil Co.	Braun #4-D	2087
232	13	18	22CAB	Energy Reserves Group, Inc.	Braun #2-B	2066
233	13	18	22CAA	Energy Reserves Group, Inc.	M. Braun #1-B	2062
234	13	18	22ADC	Energy Reserves Group, Inc.	M. Braun #1-B	2062
235	13	18	22BAA	Rains & Williamson/Clinton	Braun #1	2079
236	13	18	22ABB	Rains & Williamson Co.	Mauck #1-V	2111
237	13	18	22BAA	Rains & Williamson Oil Co.	Braun #1	2079

ID	T	R	Sec. Loc.	Company Name	Wel Name	Elevation
238	13	18	23DBB	Clinton Oil Co.	E.W. Witt #1-V	2127
239	13	18	23BCC	Graham-Michaelis	Pfeifer #2-23	2090
240	13	18	23CAC	Graham-Michaelis Corp.	Witt #1-23	2085
241	13	18	23CBB	Graham-Michaelis Corp.	Witt #2-23	2082
242	13	18	24ADB	K & E Petroleum, Inc.	Kippes #1	2133
243	13	18	24ADC	Raymond Oil Co., Inc.	Kippes #1	2158
244	13	18	24DABD	Raymond Oil Co., Inc.	Staab #1	2152
245	13	18	24ADC	Raymond Oil Co., Inc.	Kippes #1	2158
246	13	18	25DDA	Clinton Oil Co.	Gross #2-X	2073
247	13	18	25DDBB	Clinton Oil Co.	Gross #3-D	2066
248	13	18	25DDD	Clinton Oil Co.	Gross #4-D	2070
249	13	18	25CDA	Clinton Oil Co.	J.P. Gross #1-A	2057
250	13	18	25BAC	Clinton Oil Co.	Nick Geist #1-V	2078
251	13	18	25CCA	Energy Reserves Group, Inc.	J.P. Gross #3-A	2054
252	13	18	25DCB	Raymond Oil Co., Inc.	Gross #1	2058
253	13	18	36ABD	Weilert Enterprises	Dinkel #1	2054
254	13	19	3CDDB	Murfin/Nadel-Gussman/Kantor	Kreutzer #1	2077
255	13	19	4CCC	A. Scott Ritchie	Kreutzer #1	2170
256	13	19	4DBB	Raymond Oil Co., Inc.	Orth #1	2157
257	13	19	4ACC	Raymond Oil Co., Inc.	Weber #1	2151
258	13	19	5CAC	F & M Oil Co.	Slaughter #1	2094
259	13	19	5ADCC	Sun Oil Co.	Project #2	2075
260	13	19	6BCC	D.G. Hansen Trust	Akins #1	2188
261	13	19	6CBB	Petroleum, Inc.	Amrein #1	2185
262	13	19	6CCDB	Petroleum, Inc.	Amrein #2	2173
263	13	19	7CBC	Graham-Michaelis Corp.	Wolf #3-7	2096
264	13	19	7CCC	Peel-Hardman Oil Operations	Disney #1	2081
265	13	19	8AAA	Rains & Williamson/Clinton Oil	Slaughter #1	2174
266	13	19	10DDD	Davis Brothers Oil Co.	Mermis #1	2102
267	13	19	10ABD	Murfin Drilling Co.	Mermis #1-10	2142
268	13	19	10BBD	Raymond Oil Co.	Kruetzler #1	2109
269	13	19	10BAB	Raymond Oil Co.	Mermis #1	2076
270	13	19	10BADB	Raymond Oil Co.	Mermis #2	2078
271	13	19	11BCD	H.B. Mabee	Gassner #1	2137
272	13	19	13CBB	Cecil M.Keller		2140
273	13	19	13BCA	Martin & Keller	Gatschet #2	2078
274	13	19	13CBA	Martin & Keller	Sack #1	2068
275	13	19	13CAB	Martin & Keller	Sack #2	2074
276	13	19	14BCC	Okmar Oil Co.	Williams #1-A SWD	2065
277	13	19	15ACB	H.B. Mabee Oil Co.	Dreiling #3	2060
278	13	19	15ADD	H.B. Mabee Oil Co.	Dreiling #4	2058
279	13	19	15DAB	H.B. Mabee Oil Co.	Strailey #1	2039
280	13	19	15DBA	H.B. Mabee Oil Co.	Strailey #2	2066
281	13	19	15DAA	H.B. Mabee Oil Co.	Strailey #3	2038
282	13	19	15BDA	Raymond Oil Co.	Gassner #1	2061
283	13	19	16BADA	Lebsack Oil Production, Inc.	Kraus #1-16	2086
284	13	19	17DAC	Graham-Michaelis Corp.	Bemis #1-17	2070
285	13	19	17???	John O. Farmer	Bemis SWD	2066
286	13	19	18BAA	Big Creek Oil Operations	Disney #1	2074

ID	T	R	Sec. Loc.	Company Name	Wel Name	Elevation
287	13	19	18DCC	Graham-Michaelis Corp.	Adams #1-18	2151
288	13	19	18DDDB	Graham-Michaelis Corp.	Disney #1-18	2109
289	13	19	19BAB	Clinton Oil Co.	Pfeifer #2	2179
290	13	19	19ACDB	Clinton Oil Co.	Pfeifer #4-D	2126
291	13	19	19AAA	Energy Reserves Group	Pfeifer #13	2090
292	13	19	19BAA	Energy Reserves Group	Pfeifer #7	2145
293	13	19	19ABC	Energy Reserves Group	Pfeifer #9	2162
294	13	19	19BAD	Jones-Gebert/Clinton Oil Co.	Pfeifer #1	2167
295	13	19	20ABB	Woodman-Iannitti	Bemis #1	2071
296	13	19	22DCA	Abercrombie Drilling, Inc.	Rupp #1	2094
297	13	19	22ABB	H.B. Mabee Co.	Meis #1	2048
298	13	19	22DAA	Leo J. Dreiling Oil Co.	Weisner #1	2045
299	13	19	24BACC	Don E. Pratt Oil Operations	Sckenk #2-24	2048
300	13	19	24BBB	Don Pratt	Sckenk #1	2045
301	13	19	24???	John O. Farmer	Jacobs #2	2062
302	13	19	24ABBD	John O. Farmer	Jacobs #4	2061
303	13	19	28DDD	Clinton Oil Co.	Reidel-Miller #1-W	2144
304	13	19	28DCA	Landes Exploration Co.	Bemis #1	2192
305	13	19	30CCB	Kimbark Oil & Gas Co.	Orth #1	2219
306	13	19	30CCC	The Texas Co.	Mary Orth #1	2215
307	13	19	30CCD	The Texas Co.	Mary Orth #2	2196
308	13	19	31BABB	J.S. (SID) Tomlinson	Reidel #1	2231
309	13	19	31CBBD	Musgrove Petroleum Corp.	Reidel #2	2229
310	13	19	31CBCC	Musgrove Petroleum Corp.	Reidel #3	2252
311	13	19	31CBA	Musgrove Petroleum Corp.	Reidel #4	2234
312	13	19	31CCCA	Musgrove Petroleum Corp.	Reidel #5	2292
313	13	19	31CAC	The Texas Co.	G.E. Reidel #10	2223
314	13	19	31DBA	The Texas Co.	G.E. Reidel #5	2273
315	13	19	31CDA	The Texas Co.	G.E. Reidel #6	2277
316	13	19	31ADC	The Texas Co.	G.E. Reidel #7	2248
317	13	19	31CDB	The Texas Co.	G.E. Reidel #8	2223
318	13	19	31CDD	The Texas Co.	G.E. Reidel #9	2260
319	13	19	31DAA	The Texas Co.	Gus Reidel #10	2250
320	13	19	32ABC	Sid Tomlinson	Bemis #1	2260
321	13	19	32BBD	Texaco, Inc.	Guss Riedel #14	2209
322	13	19	32CBA	The Texas Co.	Guss Riedel #11	------
323	13	19	32BCC	The Texas Co.	Guss Riedel #12	2254
324	13	19	32BDC	The Texas Co.	Guss Riedel #13	2246
325	13	19	34CC	Arapaho Petroleum, Inc.	Velna Turner #1-34	2253
326	13	19	35BDC	Damar Resources, Inc.	F-Dinges #1-A	2107
327	13	19	36CDC	Artnell Co. & Leber Drlg Co.	State #1	2190
328	13	19	36CCD	Kansas Exploration Co.	State #1-B	2207
329	13	20	1ADD	D.G. Hansen	Schuster #1-A	2191
330	13	20	1DAA	D.G. Hansen Trust	Schuster #1	2187
331	13	20	1DBB	National Cooperative Refining	Flax #1	2165
332	13	20	1DAD	Petroleum, Inc.	Schuster #1-C	2188
333	13	20	2ADC	Lion Oil Co.	King #1	2185
334	13	20	2BAA	Lion Oil Co.	Werth #1	2199
335	13	20	2BCB	Petroleum, Inc.	Werth #1	2155

ID	T	R	Sec. Loc.	Company Name	Wel Name	Elevation
336	13	20	2BCD	Petroleum, Inc.	Werth #2	2164
337	13	20	3ADD	Petroleum, Inc.	Hendrickson #1	2160
338	13	20	4AAC	Clinton Oil Co.	Ebert #1-V	2168
339	13	20	4ACC	Kaiser-Francis & Leben Drlg	Ebert #1	2155
340	13	20	4CAC	Murjo Oil Royalty	Kohl #1	2117
341	13	20	5DDD	Lario Oil & Gas Co.	Younger #5	2209
342	13	20	5BCC	National Coop Refining Assoc	Werth #3	2134
343	13	20	6CCC	Carl Todd Drilling Co.	Egger #1	2153
344	13	20	6BCB	Rains & Williamson/Sunray	Bittel #1	2178
345	13	20	6DBB	Rains & Williamson Oil Co.	Clem #1	2161
346	13	20	6BBD	Sunray DX Oil Co.	Bittel #5-B	2184
347	13	20	6AABD	Sunray Oil Corp.	Bittel #4-B	2173
348	13	20	7BBC	McNames & Patterson	Gugler #1	2147
349	13	20	7BBD	Shields Oil Producers, Inc.	Gugler #2	2156
350	13	20	7BCAC	Shields Oil Producers, Inc.	Gugler #3	2140
351	13	20	8ADA	Banner Oil Co.	Union Pacific #1	2121
352	13	20	9A	Champlin Petroleum Co.	UPRR #2	2113
353	13	20	9ADD	Champlin Petroleum Co.	UPRR Ellis #1	2097
354	13	20	10BCB	Clinton Oil Co.	King #1-V	2108
355	13	20	10BCD	Clinton Oil Co.	King #2-D	2108
356	13	20	10CBD	Donald C. Slawson	Pfeifer #1-F	2107
357	13	20	11CDD	Transit Corp.	Niernberger #1	2096
358	13	20	12DAD	Graham Michaelis Corp.	Jacobs #1-12	2096
359	13	20	12BDC	Hummon Corp.	Kraus #1	2089
360	13	20	12CBD	Lindas Oil Co.	Splunker #1	------
361	13	20	13ABB	Hummon Corp.	Warren #1	2085
363	13	20	15BDB	John O. Farmer	Johnston #1	2178
364	13	20	15DCC	Jones, Shelburne, and Farmer	Hiernberger #1	2186
365	13	20	15ACC	R.G. Smith	Wegele #1	2170
366	13	20	16DDD	Gulf Oil Corp.	Schumacker #1	2241
367	13	20	16DDB	The Texas Co.	T. Gerber #1	2187
368	13	20	16CBA	V.R. Gallagher	Brungardt #5	2210
369	13	20	16BCD	V.R. Gallagher	Weisner #1	2211
370	13	20	17DCB	Guy F. Atkinson Co.	P.W. Nicholson #1	2210
371	13	20	17BCC	Imperial Drilling Co., Inc.	Raynesford #1	2216
372	13	20	17BCA	Martin Oil & Gas	Raynesford #1	2209
373	13	20	18CAD	Birmingham-Bartlett Drlg Co.	Anderson #1	2222
374	13	20	18CDDB	Birmingham-Bartlett Drlg Co.	Herbert #1	2246
375	13	20	18CCB	Graves Drilling Co.	Herbert #1	2209
376	13	20	18AAA	Imperial Oil of Kansas, Inc.	Nicholson #1	2188
377	13	20	18CBA	Martin Oil & Gas	Lang #1	2226
378	13	20	19CBB	Abercrombie Drilling, Inc.	Herbert #1	2264
379	13	20	19ABC	Sigma Petro/Damac Drlg	Lang #1	2268
380	13	20	19ABDD	Sigma Petro/Damac Drlg	Lang #2	2241
381	13	20	20DDA	Fargo Petro/Murfin Drlg	Younger #1-20	2236
382	13	20	20CCC	Imperial Drilling Co., Inc.	Flax #1	2287
383	13	20	20DDD	Imperial Drilling Co., Inc.	Younger #1	2243
384	13	20	21BDA	Burch Drilling Co., Inc.	Schumacher #1	2191
385	13	20	21CDD	Gulf Oil Co.	Schumacher #1	2241

ID	T	R	Sec. Loc.	Company Name	Wel Name	Elevation
386	13	20	21DDD	Guy F. Atkinson Co.	Peter Herman #1	2237
387	13	20	21DDB	Guy F. Atkinson Co.	Peter Herman #2	2228
388	13	20	21DCC	Guy F. Atkinson Co.	Peter Herman #3	2241
389	13	20	21BAA	Petroleum Management, Inc.	Schumaker #1	2193
390	13	20	22DCC	Imperial Oil Co.	Herman #1-A	2225
391	13	20	22CCA	Petroleum, Inc.	Herman #1-B	2233
392	13	20	22CAC	Petroleum, Inc.	Herman #2-B	2232
393	13	20	22CCD	Petroleum, Inc.	Herman #3-B	2222
394	13	20	22CAB	Petroleum, Inc.	Herman #5-B	2228
395	13	20	22CBA	Petroleum, Inc.	Herman #7-B	2233
396	13	20	22BCA	Texaco, Inc.	Honas #2	2216
397	13	20	22BDC	The Texas Co.	E. Honas #1	2231
398	13	20	22DCDA	Tivertion Petroleums, Inc.	Herbert #1	2219
399	13	20	23CDAC	Alpine Oil & Royalty Co.	Zimmerman #1	2190
400	13	20	23DCC	Alpine Oil Co., Inc.	Younger #1	2178
401	13	20	23CDB	Petroleum, Inc.	Zimmerman #1-G	2192
402	13	20	23CDD	Stecklein Oil Co.	R. Zimmerman #1 SWD	2190
403	13	20	24DDD	Globe Oil & Refining Co.	Gerken #1	2182
404	13	20	25DDC	Lario Oil & Gas Co.	Younger #4	2207
405	13	20	25DDD	Lario Oil & Gas Co.	Younger #5	2209
406	13	20	25DCA	Lario Oil & Gas Co.	Younger #6	2159
407	13	20	25DBC	Lario Oil & Gas Co.	Younger #7	2194
408	13	20	25ACB	Lario Oil & Gas Co.	Younger #8	2163
409	13	20	25ACC	Lario Oil & Gas Co.	Younger #9	2181
410	13	20	25DCD	Monsanto Co.	Orth #1 SWDW	2211
411	13	20	25BDA	Tennessee Gas Trans Co.	Mike Younger #1	2194
412	13	20	26DDC	Burch Drilling Co.	Herman #1	2181
413	13	20	26ABD	Burch Drilling Co., Inc.	Herman #2	2163
414	13	20	26DCC	Gabbert-Jones Drilling Co.	Weisner #1	------
415	13	20	26AAA	Imperial Drilling Co., Inc.	Herman #1-C	2132
416	13	20	26BAAC	J.B. Collins	Zimmerman #1	2180
417	13	20	26DDD	J.M. Huber Corp.	Weisner #1	------
418	13	20	26CCB	Sterling Drilling Co.	Weisner #1	2198
419	13	20	27CAA	Aztex Petroleum	Karlin #1-A	2229
420	13	20	27DCC	Cooperative Refining Assoc	Giebler #1-B	2214
421	13	20	27DCB	Cooperative Refining Assoc	Ok...? #2-B	2217
422	13	20	27CDD	Imperial Drilling Co.	Giebler #1	2225
423	13	20	27DDBC	Monsanto Co.	Giebler #2 SWD	------
424	13	20	27CAAD	Monsanto Co.	Giebler #2-A	2231
425	13	20	27DAC	Tilco etal	Giebler #1	2189
426	13	20	28ADD	Continental Oil Co.	A. Herman #1	2223
427	13	20	28ABC	Mendo Oil Corp.	Herman #1-A	2242
428	13	20	28ACD	Three G Oil, Inc.	Herman #1	2247
429	13	20	28AAA	Zinszer Oil Co.		------
430	13	20	29BCCA	Alpine Drilling Co., Inc.	Flax #1	2322
431	13	20	29CB	Alpine Oil Co.	Sauer #1	2325
432	13	20	29DDAC	Ames Energy Exploration	Sauer #1	2291
433	13	20	29BBD	Associates Oil & Gas, Inc.	Flax #1	2326
434	13	20	29ACC	Guy F. Atkinson Co.	Carl Flax #1	2269

ID	T	R	Sec. Loc.	Company Name	Wel Name	Elevation
435	13	20	29DDD	I.O. Miller	Sauer #1	------
436	13	20	30DCB	Birmingham-Bartlett Drlg Co.	Kaiser #1-B	2285
437	13	20	30CDA	Imperial Oil of Kansas, Inc.	Kaiser #1	2282
438	13	20	30CAA	Imperial Oil of Kansas, Inc.	Kaiser #2	2299
439	13	20	30BCAB	Texas Oil & Gas	Weber #1-A	2292
440	13	20	30DCA	Tilco etal	Boschowitzki	2210
441	13	20	31DAA	Carl Todd Drilling Co.	Boos #1	2265
442	13	20	31AAA	Imperial Drilling Co.	Kroeger #1	2281
443	13	20	31ABB	Leben Drlg/Nadel & Gussman	Kroeger #1	2276
444	13	20	32BCC	B.F. Ash	Dingel #1-A	2284
445	13	20	32DDCC	Black Beauty	Boos #1	2271
446	13	20	32DDCC	Glen Rupe & Century Oil Co.	Boos #1	2271
447	13	20	32CCC	Tilco etal	Hertel #1	2263
448	13	20	32BCD	Woodman-Iannitti/Standard	Pfeifer #1	2310
449	13	20	33CAD	Cheif Drilling Co., Inc.	Rankin #2	2297
450	13	20	33BBA	Graves Drilling Co., Inc.	Rankin #1	2264
451	13	20	33ACA	Sinclair Oil & Gas Co.	Rankin #1	2289
452	13	20	34DBB	Lewis Drilling Co.	Kingsley #2	2257
453	13	20	34BAA	Monsanto Oil Co.	Nicholson #1 SWD	2235
454	13	20	34DDB	Murfin Drilling Co.	Kingsley #2-34-B	2252
455	13	20	34DAA	Murfin Drilling Co.	Kingsley #5	2233
456	13	20	34DADA	Murfin Drilling Co.	Kingsley #6	2232
457	13	20	34CDD	Murfin Drilling Co.	Nicholson #1-34	2293
458	13	20	34DBD	Murfin Drilling Co.	Kingsley #4	2270
459	13	20	34ACD	The Texas Co.	John Storm #1-OA	2255
460	13	20	34ABD	The Texas Co.	Leo Strom #2	2238
461	13	20	34BAA	The Texas Co.	Nicholson #1	2229
462	13	20	34BDD	The Texas Co.	Nicholson #3	2249
463	13	20	34ABB	The Texas Co.	Storm #1	2209
464	13	20	34BAD	The Texas Co.	W.A. Nicholson #2	2220
465	13	20	35BD	Leavell Resources	J.A. Engel #4	2219
466	13	20	35ACD	Shields Oil Producers, Inc.	Engel #1	2215
467	13	20	35DCC	Sunbelt Petroleum, Inc.	French Mary #1	2231
468	13	20	35DAB	T.L. Ferrier	French #1	2246
469	13	20	35AA	Texaco, Inc.	J. Engel #3	2192
470	13	20	35AD	Texaco, Inc.	J.A. Engel #1	2221
471	13	20	35AB	Texaco, Inc.	J.A. Engel #4	2205
472	13	20	35BCC	The Texas Co.	Leo Storm #1-B	2224
473	13	20	36DBD	Myrle F. Hoffman	Pfeifer #1-D SWD	2227
474	13	20	36ADC	The Texas Co.	Engel #1	2214
475	13	20	36AAA	The Texas Co.	Engel #8	2215
476	13	20	36AAC	The Texas Co.	M.R. Engel #3	2202
477	13	20	36ABC	The Texas Co.	M.R. Engel #4	2202
478	13	20	36ABA	The Texas Co.	M.R. Engel #5	2173
479	13	20	36ADA	The Texas Co.	M.R. Engel #7	2233
480	13	20	36ACA	The Texas Co.	M.R. Engle #2	2200
481	13	21	1BCD	Cooperative Refining Assoc	Spilker #1-E	2180
482	13	21	1BDB	Coop. Refining/Rex & Morris	Spilker #1	2163
483	13	21	1ACB	Murfin Drilling Co.	Cromb #1	2180

ID	T	R	Sec. Loc.	Company Name	Wel Name	Elevation
484	13	21	1ACA	Murfin Drilling Co.	Cromb #5	2180
485	13	21	1ACD	Stanolind Oil & Gas Co.	A.I. Cromb #5	2179
486	13	21	1DAB	Stanolind Oil & Gas Co.	Cromb #4	2167
487	13	21	1DDA	Woodman-Iannitti Drilling Co.	Cromb #1-B	2163
488	13	21	2AAC	Energy Three Inc.	Deutscher #1	2193
490	13	21	12CAC	Birmingham-Bartlett Drlg Co.	Egger #1	2152
491	13	21	12AAA	Carl Todd Drilling	Newcomber #1	2152
492	13	21	12ADA	Petroleum, Inc.	Walle #1	2146
493	13	21	12AAD	Shields Oil Producers, Inc.	Walle #1	2154
494	13	21	12AAA	Trumart Oil Co.	Newcomber #1	2153
495	13	21	12DDB	Zenith Drilling Corp.	Newcomber #1	2175
496	13	21	13DBD	Graves Drilling	Kuhn #1	2199
497	13	21	13AAA	Graves Drilling Co., Inc.	John #1	2187
498	13	21	13DADB	Graves Drilling Co., Inc.	Kuhn #3	2207
499	13	21	13DDB	Icer Addis	Kuhn #1	2194
501	13	21	24AAAC	A.L. Abercrombie, Inc.	Mary Agnes #2	2212
502	13	21	24ADD	Abercrombie Drilling, Inc.	Mary Agnes #1	2239
503	13	21	24DDD	Imperial Oil of Kansas, Inc.	Lang #1	2273
504	13	21	24DAAB	L.G. Stepherson & Co., Inc.	Stopple #6	------
505	13	21	24CAA	Robert G. Brooks	Massier #1	2222
506	13	21	24BCD	Zenith Drilling Corp., Inc.	Massier #1	2233
507	13	21	24BDC	Zenith Drilling Corp., Inc.	Massier #2	2208
508	13	21	25DCCC	Ames Energy		2302
509	13	21	25DBD	Ames Energy Exploration	Boos #1	2289
510	13	21	25DCDB	Ames Energy Exploration	Bunker #1-A	2323
511	13	21	25CBD	Landes Exp. & St.. Resources	Dinkel #1	2335
512	13	21	25CCAC	Landes Exp. & St.. Resources	Dinkel #2	2332
514	13	21	36ADD	The Kimbark Co.	Kroeger #1	2300
515	13	21	36DBD	Transit Corp.	Kroeger #1	2282
519	14	16	6AAB	Range Oil Co.	Kippes Heirs #1	1969
520	14	16	6AAD	Range Oil Co.	Kippes Heirs #2	1968
521	14	16	7BAA	Dreiling, LTD	Harwood #2	2261
526	14	16	18BCA	Dreiling Resources, Inc.	Wagner #2	1915
527	14	16	29CCDD	Clinton Oil Co.	O.F. Dreiling #1-X	1917
528	14	16	32CAC	Clinton Oil Co.	Wellbrock #1-X	1919
529	14	17	2ABC	Birmingham & Bartlett	Ray Braun #2	1928
530	14	17	2CA	Clark Knight	Braun #1	1951
531	14	17	2CBA	R.P. Nixon Oil Operations	J. Braun SWD	1972
532	14	17	3ABB	Dreiling, LTD	Sander #1	1970
533	14	17	4AAA	Musgrove Petroleum Corp.	Dreiling #1	1991
534	14	17	4CCBD	R.P. Nixon Oil Operations	Lang B SWD	1935
535	14	17	5BDC	Frontier Oil Co.	Pfeifer #1	2025
536	14	17	5CAC	Ladd Petroleum Corp.	Pfeifer #2	2028
537	14	17	5CAA	Ladd Petroleum Corp.	Pfeifer SWD	2019
538	14	17	5CAB	Leben Drilling Co.	Pfeifer #1	2024
539	14	17	5CDA	Leo J. Dreiling	Pfeifer #1	2023
540	14	17	5DDC	Oil Producers, Inc. of Kansas	Hoffman SWD #1	2019
541	14	17	5CBD	Sun Production Division	Pfeifer #3-C	2027
542	14	17	5AAA	Sunray DX Oil Co.	George #4	2034

ID	T	R	Sec. Loc.	Company Name	Wel Name	Elevation
543	14	17	5AAD	Sunray DX Oil Co.	George Dinkle #3	2030
544	14	17	5ABB	Weilert Enterprises	Dinkel East	2032
545	14	17	6BBBB	A. Scott Ritchie	Prewo #1	2013
546	14	17	6ABC	Dreiling, LTD	Francis #1	2027
547	14	17	6ADA	Leben Drilling, Inc.	Younger #1-B	2004
548	14	17	6CCDA	TGT Petroleum Corp.	Hoffman #1	2007
549	14	17	7AAA	Anschutz Drilling Co.	Younger #1	1999
550	14	17	7AAD	Dreiling, LTD	B. Younger #1	1999
551	14	17	7BDB	Dreiling, LTD	Wasinger #1	2005
552	14	17	8ABC	Amerada Oil Co.	Lang #1	2011
553	14	17	8ACA	Armstrong-Jackman	Lang #2	2017
554	14	17	9ABA	Kathol Petroleum Co.	Sanders #1	2023
555	14	17	10BDC	Phoenix Drilling Co.	Sanders #2	2020
556	14	17	12BCC	Franco Central Oil Co.	Lang #1	1966
557	14	17	14CAA	Murfin Drilling Co.	Lang #1	1982
558	14	17	14BBC	Okmar Oil Co.	Brungart #2	------
559	14	17	16ADC	D Oil Operations	Lang #1-B	2001
560	14	17	16DCC	Dreiling, LTD of Colorado	Herl #1	1978
561	14	17	16BDD	Leben Drilling Co.	Dinkel #1	1989
562	14	17	16BDB	Leben Oil Producers	Dinkel #2	1995
563	14	17	17CBB	Anschutz Drilling Co.	Stecklein #1	1982
564	14	17	17DAAC	Okmar Oil Co.	Pfannensteil #3	1996
565	14	17	17CDD	Sinclair Oil & Gas Co.	J.J. Stecklein #1	1967
566	14	17	17ACC	TGT Petroleum Corp.	Pfeifer #1	1989
567	14	17	18DCDD	Sunray Mid-Continent Oil Co.	Margret Dinkel #1	1955
568	14	17	20BABB	Black Petroleum Co.	Dinkel #1	1960
569	14	17	20BDB	Elmar Karst	Dinkel - Staab #1 SWD	1967
570	14	17	20ABC	Sierra Petroleum Co., Inc.	Hammerschmidt #1	1973
571	14	17	20BAA	Stearns Petroleum, Inc.	Heyl #1	1974
572	14	17	21BBC	Bea Drilling Co., Inc.	Stecklein #4	------
573	14	17	22DDAC	K & E Petroleum, Inc.	Steffen #1	1969
574	14	17	22BCBA	The Atlantic Refining Co.	John P.A. Dreiling #3	1892
575	14	17	23DBB	Icer Addis	Schumaker #1	1966
576	14	17	24???	Backus Oil Co.	Gerstner #2 SWD	1962
577	14	17	24CAD	Hummon Oil, Inc.	F. Gerstner #1	1960
578	14	17	25BAC	T.O. Lilystrand JR	Ruder #1	1853
579	14	17	27BBA	Charles Crow	Herl #2	1975
580	14	17	27CBC	Lion Oil Co.	Catherine #1	1966
581	14	17	27CCB	Lion Oil Co.	Jerome #1	1963
582	14	17	28ADD	Circle Crow Drilling Co.	Dinkel #3	------
583	14	17	28ABD	Circle Oil Co., Inc.	Dinkel #1	1972
584	14	17	28ADA	Lion Oil Co.	Dinkel #2	1959
585	14	17	28DDA	Lion Oil Co.	Gross #1	------
586	14	17	28DBD	Lion Oil Co.	Herl #3	1962
587	14	17	28DAD	Lion Oil Co.	Herl #4	1950
588	14	17	30ADB	Petroleum Management, Inc.	Grabee #1	1945
589	14	17	30???	T. Dreiling Oil Co.	Pfanenstiel #1	1964
590	14	17	32DCC	Clinton Oil Co.	Phillip #1-V	1925
591	14	17	34BCB	Raymond Oil Co.	Brull #1	1967

ID	T	R	Sec. Loc.	Company Name	Wel Name	Elevation
592	14	18	6CBB	J.E. Hall	K-State #1	2093
593	14	18	7BAB	National Associated Petro Co.	Pfeifer #1	2088
594	14	18	8???	Well: Fort Hayes State SWD	Fort Hayes State S.W.D.	2048
595	14	18	11ACC	Kansas Exploration Co.	Leiker #1	1985
596	14	18	11BDD	Midway Drilling	Josephine Leiker #3	1984
597	14	18	13DDBD	Hanhoff Oil & Gas Co.	Herl #1	------
598	14	18	13DDAC	Hanhoff Oil & Gas Co.	Herl #2	1990
599	14	18	14DDB	Woodman & Iannitti	Brull #1	1859
600	14	18	17DBD	Petroleum Management, Inc.	Schaffer #1	2044
601	14	18	18AADB	National Associated Petro Co.	State of Kansas #1	2069
602	14	18	18ACC	TXO Production Corp.	State Of Kansas #1-A	2092
603	14	18	19DBB	Leben Drilling Co.	Rohr #1	2105
604	14	18	19DBD	N-B Co. & Lexicon Resources	Rohr #1	2102
605	14	18	19BDD	Shamrock Energy Corp.	Johnson #1	2112
606	14	18	20BC	Nelson Enterprises	Rohr #1	2098
607	14	18	20BAC	Sabre Exploration, Inc.	Pfannenstiel #1	2056
608	14	18	21BB	Woodman & Iannitti	Pfannenstiel #1	2031
609	14	18	24CDD	Hanhoff Oil & Gas	D.J. Pfannenstiel #1	1954
610	14	18	25ADDB	Hanhoff Oil & Gas Co.	Stecklein #1	1965
611	14	18	27CCD	Clinton Oil Co.	Engel #2-D	2064
612	14	18	27CBB	Osage Oil & Gas Co.	Engel #1	2066
613	14	18	28CDD	Lindas Co.	Stecklein #1-A	2065
614	14	18	29BAA	Alpine Oil & Royalty	Engel #1	2087
615	14	18	29CCAB	Dreiling Ltd of Colorado		2058
616	14	18	29ADC	Hudson Petroleum Co.	Menhan #1	2085
617	14	18	29DA	Raymond Oil Co., Inc.	Menhan #1	2071
618	14	18	30DCDA	Myrle F. Hoffman	Gerald Schnelker #1	2050
619	14	18	31DAB	Clinton Oil Co.	Edwin Ruder #1-V	2045
620	14	18	31ADD	Dreiling Ltd of Colorado	Ruder #1-31	2035
621	14	18	31ADA	Dreiling Ltd of Colorado	Ruder #2-31	2038
622	14	18	31BDD	Sterling Drilling Co.	Rupp #1	2048
624	14	18	32BCDB	Dreiling, Ltd	Rohr-Engel #1	2052
625	14	18	32AAB	Dreiling Ltd of Colorado	Mary Engel #1	2044
626	14	18	32BCCB	Dreiling Ltd of Colorado	Rohr-Engel #3	2043
627	14	18	32BDCB	Dreiling Ltd of Colorado	Rohr-Engels #2	2050
628	14	18	32CCC	General American Oil of Texas	Pfannensteil #1	2026
629	14	18	32DCA	Omega Drilling, Inc.	Pfannensteil #1	2039
630	14	18	32ADCB	Pittman & Associates	Wright #33-32	2038
631	14	18	33CAA	C & R Drilling Co.	Stecklein #1	2044
632	14	18	33AAA	Clarence Dreiling	Adeline Engel #2	2061
633	14	18	33CABB	Dreiling, LTD	Stecklein #2	2045
634	14	18	33BCC	El Dorado Refining Co.	Engel #1	2042
635	14	18	33DDD	Herman G. Kaiser	Engel #1	2036
636	14	18	33DAA	Omega Drilling Co.	Carl Engel #1	2039
637	14	18	33ADC	Omega Drilling, Inc. etal	Engel #1	2043
638	14	18	33BCA	Pendleton Land & Exp.	Engel #1	2057
639	14	18	33BAC	Pendleton Land & Exp.	Engel #2	2056
640	14	18	33BDD	Pendleton Land & Exp.	Engel #3	2051
641	14	18	33CDD	Pendleton Land & Exp.	Legleiter #2	2041

ID	T	R	Sec. Loc.	Company Name	Wel Name	Elevation
642	14	18	34BBA	Coastal Oil & Gas	Engel #3-V	2060
643	14	18	34BAB	Coastal Oil & Gas	Engel #6-J	2060
644	14	18	34BDA	Coastal Oil & Gas Co.	Engel #1	2052
645	14	18	34ACC	Colorado Oil & Gas Co.	Engel #2-A	2051
646	14	18	34ABC	Colorado Oil & Gas Co.	Engle #1-A	2053
647	14	18	34BAC	Colorado Oil & Gas Co.	Engle #2	2055
648	14	18	34DBB	Woodman-Iannitti/E.J. Carter	Engel #1	2052
649	14	18	35ADD	Beacon Resources	Phannensteil #1	2015
650	14	18	35CCC	Globe Oil & Refining Co.	Dechant #1	2026
651	14	18	35BDC	Globe Oil & Refining Co.	Phannensteil #1	2022
652	14	19	1CBA	D.R. Lauck Oil Co., Inc.	State #1	2185
653	14	19	1BAA	Leben Drilling Co.	State #1	2145
654	14	19	1ABB	Leben Drlg & RSC Oil	State #1-A	2142
655	14	19	1CAA	Pendleton Land & Exp.	State #1	2151
656	14	19	1DAB	Sunray & Lindas	State Land #1	2115
657	14	19	2ADA	Roberts E. Campbell	Jacobs #1	2212
658	14	19	2CCD	Sid Tomlinson	Stabelman #1	2201
659	14	19	2CCAA	Sid Tomlinson	Stabelman #2	2198
660	14	19	2CCC	Sid Tomlinson	Stabelman #3	2221
661	14	19	3ACC	C.W. Smith	Orth #2	2174
662	14	19	3BDA	C.W. Smith	Orth #3	2171
663	14	19	3BDB	C.W. Smith	Orth #4	2179
664	14	19	3BAC	C.W. Smith	Orth #5	2197
665	14	19	3BAD	C.W. Smith	Orth #6	2180
666	14	19	3ADC	C.W. Smith	Pfeifer #1	2186
667	14	19	3DBB	C.W. Smith	Weiland #1	2190
668	14	19	3DBA	C.W. Smith	Weiland #2	2173
669	14	19	3CBA	C.W. Smith & Associates	Stabelman #2	2191
670	14	19	3CAA	O-Frac	Stabelman #1	2193
671	14	19	3CCC	Tennessee Gas/Shelly-Miller	Stabelman #1	2242
672	14	19	3BDD	Transit Corp.	Orth #1	2154
673	14	19	4DDD	C.W. Smith	Stadelman #1-A	2220
674	14	19	4CCB	Tenneco Oil Co.	Eral L. Orth #1-4	2247
675	14	19	4CCCA	Tenneco Oil Co.	Orth #2-4	2268
676	14	19	4BDB	Three G Oil Co.	Orth #1	2267
677	14	19	4BBA	Thunderbird Drilling, Inc.	Orth #1	2258
678	14	19	4CAA	Victor Drilling Co.	Orth #1	2222
679	14	19	5DDB	Braden Drilling Co.	Orth #2	2263
680	14	19	5ADB	Braden Drilling Co.	Werth #1	------
681	14	19	5AACD	Braden Drilling, Inc.	Werth #4	2270
682	14	19	5CABC	Coastal Oil & Gas	Riedel #6-J	2258
683	14	19	5CBB	Coastal Oil & Gas, Inc.	Riedel #7-J	2255
684	14	19	5CAC	Colorado Oil & Gas Co.	Riedel #3	2273
685	14	19	5CAAC	Colorado Oil & Gas Corp.	Riedel #4	2271
686	14	19	5CCB	Pan American Petroleum Corp.	Riedel #1-B	2229
687	14	19	5???	Petroleum Energy, Inc.	Riedel #1	2258
688	14	19	5CCD	Stanolind Oil & Gas Co.	Gus Riedel #2-B	2236
689	14	19	6???	Aztec Petroleum	Riedel #1-A	2279
690	14	19	6CBA	Clarence Drilling	Irvin #2-6	2278

ID	T	R	Sec. Loc.	Company Name	Wel Name	Elevation
691	14	19	6BCB	Nadel & Gussman Oil Prod.	Strohmeier #1	2269
692	14	19	6DAD	Pan American Petroleum Corp.	L.V. Irvin Unit #2	2242
693	14	19	6DDAC	R.R. Rhyne Co.	Irvin #5	2246
694	14	19	6CBB	Rains & Williamson Oil Co.	Irvin #1	2253
695	14	19	6ABBD	Stanolind Oil & Gas Co.	G. Riedel #2-D	2283
696	14	19	6ACA	Stanolind Oil & Gas Co.	Irvin #2	2273
697	14	19	6DDD	Stanolind Oil & Gas Co.	L.V. Irvin Unit #1	2240
698	14	19	6AAB	Stanolind Oil & Gas Co.	Mae Schwaller #1	2284
699	14	19	6AAD	Stanolind Oil & Gas Co.	Mae Schwaller #2	2276
700	14	19	6ABA	Stanolind Oil & Gas Co.	Riedel #1-C	2287
701	14	19	7DCC	Bay Petroleum Corp.	Krammer #1	2228
702	14	19	7DCA	Cattleman's Oil Operations	Krammer #1-C	2230
703	14	19	7DBC	Chief Drilling Co.	Krammer #1	2237
704	14	19	7BAD	Dreilling, LTD	Harwood #1	2274
705	14	19	8BCDB	Al Tipton	Riedel #1	2204
706	14	19	8CA	Al Tipton	Riedel #2	2208
707	14	19	8ADD	Colorado Oil & Gas Corp.	Kinderknecht #2	2226
708	14	19	8DBD	Davis Brothers	Kinderknecht #2	2212
709	14	19	8DCC	Frontier Oil Co.	Kinderknecht #10-B	2198
710	14	19	8BBD	Frontier Oil Co.	Louis Riedel #1	2224
711	14	19	8CBB	Frontier Oil Co.	Riedel #1	2216
712	14	19	9BCC	Colorado Oil & Gas Co.	Von Feldt #1	2223
713	14	19	9BAD	Tenneco Oil Co.	Meis #1	2222
714	14	19	10CAA	Bankoff Oil Co.	Weisnell #1	2223
715	14	19	10ABB	Mike Weilert Oil Co.	Kisner #1	2198
716	14	19	11ACAC	L.G. Stephenson & Co., Inc.	Stadelman #2	2218
717	14	19	11BAB	Raymond Oil Co.	Orth #1	2194
718	14	19	11DBD	Three G Oil Co.	Kisner #1	2188
719	14	19	12BCC	Herman George Kaiser	Befort #1	2196
720	14	19	12ABD	Pendleton Land & Exp.	Kingsley #1	2206
721	14	19	12DCB	Three G Oil Co.	J. Befort #1	2175
722	14	19	12CAD	Three G Oil Co.	Wiesner #1	2191
723	14	19	13DAA	C & C Exploration	Pfannenstiel #2	2132
724	14	19	13DAC	C & C Exploration	Pfannenstiel #5	2113
725	14	19	13ADC	C & C Exploration	Sunley #3-A	2134
726	14	19	14DBA	Amber Exploration Co.	Metz #1-14	1928
727	14	19	14DCC	Anschutz Drilling Co.	Wiesner #1	2153
728	14	19	16CAA	Gas Futures LTD	Kraus #1	2158
729	14	19	16???	J&W Oil Co.	Kraus #1 SWD	2170
730	14	19	16BCC	Petroleum, Inc.	Kinderknecht #1	2187
731	14	19	16BBCC	Petroleum, Inc.	Kinderknecht #1-B	2180
732	14	19	16BCAC	Petroleum, Inc.	Kinderknecht #2-B	2175
733	14	19	17CDD	Cattleman Oil Co.	Kraus #1	2191
734	14	19	17AAA	Coppinger Drilling, Inc.	Kramer #1	2192
735	14	19	17DAA	National Coop Refining Assoc	Seitz #1-A	2193
736	14	19	17DAC	National Coop Refining Assoc	Seitz #2-A	2179
737	14	19	17ADAA	Petroleum, Inc.	Kramer #1	2194
738	14	19	17ADB	Petroleum, Inc.	Kramer #2	2199
739	14	19	18ADB	Hummon Oil, Inc.	Kraus #1	2208

ID	T	R	Sec. Loc.	Company Name	Wel Name	Elevation
740	14	19	18AAB	National Associated Petro	Kraus #1	------
741	14	19	18BCB	Raymond Oil Co., Inc.	Wilfred Kraus #1	2179
742	14	19	18BCC	Raymond Oil Co., Inc.	Wilfred Kraus #2	2190
743	14	19	18???	Raymond Oil Co., Inc.	Kraus #3 SWD	2197
744	14	19	19AACA	Triple H Oil Operations	Barnes #1	2194
745	14	19	20BDAC	Aikins & ower	Kraus #1	2224
746	14	19	20DAA	Coppinger Drilling Co., Inc.	Kraus #1	2224
747	14	19	21CBB	Colorado Oil & Gas Co.	Kraus #1-A	2211
748	14	19	21BACD	J.R. Green Oil Operation	Kraus #3	2168
749	14	19	21BAA	Tennessee Gas & Oil Co.	Esther M. Kraus #2	2185
750	14	19	21BAD	Tennessee Gas & Oil Co.	Esther M. Kraus #4	2166
751	14	19	21BDD	Tennessee Gas Trans. Co.	Esther M. Kraus #1	2151
752	14	19	21BAB	Tennessee Gas Trans. Co.	Kraus #3	2175
753	14	19	22B	Mike Weilert Oil Co.	Kraus #1-H	2152
754	14	19	22BCDB	Weilert Enterprises	H. Kraus #5 SWD	2114
755	14	19	23CBAD	S & K Oil Co.	Befort #1	2123
756	14	19	24D	Panhandle Petroleum	Phannenstiel #1	2093
757	14	19	26DCA	Beacon Resources	Copeland #1	2059
758	14	19	26ACC	Beacon Resources Corp.	Copeland #2	2073
759	14	19	27DAAC	N-B Co., Inc.	Copeland #1 SWD	2084
760	14	19	28DBAA	Barnett Oil Co.	Sunley-Moser #2	2137
761	14	19	28CAA	Brunson Production & Exp.	Weber #1	2136
762	14	19	28CDBA	N-B Co., Inc.	Weber SWD	------
763	14	19	28CDC	Raymond Oil Co.	Weber #1	2126
764	14	19	28BAA	Walters Drilling Co.	Feitz #1	2214
765	14	19	29BBD	Rains-Williamson Oil Co.	Kuhn #1	2158
766	14	19	29ACC	Raymond Oil Co.	Wilson #1	2120
767	14	19	30BB	Murfin Drilling & Kern Drlg	Rohr #1	2161
768	14	19	30ACD	Petroleum Management, Inc.	Lily Johnson #1	2149
769	14	19	30AAA	Woodman-Iannitti/Bion Allen	Johnson #1	2167
770	14	19	32BAA	Leben Drilling, Inc.	Wassinger #1	2097
771	14	19	32DCB	Pam-Kar Drilling Co., Inc.	Moore #1	2073
772	14	19	33ACCA	Black Petroleum Co.	Gabel #1	2102
773	14	19	33BDD	Burch Drilling Co., Inc.	Moore #1	2113
774	14	19	33CAC	Fundamental Oil Corp.	Millard Moore #1	2099
775	14	19	34CDAC	Reif Oil Operations	Maxwell #1	2087
776	14	19	34BBA	Three G Oil Co., Inc.	Feitz #1	2118
777	14	19	34BAB	Three G Oil Co., Inc.	Feitz #2	2129
778	14	19	34BBD	Three G Oil Co., Inc.	Feitz #3	2110
779	14	19	34BAC	Three G Oil Co., Inc.	Feitz #4	2123
780	14	19	34CBB	Woodman & Iannitti Drlg	Haas #1	2093
781	14	19	35ADB	American Energies Corp.	Younker #1-A	2095
782	14	19	35ACA	American Energies Corp.	Younker #1-C	2092
783	14	19	35BAD	Beacon Resources Corp.	Herl #1	2097
784	14	19	35BDA	Beacon Resources Corp.	Herl #2	2117
785	14	19	35BAA	Beacon Resources Corp.	Herl #3	2079
786	14	19	35BAC	Beacon Resources Corp.	Herl #4	2111
787	14	19	35ACB	Beacon Resources Corp.	Younker #1	2101
788	14	19	35ABD	Beacon Resources Corp.	Younker #4	2080

ID	T	R	Sec. Loc.	Company Name	Wel Name	Elevation
789	14	19	35ABB	Beacon Resources Corp.	Yonker #3	2075
790	14	19	35DDB	Three G Oil Co.	Speier #1	2114
791	14	19	35DAC	Three G Oil Co.	Spier #2	2118
792	14	19	36BCC	Black Petroleum, Inc.	Younker #1	2080
793	14	19	36DDB	ET-AL, Inc.	Befort #1	2058
794	14	19	36CBB	Frontier Oil Co.	Befort #1-A	2087
795	14	19	36DDD	Petroleum, Inc.	Befort #1	2052
796	14	19	36CDD	Three G Oil Co.	Befort #1	2095
797	14	19	36CDB	Three G Oil Co.	Befort #2	2092
798	14	20	1BDD	American Warrior, Inc.	Honus #3-1A	2215
799	14	20	1A	Aztec Petroleum, Inc.	Hertel #2-A	2247
800	14	20	1AAB	Aztec Petroleum, Inc.	Pfeifer #1-A	2233
801	14	20	1BAD	Chief Drilling Co., Inc.	Schlyer #1	2227
802	14	20	1BAD	Oil Mark, Inc.	Honas #1	------
803	14	20	1BDA	Oil Mark, Inc.	Honas #2	2217
804	14	20	1BBB	Oil Mark, Inc.	Honas #3 SWD	2261
805	14	20	1AAC	Rebel Production	Hertel #3-A	2267
806	14	20	2ACCC	Central Kansas Oil & Gas	Luea #1	2271
807	14	20	2DBB	Central Kansas Oil & Gas	Pfiefer #1	2264
808	14	20	2BBB	Rebel Petroleum	Luea #1	2232
809	14	20	2DCC	Sunray Oil Corp.	Pfiefer #3-A	2226
810	14	20	3CCC	D.G. Hansen	Giebler #1	2268
811	14	20	3ABB	D.G. Hansen Trust	Dinkel #6	2278
812	14	20	3DBA	Erbert Oil Co.	Dinkle #6	2240
813	14	20	3DBB	Harold Erbert	Dinkle #8	2227
814	14	20	3DBD	Lewis Drilling Co.	Dinkel #1	2236
815	14	20	3BDD	Zinszer Oil Co.	Dinkel #1	2293
816	14	20	4CBC	A.L. Abercrombie	Kisner #1	2273
817	14	20	4CCB	A.L. Abercrombie Drilling	Kisner #2	2252
818	14	20	4ACA	Mack Oil Co.	Gottschalk #2	2308
819	14	20	5DAA	Abercrombie Drilling	Boos #1	2246
820	14	20	5DBA	Abercrombie Drilling	Gabel #1	2239
821	14	20	5AAA	Imperial Drilling Co.	Gabel #1	2311
822	14	20	5ABD	Three G Oil, Inc.	Gabel #1	2268
823	14	20	6DDD	Kern Drilling Co., Inc.	Gottschalk #1	2214
824	14	20	6AAD	Tilco etal	Gottschalk #2	2239
825	14	20	6BDD	White Eagle Oil Co.	John Dinkel #1	2216
826	14	20	7ACC	John O. Farmer, Inc.	Weber #1	2229
827	14	20	9BAA	Abercrombie Drilling	Lang #1-A	2212
828	14	20	10ABB	Aztec Petroleum	P. Gottschalk #2-A	2193
829	14	20	10DAD	Canaday Oil Corp.	Gottschalk #1-A	2171
830	14	20	10ACB	DaMar Oil Operations	Gottschalk #1-A	2203
831	14	20	10BAD	Dunne-Gardner Petro, Inc.	Gottschalk #1	2237
832	14	20	10ADD	National Drilling Co.	Pfannenstiel #1	2192
833	14	20	11ADD	Bea Drilling Co.	Befort #1	2238
834	14	20	11ADB	Bea Drilling Co.	Befort #5 SWD	2231
835	14	20	11DCB	Canaday Oil Corp.	Befort #1	2231
836	14	20	11B	Central Kansas Oil & Gas	Josephine #1	2242
837	14	20	11DDB	Grand Mesa Operating Co.	Befort #1-11	2180

ID	T	R	Sec. Loc.	Company Name	Wel Name	Elevation
838	14	20	11CDB	Murfin Drilling Co.	Honas #1	2203
839	14	20	11CBA	Rains & Williamson Oil Co.	Weber Honas #1	2228
840	14	20	11BDAB	Sunray Mid-Continent Oil Co.	Josephine #4	2245
841	14	20	11BABD	Sunray Oil Corp.	Josephine #2	2248
842	14	20	11BBDC	The National Oil Co.	Pfeifer #1	2238
843	14	20	12CDA	Aztec Petroleum	Kisner #1-A	2158
844	14	20	12DCC	L & F Oil Operations	Gottschalk #1	2202
845	14	20	12DBB	Pam-Kar & Nat'l Coop. Rfng.	P. Zimmerman #1	2198
846	14	20	12DDC	Tilco etal	Kraus #1	2228
847	14	20	13???	Hummon Oil Co.	Kirkman #1	2194
848	14	20	13DABB	Lario Oil & Gas Co.	Kirkman #1	2199
849	14	20	13ACD	Okmar Oil Corp.	Kirkman #1	2181
850	14	20	13BDD	Omega Drilling, Inc.	Dinkel #1	2144
851	14	20	13???	Trumart Oil Co.	Kirkman #1	2194
852	14	20	14AAA	K & E Drilling, Inc.	Cerney #2	2198
853	14	20	14ABB	Lindas Oil Co.	Cerney #1	2212
854	14	20	14DBD	Shields Oil Producers	Cerney #1	2128
855	14	20	15DDC	Birmingham-Bartlett Drlg Co.	C. Cerney #1	2207
856	14	20	15CDA	Rains & Williamson Oil Co.	Haselhorst #1-A	2228
857	14	20	15CBA	Rains & Williamson Oil Co.	Haselhorst #2	2235
858	14	20	15ACB	Stanolind Oil & Gas Co.	Betty Nye #1	2240
859	14	20	16DDA	Donald C. Slawson	Seibel #1-B	2233
860	14	20	17DB	Mull Drilling, Inc.	Kingsley #1	2157
861	14	20	17DA	Mull Drilling, Inc.	Kingsley #2	2159
862	14	20	19CAA	Pickrell Drilling Co.	Kingsley #1	2231
863	14	20	19DAB	Source Petroleum	Kingsley #1-B	2237
864	14	20	20DDDB	A. Scott Ritchie	Weigel #1	2122
865	14	20	21ADA	Rocket Drilling Co.	Seibel #1	2243
866	14	20	22DDDB	Oxford Exploration	Augie Befort #22-11	2137
867	14	20	22CBD	Sage Drilling Co.	Soloman #1	2216
868	14	20	23BDD	Don E. Pratt	Keller #1	2140
869	14	20	23CADB	Imperial Oil Co.	Befort #1	2135
870	14	20	24CDD	Davis Brothers	Moore #1-A	2094
871	14	20	24CBB	Lewis Drilling Co.	Moore #1	2096
872	14	20	25DBB	Kern-Landis & Murfin Drlg	Leiker #1	2092
873	14	20	27BCD	Shields Oil Prod./DC Slawson	Kingsley-Blake-Harwood#1	2134
874	14	20	27DDA	Shields Oil Producers, Inc.	R.Young #1-A	2098
875	14	20	28AAC	Rains & Williamson Oil Co.	Soloman-Burnett #1	2154
876	14	20	28ADA	Rains & Williamson Oil Co.	Soloman-Burnett #2	2142
877	14	20	28ABA	Rains & Williamson Oil Co.	Soloman-Burnett #3	2161
878	14	20	28ACA	Rains & Williamson Oil Co.	Soloman-Burnett #4	2148
879	14	20	28ADC	Rains & Williamson Oil Co.	Soloman-Burnett #5	2137
880	14	20	28ABC	Rains & Williamson Oil Co.	Soloman-Burnett #6	2137
881	14	20	28DAA	Rains & Williamson Oil Co.	Zonker #1	2129
882	14	20	29AAA	Thunderbird Drilling, Inc.	Groff #1	2098
883	14	20	34BAB	Rains & Williamson Oil Co.	Ward #1	2091
884	14	20	34BBC	Rains & Williamson Oil Co.	Ward #2	2093
885	14	20	35BDC	Murjo Oil & Royalty	Irvin #1	2064
886	14	20	35AAC	Rains & Williamson Oil Co.	Irvin #1	2074

ID	T	R	Sec. Loc.	Company Name	Wel Name	Elevation
887	14	21	1ABB	Dunne-Gardner Petro, Inc.	Dinkel #1	2251
888	14	21	1ACCA	F & M Oil Co., Inc.	Dinkel #1	2244
889	14	21	1ADC	F & M Oil Co., Inc.	Dinkel #1-A	2268
890	14	21	1ACAC	F & M Oil Co., Inc.	Dinkel #2	2255
891	14	21	1DBBD	F & M Oil Co., Inc.	Luea #1	2237
893	14	21	11BAA	Dakota Resources, Inc.	Pfiefer #1	2263
894	14	21	11CB	Prickrell Drilling Co.	Clemens #1-A	2236
895	14	21	13DBC	Solar Oil Co.	Luea #1	2233
898	14	21	23AAA	R.W. Shields	Gabel #1	2181
899	14	21	23ACA	Rains & Williamson Oil Co.	Dinkel #1	2222
903	14	21	35BB	John O. Farmer	Holtsinger #3-A	2095
904	14	21	35CDB	Sunray DX Oil Co.	Holtzinger #4	2070
905	14	21	36CBC	Guy F. Atkinson Co.	Otto Wagner #1	2074
906	15	16	5DAD	Driscoll Leasing Co.	Rajewski #1	1851
907	15	16	8BBB	Bergman Drilling Co., Inc.	Braun #1	1865
908	15	16	32CAA	Leo J. Dreilling Oil Co.	Dome #1	1867
909	15	17	6DB	Collins & Collins	Stecklein #2 SWD	1990
910	15	17	6DBC	John O. Farmer, Inc.	Stecklein #1	1995
911	15	17	6BDB	Raymond Oil Co., Inc.	Stecklein #1	1993
912	15	17	6CAA	Raymond Oil Co., Inc.	Strecklein #1	1999
913	15	17	7DAA	Cheif Drilling	Werth #1	1965
914	15	17	9CDAB	Dreilling, LTD	Philip #1	1954
915	15	17	10CAA	Clinton Oil Co.	A. Phillips #1-V	1933
916	15	17	10CDD	R.W. Shields	Phillips #1	1951
917	15	17	11CCC	Tilco etal	Phillips Ranch #1	1955
918	15	17	13BBB	National Coop Refinery Assoc	Lieker #1	1987
919	15	17	15CBB	Bay Petroleum Corp.	Degenhart #1	1955
920	15	17	15CCB	Bay Petroleum Corp.	Degenhart #2	------
921	15	17	15CAD	Tennessee Gas Trans. Co.	John J. Degenhart #4	1980
922	15	17	16BDA	Allen Oil Co.	Vonfeldt #1	1970
923	15	17	16DBC	American Energies Corp.	Roth #1-B	1978
924	15	17	16DAD	F & R Oil	Roth #1	------
925	15	17	16ABC	Three G Oil, Inc.	Roth #1	1967
926	15	17	17BDC	Petroleum Management, Inc.	Gross #2	1977
927	15	17	17CBB	Petroleum Management, Inc.	Leiker #1-B	1984
928	15	17	17CCA	Petroleum Management, Inc.	Leiker #1-D	1996
929	15	17	17BCB	Petroleum Management, Inc.	Leiker #2-C	1971
930	15	17	17CBA	Petroleum Management, Inc.	Leiker #3-B	1992
931	15	17	17BCD	Petroleum Management, Inc.	Leiker #3-C	------
932	15	17	17CBC	Petroleum Management, Inc.	Leiker #4-B	1990
933	15	17	17BCA	Petroleum Management, Inc.	Leiker #4-C	1975
934	15	17	18ACB	Allen Oil Co.	Gross #1-18	1985
935	15	17	18ADA	Petroleum Management	Gross #2-18	1972
936	15	17	18ADD	Petroleum Management, Inc.	Gross #1	1978
937	15	17	18BCDD	Petroleum Management, Inc.	Leiker #4	2003
938	15	17	18DDC	Petroleum Management, Inc.	Stecklein #5	1995
939	15	17	18DAA	Petroleum Management, Inc.	Stecklein #7	1977
940	15	17	19ADB	Earl L. Thomason	Leiker #1-B	1998
941	15	17	19ADD	Edward P. Leiker	Leiker #2	1992

ID	T	R	Sec. Loc.	Company Name	Wel Name	Elevation
942	15	17	19CCB	Glenn W. Peel Estate	Dumler #6	1998
943	15	17	19BDCB	Gross Oil Operations	Leiker #1	2020
944	15	17	19ADD	National Oil Co., Inc.	Leiker #2	1987
945	15	17	19CCC	Peel & Hardman	Dumler #1	1991
946	15	17	20CBD	Continental Oil Co.	A. Boos #2	1968
947	15	17	20CBB	Continental Oil Co.	A. Boos #3	1979
948	15	17	20CDB	Continental Oil Co.	Boos #1	1957
949	15	17	20DCBB	Dreilling, LTD	Gross #2	1957
950	15	17	21CBC	E.K. Ediston	Dinkel #1	1974
951	15	17	21CCC	Oil Producing, Inc.	Dinkel #1	1971
952	15	17	22BBB	Bay Petroleum Corp.	Schmidt #1	1969
953	15	17	22BCA	Tennessee Gas Trans. Co.	Eugene Schmidt #1	1959
954	15	17	28DDC	Clinton Oil Co.	Applonia Roth #1-V	1883
955	15	17	28CAA	Graves Drlg Co. & Phillips Oil	Rajewski #1	1861
956	15	17	28DBB	Jay Bee Oil Co.	Roth #1	1868
957	15	17	28BCB	TXO Productions Corp.	Rajewski #1	1953
958	15	17	29BBB	Energy Reserves Group, Inc.	Werth #6	1975
959	15	17	30CBB	National Coop Refinery Assoc	Lieker #1	1956
960	15	17	30BBB	National Coop Refinery Assoc	Lieker #1	1987
961	15	17	30AAD	Vincent Oil Co.	Cambell #3	1980
962	15	17	30ADD	Vincent Oil Corp.	Cambell #2	1979
964	15	17	30DBC	Vincent Oil Corp.	Cambell #4	1950
965	15	17	32ACA	Landes Exploration	Urban #1	1883
966	15	17	34DCC	Clinton Oil Co.	Jacobs #1-V	1910
967	15	17	34CBDA	Graham-Michaelis Corp.	Strecker #1-34-A	1903
968	15	17	35ACA	Clinton Oil Co.	Jacobs #1-V	1890
969	15	17	35DCA	Graham-Michaelis Corp.	Klein #1-35	1898
970	15	17	36CCB	Clinton Oil Co.	Mary Taylor #1-V	1893
971	15	18	2ACC	V.R. Gallagher	Phannenstiel #1	2013
972	15	18	3DBD	Damar Resources, Inc.	Gabe Brull #1	2028
973	15	18	3ACA	Petroleum, Inc.	Phannenstiel #1-D	2011
974	15	18	3ACD	Petroleum, Inc.	Phannenstiel #3-E	2009
975	15	18	3DBC	Petroleum, Inc.	Wiesner #1-G	2031
976	15	18	4???	D Oil Operations	Oldham #3	2016
977	15	18	4BACC	D Oil Operations	Oldham #3	2016
978	15	18	4BDB	D Oil Operations	Ruder #1-A	2021
979	15	18	4BAB	D Oil Operations & Dreiling	Oldham #2	2024
980	15	18	4BBA	Dreilling, LTD	Oldham #5	2028
981	15	18	4DAA	Dreilling, LTD	Staab #1	2026
982	15	18	4ADB	National Coop Refinery Assoc	Ruder #1	2030
983	15	18	4BCBD	Thornton E. Anderson	Ruder #3	2016
984	15	18	5ABCC	H & C Oil Operations	Hoobs #4	2035
985	15	18	5DDCC	Petro Land & Exploration	Hoobs #1	2017
986	15	18	5DAA	Thornton E. Anderson	Munsch #1	2007
987	15	18	5DACA	Thornton E. Anderson	Munsch #2	2012
988	15	18	6BBC	Petroleum, Inc.	Ryan #2	2037
989	15	18	6CDA	Thunderbird Drilling Co.	Dechant #2	2025
990	15	18	6DCC	Woodman-Iannitti Oil Co.	Dechant #1	2015
991	15	18	7ACC	Burch Drilling Co., Inc.	Nickel #1	2028

ID	T	R	Sec. Loc.	Company Name	Wel Name	Elevation
992	15	18	7CBD	Dreiling Limited of Colorado	Shires #2	2065
993	15	18	7CCD	Dreiling Limited of Colorado	Shires #4	2080
994	15	18	7BBBD	F & M Oil Co., Inc.	Urban #1	2061
995	15	18	8CDBB	Gulf Oil Corporation	J.A. Swires #3	1996
996	15	18	8CDB	Gulf Oil Corporation	James A. Swires #5-W	2001
997	15	18	9DBC	Dreiling Limited of Colorado	Munsch #1	2032
998	15	18	9ADA	Frontier Oil Co.	Fidelis Dinges #1	2030
999	15	18	9DCCA	Kewanee Oil Co.	Befort #2	2032
1000	15	18	9BCAB	Rosel Energy, Inc.	Saab #1	1995
1001	15	18	9BABC	Thornton E. Anderson	Staab #1	2020
1002	15	18	10BBA	Colorado Oil & Gas Corp.	Dinges #1-A	2029
1003	15	18	10BAC	Colorado Oil & Gas Corp.	Dinges #2-A	2029
1004	15	18	10BBC	Colorado Oil & Gas Corp.	Dinges #3-A	2025
1005	15	18	10D	Francis Oil & Gas		2000
1006	15	18	10ABC	Kewanee Oil Co.	Leiker #1-A	2029
1007	15	18	10CAD	Okmar Oil Co.	Kings SWD	2013
1008	15	18	11ADB	E.K. Carey Drilling Co., Inc.	Gross #1	2018
1009	15	18	11ADA	E.K. Carey Drilling Co., Inc.	Gross #5	2017
1010	15	18	11CCC	Frontier Oil Co.	Wasinger #1	1993
1011	15	18	11DDA	Phillips Petroleum	John #3-A	2022
1012	15	18	11DAC	Phillips Petroleum	John #4-A	2023
1013	15	18	11DAB	Phillips Petroleum	John #5-A	2025
1014	15	18	11DAA	Phillips Petroleum	John #6-A	2019
1015	15	18	12CBC	Hawn Petroleum, Inc.	Brock #10	2020
1016	15	18	13BBD	Alpine Oil & Royality Co.	T.S. Leiker #3	2016
1017	15	18	13BBB	Alpine Oil & Royality Co.	T.S. Leiker #6	2019
1018	15	18	13CBB	Alpine Oil & Royality Co.	T.S. Leiker #9	2018
1019	15	18	13BBC	Alpine Oil & Royality Co.	T.S. Leiker #9	2018
1020	15	18	14C	Aylward Drilling Co.	Graf #4	1992
1021	15	18	14CBB	Frontier Oil Co.	Graf #1	1997
1022	15	18	14AAA	Woodriver Oil & Refinery Co.	Dechant #1	2019
1023	15	18	14AAA	Woodriver Oil & Refinery Co.	Dechant #5	2022
1024	15	18	15ADC	Baruch-Foster Corporation	Paul Wasinger #2	2007
1025	15	18	15ADAC	Frontier Oil Company	Wasinger #1	2007
1026	15	18	15CCBD	Grant Oil, Inc. & Alta, Inc.	Wetta #1-24	2051
1027	15	18	15???	Phillips Petroleum Co.	Wasinger #2	------
1028	15	18	15AADB	Phillips Petroleum Co.	Wasinger #3	2005
1029	15	18	15ABD	Phillips Petroleum Co.	Wasinger #4	2017
1030	15	18	15ABC	Phillips Petroleum Co.	Wasinger #5	2020
1031	15	18	16BDB	Mid-Western Petro & Exp.	Wolf #2	2038
1032	15	18	16BAD	Okmar Oil Company	Wolf #3	------
1033	15	18	16???	Okmar Oil Company	Wolfe #3	2013
1034	15	18	17ACAD	Dreiling Oil Company	Grabbe #6	1984
1035	15	18	17DBAC	Graves Drilling Company	Roth #1	1975
1036	15	18	18BCC	Burch Drilling Company	Phannenstiel #1	2065
1037	15	18	18CCC	C & G Drilling	Wasinger #1	2019
1038	15	18	18AAA	C.H. Spoor	Ruder #1	2022
1039	15	18	18ADBD	F & M Oil Company, Inc.	Ruder #1-A	2054
1040	15	18	18BDD	Fundamental Oil Corporation	Schmidtberger #1	------

ID	T	R	Sec. Loc.	Company Name	Wel Name	Elevation
1041	15	18	18ADD	K & E Drilling Co. & BOA	Ruder #1	2037
1042	15	18	18DDC	The National Oil Company	Wasinger #1	2028
1043	15	18	19CDB	F & M Oil Company	Klaus #1	1973
1044	15	18	19BBBD	F & M Oil Company	Klaus #1-A	2009
1045	15	18	19ABA	Fundamental Oil Corporation	Felx Roth #1	2035
1046	15	18	19CCA	Lew-Thom Energies, Inc.	Klaus #1	1977
1047	15	18	20DDD	Artnell Company	Weisner #1	1948
1048	15	18	21BDD	Tilco etal	Roth #1	2023
1049	15	18	22ACBD	Okmar Oil Company		2010
1050	15	18	22CD	Union Texas Petroleum	Pivonka #3-A	2017
1051	15	18	23CDAA	Alta, Inc.	Ruder #1-23	2000
1052	15	18	23DDA	Jones, Shelburne, & Farmer	Pfannensteil #1	1959
1053	15	18	24DCC	Chief Drilling Company	Herald #1	1989
1054	15	18	24CDD	Hummon Oil Company	Werth #1	1971
1055	15	18	24BDA	Wilkon Drilling Company	Kansas State College #1	1994
1056	15	18	25BDCA	Landmark Oil Exploration, Inc.	Werth #_	1954
1057	15	18	25CCC	The P.M.O. Corporation	Wolf #1	1903
1058	15	18	26BCCD	Pendleton Land & Exploration	Madden #1	1965
1059	15	18	27BAB	Rains & Williamson Oil Co.	Roth #1	2023
1060	15	18	27BBD	Rains & Williamson Oil Co.	Roth #2	2008
1061	15	18	28DBBA	Hunter Oil Company	Zimmerman #1	1908
1062	15	18	28ABB	Martin Oil & Gas	Herklotz #1	2001
1063	15	18	28ACC	Osage Oil & Gas Company	Herklotz #1	1936
1064	15	18	28DAB	Tilco etal	Zimmerman #1	1922
1065	15	18	30BDA	Allen Drilling Company	Werth #1-30	1936
1066	15	18	30DCC	Allen Drilling Company	Werth #1-30-B	1951
1067	15	18	30CA	Energy Exploration	Bircher #1	1924
1068	15	18	30BBB	Woodman Iannitti Drlg Co.	Gottschalk Brothers #1	1970
1069	15	18	31DDD	Hi Plains Oil Exploration	Zimmerman #1	1971
1070	15	18	34BBA	F & M Oil Company, Inc.	Bieker #1	1911
1071	15	18	35BAA	Kewanee Oil Company	Schaefer #1	1915
1072	15	18	35AAC	Tennessee Gas & Oil	Werth #1	1931
1073	15	18	36BDDB	A. Scott Ritchie	Schlegel #1-A	1902
1074	15	18	36ACD	Scott Ritchie	Werth #1	1810
1075	15	19	1CAA	Alpine Oil & Royalty Co.	Dechant #1	2105
1076	15	19	1BAA	Alpine Oil & Royalty Co.	Pfannenstiel #4	2098
1077	15	19	1ABB	Imperial Oil Company	Wilson #3	2084
1078	15	19	1ADCC	Imperial Oil Company	Wilson #5	2070
1079	15	19	1DBB	Imperial Oil of Kansas	Pfannenstiel #1-B	2092
1080	15	19	1AAD	Petroleum, Inc.	Wilson #1-B	2049
1081	15	19	1ADA	Petroleum, Inc.	Wilson #2-B	2054
1082	15	19	1CABB	Thornton E. Anderson	Dechant #5	2083
1083	15	19	1BDCC	Thornton E. Anderson	Pfannenstiel #5	2092
1084	15	19	1BDBB	Thornton E. Anderson	Pfannenstiel #7	2106
1085	15	19	1BBAA	Thornton E. Anderson	Pfannenstiel #9	2111
1086	15	19	2AAAB	Aztex Petroleum	Haas #1-A	2111
1087	15	19	2ADD	Imperial Oil Company	Haas #1	2093
1088	15	19	2BBD	Jay Bee Oil Company	Saver #1	2071
1089	15	19	2DBC	Thornton E. Anderson	Haas #2-A	2090

ID	T	R	Sec. Loc.	Company Name	Wel Name	Elevation
1090	15	19	2DAA	Thornton E. Anderson	Haas #3	2082
1091	15	19	3ABD	The National Oil Company	Dechant #1	2073
1092	15	19	4DDC	Raymond Oil Company, Inc.	Gross #1	2052
1093	15	19	6DAA	Herdon Drillion Company	Younger #1	2054
1094	15	19	7BDD	Rains & Williamson Oil Co.	Younger #1	2034
1095	15	19	7ABB	Skelly Oil Company	Anderson #7	1821
1096	15	19	11ADD	Gabbert & Jones	Gross #1	2044
1097	15	19	12CDA	Isern Brothers	Huser #1	2055
1098	15	19	12DBB	Raymond Oil Company, Inc.	Urban #1	2067
1099	15	19	12DBB	Source Petroleum	Urban #1	2069
1100	15	19	12CDAA	Source Petroleum	Urban #3	2057
1101	15	19	13DAB	F & M Oil Company, Inc.	Wasinger #1	2025
1102	15	19	13ADC	F & M Oil Company, Inc.	Wasinger #2	2024
1103	15	19	13DBA	F & M Oil Company, Inc.	Wasinger #3	2023
1104	15	19	13AAD	F & M Oil Company, Inc.	Wolf #2	2048
1105	15	19	16DAA	Continental oil Company	M.J. Unrien #1	1999
1106	15	19	16AB	John O. Framer, Inc.	Kraus #1	2016
1107	15	19	16CBB	Musgrove Petroleum	Hauschild #2	1999
1108	15	19	16CCC	Raymond Oil Company	Hauschild #1	1976
1109	15	19	17DDD	Bridgeport Oil Company, Inc.	Hauschild #1	1977
1110	15	19	20ACA	F & M Oil Company, Inc.	Bieler #1	1993
1111	15	19	22ABA	Raymond Oil	Werth #1	1996
1112	15	19	23BDD	John O. Farmer, Inc.	Rischert #1	1975
1113	15	19	24BDB	Allen Drilling Company	L. Gross #1-24	1970
1114	15	19	24ADA	F & M Oil Company, Inc.	Wasinger #2-A	1994
1115	15	19	27DAA	L & H Oil Operations	Legleiter #2	2003
1116	15	19	27DAD	L & H Oil Operations	Legletier #3	2020
1117	15	19	27CCB	Rains & Williamson Oil Co.	Legge #1	2028
1118	15	19	28DAB	John O. Farmer, Inc.	Dinkel #1	2030
1119	15	19	29DAC	Kewanee Oil Company	Berrick #10	------
1120	15	19	31DCB	Mull Drilling Company	Reidel #1	2091
1121	15	19	31CD	Mull Drilling Company	Reidel #2	2097
1122	15	19	31CA	Mull Drilling Company	Riedel #3	2103
1123	15	19	33DDD	Anador Resources, Inc.	Werth #1-33	2012
1124	15	19	33AAA	Herman Kaiser	Randa #1	2038
1125	15	19	33BD	Pickrell Drilling Company	Werth #1-E	2055
1126	15	19	34CAC	Jet Drilling Company	Doerr #1	2050
1127	15	19	35DCC	Chief Drilling Company etal	Zimmerman #1	2001
1128	15	19	35CDB	Donald C. Slawson	Seelye #3-B	2024
1129	15	19	35AB	McClure & J. O. Farmer	Zimmerman #1	2009
1130	15	19	36BCD	Clinton Oil Company	Zimmerman #1-V	2014
1131	15	20	2DBC	Rains & Williamson Oil Co.	Jacobs #1	2043
1132	15	20	3ABC	Colorado Oil Company	Stephens #1	2258
1133	15	20	5ADA	Rains & Williamson Oil Co.	Honas #1	2070
1134	15	20	6BBB	Bankoff Oil Company	Bollig #1	2023
1135	15	20	7AB	Gabbert-Jones, Inc	King #1-A	2075
1136	15	20	7DCD	Geneses Oil & Gas, Inc.	Meserve Ranch #1	2150
1137	15	20	7CC	Imperial Oil Company	King #1	2166
1138	15	20	8ADD	Rains & Williamson Oil Co.	Meserve #1-A	2001

ID	T	R	Sec. Loc.	Company Name	Wel Name	Elevation
1139	15	20	8A	Woodman Iannitti Drilling Co.	Meserve #1	2044
1140	15	20	10CAB	E. H. Riggs	#1 Trust	2014
1141	15	20	10BA	Godsey-Earlougher Division	Bentley #1	2025
1142	15	20	12ADA	Abercrombie Drilling	Menehan #1	2037
1143	15	20	12DBA	Rains & Williamson Oil Co.	Menehan #1	2019
1144	15	20	12BBB	Rains & Williamson Oil Co.	Wann-Rohr #1	2045
1145	15	20	18CBA	John O. Farmer	Meserve #1-B	2209
1146	15	20	18BCC	Rains & Williamson Oil Co.	Meserve #1	2198
1147	15	20	18BBC	Rains & Williamson Oil Co.	Meserve #2	2153
1148	15	20	19ABC	Rains & Williamson Oil Co.	North #1	2135
1149	15	20	20CDC	Amerada Petroleum Company	Fred Bullock #1	2170
1150	15	20	20CCD	Don Pratt etal	North #1	2157
1151	15	20	20CCA	John O. Farmer, Inc.	North Bullock #1	2152
1152	15	20	21BDD	Don Pratt	North #1	2138
1153	15	20	21DDD	Don Pratt	North (Albert) #1	2204
1154	15	20	21DAA	Rains & Williamson Oil Co.	North #1-C	2149
1155	15	20	24DAA	Pickrell Drlg & SW Petro-Chem	Wearth #1-A	2099
1156	15	20	27CB	Barker Exploration Company	Crotinger #1	2283
1157	15	20	27CAD	Rains & Williamson Oil Co.	Crotinger #1	2262
1158	15	20	27DDD	Rains & Williamson Oil Co.	Crotinger #1-A	2161
1159	15	20	27AC	Spines Exploration, Inc.	Graham #1	2151
1160	15	20	28CD	Barker Exploration Company	North #1	2295
1161	15	20	28BCC	Buffalo Oil & Rine etal	Mutual #1	2192
1162	15	20	28CCC	Rains & Williamson Oil Co.	North #1-A	2266
1163	15	20	28CCA	Rains & Williamson Oil Co.	North #2-A	2256
1164	15	20	28BBB	Rains & Williamson Oil Co.	North #2-B	2175
1165	15	20	28DBD	Rains & Williamson Oil Co.	North #6	2272
1166	15	20	29ABD	John O. Farmer	North #2	2192
1167	15	20	29ADB	John O. Farmer, Inc	North #1	2229
1168	15	20	29ABD	John O. Farmer, Inc	North #2	2192
1169	15	20	29DDD	Rains & Williamson Oil Co.	Bullock #1	2274
1170	15	20	30BCC	John O. Farmer, Inc	North #1-30	2334
1171	15	20	31BDD	John O. Farmer, Inc	Sumner #1-31	2316
1172	15	20	32AAA	Oxford Exploration Company	North #32-11	2306
1173	15	20	33AAC	Colorado Oil Company	Stephens #2	2259
1174	15	20	33ADC	Colorado Oil Company	Stephens #3	2230
1175	15	20	33CAAC	Rains & Williamson Oil Co.	Edwards #1	2285
1176	15	20	33DBB	Rains & Williamson Oil Co.	Moran #1	2252
1177	15	20	33DADB	Rains & Williamson Oil Co.	Moran #2	2229
1178	15	20	33DAB	Rains & Williamson Oil Co.	Moran #3	2222
1179	15	20	33DBD	Rains & Williamson Oil Co.	Moran #4	2235
1180	15	20	33ABA	Rains & Williamson Oil Co.	Stephens #1-A	2260
1181	15	20	33ACA	Rains & Williamson Oil Co.	Stephens #2-A	2238
1182	15	20	33BCA	Rains & Williamson Oil Co.	Wallace #5	2286
1183	15	20	33BBB	Rains & Williamson Oil Co.	Wallace #1	2269
1184	15	20	33CAA	White & Ellis Drilling, Inc.	Black #1	2273
1185	15	20	34CBCA	E. K. Edmiston	Bee #1	2241
1186	15	20	34DCC	F & M Oil Company, Inc.	Bee #1	2218
1187	15	20	34CCAC	John O. Farmer, Inc.	Ree #1-B	2224

ID	T	R	Sec. Loc.	Company Name	Wel Name	Elevation
1188	15	20	34CA	Kaiser-Francis	Singleton #1	2248
1189	15	20	34CDC	Marshel Oil & Gas	Singleton #1	2221
1190	15	20	35DCC	Donald C. Slawson	Elmore #1-M	2155
1191	15	20	35CDAC	Raymond Oil company	Elmore #1-B	2162
1192	15	21	1CCA	Abercrombie Drilling, Inc.	Tom Moore #1	2049
1193	15	21	1BDC	Deep Rock Oil Corporation	Moore #1-A	2065
1194	15	21	1ACC	Pickrell Drilling Company	Milberger #1-A	2032
1195	15	21	12CD	Abercrombie Drilling, Inc.	Brenner #1-A	2187
1196	15	21	12DC	John O. Farmer	King #1-C	2157
1197	15	21	12DBC	John O. Farmer	King #2-C	2143
1198	15	21	12ABDD	John O. Farmer, Inc.	King #1-A-E	2119
1199	15	21	12ABC	John O. Farmer, Inc.	King #3-E	2117
1200	15	21	13AB	John O. Farmer	Benner #1-B	2178
1201	15	21	13ADA	John O. Farmer	Brenner #2-B	2187
1202	15	21	13AA	John O. Farmer	Brenner #3-B	2161
1203	15	21	13AD	Rains & Williamson Oil Co.	Brenner #1	2213
1204	15	21	13DAAC	Rains & Williamson Oil Co.	Brenner #1-B	2258
1205	15	21	24CADC	John O. Farmer	North #1-E	2250
1206	15	21	24CDAC	John O. Farmer	North #3	2261
1207	15	21	24DBB	John O. Farmer, Inc.	North #1-24	2259
1208	15	21	24CBB	John O. Farmer, Inc.	North #2-24	2224
1209	15	21	24CCC	Welch & Olsson Drilling Co.	D.K. North #1	2291
1210	15	21	25BAA	John O. Farmer, Inc.	North #1-H	2269
1211	15	21	35DCC	Berexo, Inc.	Leo Twin #1	2310
1212	15	21	35BA	Walters Drilling Company	North #1-F	2324
1213	15	21	36AAA	Don E. Pratt	D.K. North #1-A	2317
1216	16	17	2DCD	Graham-Michaelis Corp.	Solomon Estates #1-2	1943
1217	16	17	3ACDB	D & G Oil Operations	Roth #1	1946
1218	16	17	3CDC	Donald C. Slawson	Urban #1-A	1962
1219	16	17	3ACD	Jay Bee Oil Company, Inc.	Roth #1-B	1954
1220	16	17	3BBAC	Witchita Iron & Metal	Klein #2	1919
1221	16	17	4AAA	Clinton Oil Company	D.R. Roth #3-D	1919
1222	16	17	4AAB	Real Petroleum	Roth #1-V	1920
1223	16	17	5DCA	Lario Oil & Gas Company	Basgall #1	1991
1224	16	17	5ADC	Lario Oil & Gas Company	Jacobs #1-B	1928
1225	16	17	6???	M.B. Armer	Pfiefer #1	1903
1228	16	18	6DDC	Omega Drilling, Inc.	Bieker #2-A	2019
1229	16	18	6CBA	Sunburst Exploration Co.	Bieker #1	2014
1230	16	18	8BBA	Omaga Drilling, Inc.	Nora Benbow #1	2037
1231	16	18	8ADD	Omega Drlg & Buttes Oil & Gas	Sdilia Herrman #1	2015
1232	16	18	9CDC	John O. Farmer, Inc.	Bahr #1	1989
1233	16	18	11AAB	Imperial Oil of Kansas, Inc.	Werth #1	1994
1234	16	18	11AADA	Prairie Oil, Inc.	Werth #1	1994
1235	16	18	12BAA	Imperial Oil of Kansas, Inc.	Herrman #1	1967
1236	16	18	12BBB	Imperial Oil of Kansas, Inc.	Herrman #2-A	1989
1238	16	19	2CAC	Clinton Oil Company	Kurn #1-V	2019
1239	16	19	2BDD	McClure Oil & Abercrombie Drlg	Zimmerman #1	2027
1240	16	19	2CAA	Triple H Oil Operations	Oelkers #1-A	2033
1241	16	19	3DCB	Anschutz Drilling Company	Seelye #1	2043

ID	T	R	Sec. Loc.	Company Name	Wel Name	Elevation
1242	16	19	3DAB	Ram Petroleum Corporation	Crotinger #1	2154
1243	16	19	3AAB	Raymond Oil/Rains&Williamson	Seelye #1-A	2017
1244	16	19	3AAAC	Raymond Oil Company	Seelye #2 SWD	2031
1245	16	19	6BB	Muir-Thompson, Inc.	Schutte #1	2085
1247	16	20	1BCC	Darby & Bothwell, Inc.	Weitzel #1	2114
1248	16	20	1AABC	Madeira Oil Company	Watson #1	2086
1249	16	20	1BCC	Rains & Williamson Oil	Weitzel #1	2116
1250	16	20	1DBA	Ram Petroleum Corporation	Pfeifer #1	2094
1251	16	20	1ACD	Ram Petroleum Corporation	Watson #1	2095
1252	16	20	1ADA	Ram Petroleum Corporation	Watson #2	2073
1253	16	20	1CAA	Ram Petroleum Corporation	Watson #3	2100
1254	16	20	1ACB	Ram Petroleum Corporation	Watson #4	2094
1255	16	20	1ACC	Ram Petroleum Corporation	Watson #5	2095
1256	16	20	1CAB	Ram Petroleum Corporation	Watson #6	2102
1257	16	20	1AABC	Ram Petroleum Corporation	Watson #7	2089
1258	16	20	2ABD	Dixie Oil Company	Ree #1-A	2123
1259	16	20	2BAD	Dixie Oil Company	Wassinger #1	2122
1260	16	20	3AA	Donald C. Slawson	Crotinger #1-B	2147
1261	16	20	3ABAC	National Oil Company	Crotinger #1	2250
1262	16	20	3AAB	Raymond Oil Company, Inc.	Crotinger #1	2157
1263	16	20	3BCB	The Reach Group	Crotinger #1	2189
1264	16	20	4ABB	E.K. Edmiston	Bullock #1	2212
1265	16	20	4BBB	John O. Farmer, Inc.	Ree #1	2226
1266	16	20	4BACC	National Coop Refining Assoc	Frank #2	2186
1267	16	20	5CC	Barnett Oil Company	Royce #1	2229
1268	16	20	7BDD	Rains & Williamson Oil Co.	Grumbein #1	2288
1269	16	20	12ABD	Ram Petroleum Corporation	Watson #1-B	2104
1271	16	21	1DBC	American Penn Energies	Sarvis #1-1	2261
1272	16	21	1CAA	John O. Farmer	Sarvis #1	2255

Appendix 2: Stratigraphic Thicknesses from Well Logs

The following table lists the data gathered from the gamma-ray logs from Appendix 1. An ID number is used to relate the information in this table with the information in the previous appendix. Included in the table are the depth to the top of the upper Dakota aquifer, the aquifer (sand) and aquitard (shale) subunit thicknesses in the three zones, and the thickness of the Kiowa shale aquitard. The thicknesses are recorded in feet because the gamma-ray logs are graduated in tens of feet. Values are given in feet because the logs were calibrated in feet (1 ft = 0.3048 m).

	Depth	Zone 1		Zone 2		Zone 3		Total		Percent	Total	Kiowa Sh.
ID	to Top	Sand	Shale	Sand	Shale	Sand	Shale	Sand	Shale	Sand	Thickness	Thickness
1	320	10	70	10	90	50	60	70	220	24%	290	40
2	370	20	80	20	80	50	20	90	180	33%	270	60
3	370	10	70	20	110	50	20	80	200	29%	280	70
4	380	30	60	90	40	20	20	140	120	54%	260	30
5	420	20	60	10	110	30	50	60	220	21%	280	40
6	360	20	60	90	40	20	40	130	140	48%	270	40
7	400	20	80	10	80	5	110	35	270	11%	305	0
8	350	20	90	20	90	50	30	90	210	30%	300	40
9	370	0	140	20	50	25	40	45	230	16%	275	10
10	380	0	100	50	70	50	20	100	190	34%	290	20
11	400	10	100	10	100	20	50	40	250	14%	290	0
12	330	30	110	0	80	60	30	90	220	29%	310	30
13	370	10	100	0	90	50	40	60	230	21%	290	50
14	420	20	60	0	150	30	80	50	290	15%	340	10
15	450	0	130	30	90	50	60	80	280	22%	360	20
17	420	10	140	30	100	40	60	80	300	21%	380	50
18	380	10	90	30	140	40	70	80	300	21%	380	50
19	390	40	80	50	70	60	30	150	180	45%	330	10
20	360	20	100	20	105	20	60	60	265	18%	325	0
21	350	40	60	150	70	10	20	200	150	57%	350	0
22	370	10	100	60	80	50	10	120	190	39%	310	0
23	325	40	70	30	40	160	0	230	110	68%	340	0
24	340	40	60	50	40	110	20	200	120	63%	320	20
25	365	20	60	30	80	100	10	150	150	50%	300	0
26	350	40	60	30	130	30	40	100	230	30%	330	0
27	360	10	75	40	120	60	30	110	225	33%	335	30
28	345	30	70	70	70	30	70	130	210	38%	340	20
29	330	60	50	40	10	110	20	210	80	72%	290	40
30	330	100	60	0	60	60	10	160	130	55%	290	40
31	340	60	70	40	50	30	80	130	200	39%	330	0
32	465	15	70	10	90	70	40	95	200	32%	295	30
33	470	10	70	20	130	30	30	60	230	21%	290	30
34	450	20	90	30	110	30	20	80	220	27%	300	20
35	430	70	100	10	60	70	10	150	170	47%	320	10
36	440	30	120	20	80	50	30	100	230	30%	330	0
37	430	60	80	30	40	40	50	130	170	43%	300	20

ID	Depth to Top	Zone 1 Sand	Zone 1 Shale	Zone 2 Sand	Zone 2 Shale	Zone 3 Sand	Zone 3 Shale	Total Sand	Total Shale	Percent Sand	Total Thickness	Kiowa Thickness
38	430	0	100	0	110	40	50	40	260	13%	300	20
39	450	0	130	40	80	20	60	60	270	18%	330	10
40	450	40	60	0	110	30	30	70	200	26%	270	20
41	420	10	80	0	90	30	70	40	240	14%	280	30
42	410	20	80	0	90	30	60	50	230	18%	280	20
43	420	60	60	0	90	30	60	90	210	30%	300	10
44	440	10	70	10	70	70	50	90	190	32%	280	30
45	440	30	70	0	90	50	40	80	200	29%	280	30
46	450	40	70	30	50	50	50	120	170	41%	290	40
47	460	60	60	20	50	40	50	120	160	43%	280	50
48	470	40	50	50	60	10	80	100	190	34%	290	20
49	430	70	70	30	40	40	50	140	160	47%	300	50
50	440	70	70	40	60	20	40	130	170	43%	300	50
51	470	60	60	30	80	30	30	120	170	41%	290	40
53	450	50	50	0	90	0	80	50	220	19%	270	0
54	430	50	70	0	100	30	40	80	210	28%	290	40
55	430	50	70	0	80	30	50	80	200	29%	280	50
56	430	70	60	0	90	40	30	110	180	38%	290	50
57	470	50	60	10	110	20	30	80	200	29%	280	50
58	450	20	70	0	120	40	30	60	220	21%	280	40
59	450	40	50	10	80	70	10	120	140	46%	260	20
60	450	70	40	20	30	60	60	150	130	54%	280	10
61	440	40	70	0	110	30	30	70	210	25%	280	50
62	460	70	60	0	80	40	40	110	180	38%	290	30
63	460	80	60	0	70	30	40	110	170	39%	280	30
64	460	70	40	20	70	40	30	130	140	48%	270	30
65	450	30	80	40	50	40	40	110	170	39%	280	40
66	430	30	70	20	90	30	30	80	190	30%	270	40
67	470	70	60	20	60	50	50	140	170	45%	310	30
68	450	60	50	10	120	40	30	110	200	35%	310	40
69	460	40	90	0	120	50	20	90	230	28%	320	30
70	470	30	80	10	110	30	30	70	220	24%	290	40
72	310	30	80	10	90	80	30	120	200	38%	320	0
73	310	40	20	30	50	10	90	80	160	33%	240	0
74	310	20	50	0	150	10	50	30	250	11%	280	0
75	300	120	70	0	50	40	10	160	130	55%	290	10
80	260	50	40	10	80	10	50	70	170	29%	240	20
81	280	40	50	0	90	50	10	90	150	38%	240	20
82	250	20	40	20	70	50	10	90	120	43%	210	20
84	230	10	60	10	60	70	10	90	130	41%	220	0
85	200	30	40	0	90	30	70	60	200	23%	260	30
86	230	10	80	20	50	20	80	50	210	19%	260	0
87	250	10	70	10	90	40	40	60	200	23%	260	30
88	200	0	110	0	70	120	20	120	200	38%	320	0
89	260	0	100	0	100	20	30	20	230	8%	250	0
90	190	0	110	10	60	40	40	50	210	19%	260	30
91	360	20	50	0	150	40	30	60	230	21%	290	20
92	320	20	70	30	60	60	60	110	190	37%	300	40

ID	Depth to Top	Zone 1 Sand	Zone 1 Shale	Zone 2 Sand	Zone 2 Shale	Zone 3 Sand	Zone 3 Shale	Total Sand	Total Shale	Percent Sand	Total Thickness	Kiowa Thickness
93	360	10	90	10	90	30	40	50	220	19%	270	30
94	300	20	110	50	60	0	80	70	250	22%	320	0
95	330	10	60	20	80	30	50	60	190	24%	250	50
96	340	30	70	20	100	40	50	90	220	29%	310	50
97	330	30	70	0	70	90	20	120	160	43%	280	70
98	360	40	40	40	90	40	30	120	160	43%	280	40
99	350	30	50	20	90	70	40	120	180	40%	300	40
100	320	30	50	100	10	0	90	130	150	46%	280	40
101	340	40	70	10	40	10	60	60	170	26%	230	50
102	370	40	60	10	80	60	30	110	170	39%	280	30
103	360	30	80	10	100	20	60	60	240	20%	300	20
104	330	60	60	0	80	30	10	90	150	38%	240	40
105	330	60	60	20	80	30	50	110	190	37%	300	20
106	320	70	60	0	90	20	60	90	210	30%	300	30
107	320	30	70	50	90	60	60	140	220	39%	360	30
108	280	30	70	40	100	90	30	160	200	44%	360	30
109	340	20	80	40	70	70	30	130	180	42%	310	40
110	280	20	70	0	80	70	20	90	170	35%	260	40
111	330	10	80	0	110	10	70	20	260	7%	280	20
112	300	40	50	10	70	20	100	70	220	24%	290	30
113	320	30	60	10	50	20	110	60	220	21%	280	0
114	330	20	70	10	100	0	80	30	250	11%	280	30
115	310	20	70	20	60	20	50	60	180	25%	240	20
116	290	0	100	100	10	0	90	100	200	33%	300	20
117	270	50	100	0	110	30	50	80	260	24%	340	30
118	320	20	50	20	130	20	40	60	220	21%	280	20
119	270	0	80	20	50	60	20	80	150	35%	230	80
120	300	20	80	0	100	20	60	40	240	14%	280	40
121	250	30	70	0	70	40	20	70	160	30%	230	20
122	260	30	70	0	70	50	20	80	160	33%	240	50
123	310	20	90	0	80	30	40	50	210	19%	260	30
124	300	0	80	20	70	10	70	30	220	12%	250	20
125	300	40	80	0	120	40	20	80	220	27%	300	50
126	320	30	70	0	100	90	20	120	190	39%	310	50
127	310	30	80	10	70	80	20	120	170	41%	290	80
128	420	60	60	20	60	30	60	110	180	38%	290	30
129	300	30	70	10	90	80	50	120	210	36%	330	30
131	400	10	70	0	50	100	0	110	120	48%	230	100
132	370	30	60	0	30	90	20	120	110	52%	230	60
134	340	20	80	0	110	15	45	35	235	13%	270	70
135	310	20	80	30	90	20	40	70	210	25%	280	20
136	330	30	80	20	95	20	50	70	225	24%	295	0
137	300	70	20	65	30	40	65	175	115	60%	290	20
138	250	20	80	90	50	50	50	160	180	47%	340	40
139	270	0	70	50	50	0	100	50	220	19%	270	20
140	250	10	90	70	60	30	70	110	220	33%	330	40
141	230	80	60	70	20	40	10	190	90	68%	280	20
142	210	70	60	110	0	70	10	250	70	78%	320	20

ID	Depth to Top	Zone 1 Sand	Zone 1 Shale	Zone 2 Sand	Zone 2 Shale	Zone 3 Sand	Zone 3 Shale	Total Sand	Total Shale	Percent Sand	Total Thickness	Kiowa Thickness
144	240	70	40	70	20	30	60	170	120	59%	290	50
145	240	80	70	30	80	30	20	140	170	45%	310	30
146	240	80	40	50	50	30	40	160	130	55%	290	30
147	230	70	60	110	20	40	20	220	100	69%	320	20
148	220	50	60	90	50	60	10	200	120	63%	320	60
149	220	50	110	70	10	20	40	140	160	47%	300	40
150	240	70	70	50	40	20	40	140	150	48%	290	40
151	260	70	40	30	90	20	30	120	160	43%	280	40
152	260	100	40	30	70	50	40	180	150	55%	330	30
153	250	60	80	60	30	20	50	140	160	47%	300	30
154	270	70	40	30	100	30	30	130	170	43%	300	50
155	260	70	40	20	90	30	30	120	160	43%	280	50
156	250	80	50	30	80	50	50	160	180	47%	340	30
157	260	30	80	90	40	30	20	150	140	52%	290	70
158	250	60	60	70	30	60	20	190	110	63%	300	70
159	300	80	70	60	30	20	40	160	140	53%	300	40
160	320	90	40	0	40	90	0	180	80	69%	260	30
161	300	60	90	80	40	40	40	180	170	51%	350	30
162	350	10	90	20	130	50	30	80	250	24%	330	30
163	360	100	120	10	60	20	20	130	200	39%	330	30
164	400	20	80	40	50	0	100	60	230	21%	290	30
165	370	10	130	30	90	50	10	90	230	28%	320	30
166	320	30	80	40	50	10	50	80	180	31%	260	30
167	300	0	140	60	30	20	40	80	210	28%	290	60
168	280	0	90	70	70	0	70	70	230	23%	300	0
169	275	0	100	90	50	10	40	100	190	34%	290	30
170	280	80	40	40	80	30	70	150	190	44%	340	20
171	290	60	60	70	40	0	80	130	180	42%	310	50
173	300	50	40	120	0	10	70	180	110	62%	290	70
174	290	70	40	50	70	60	50	180	160	53%	340	20
175	300	60	40	40	50	30	90	130	180	42%	310	40
176	240	90	60	0	60	30	20	120	140	46%	260	40
177	250	80	50	10	30	60	20	150	100	60%	250	40
178	230	60	60	10	50	0	60	70	170	29%	240	20
179	310	50	60	10	110	30	50	90	220	29%	310	40
180	280	40	70	0	120	30	50	70	240	23%	310	30
181	280	50	40	50	80	10	90	110	210	34%	320	10
182	220	30	100	0	50	90	10	120	160	43%	280	50
183	210	80	70	0	90	30	20	110	180	38%	290	40
184	200	70	40	0	70	30	80	100	190	34%	290	30
185	210	80	30	0	90	70	10	150	130	54%	280	30
186	180	70	60	30	80	20	40	120	180	40%	300	60
187	190	80	30	0	100	60	60	140	190	42%	330	30
188	200	40	50	0	90	70	40	110	180	38%	290	60
189	220	80	30	0	70	40	70	120	170	41%	290	20
190	220	40	90	0	100	20	40	60	230	21%	290	100
191	340	40	70	80	70	60	30	180	170	51%	350	30
192	330	50	70	0	120	60	30	110	220	33%	330	20

ID	Depth to Top	Zone 1 Sand	Zone 1 Shale	Zone 2 Sand	Zone 2 Shale	Zone 3 Sand	Zone 3 Shale	Total Sand	Total Shale	Percent Sand	Total Thickness	Kiowa Thickness
193	320	40	60	10	60	80	10	130	130	50%	260	20
194	370	40	60	10	110	70	30	120	200	38%	320	10
195	360	40	60	20	100	70	40	130	200	39%	330	20
196	360	50	110	0	80	20	30	70	220	24%	290	0
197	365	50	50	50	120	50	20	150	190	44%	340	40
198	440	50	60	20	90	40	40	110	190	37%	300	30
199	460	10	60	50	30	30	60	90	150	38%	240	30
200	460	70	60	0	70	100	10	170	140	55%	310	20
201	450	60	80	10	80	30	50	100	210	32%	310	20
203	460	20	100	20	80	20	70	60	250	19%	310	0
204	430	60	90	10	70	60	20	130	180	42%	310	20
205	460	25	80	30	110	20	50	75	240	24%	315	40
206	440	60	80	20	100	30	40	110	220	33%	330	80
207	450	50	50	0	100	40	40	90	190	32%	280	70
208	430	60	50	0	100	60	90	120	240	33%	360	30
209	460	40	70	20	60	60	40	120	170	41%	290	50
210	450	40	60	30	100	40	40	110	200	35%	310	40
211	370	40	60	20	120	40	30	100	210	32%	310	40
212	420	80	50	0	70	30	50	110	170	39%	280	80
213	450	40	60	10	80	20	60	70	200	26%	270	40
214	440	70	50	10	50	50	40	130	140	48%	270	60
215	360	60	100	0	40	50	40	110	180	38%	290	50
216	360	50	60	20	60	70	30	140	150	48%	290	60
217	390	80	50	50	60	40	20	170	130	57%	300	30
218	370	80	50	0	100	30	30	110	180	38%	290	30
219	410	100	50	30	60	20	40	150	150	50%	300	30
220	430	50	90	0	80	30	30	80	200	29%	280	30
221	400	50	50	20	100	20	15	90	165	35%	255	0
222	440	70	70	30	90	20	90	120	250	32%	370	40
223	400	80	80	15	75	40	30	135	185	42%	320	30
224	400	0	150	70	50	40	60	110	260	30%	370	30
225	420	40	70	10	90	30	30	80	190	30%	270	0
226	370	20	60	10	130	20	50	50	240	17%	290	20
227	270	110	60	0	70	30	30	140	160	47%	300	30
228	270	40	90	20	80	30	20	90	190	32%	280	40
229	330	60	70	0	120	20	40	80	230	26%	310	40
230	340	90	40	40	60	30	20	160	120	57%	280	30
231	370	60	50	40	80	30	30	130	160	45%	290	50
232	350	20	80	10	110	20	30	50	220	19%	270	50
233	335	60	40	50	90	20	15	130	145	47%	275	30
234	330	20	70	20	80	50	40	90	190	32%	280	30
235	350	80	50	0	80	30	50	110	180	38%	290	100
236	380	80	40	40	60	30	40	150	140	52%	290	60
237	350	80	40	0	90	40	40	120	170	41%	290	110
238	410	50	80	10	55	10	40	70	175	29%	245	30
239	360	70	50	10	80	20	50	100	180	36%	280	40
240	355	40	60	40	80	20	40	100	180	36%	280	50
241	360	80	45	0	100	20	30	100	175	36%	275	55

ID	Depth to Top	Zone 1 Sand	Zone 1 Shale	Zone 2 Sand	Zone 2 Shale	Zone 3 Sand	Zone 3 Shale	Total Sand	Total Shale	Percent Sand	Total Thickness	Kiowa Thickness
242	400	80	70	60	10	10	35	150	115	57%	265	20
243	420	0	70	150	20	20	110	170	200	46%	370	20
244	420	50	70	70	60	20	70	140	200	41%	340	10
245	420	0	80	150	0	0	60	150	140	52%	290	60
246	350	10	90	0	120	20	60	30	270	10%	300	40
247	340	0	100	10	130	10	70	20	300	6%	320	30
248	330	40	80	15	130	40	30	95	240	28%	335	20
249	340	0	90	10	80	20	20	30	190	14%	220	110
250	350	30	50	25	110	30	30	85	190	31%	275	50
251	330	20	70	20	70	40	50	80	190	30%	270	60
252	350	0	80	0	100	40	50	40	230	15%	270	50
253	330	0	120	20	70	30	40	50	230	18%	280	20
254	380	20	110	0	90	40	30	60	230	21%	290	40
255	450	30	90	0	80	30	50	60	220	21%	280	60
256	440	30	100	20	60	30	40	80	200	29%	280	20
257	430	40	80	0	80	20	50	60	210	22%	270	70
258	380	40	90	20	50	20	70	80	210	28%	290	50
260	470	30	90	0	80	30	30	60	200	23%	260	50
261	470	40	70	0	80	40	40	80	190	30%	270	50
262	450	30	80	10	90	30	40	70	210	25%	280	50
263	370	40	70	0	90	40	30	80	190	30%	270	50
264	360	30	40	10	90	40	70	80	200	29%	280	30
265	450	70	50	10	90	30	40	110	180	38%	290	40
266	370	10	120	10	40	20	90	40	250	14%	290	30
267	430	30	70	50	70	10	50	90	190	32%	280	60
268	380	50	70	80	40	20	40	150	150	50%	300	50
269	350	20	110	30	30	30	70	80	210	28%	290	50
270	360	40	70	60	60	30	30	130	160	45%	290	50
271	450	0	50	0	120	40	50	40	220	15%	260	50
273	350	0	70	60	60	20	70	80	200	29%	280	60
274	330	0	60	80	70	20	30	100	160	38%	260	70
275	340	10	100	50	30	40	60	100	190	34%	290	50
276	320	70	50	10	100	30	40	110	190	37%	300	20
277	300	50	60	0	110	80	0	130	170	43%	300	50
278	330	50	70	0	100	30	30	80	200	29%	280	50
279	310	0	100	10	90	50	20	60	210	22%	270	50
280	340	0	90	0	100	40	50	40	240	14%	280	50
281	310	10	130	0	70	40	30	50	230	18%	280	50
282	310	70	60	10	80	60	20	140	160	47%	300	50
283	350	0	70	0	110	60	30	60	210	22%	270	60
284	330	10	70	0	80	100	30	110	180	38%	290	50
285	330	0	80	0	100	80	30	80	210	28%	290	50
286	340	30	100	20	70	30	30	80	200	29%	280	50
287	410	30	60	0	110	50	30	80	200	29%	280	50
288	360	70	50	10	90	30	40	110	180	38%	290	50
289	440	20	60	0	120	30	30	50	210	19%	260	50
290	380	20	90	0	100	40	10	60	200	23%	260	70
291	350	0	80	0	100	60	20	60	200	23%	260	60

ID	Depth to Top	Zone 1 Sand	Zone 1 Shale	Zone 2 Sand	Zone 2 Shale	Zone 3 Sand	Zone 3 Shale	Total Sand	Total Shale	Percent Sand	Total Thickness	Kiowa Thickness
292	400	0	100	0	100	20	30	20	230	8%	250	80
293	420	0	80	0	100	40	60	40	240	14%	280	50
294	430	20	50	0	130	30	40	50	220	19%	270	50
295	330	0	70	0	100	60	50	60	220	21%	280	50
296	340	70	60	0	110	40	20	110	190	37%	300	40
297	310	0	90	0	100	30	50	30	240	11%	270	50
298	300	30	70	0	120	30	20	60	210	22%	270	60
299	300	20	120	80	0	20	50	120	170	41%	290	60
300	320	20	80	0	130	30	20	50	230	18%	280	50
301	340	10	110	0	80	10	40	20	230	8%	250	70
302	330	10	110	0	100	20	30	30	240	11%	270	60
303	400	50	70	10	70	30	50	90	190	32%	280	40
304	450	0	110	10	70	30	50	40	230	15%	270	30
305	460	0	70	0	100	50	60	50	230	18%	280	40
307	450	10	40	0	120	50	30	60	190	24%	250	30
308	470	70	50	30	60	40	20	140	130	52%	270	50
309	470	0	130	10	70	30	30	40	230	15%	270	50
310	500	20	50	10	100	30	60	60	210	22%	270	50
311	480	0	110	20	60	20	60	40	230	15%	270	40
312	540	10	50	0	100	20	90	30	240	11%	270	50
313	460	0	80	0	90	40	60	40	230	15%	270	50
314	510	10	90	0	110	30	70	40	270	13%	310	30
315	510	0	90	0	100	80	10	80	200	29%	280	50
316	490	10	90	0	60	50	30	60	180	25%	240	40
317	450	40	60	0	100	40	20	80	180	31%	260	80
318	490	30	90	10	80	50	10	90	180	33%	270	50
319	510	0	90	20	60	30	30	50	180	22%	230	40
320	510	0	90	0	90	70	10	70	190	27%	260	40
321	450	0	90	10	90	90	20	100	200	33%	300	40
322	440	0	100	0	80	30	20	30	200	13%	230	30
323	500	0	110	0	90	20	60	20	260	7%	280	30
324	510	0	110	0	80	30	50	30	240	11%	270	30
325	520	0	80	0	60	40	60	40	200	17%	240	70
326	440	10	100	20	60	30	50	60	210	22%	270	40
327	430	10	120	10	70	30	30	50	220	19%	270	40
328	440	0	110	30	40	50	40	80	190	30%	270	50
329	470	10	90	0	80	40	40	50	210	19%	260	40
330	460	40	70	0	80	20	60	60	210	22%	270	50
331	450	40	60	0	90	20	60	60	210	22%	270	40
332	450	70	50	0	70	50	50	120	170	41%	290	40
333	450	30	80	10	90	20	60	60	230	21%	290	30
334	470	40	80	30	50	20	50	90	180	33%	270	40
335	420	30	60	30	80	60	30	120	170	41%	290	30
336	420	50	60	0	100	70	20	120	180	40%	300	30
337	420	30	130	0	70	30	40	60	240	20%	300	30
338	460	30	70	0	100	30	50	60	220	21%	280	40
339	440	30	60	0	100	30	50	60	210	22%	270	40
340	400	10	100	0	80	20	60	30	240	11%	270	40

ID	Depth to Top	Zone 1 Sand	Zone 1 Shale	Zone 2 Sand	Zone 2 Shale	Zone 3 Sand	Zone 3 Shale	Total Sand	Total Shale	Percent Sand	Total Thickness	Kiowa Thickness
341	470	0	100	0	90	30	30	30	220	12%	250	50
342	390	60	50	0	120	20	50	80	220	27%	300	50
343	430	50	90	0	70	30	30	80	190	30%	270	50
344	440	40	90	10	70	20	60	70	220	24%	290	40
345	420	60	40	10	100	20	50	90	190	32%	280	50
346	450	70	30	30	90	30	50	130	170	43%	300	50
347	430	80	50	10	80	40	30	130	160	45%	290	50
348	430	40	80	0	80	20	50	60	210	22%	270	40
349	430	20	110	0	80	20	40	40	230	15%	270	50
350	410	20	110	0	90	20	40	40	240	14%	280	40
351	370	50	80	20	90	20	40	90	210	30%	300	40
352	370	40	80	10	100	20	40	70	220	24%	290	40
353	360	20	90	10	90	30	40	60	220	21%	280	40
354	350	30	90	20	100	30	40	80	230	26%	310	40
355	370	20	90	0	110	40	30	60	230	21%	290	40
356	380	10	100	20	80	30	30	60	210	22%	270	50
357	380	30	80	0	90	40	40	70	210	25%	280	50
358	360	60	70	0	60	50	30	110	160	41%	270	40
359	330	80	50	20	50	50	40	150	140	52%	290	50
360	340	50	70	30	30	50	50	130	150	46%	280	50
361	350	30	60	20	80	30	50	80	190	30%	270	40
363	450	30	70	30	90	20	40	80	200	29%	280	50
364	470	30	50	20	80	50	50	100	180	36%	280	70
365	450	20	90	10	60	20	70	50	220	19%	270	50
366	500	20	80	20	60	20	50	60	190	24%	250	50
367	450	60	50	20	110	20	30	100	190	34%	290	70
368	460	50	40	80	10	10	100	140	150	48%	290	50
369	470	70	40	40	20	30	70	140	130	52%	270	50
370	460	50	70	20	80	40	20	110	170	39%	280	50
371	480	50	40	0	100	20	70	70	210	25%	280	40
372	480	50	70	0	100	20	30	70	200	26%	270	50
373	470	50	70	10	90	30	40	90	200	31%	290	40
374	500	30	50	50	40	20	80	100	170	37%	270	50
375	470	50	90	20	50	20	40	90	180	33%	270	60
376	440	80	50	0	90	20	50	100	190	34%	290	40
377	460	0	70	130	0	30	80	160	150	52%	310	40
378	500	60	30	10	90	10	60	80	180	31%	260	60
379	500	100	40	0	90	20	40	120	170	41%	290	60
380	460	70	70	0	70	0	70	70	210	25%	280	70
381	490	10	100	10	80	20	50	40	230	15%	270	50
382	540	30	50	30	70	0	110	60	230	21%	290	30
383	500	30	70	10	70	30	60	70	200	26%	270	40
384	450	0	90	30	70	30	60	60	220	21%	280	40
385	490	20	100	20	60	20	40	60	200	23%	260	40
386	490	20	50	0	90	50	70	70	210	25%	280	40
387	450	0	110	20	70	30	70	50	250	17%	300	50
388	490	10	70	20	100	30	60	60	230	21%	290	40
389	450	30	70	30	70	20	50	80	190	30%	270	20

ID	Depth to Top	Zone 1 Sand	Zone 1 Shale	Zone 2 Sand	Zone 2 Shale	Zone 3 Sand	Zone 3 Shale	Total Sand	Total Shale	Percent Sand	Total Thickness	Kiowa Thickness
390	440	0	110	30	70	40	50	70	230	23%	300	70
391	490	40	90	0	80	10	50	50	220	19%	270	50
392	480	10	90	20	90	30	40	60	220	21%	280	40
393	470	10	90	10	70	60	40	80	200	29%	280	40
394	490	20	80	10	100	30	40	60	220	21%	280	40
395	500	10	90	10	100	20	40	40	230	15%	270	60
396	470	40	80	10	90	30	40	80	210	28%	290	50
397	490	30	70	10	100	20	50	60	220	21%	280	50
398	470	10	70	0	110	30	50	40	230	15%	270	50
399	450	10	100	0	90	10	60	20	250	7%	270	50
400	440	0	70	0	90	20	60	20	220	8%	240	80
401	460	20	70	0	90	30	60	50	220	19%	270	50
402	435	10	65	30	70	10	75	50	210	19%	260	50
403	460	20	70	0	90	30	50	50	210	19%	260	60
404	460	0	90	10	90	20	50	30	230	12%	260	50
405	460	0	100	0	100	40	20	40	220	15%	260	50
406	420	0	90	0	90	30	50	30	230	12%	260	40
407	450	10	80	30	70	30	50	70	200	26%	270	50
408	420	10	80	10	90	30	70	50	240	17%	290	40
409	440	20	90	10	80	30	50	60	220	21%	280	40
410	446	20	94	0	100	10	80	30	274	10%	304	40
411	460	20	80	0	100	20	60	40	240	14%	280	60
412	440	10	70	0	130	20	40	30	240	11%	270	60
413	430	0	90	0	110	20	50	20	250	7%	270	40
414	430	20	90	0	90	30	40	50	220	19%	270	40
415	400	10	90	0	100	50	50	60	240	20%	300	40
416	450	20	80	0	80	30	30	50	190	21%	240	80
417	450	10	100	20	60	40	40	70	200	26%	270	50
418	430	40	50	100	0	40	80	180	130	58%	310	50
419	470	20	110	30	60	30	30	80	200	29%	280	50
420	460	0	100	0	80	30	70	30	250	11%	280	40
421	460	0	110	10	70	20	60	30	240	11%	270	50
422	470	10	80	10	90	20	60	40	230	15%	270	30
424	470	0	95	10	80	30	60	40	235	15%	275	50
425	450	30	80	0	90	30	40	60	210	22%	270	40
426	460	0	80	0	90	80	30	80	200	29%	280	50
427	490	10	100	10	100	10	60	30	260	10%	290	30
428	490	10	100	10	60	20	50	40	210	16%	250	60
430	580	20	80	20	50	20	60	60	190	24%	250	60
431	575	0	105	0	90	30	30	30	225	12%	255	60
432	540	0	120	0	90	40	30	40	240	14%	280	50
433	570	40	70	10	70	40	40	90	180	33%	270	60
434	530	0	100	20	50	30	90	50	240	17%	290	30
435	520	0	80	0	100	30	70	30	250	11%	280	40
436	520	20	90	20	90	10	50	50	230	18%	280	40
437	520	30	50	0	100	0	100	30	250	11%	280	40
438	540	60	20	20	80	50	30	130	130	50%	260	60
439	530	40	50	10	90	10	70	60	210	22%	270	30

ID	Depth to Top	Zone 1 Sand	Zone 1 Shale	Zone 2 Sand	Zone 2 Shale	Zone 3 Sand	Zone 3 Shale	Total Sand	Total Shale	Percent Sand	Total Thickness	Kiowa Thickness
440	450	30	50	0	100	60	40	90	190	32%	280	50
441	680	30	70	20	50	10	90	60	210	22%	270	60
442	520	70	50	0	80	30	40	100	170	37%	270	50
443	510	40	40	20	80	40	50	100	170	37%	270	60
444	510	50	30	40	50	30	60	120	140	46%	260	40
445	510	10	80	0	90	30	60	40	230	15%	270	50
446	510	0	90	0	100	40	50	40	240	14%	280	30
447	500	50	40	0	100	20	60	70	200	26%	270	50
448	550	50	50	10	80	30	30	90	160	36%	250	60
449	520	0	90	0	90	70	30	70	210	25%	280	40
450	510	0	80	20	50	90	40	110	170	39%	280	50
451	520	0	70	10	90	90	30	100	190	34%	290	50
452	490	30	70	10	100	20	30	60	200	23%	260	50
454	490	20	80	10	60	20	80	50	220	19%	270	50
455	470	20	90	30	80	30	50	80	220	27%	300	40
456	470	20	60	40	50	20	80	80	190	30%	270	80
457	530	0	85	10	85	20	55	30	225	12%	255	70
458	510	10	80	10	70	30	50	50	200	20%	250	60
459	480	10	80	20	80	25	65	55	225	20%	280	80
460	470	30	80	10	60	20	55	60	195	24%	255	90
462	490	15	80	10	60	20	70	45	210	18%	255	50
463	460	0	85	0	90	30	60	30	235	11%	265	40
464	470	0	80	25	75	20	50	45	205	18%	250	60
465	465	15	55	35	65	20	80	70	200	26%	270	50
466	440	50	40	30	70	20	70	100	180	36%	280	40
467	470	10	70	20	80	30	70	60	220	21%	280	40
468	470	70	60	20	50	20	70	110	180	38%	290	50
469	450	0	100	0	80	10	70	10	250	4%	260	70
470	465	20	40	30	70	10	80	60	190	24%	250	60
471	455	30	70	20	80	25	50	75	200	27%	275	50
472	460	20	90	0	70	30	70	50	230	18%	280	45
473	470	20	90	0	90	50	20	70	200	26%	270	40
474	440	95	50	20	65	10	40	125	155	45%	280	55
476	460	0	90	0	70	20	60	20	220	8%	240	20
477	460	0	90	30	70	10	50	40	210	16%	250	50
478	430	10	100	30	70	10	50	50	220	19%	270	50
479	450	120	60	20	50	0	50	140	160	47%	300	50
480	440	50	60	0	100	20	50	70	210	25%	280	50
481	450	40	60	0	100	30	50	70	210	25%	280	40
482	420	30	80	20	100	20	50	70	230	23%	300	40
483	440	40	60	0	90	50	50	90	200	31%	290	20
484	440	30	50	0	110	10	60	40	220	15%	260	50
485	440	40	60	10	80	40	40	90	180	33%	270	30
486	430	40	100	0	80	10	40	50	220	19%	270	50
487	430	40	100	0	70	10	60	50	230	18%	280	40
488	450	50	50	0	100	40	60	90	210	30%	300	30
490	420	20	90	10	90	40	30	70	210	25%	280	40
491	420	40	110	0	80	10	40	50	230	18%	280	40

ID	Depth to Top	Zone 1 Sand	Zone 1 Shale	Zone 2 Sand	Zone 2 Shale	Zone 3 Sand	Zone 3 Shale	Total Sand	Total Shale	Percent Sand	Total Thickness	Kiowa Thickness
492	430	50	80	0	80	20	40	70	200	26%	270	40
493	430	80	60	0	80	20	30	100	170	37%	270	50
494	420	90	60	0	80	10	40	100	180	36%	280	40
495	440	80	70	0	80	20	40	100	190	34%	290	50
496	450	70	50	0	100	20	40	90	190	32%	280	50
497	450	30	90	0	70	10	80	40	240	14%	280	60
498	460	70	70	0	70	10	60	80	200	29%	280	50
499	420	100	60	20	60	30	30	150	150	50%	300	50
501	470	50	80	20	80	20	40	90	200	31%	290	40
502	480	50	40	20	70	0	80	70	190	27%	260	50
503	520	20	60	10	90	10	90	40	240	14%	280	30
505	450	90	50	0	70	40	30	130	150	46%	280	50
506	470	80	30	0	90	40	70	120	190	39%	310	30
507	440	90	30	20	60	30	60	140	150	48%	290	40
509	520	40	70	10	110	10	40	60	220	21%	280	40
510	540	70	30	0	120	60	10	130	160	45%	290	40
511	560	70	40	0	110	20	40	90	190	32%	280	40
512	570	0	70	0	110	30	50	30	230	12%	260	40
514	530	50	60	0	130	30	30	80	220	27%	300	30
515	520	50	30	0	110	20	40	70	180	28%	250	60
519	200	20	70	0	110	110	0	130	180	42%	310	10
520	200	30	50	0	120	70	30	100	200	33%	300	20
521	480	70	60	20	60	40	40	130	160	45%	290	40
526	140	70	70	0	70	70	20	140	160	47%	300	20
529	230	50	20	20	80	30	90	100	190	34%	290	10
530	210	40	50	0	100	30	50	70	200	26%	270	30
531	220	60	70	50	30	30	80	140	180	44%	320	15
532	230	50	60	0	100	30	50	80	210	28%	290	30
533	220	110	60	0	60	30	40	140	160	47%	300	40
535	265	90	50	10	80	0	60	100	190	34%	290	75
536	270	110	40	0	90	0	40	110	170	39%	280	80
537	270	60	40	20	60	10	90	90	190	32%	280	30
538	270	70	40	0	100	0	60	70	200	26%	270	80
539	260	60	40	50	40	30	60	140	140	50%	280	40
540	260	60	40	30	50	60	40	150	130	54%	280	0
542	300	70	90	10	90	30	30	110	210	34%	320	30
543	290	70	60	0	110	20	30	90	200	31%	290	70
544	300	60	30	20	80	50	40	130	150	46%	280	30
545	270	20	90	10	110	30	60	60	260	19%	320	30
546	310	20	100	0	90	10	70	30	260	10%	290	20
548	250	30	100	0	100	50	50	80	250	24%	330	30
549	230	120	50	0	50	30	60	150	160	48%	310	20
550	230	110	60	0	50	20	40	130	150	46%	280	40
551	240	60	100	0	60	30	30	90	190	32%	280	40
552	250	90	50	20	80	10	40	120	170	41%	290	70
553	270	40	40	40	80	20	40	100	160	38%	260	40
554	280	20	110	10	80	10	50	40	240	14%	280	30
555	260	90	40	40	50	30	40	160	130	55%	290	50

ID	Depth to Top	Zone 1 Sand	Zone 1 Shale	Zone 2 Sand	Zone 2 Shale	Zone 3 Sand	Zone 3 Shale	Total Sand	Total Shale	Percent Sand	Total Thickness	Kiowa Thickness
557	210	30	30	0	130	80	30	110	190	37%	300	30
558	240	20	70	0	70	60	60	80	200	29%	280	30
559	230	50	50	0	130	20	40	70	220	24%	290	30
560	180	60	50	10	110	50	20	120	180	40%	300	30
561	230	40	50	0	150	25	35	65	235	22%	300	20
562	235	0	100	0	125	20	50	20	275	7%	295	50
563	230	0	90	0	70	90	20	90	180	33%	270	30
564	230	0	100	0	110	40	40	40	250	14%	290	50
565	200	20	100	0	60	70	30	90	190	32%	280	30
566	260	0	140	60	10	20	60	80	210	28%	290	30
567	170	20	70	20	90	20	70	60	230	21%	290	30
568	170	10	90	20	50	90	0	120	140	46%	260	0
569	200	10	80	40	50	30	70	80	200	29%	280	30
570	190	0	110	40	50	30	60	70	220	24%	290	30
573	185	60	40	50	60	20	60	130	160	45%	290	30
574	130	30	50	0	100	40	65	70	215	25%	285	100
575	170	20	80	40	90	20	60	80	230	26%	310	20
576	170	20	80	40	60	10	60	70	200	26%	270	40
577	150	80	50	10	90	20	55	110	195	36%	305	40
579	190	0	100	40	70	30	50	70	220	24%	290	20
582	160	60	50	20	30	30	70	110	150	42%	260	90
583	160	40	80	20	80	30	60	90	220	29%	310	50
588	130	0	150	50	30	30	30	80	210	28%	290	40
589	150	10	100	10	80	30	50	50	230	18%	280	20
590	120	30	40	20	90	10	90	60	220	21%	280	30
591	150	60	40	0	100	40	60	100	200	33%	300	30
592	300	30	80	40	60	30	40	100	180	36%	280	40
593	300	20	90	120	10	40	30	180	130	58%	310	30
594	290	10	60	10	90	30	70	50	220	19%	270	45
595	310	50	60	60	40	20	30	130	130	50%	260	10
596	200	0	100	0	100	60	30	60	230	21%	290	30
597	200	90	50	0	80	20	50	110	180	38%	290	50
598	200	50	60	0	80	10	80	60	220	21%	280	50
599	180	30	100	0	90	30	30	60	220	21%	280	30
600	250	30	120	0	90	10	30	40	240	14%	280	40
601	320	10	70	10	90	30	50	50	210	19%	260	40
602	320	0	130	20	40	0	80	20	250	7%	270	50
603	320	0	90	20	110	45	10	65	210	24%	275	80
604	320	10	90	30	100	25	35	65	225	22%	290	30
605	330	0	100	20	100	50	10	70	210	25%	280	10
606	320	0	100	50	50	10	70	60	220	21%	280	60
607	250	40	70	70	20	0	90	110	180	38%	290	60
608	230	20	80	0	90	10	70	30	240	11%	270	50
609	160	40	100	0	100	30	20	70	220	24%	290	30
610	150	40	110	20	80	30	20	90	210	30%	300	30
611	250	20	80	30	50	30	60	80	190	30%	270	70
612	250	30	110	10	70	30	50	70	230	23%	300	30
613	245	0	100	15	75	30	60	45	235	16%	280	40

ID	Depth to Top	Zone 1 Sand	Zone 1 Shale	Zone 2 Sand	Zone 2 Shale	Zone 3 Sand	Zone 3 Shale	Total Sand	Total Shale	Percent Sand	Total Thickness	Kiowa Thickness
614	295	10	80	20	100	30	30	60	210	22%	270	60
616	275	10	80	10	105	20	50	40	235	15%	275	90
617	250	0	90	0	120	30	35	30	245	11%	275	60
618	240	20	80	10	90	60	30	90	200	31%	290	70
619	200	0	100	0	80	80	30	80	210	28%	290	50
621	230	20	50	0	100	20	60	40	210	16%	250	70
623	210	0	100	30	70	30	50	60	220	21%	280	80
624	220	10	80	0	120	20	40	30	240	11%	270	50
625	230	0	120	0	100	30	20	30	240	11%	270	80
626	210	10	140	0	80	30	20	40	240	14%	280	50
628	180	10	110	0	80	10	70	20	260	7%	280	60
629	200	0	130	50	30	30	40	80	200	29%	280	60
630	210	10	80	0	110	40	30	50	220	19%	270	60
632	250	20	80	0	100	10	60	30	240	11%	270	60
635	240	0	70	0	80	30	70	30	220	12%	250	50
637	230	10	80	0	80	50	50	60	210	22%	270	60
638	230	0	100	10	70	50	50	60	220	21%	280	80
639	240	0	70	0	100	30	70	30	240	11%	270	60
640	280	20	60	0	60	40	40	60	160	27%	220	80
641	230	20	60	0	100	50	30	70	190	27%	260	60
644	240	60	90	10	70	30	20	100	180	36%	280	40
645	240	30	100	0	50	30	70	60	220	21%	280	60
647	250	15	85	0	95	20	50	35	230	13%	265	60
648	250	0	110	10	85	40	30	50	225	18%	275	30
649	190	20	40	0	100	40	10	60	150	29%	210	20
652	400	50	70	0	70	50	50	100	190	34%	290	40
653	380	40	100	20	50	30	40	90	190	32%	280	30
654	370	20	110	50	50	30	30	100	190	34%	290	40
655	370	40	70	60	60	40	30	140	160	47%	300	40
656	340	60	50	20	80	40	30	120	160	43%	280	0
657	420	50	90	70	30	20	40	140	160	47%	300	30
658	440	10	100	60	30	10	70	80	200	29%	280	40
659	440	10	60	90	70	30	20	130	150	46%	280	40
660	440	0	120	90	10	20	40	110	170	39%	280	40
661	400	20	90	80	50	40	20	140	160	47%	300	70
662	410	20	80	40	45	40	60	100	185	35%	285	70
663	430	20	70	30	90	25	45	75	205	27%	280	70
664	450	0	90	0	100	50	40	50	230	18%	280	50
665	435	50	70	40	40	20	90	110	200	35%	310	30
666	435	40	70	65	45	15	40	120	155	44%	275	50
667	435	30	70	40	70	0	65	70	205	25%	275	80
668	395	30	80	80	45	35	25	145	150	49%	295	70
669	410	30	70	60	50	40	40	130	160	45%	290	50
670	420	30	80	70	75	20	20	120	175	41%	295	70
671	490	30	90	20	40	40	50	90	180	33%	270	50
672	390	30	80	30	90	35	25	95	195	33%	290	50
673	470	40	80	60	30	20	40	120	150	44%	270	40
674	470	20	90	40	70	20	50	80	210	28%	290	40

ID	Depth to Top	Zone 1 Sand	Zone 1 Shale	Zone 2 Sand	Zone 2 Shale	Zone 3 Sand	Zone 3 Shale	Total Sand	Total Shale	Percent Sand	Total Thickness	Kiowa Thickness
675	510	50	70	20	70	10	30	80	170	32%	250	50
676	520	0	110	0	80	20	40	20	230	8%	250	50
677	520	20	60	10	70	30	70	60	200	23%	260	50
678	530	40	50	20	60	30	40	90	150	38%	240	60
679	500	50	80	0	70	20	50	70	200	26%	270	50
680	510	10	80	20	80	20	40	50	200	20%	250	60
681	530	0	100	0	90	20	30	20	220	8%	240	50
682	500	10	70	0	90	30	80	40	240	14%	280	30
683	490	20	70	10	110	40	40	70	220	24%	290	30
684	510	10	120	0	70	30	50	40	240	14%	280	30
685	510	0	80	0	90	30	40	30	210	13%	240	60
686	450	20	50	40	40	30	80	90	170	35%	260	20
687	440	10	90	60	40	20	80	90	210	30%	300	20
688	450	60	60	20	90	40	40	120	190	39%	310	20
689	510	10	100	0	90	40	10	50	200	20%	250	70
690	500	10	120	0	80	40	10	50	210	19%	260	70
691	500	50	30	20	110	40	10	110	150	42%	260	70
692	470	0	110	10	70	40	60	50	240	17%	290	30
693	455	80	40	0	90	60	30	140	160	47%	300	30
694	470	30	50	10	110	30	20	70	180	28%	250	15
695	520	0	90	0	80	40	40	40	210	16%	250	20
696	520	0	100	0	90	20	20	20	210	9%	230	80
697	455	100	50	0	100	0	60	100	210	32%	310	20
698	515	0	90	0	120	40	10	40	220	15%	260	70
699	515	10	65	10	120	30	10	50	195	20%	245	70
700	525	0	80	0	140	20	20	20	240	8%	260	80
701	440	0	110	0	100	60	30	60	240	20%	300	30
702	450	0	100	30	80	50	30	80	210	28%	290	30
703	450	0	110	20	90	60	20	80	220	27%	300	30
704	500	20	70	10	100	20	60	50	230	18%	280	40
705	440	20	110	0	90	20	30	40	230	15%	270	40
706	440	20	120	0	80	20	30	40	230	15%	270	40
707	450	10	90	50	50	20	40	80	180	31%	260	50
708	450	0	100	20	90	20	30	40	220	15%	260	40
709	430	10	60	10	80	20	50	40	190	17%	230	50
710	440	0	120	30	60	40	40	70	220	24%	290	20
711	430	0	90	30	70	30	70	60	230	21%	290	30
712	460	0	90	30	60	20	60	50	210	19%	260	50
713	450	0	100	60	50	20	50	80	200	29%	280	40
714	470	30	110	20	80	40	50	90	240	27%	330	30
715	440	0	110	30	70	30	100	60	280	18%	340	30
716	450	0	110	25	85	40	40	65	235	22%	300	30
717	430	0	110	30	70	60	20	90	200	31%	290	20
718	430	40	90	0	80	40	40	80	210	28%	290	20
719	450	20	80	15	110	45	10	80	200	29%	280	20
720	460	10	70	60	40	60	50	130	160	45%	290	20
721	420	0	95	20	100	30	55	50	250	17%	300	20
722	430	0	80	0	150	40	10	40	240	14%	280	30

ID	Depth to Top	Zone 1 Sand	Zone 1 Shale	Zone 2 Sand	Zone 2 Shale	Zone 3 Sand	Zone 3 Shale	Total Sand	Total Shale	Percent Sand	Total Thickness	Kiowa Thickness
723	350	0	120	80	30	35	15	115	165	41%	280	40
724	340	20	70	0	90	40	60	60	220	21%	280	40
725	350	10	95	100	10	30	40	140	145	49%	285	50
726	280	20	70	20	90	60	30	100	190	34%	290	50
728	380	0	80	0	80	30	60	30	220	12%	250	70
729	370	0	90	0	100	70	40	70	230	23%	300	30
730	400	0	100	0	100	80	20	80	220	27%	300	20
731	390	10	100	20	80	100	0	130	180	42%	310	30
732	390	15	105	10	80	100	10	125	195	39%	320	40
733	390	40	70	0	90	80	20	120	180	40%	300	30
734	420	0	100	20	90	50	20	70	210	25%	280	30
735	420	0	120	10	70	50	40	60	230	21%	290	20
736	400	0	100	10	90	70	30	80	220	27%	300	30
737	410	10	100	10	80	70	20	90	200	31%	290	30
738	420	0	80	20	80	70	40	90	200	31%	290	30
739	430	0	110	20	50	20	70	40	230	15%	270	40
740	440	0	110	30	50	30	60	60	220	21%	280	30
741	400	20	90	10	70	20	70	50	230	18%	280	30
742	410	30	80	10	80	40	20	80	180	31%	260	30
743	420	50	60	10	80	50	30	110	170	39%	280	40
744	400	30	70	10	90	70	30	110	190	37%	300	30
745	420	40	90	0	90	70	10	110	190	37%	300	20
746	420	50	80	0	110	100	0	150	190	44%	340	50
747	410	10	90	30	80	50	50	90	220	29%	310	30
748	370	10	90	40	60	60	30	110	180	38%	290	40
749	390	0	100	70	40	40	50	110	190	37%	300	30
750	380	0	110	50	40	60	40	110	190	37%	300	30
752	380	0	100	80	30	40	60	120	190	39%	310	30
753	360	0	60	90	30	20	80	110	170	39%	280	60
754	330	0	100	60	20	30	70	90	190	32%	280	50
755	350	0	90	0	90	30	60	30	240	11%	270	20
756	310	0	70	10	90	10	90	20	250	7%	270	20
757	270	30	70	20	70	0	90	50	230	18%	280	50
758	280	20	80	10	90	20	50	50	220	19%	270	50
759	300	0	80	60	40	40	60	100	180	36%	280	70
760	340	10	90	0	90	70	30	80	210	28%	290	40
761	330	0	120	0	90	70	20	70	230	23%	300	40
763	330	10	90	0	100	60	30	70	220	24%	290	60
764	410	50	80	0	80	70	20	120	180	40%	300	30
765	350	0	110	20	60	70	40	90	210	30%	300	40
766	320	20	80	20	90	70	20	110	190	37%	300	80
767	370	20	80	30	70	70	30	120	180	40%	300	30
768	390	10	60	40	50	50	50	100	160	38%	260	30
769	360	0	100	10	80	80	30	90	210	30%	300	50
771	250	0	90	30	90	80	10	110	190	37%	300	60
772	300	40	40	0	120	30	60	70	220	24%	290	60
773	300	30	80	40	90	70	10	140	180	44%	320	70
774	290	10	80	0	90	80	40	90	210	30%	300	40

ID	Depth to Top	Zone 1 Sand	Zone 1 Shale	Zone 2 Sand	Zone 2 Shale	Zone 3 Sand	Zone 3 Shale	Total Sand	Total Shale	Percent Sand	Total Thickness	Kiowa Thickness
775	300	30	70	10	80	20	40	60	190	24%	250	70
776	320	20	70	10	90	50	40	80	200	29%	280	30
777	340	0	100	0	90	30	50	30	240	11%	270	30
778	310	0	100	0	90	30	60	30	250	11%	280	40
779	340	10	50	10	90	50	50	70	190	27%	260	60
780	310	10	100	10	90	30	40	50	230	18%	280	40
782	300	10	60	20	90	20	70	50	220	19%	270	60
783	300	40	70	10	80	10	70	60	220	21%	280	50
784	310	30	80	20	70	30	50	80	200	29%	280	50
785	280	30	70	10	90	30	50	70	210	25%	280	50
786	320	50	70	10	70	30	50	90	190	32%	280	50
787	300	60	60	10	70	40	40	110	170	39%	280	20
789	270	20	80	0	90	30	60	50	230	18%	280	50
790	310	10	80	0	100	30	50	40	230	15%	270	40
791	310	30	60	0	100	30	50	60	210	22%	270	50
792	280	20	80	0	70	30	80	50	230	18%	280	40
793	230	20	50	0	100	30	70	50	220	19%	270	60
794	280	40	70	0	90	50	30	90	190	32%	280	50
795	240	10	70	0	100	20	60	30	230	12%	260	50
796	270	10	60	20	80	60	40	90	180	33%	270	60
797	270	30	80	10	80	30	50	70	210	25%	280	50
798	450	20	35	30	130	20	10	70	175	29%	245	80
800	470	0	90	10	90	20	40	30	220	12%	250	70
801	460	30	40	10	90	40	60	80	190	30%	270	60
802	460	30	30	10	120	40	40	80	190	30%	270	50
803	450	0	90	20	90	30	30	50	210	19%	260	50
804	500	0	100	10	80	30	50	40	230	15%	270	30
805	500	20	30	20	100	30	80	70	210	25%	280	40
806	500	30	80	0	100	10	60	40	240	14%	280	30
807	490	30	90	0	70	20	70	50	230	18%	280	30
809	440	60	80	0	70	40	30	100	180	36%	280	40
810	510	0	80	0	120	10	100	10	300	3%	310	60
811	520	0	80	0	100	40	50	40	230	15%	270	40
812	470	0	90	20	50	20	90	40	230	15%	270	40
813	450	20	70	10	80	10	70	40	220	15%	260	40
814	470	10	90	0	80	30	50	40	220	15%	260	40
815	530	10	90	0	90	20	60	30	240	11%	270	40
816	500	0	90	0	110	40	40	40	240	14%	280	30
817	480	10	60	20	80	30	60	60	200	23%	260	50
818	540	20	60	10	90	20	80	50	230	18%	280	30
819	490	30	70	30	80	20	80	80	230	26%	310	50
820	480	10	100	0	100	20	30	30	230	12%	260	50
821	550	0	100	10	90	10	60	20	250	7%	270	30
822	510	0	80	0	100	10	80	10	260	4%	270	40
823	450	40	60	0	70	10	80	50	210	19%	260	50
824	470	30	60	50	60	30	40	110	160	41%	270	50
825	440	30	60	20	80	30	50	80	190	30%	270	50
826	440	20	60	10	70	20	80	50	210	19%	260	50

ID	Depth to Top	Zone 1 Sand	Zone 1 Shale	Zone 2 Sand	Zone 2 Shale	Zone 3 Sand	Zone 3 Shale	Total Sand	Total Shale	Percent Sand	Total Thickness	Kiowa Thickness
827	430	0	120	60	40	0	50	60	210	22%	270	40
829	360	30	100	60	40	10	70	100	210	32%	310	30
830	280	40	60	50	70	0	80	90	210	30%	300	60
831	460	0	110	0	100	10	40	10	250	4%	260	50
832	410	30	80	20	80	30	20	80	180	31%	260	50
833	460	10	50	60	60	20	60	90	170	35%	260	40
835	420	20	40	60	40	70	60	150	140	52%	290	40
836	450	40	70	10	50	40	50	90	170	35%	260	60
837	390	10	100	50	40	30	30	90	170	35%	260	60
838	400	30	40	30	60	70	30	130	130	50%	260	60
839	420	60	40	10	80	30	60	100	180	36%	280	50
840	450	30	90	10	80	40	30	80	200	29%	280	50
841	460	20	80	0	80	20	70	40	230	15%	270	60
842	460	10	90	0	80	20	70	30	240	11%	270	40
843	360	30	100	60	30	0	70	90	200	31%	290	40
844	410	30	80	60	30	20	70	110	180	38%	290	40
845	430	0	80	20	70	20	50	40	200	17%	240	40
846	440	10	80	60	50	30	50	100	180	36%	280	40
847	420	30	80	0	80	60	30	90	190	32%	280	40
848	420	20	80	0	80	50	50	70	210	25%	280	30
849	400	30	80	0	80	50	30	80	190	30%	270	30
850	370	20	90	0	80	30	60	50	230	18%	280	40
851	420	30	90	0	70	50	40	80	200	29%	280	40
852	410	20	80	10	80	40	40	70	200	26%	270	40
853	420	40	70	10	60	20	60	70	190	27%	260	60
854	340	0	100	30	60	30	30	60	190	24%	250	30
855	410	40	70	0	90	20	60	60	220	21%	280	30
856	500	20	60	30	90	10	70	60	220	21%	280	30
857	430	10	60	40	60	50	70	100	190	34%	290	30
858	440	30	40	50	40	50	80	130	160	45%	290	40
859	430	20	50	40	60	30	70	90	180	33%	270	40
860	370	30	40	0	110	30	70	60	220	21%	280	30
861	360	40	60	0	90	30	60	70	210	25%	280	50
862	440	40	70	0	90	20	60	60	220	21%	280	30
863	430	40	70	10	60	20	70	70	200	26%	270	50
864	320	30	60	20	70	10	70	60	200	23%	260	60
865	460	30	50	20	50	30	70	80	170	32%	250	40
866	320	40	50	70	10	30	70	140	130	52%	270	60
867	410	20	70	40	60	30	40	90	170	35%	260	60
868	320	0	110	20	60	20	40	40	210	16%	250	50
869	320	0	90	40	40	20	60	60	190	24%	250	60
870	290	40	90	0	70	30	30	70	190	27%	260	50
871	280	0	70	40	50	50	60	90	180	33%	270	60
872	280	0	90	30	70	50	50	80	210	28%	290	40
873	330	10	80	10	90	40	40	60	210	22%	270	50
874	290	20	70	10	90	40	50	70	210	25%	280	40
875	330	0	110	80	0	50	40	130	150	46%	280	50
876	330	10	80	20	50	30	60	60	190	24%	250	50

ID	Depth to Top	Zone 1 Sand	Zone 1 Shale	Zone 2 Sand	Zone 2 Shale	Zone 3 Sand	Zone 3 Shale	Total Sand	Total Shale	Percent Sand	Total Thickness	Kiowa Thickness
878	330	0	100	60	40	40	40	100	180	36%	280	30
879	310	10	90	20	70	20	80	50	240	17%	290	30
880	320	20	60	70	30	20	40	110	130	46%	240	20
881	310	20	80	10	60	20	80	50	220	19%	270	50
882	310	30	60	0	80	0	60	30	200	13%	230	20
883	270	10	80	10	100	20	50	40	230	15%	270	60
884	270	20	70	10	100	60	20	90	190	32%	280	50
886	260	20	70	20	90	20	60	60	220	21%	280	50
887	470	60	40	0	100	50	30	110	170	39%	280	40
888	460	50	40	20	70	30	70	100	180	36%	280	50
889	490	30	60	20	90	30	40	80	190	30%	270	40
890	470	60	40	10	90	20	60	90	190	32%	280	60
891	440	40	50	20	70	40	70	100	190	34%	290	40
893	470	60	40	20	80	20	60	100	180	36%	280	60
894	480	30	70	0	100	20	50	50	220	19%	270	40
895	420	20	50	80	30	50	50	150	130	54%	280	70
898	390	80	30	30	50	40	50	150	130	54%	280	80
899	450	70	30	30	70	0	80	100	180	36%	280	40
903	260	0	110	80	0	50	50	130	160	45%	290	70
904	360	60	20	70	40	30	70	160	130	55%	290	30
906	70	80	30	10	80	10	80	100	190	34%	290	30
907	70	20	70	20	80	30	70	70	220	24%	290	0
908	40	90	30	10	90	40	60	140	180	44%	320	20
910	190	10	90	0	70	30	50	40	210	16%	250	40
911	170	20	60	0	100	80	30	100	190	34%	290	30
912	180	20	10	0	110	40	60	60	180	25%	240	30
914	120	10	40	0	140	60	20	70	200	26%	270	80
915	110	0	110	30	60	20	70	50	240	17%	290	50
916	130	20	40	10	135	20	40	50	215	19%	265	0
917	130	30	30	10	110	90	10	130	150	46%	280	75
918	120	10	40	110	80	20	35	140	155	47%	295	40
919	140	20	60	20	70	50	50	90	180	33%	270	60
920	140	20	70	90	30	10	60	120	160	43%	280	60
922	130	20	80	10	90	60	40	90	210	30%	300	50
923	140	20	90	60	30	30	60	110	180	38%	290	50
924	150	60	70	20	50	20	60	100	180	36%	280	60
926	130	20	40	20	150	35	20	75	210	26%	285	60
927	130	60	60	10	90	40	20	110	170	39%	280	0
928	150	30	90	0	90	10	70	40	250	14%	290	0
929	120	0	100	10	90	40	80	50	270	16%	320	0
930	140	0	80	20	80	30	60	50	220	19%	270	0
931	130	10	90	20	80	30	50	60	220	21%	280	0
932	130	40	70	10	60	30	70	80	200	29%	280	0
933	130	0	70	10	100	10	80	20	250	7%	270	30
934	135	10	55	40	110	20	50	70	215	25%	285	50
935	120	10	40	60	130	30	50	100	220	31%	320	25
936	140	30	90	10	70	20	50	60	210	22%	270	40
937	155	20	45	40	130	30	25	90	200	31%	290	50

ID	Depth to Top	Zone 1 Sand	Zone 1 Shale	Zone 2 Sand	Zone 2 Shale	Zone 3 Sand	Zone 3 Shale	Total Sand	Total Shale	Percent Sand	Total Thickness	Kiowa Thickness
939	130	60	60	10	90	30	40	100	190	34%	290	40
940	140	0	80	120	0	50	80	170	160	52%	330	0
942	160	0	80	50	50	20	70	70	200	26%	270	60
944	130	20	50	100	20	30	70	150	140	52%	290	20
945	150	20	60	50	70	20	80	90	210	30%	300	30
948	220	10	70	20	80	10	80	40	230	15%	270	0
949	110	10	90	0	90	10	90	20	270	7%	290	50
950	120	20	80	20	80	40	50	80	210	28%	290	60
952	120	20	60	70	20	50	60	140	140	50%	280	50
953	110	30	70	140	0	20	50	190	120	61%	310	50
957	100	40	50	30	90	30	50	100	190	34%	290	50
958	130	0	90	10	90	30	60	40	240	14%	280	50
960	130	30	50	90	10	60	50	180	110	62%	290	50
961	140	10	110	40	50	30	50	80	210	28%	290	50
962	140	20	40	50	60	20	80	90	180	33%	270	60
963	130	0	90	20	90	20	70	40	250	14%	290	50
964	90	10	100	0	110	20	70	30	280	10%	310	30
965	20	20	60	0	100	70	30	90	190	32%	280	40
967	50	70	50	20	80	50	20	140	150	48%	290	40
968	60	10	80	20	80	30	60	60	220	21%	280	60
969	70	30	80	10	60	30	70	70	210	25%	280	40
970	50	40	80	30	70	40	40	110	190	37%	300	30
972	200	20	60	40	60	50	50	110	170	39%	280	40
973	200	10	60	0	100	20	80	30	240	11%	270	40
974	180	20	80	0	70	70	30	90	180	33%	270	30
975	210	0	80	0	90	60	40	60	210	22%	270	60
978	170	20	80	0	80	70	40	90	200	31%	290	50
979	200	20	80	0	100	30	40	50	220	19%	270	50
980	200	0	80	0	90	60	40	60	210	22%	270	80
981	180	10	90	0	80	50	60	60	230	21%	290	50
983	180	0	90	0	80	30	70	30	240	11%	270	40
984	200	20	50	10	90	40	60	70	200	26%	270	30
985	180	0	100	0	100	20	60	20	260	7%	280	50
986	170	20	80	0	80	40	60	60	220	21%	280	50
987	180	0	90	0	80	50	50	50	220	19%	270	50
988	210	30	70	0	80	20	70	50	220	19%	270	50
989	180	30	70	0	90	30	60	60	220	21%	280	60
990	160	0	70	40	70	30	70	70	210	25%	280	60
991	190	0	100	0	90	30	70	30	260	10%	290	30
994	230	0	100	0	80	30	50	30	230	12%	260	60
995	140	20	80	0	100	30	50	50	230	18%	280	50
996	140	20	80	0	100	50	30	70	210	25%	280	60
997	190	10	80	0	90	40	50	50	220	19%	270	40
999	180	20	90	20	60	30	50	70	200	26%	270	20
1001	180	0	70	0	100	20	80	20	250	7%	270	20
1004	190	20	90	0	80	30	60	50	230	18%	280	50
1007	160	0	90	40	60	20	70	60	220	21%	280	50
1008	170	10	90	40	50	60	40	110	180	38%	290	40

ID	Depth to Top	Zone 1 Sand	Zone 1 Shale	Zone 2 Sand	Zone 2 Shale	Zone 3 Sand	Zone 3 Shale	Total Sand	Total Shale	Percent Sand	Total Thickness	Kiowa Thickness
1009	180	0	100	40	60	60	30	100	190	34%	290	50
1011	190	10	100	20	80	20	50	50	230	18%	280	50
1012	180	0	110	20	70	50	40	70	220	24%	290	50
1013	180	0	110	20	70	60	30	80	210	28%	290	50
1014	180	0	100	20	80	60	30	80	210	28%	290	50
1015	190	10	80	10	80	40	60	60	220	21%	280	50
1016	150	0	90	60	40	40	70	100	200	33%	300	50
1017	180	10	90	10	80	30	60	50	230	18%	280	50
1018	160	30	50	40	110	30	20	100	180	36%	280	0
1019	170	20	100	20	90	60	20	100	210	32%	310	20
1020	130	0	65	70	90	50	15	120	170	41%	290	0
1021	140	0	60	20	140	30	30	50	230	18%	280	0
1022	160	10	100	20	70	50	40	80	210	28%	290	20
1023	180	20	100	20	70	40	20	80	190	30%	270	15
1024	155	0	70	20	140	30	25	50	235	18%	285	30
1025	210	20	60	0	80	20	40	40	180	18%	220	20
1026	170	0	90	70	40	50	50	120	180	40%	300	40
1027	160	10	80	30	70	50	40	90	190	32%	280	50
1028	160	30	70	30	60	30	60	90	190	32%	280	50
1029	160	0	80	60	40	20	80	80	200	29%	280	50
1030	165	10	40	90	80	20	45	120	165	42%	285	50
1031	180	0	90	30	100	0	70	30	260	10%	290	35
1032	185	20	60	40	80	10	40	70	180	28%	250	70
1033	190	10	70	40	80	10	70	60	220	21%	280	40
1034	120	30	70	10	80	30	60	70	210	25%	280	40
1035	125	20	70	30	85	15	45	65	200	25%	265	30
1036	270	10	90	10	80	20	80	40	250	14%	290	10
1037	150	30	80	40	50	30	40	100	170	37%	270	50
1038	170	20	80	10	80	40	50	70	210	25%	280	40
1039	200	20	40	10	90	30	70	60	200	23%	260	60
1040	230	10	90	30	50	30	40	70	180	28%	250	60
1042	160	0	85	10	110	20	40	30	235	11%	265	50
1043	120	10	70	0	90	40	60	50	220	19%	270	30
1044	145	50	80	0	70	30	25	80	175	31%	255	50
1046	120	0	80	0	80	60	40	60	200	23%	260	50
1048	170	60	60	30	40	40	40	130	140	48%	270	60
1051	130	30	70	60	30	50	40	140	140	50%	280	50
1053	190	30	50	40	60	50	50	120	160	43%	280	50
1054	90	10	70	120	0	10	90	140	160	47%	300	50
1055	120	20	60	90	20	40	60	150	140	52%	290	50
1056	90	20	80	90	20	30	50	140	150	48%	290	40
1057	40	0	100	0	80	70	40	70	220	24%	290	50
1058	80	0	90	40	60	30	70	70	220	24%	290	50
1059	140	20	60	10	90	70	30	100	180	36%	280	50
1060	130	40	60	0	80	50	50	90	190	32%	280	30
1062	190	40	70	40	60	20	80	100	210	32%	310	30
1064	40	50	70	40	60	30	40	120	170	41%	290	40
1066	90	0	100	0	80	30	50	30	230	12%	260	50

ID	Depth to Top	Zone 1 Sand	Zone 1 Shale	Zone 2 Sand	Zone 2 Shale	Zone 3 Sand	Zone 3 Shale	Total Sand	Total Shale	Percent Sand	Total Thickness	Kiowa Thickness
1069	110	40	80	0	80	10	60	50	220	19%	270	50
1071	50	0	50	0	100	50	70	50	220	19%	270	40
1072	30	0	120	0	100	30	60	30	280	10%	310	50
1073	70	20	90	10	70	40	30	70	190	27%	260	50
1075	290	10	90	0	80	10	70	20	240	8%	260	40
1076	280	10	80	0	80	20	80	30	240	11%	270	50
1077	260	30	80	0	80	20	70	50	230	18%	280	50
1078	240	10	90	20	80	30	50	60	220	21%	280	40
1079	270	10	90	0	110	20	40	30	240	11%	270	50
1080	230	10	90	0	80	30	60	40	230	15%	270	50
1081	230	0	110	0	70	40	50	40	230	15%	270	40
1082	260	10	100	0	70	20	70	30	240	11%	270	40
1083	270	0	100	10	80	0	80	10	260	4%	270	50
1084	280	0	120	10	70	10	60	20	250	7%	270	60
1085	300	0	100	0	80	40	50	40	230	15%	270	40
1086	280	0	100	50	40	20	70	70	210	25%	280	50
1087	260	0	120	20	70	30	40	50	230	18%	280	50
1088	250	0	70	0	110	10	90	10	270	4%	280	40
1089	260	0	100	30	60	20	50	50	210	19%	260	60
1090	250	10	100	30	60	10	70	50	230	18%	280	50
1091	260	20	70	20	80	10	70	50	220	19%	270	40
1092	220	50	40	20	90	60	30	130	160	45%	290	50
1093	230	10	90	0	90	40	60	50	240	17%	290	30
1094	240	20	70	0	70	50	50	70	190	27%	260	40
1095	50	50	60	40	60	0	90	90	210	30%	300	20
1096	190	40	40	0	110	20	80	60	230	21%	290	50
1097	210	0	90	0	100	20	70	20	260	7%	280	40
1099	220	20	40	10	110	20	80	50	230	18%	280	50
1100	220	10	70	10	90	40	50	60	210	22%	270	30
1101	180	0	70	20	80	40	60	60	210	22%	270	30
1102	180	10	80	20	80	20	60	50	220	19%	270	30
1103	180	10	60	10	90	20	80	40	230	15%	270	40
1104	200	10	90	20	70	60	30	90	190	32%	280	50
1106	170	10	70	0	100	90	10	100	180	36%	280	70
1108	115	20	40	40	100	50	15	110	155	42%	265	20
1109	100	10	60	50	110	40	20	100	190	34%	290	40
1110	135	10	40	20	120	50	30	80	190	30%	270	60
1111	130	25	50	70	80	50	20	145	150	49%	295	20
1112	120	10	35	30	80	0	50	40	165	20%	205	50
1113	100	30	80	10	80	40	30	80	190	30%	270	45
1114	120	40	90	0	100	0	45	40	235	15%	275	40
1115	130	30	80	20	80	60	20	110	180	38%	290	40
1116	150	20	80	20	80	40	50	80	210	28%	290	30
1117	160	10	90	0	70	30	60	40	220	15%	260	60
1118	170	10	80	10	70	30	60	50	210	19%	260	50
1120	220	0	80	60	30	30	80	90	190	32%	280	50
1121	220	0	80	70	30	40	60	110	170	39%	280	40
1122	230	30	40	100	10	50	60	180	110	62%	290	40

ID	Depth to Top	Zone 1 Sand	Zone 1 Shale	Zone 2 Sand	Zone 2 Shale	Zone 3 Sand	Zone 3 Shale	Total Sand	Total Shale	Percent Sand	Total Thickness	Kiowa Thickness
1123	150	0	90	0	90	30	60	30	240	11%	270	50
1125	180	30	60	10	80	40	60	80	200	29%	280	30
1126	190	0	80	0	100	30	50	30	230	12%	260	50
1127	150	10	80	10	70	20	70	40	220	15%	260	50
1128	160	20	80	0	90	20	70	40	240	14%	280	50
1129	140	10	90	0	100	20	70	30	260	10%	290	20
1130	150	0	100	20	80	70	10	90	190	32%	280	30
1131	220	30	50	10	90	30	60	70	200	26%	270	50
1133	230	50	40	10	70	30	70	90	180	33%	270	60
1134	200	0	80	10	70	40	60	50	210	19%	260	40
1135	240	10	80	0	90	80	20	90	190	32%	280	60
1136	310	10	100	30	50	60	40	100	190	34%	290	70
1137	320	10	70	0	80	80	20	90	170	35%	260	100
1138	200	0	90	0	100	50	40	50	230	18%	280	50
1139	190	50	60	0	80	70	20	120	160	43%	280	70
1141	320	0	70	0	90	70	20	70	180	28%	250	70
1142	200	20	80	10	90	40	30	70	200	26%	270	70
1143	180	10	60	20	80	40	50	70	190	27%	260	70
1144	210	10	80	0	80	60	30	70	190	27%	260	40
1145	360	10	70	0	100	50	50	60	220	21%	280	60
1146	350	10	80	10	100	50	40	70	220	24%	290	50
1147	300	20	70	0	90	60	30	80	190	30%	270	70
1148	290	20	80	10	90	30	50	60	220	21%	280	80
1149	310	10	50	40	80	70	20	120	150	44%	270	60
1150	290	40	70	20	80	10	60	70	210	25%	280	60
1151	290	10	100	10	90	0	90	20	280	7%	300	40
1152	290	40	50	0	80	60	30	100	160	38%	260	100
1153	350	0	90	40	40	40	30	80	160	33%	240	130
1154	280	10	60	90	0	30	40	130	100	57%	230	140
1155	240	0	90	10	70	20	70	30	230	12%	260	40
1156	420	10	80	110	0	20	80	140	160	47%	300	50
1157	390	0	90	110	10	20	60	130	160	45%	290	90
1158	280	30	80	80	20	60	30	170	130	57%	300	70
1159	280	0	90	120	10	20	60	140	160	47%	300	60
1160	430	20	90	60	40	10	60	90	190	32%	280	80
1161	320	10	80	30	60	10	100	50	240	17%	290	80
1162	400	20	80	0	100	10	90	30	270	10%	300	40
1163	380	0	100	50	60	10	70	60	230	21%	290	60
1164	320	20	90	0	80	20	70	40	240	14%	280	60
1165	420	0	80	10	100	10	70	20	250	7%	270	60
1166	340	0	90	20	70	20	100	40	260	13%	300	40
1167	380	0	100	10	90	10	70	20	260	7%	280	90
1168	350	0	80	20	70	10	90	30	240	11%	270	60
1169	400	0	90	0	100	10	70	10	260	4%	270	60
1170	480	50	80	10	80	0	80	60	240	20%	300	60
1171	460	60	80	20	70	10	60	90	210	30%	300	40
1172	460	20	70	10	100	20	60	50	230	18%	280	50
1173	380	10	90	90	10	20	60	120	160	43%	280	60

ID	Depth to Top	Zone 1 Sand	Zone 1 Shale	Zone 2 Sand	Zone 2 Shale	Zone 3 Sand	Zone 3 Shale	Total Sand	Total Shale	Percent Sand	Total Thickness	Kiowa Thickness
1174	350	10	100	30	60	40	50	80	210	28%	290	40
1175	400	0	110	60	30	20	60	80	200	29%	280	15
1176	380	0	100	50	40	10	70	60	210	22%	270	40
1177	350	20	80	70	40	30	50	120	170	41%	290	50
1178	340	30	80	50	50	20	60	100	190	34%	290	50
1179	360	20	70	40	60	10	90	70	220	24%	290	30
1180	380	0	80	120	0	0	80	120	160	43%	280	50
1181	360	10	80	80	30	20	60	110	170	39%	280	50
1182	410	20	80	100	0	10	100	130	180	42%	310	40
1183	400	10	90	20	90	10	50	40	230	15%	270	60
1184	400	0	90	60	40	30	70	90	200	31%	290	50
1185	360	20	80	70	30	40	60	130	170	43%	300	40
1186	350	20	80	30	80	10	80	60	240	20%	300	50
1187	350	0	110	50	50	10	80	60	240	20%	300	70
1188	370	30	70	70	30	30	50	130	150	46%	280	50
1189	350	30	60	30	70	70	30	130	160	45%	290	50
1190	280	0	80	40	50	50	50	90	180	33%	270	110
1191	280	0	70	20	80	40	50	60	200	23%	260	35
1194	370	50	30	60	60	50	30	160	120	57%	280	40
1195	330	40	30	0	110	50	40	90	180	33%	270	60
1196	310	0	80	0	80	90	30	90	190	32%	280	60
1197	300	40	70	0	70	30	50	70	190	27%	260	40
1198	300	0	80	0	80	30	50	30	210	13%	240	70
1199	300	10	70	30	50	30	60	70	180	28%	250	40
1200	330	0	90	0	80	50	50	50	220	19%	270	90
1201	330	10	70	0	100	60	20	70	190	27%	260	80
1202	310	0	80	10	70	90	10	100	160	38%	260	90
1203	350	0	100	20	80	50	20	70	200	26%	270	80
1204	410	0	90	0	90	60	10	60	190	24%	250	70
1205	410	0	100	10	80	40	60	50	240	17%	290	60
1206	420	10	100	20	70	30	50	60	220	21%	280	60
1207	420	0	110	20	70	40	40	60	220	21%	280	70
1208	400	10	100	0	100	30	70	40	270	13%	310	50
1209	450	40	60	30	70	50	30	120	160	43%	280	50
1210	420	20	70	10	100	40	30	70	200	26%	270	80
1211	450	20	60	50	50	40	50	110	160	41%	270	60
1212	470	10	80	30	70	50	40	90	190	32%	280	90
1216	80	30	70	70	30	80	20	180	120	60%	300	50
1217	100	20	80	30	60	100	10	150	150	50%	300	30
1218	100	40	60	50	50	60	40	150	150	50%	300	30
1219	120	30	60	60	50	80	20	170	130	57%	300	35
1221	50	0	120	10	90	70	30	80	240	25%	320	30
1222	50	30	60	20	100	90	10	140	170	45%	310	40
1223	130	20	50	30	70	40	60	90	180	33%	270	40
1224	60	50	50	10	100	30	60	90	210	30%	300	30
1225	50	40	60	20	80	40	60	100	200	33%	300	20
1228	140	40	60	60	30	60	50	160	140	53%	300	30
1229	120	10	90	70	40	70	40	150	170	47%	320	30

ID	Depth to Top	Zone 1 Sand	Zone 1 Shale	Zone 2 Sand	Zone 2 Shale	Zone 3 Sand	Zone 3 Shale	Total Sand	Total Shale	Percent Sand	Total Thickness	Kiowa Thickness
1230	160	20	60	70	30	10	90	100	180	36%	280	50
1231	150	0	90	0	90	20	70	20	250	7%	270	50
1232	110	30	40	0	80	20	100	50	220	19%	270	40
1233	130	40	40	30	60	70	30	140	130	52%	270	50
1234	120	40	60	0	80	30	60	70	200	26%	270	20
1235	100	20	70	0	80	30	70	50	220	19%	270	40
1236	110	60	50	20	60	30	70	110	180	38%	290	50
1238	160	10	70	40	70	30	60	80	200	29%	280	30
1239	160	20	70	30	70	50	50	100	190	34%	290	40
1240	170	10	80	0	100	40	50	50	230	18%	280	40
1242	120	80	40	10	80	50	40	140	160	47%	300	30
1243	150	20	80	20	60	30	60	70	200	26%	270	40
1244	170	30	60	20	80	40	40	90	180	33%	270	40
1245	210	10	70	80	10	70	40	160	120	57%	280	50
1247	240	10	70	20	80	40	40	70	190	27%	260	60
1248	210	0	90	30	50	40	60	70	200	26%	270	40
1249	230	20	70	20	60	40	50	80	180	31%	260	60
1250	220	10	80	30	60	70	30	110	170	39%	280	50
1251	200	20	100	40	40	60	40	120	180	40%	300	50
1252	200	0	80	50	50	50	50	100	180	36%	280	40
1253	220	30	60	10	100	70	30	110	190	37%	300	50
1254	220	0	80	30	70	40	60	70	210	25%	280	30
1255	220	0	80	40	60	60	40	100	180	36%	280	50
1256	220	20	60	50	50	50	50	120	160	43%	280	50
1257	210	0	100	50	50	40	50	90	200	31%	290	40
1258	250	0	100	10	70	50	40	60	210	22%	270	50
1259	240	20	90	60	40	40	60	120	190	39%	310	60
1260	280	20	90	20	60	40	40	80	190	30%	270	50
1261	280	0	80	30	60	30	40	60	180	25%	240	110
1262	260	0	80	60	40	40	40	100	160	38%	260	110
1263	310	30	60	80	40	30	50	140	150	48%	290	50
1264	340	40	60	30	80	0	90	70	230	23%	300	60
1265	350	10	100	30	60	40	60	80	220	27%	300	50
1266	330	80	30	10	90	40	50	130	170	43%	300	50
1267	340	10	70	40	50	20	100	70	220	24%	290	70
1268	260	80	50	30	60	80	20	190	130	59%	320	70
1269	210	20	90	40	60	60	30	120	180	40%	300	80
1271	400	40	60	30	80	10	80	80	220	27%	300	40
1272	400	60	50	20	70	20	80	100	200	33%	300	40

Appendix 3: Collection of Modeled Directional Semivariograms

The following figures show all of the directional semivariograms produced for this project. There were eight directional semivariograms produced for each of the three zones for an total of 24 directional semivariograms. The semivariograms were produced at 22.5° increments starting at 0° or north. The other seven directions included 22.5°, 45.0°, 67.5°, 90.0°, 112.5°, 135.0°, and 157.5°. There are only eight directions because the 90° or east direction is also equivalent to the 270° or west direction and so on.

The exponential model was used to model all of the semivariograms along with various nested structures superimposed on the exponential model. All of the semivariograms had pronounced nugget effects, but only the semivariograms from Zones 2 and 3 showed hole effects. The nugget effect was modeled by adding an origin shift so that the semivariograms had a non-zero starting point on the semivariance axis. The hole effect were modeled by superimposing a sine function on the exponential model. Model fitting was accomplished by eye on a trial and error basis.

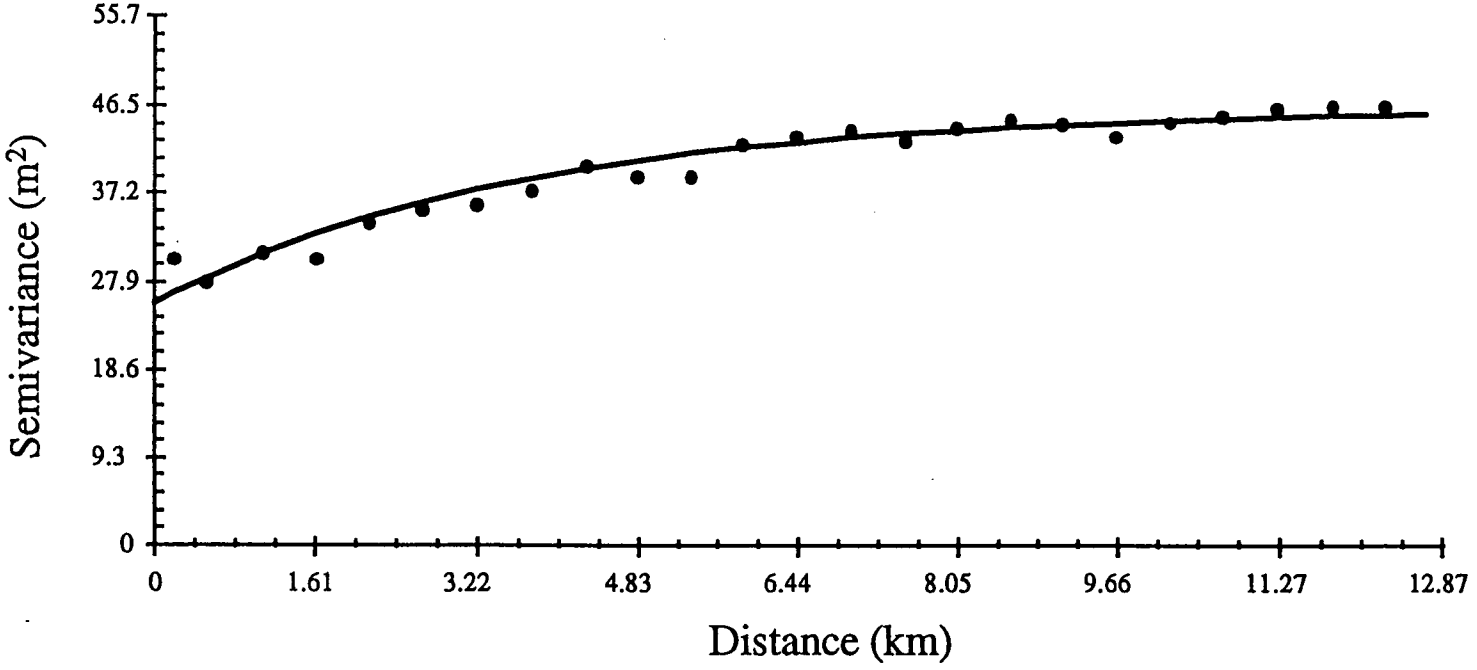

Figure A3.1: Direcrtional semivariogram in Zone 1. The direction is 0 degrees. The range is 11.27 km (7 mi). The sill is 46.5 m^2 (500 ft^2) and the nugget effect is 25.5 m^2 (275 ft^2). The lag distance is 1/3 of a mile (0.54 km).

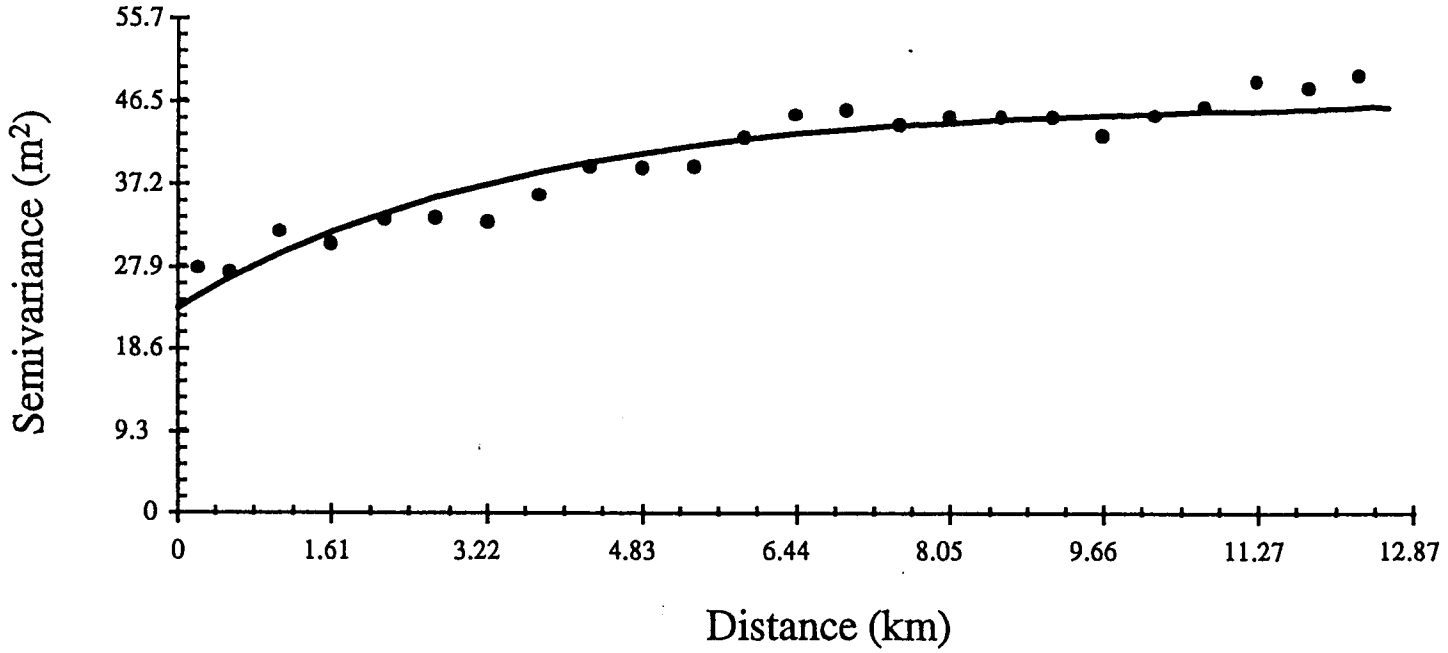

Figure A3.2: Direcrtional semivariogram in Zone 1. The direction is 22.5 degrees. The range is 10.5 km (6.5 mi). The sill is 46.5 m^2 (500 ft^2) and the nugget effect is 23.2 m^2 (250 ft^2). The lag distance is 1/3 of a mile (0.54 km).

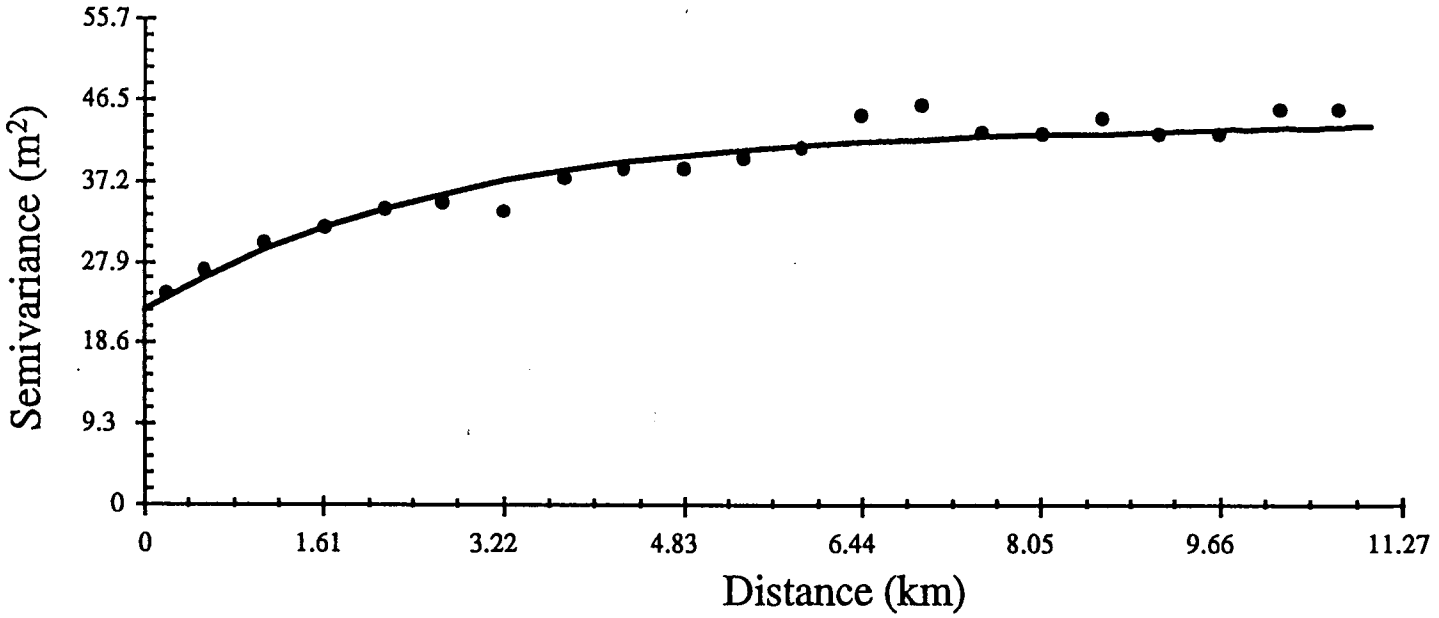

Figure A3.3: Direcrtional semivariogram in Zone 1. The direction is 45 degrees. The range is 8.05 km (5 mi). The sill is 43.7 m^2 (470 ft^2) and the nugget effect is 22.3 m^2 (240 ft^2). The lag distance is 1/3 of a mile (0.54 km).

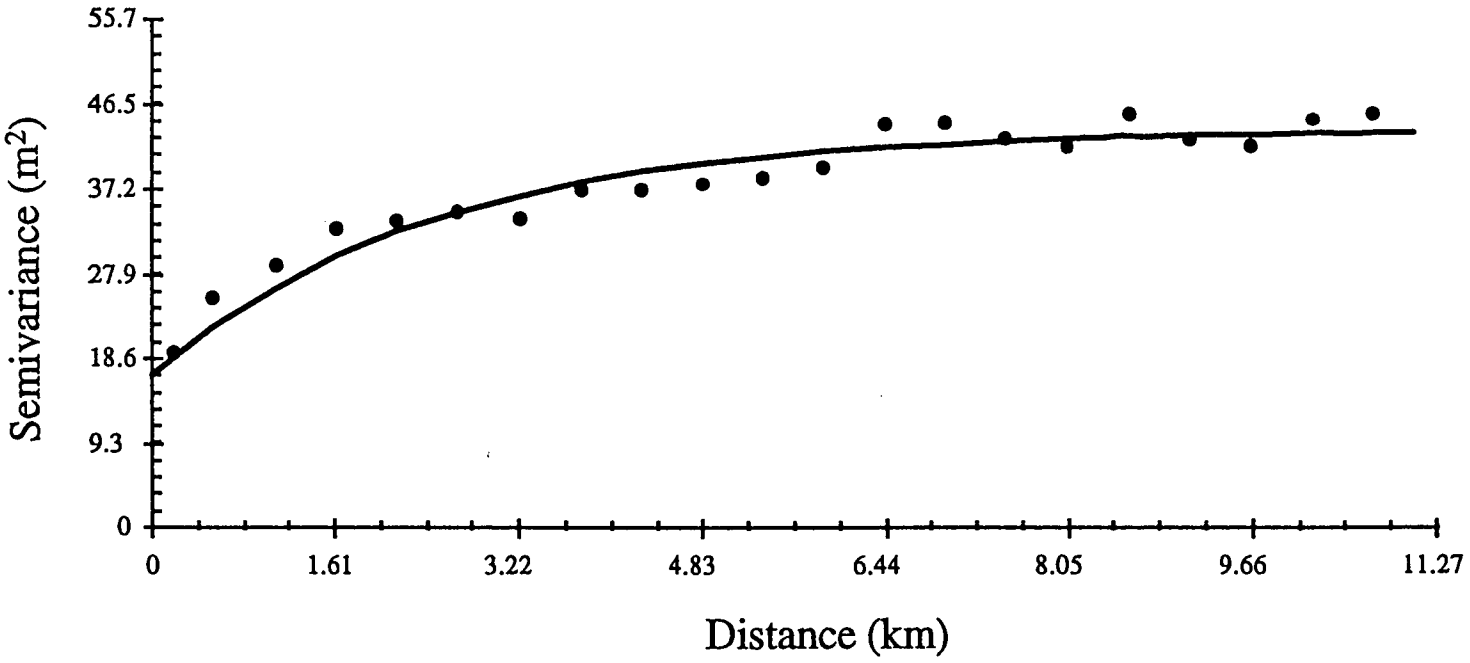

Figure A3.4: Direcrtional semivariogram in Zone 1. The direction is 67.5 degrees. The range is 7.24 km (4.5 mi). The sill is 43.7 m^2 (470 ft^2) and the nugget effect is 16.7 m^2 (180 ft^2). The lag distance is 1/3 of a mile (0.54 km).

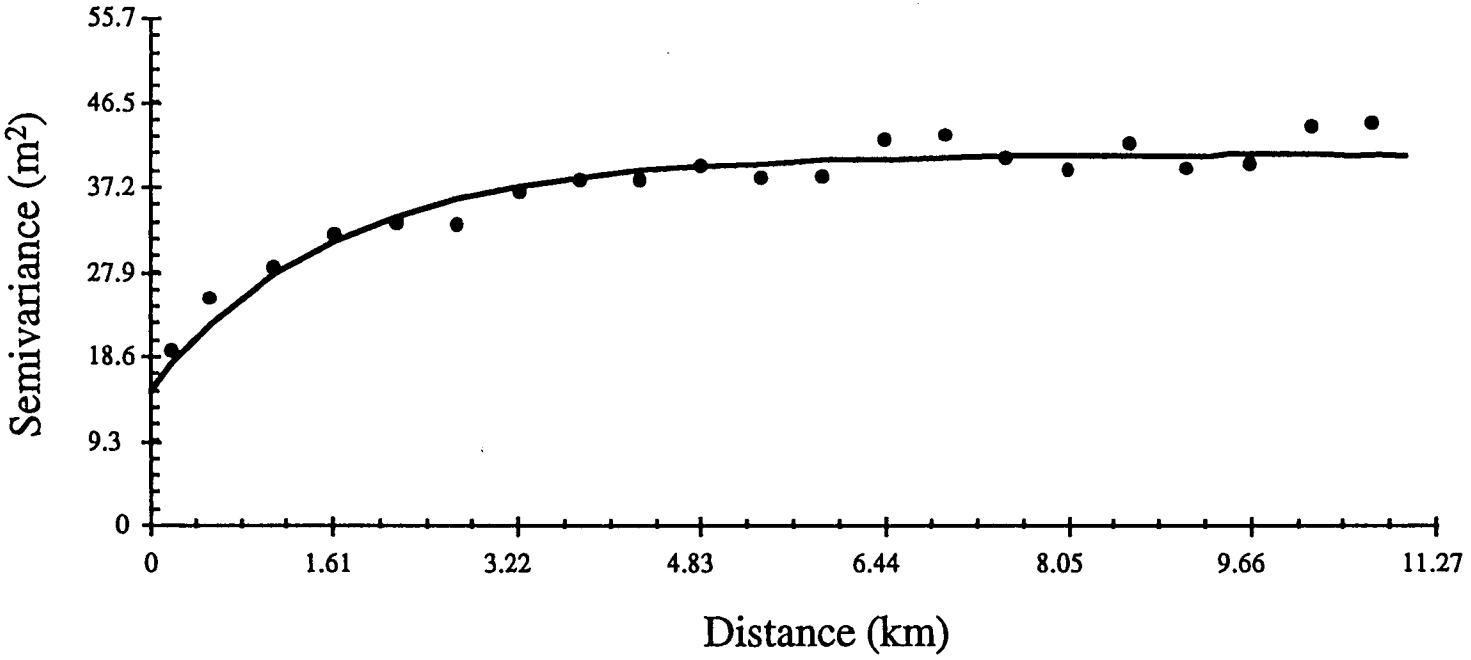

Figure A3.5: Direcrtional semivariogram in Zone 1. The direction is 90 degrees. The range is 4.83 km (3 mi). The sill is 40.9 m^2 (440ft^2) and the nugget effect is 14.9 m^2 (160 ft^2). The lag distance is 1/3 of a mile (0.54 km).

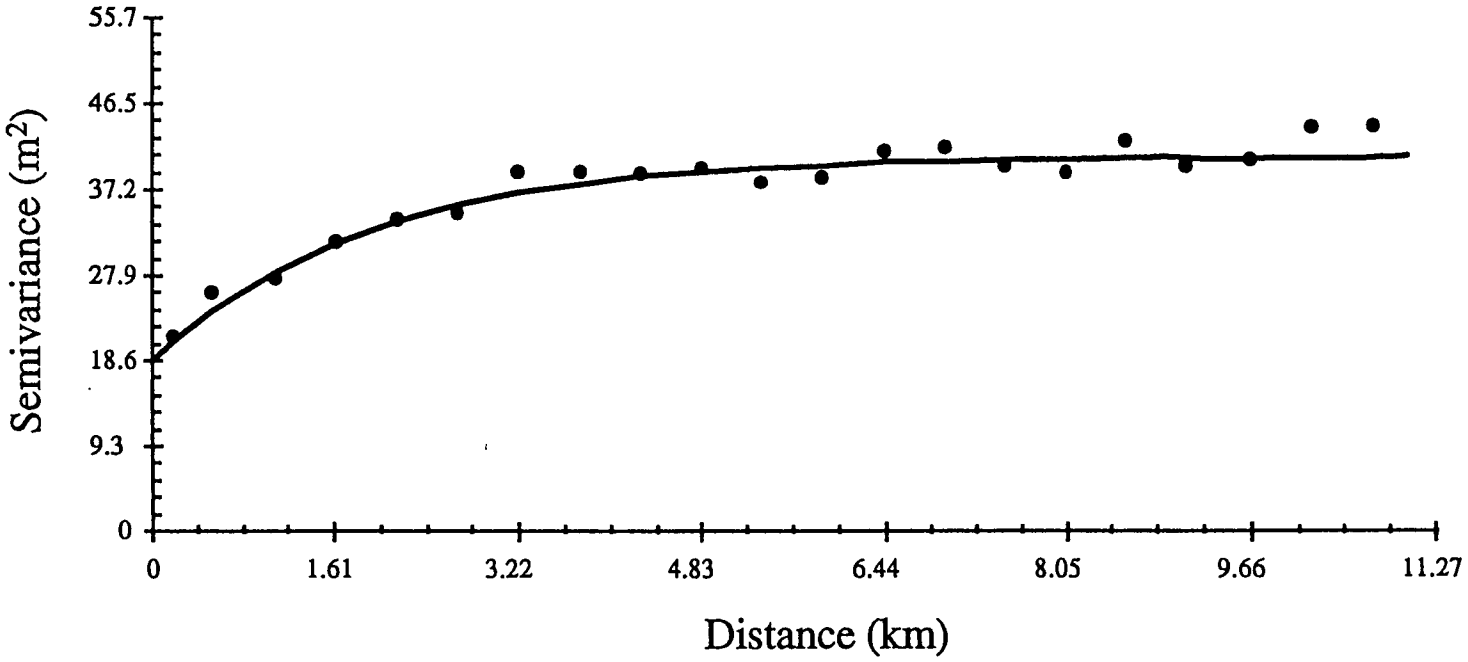

Figure A3.6: Direcrtional semivariogram in Zone 1. The direction is 112.5 degrees. The range is 5.63 km (3.5 mi). The sill is 40.9 m^2 (440ft^2) and the nugget effect is 18.6 m^2 (200ft^2). The lag distance is 1/3 of a mile (0.54 km).

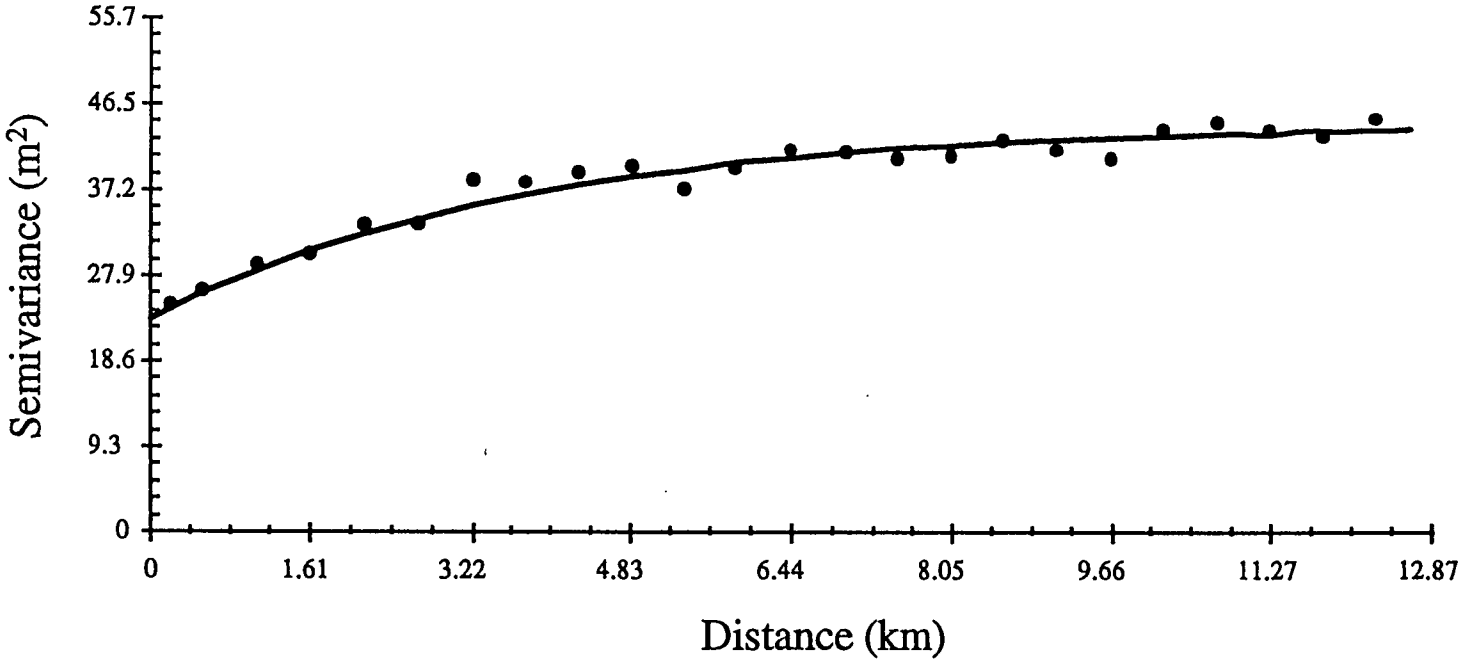

Figure A3.7: Direcrtional semivariogram in Zone 1. The direction is 135 degrees. The range is 11.27 km (7 mi). The sill is 44.6 m^2 (480 ft^2) and the nugget effect is 23.2 m^2 (250 ft^2). The lag distance is 1/3 of a mile (0.54 km).

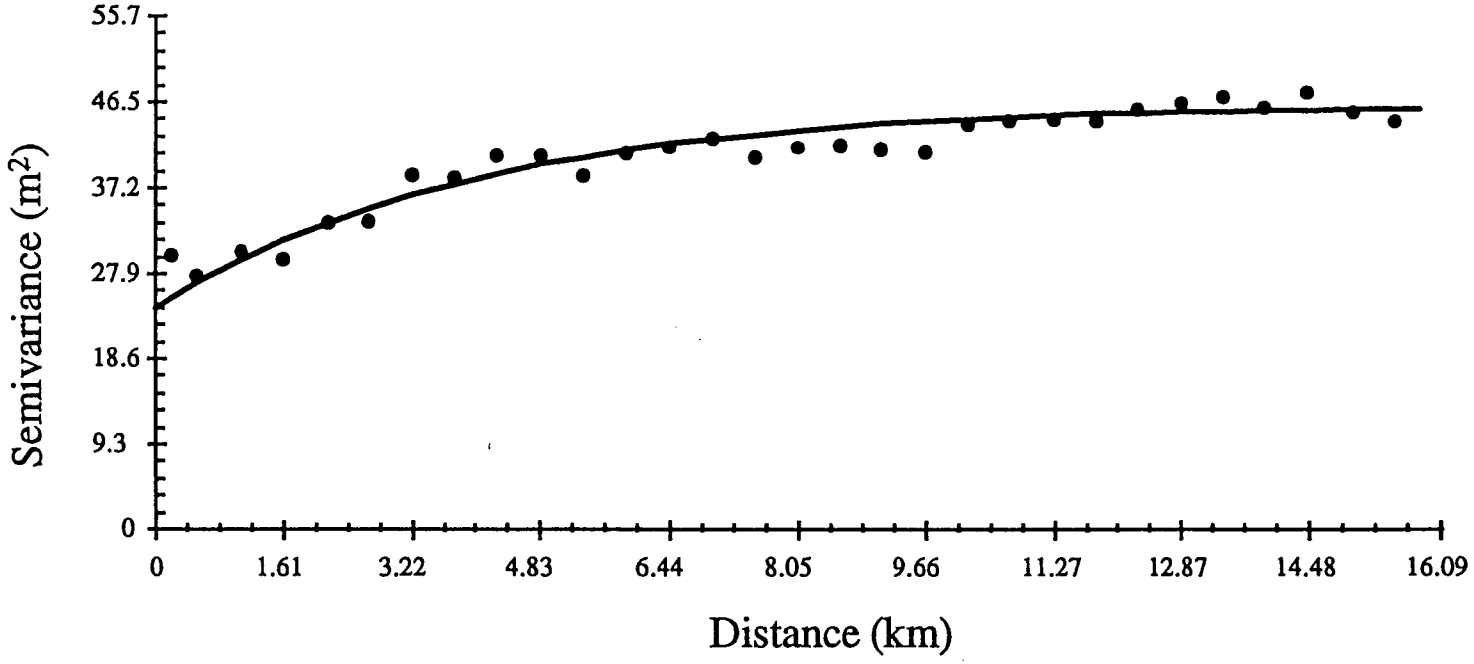

Figure A3.8: Direcrtional semivariogram in Zone 1. The direction is 157.5 degrees. The range is 12.07 km (7.5 mi). The sill is 46.5 m^2 (500 ft^2) and the nugget effect is 24.2 m^2 (260 ft^2). The lag distance is 1/3 of a mile (0.54 km).

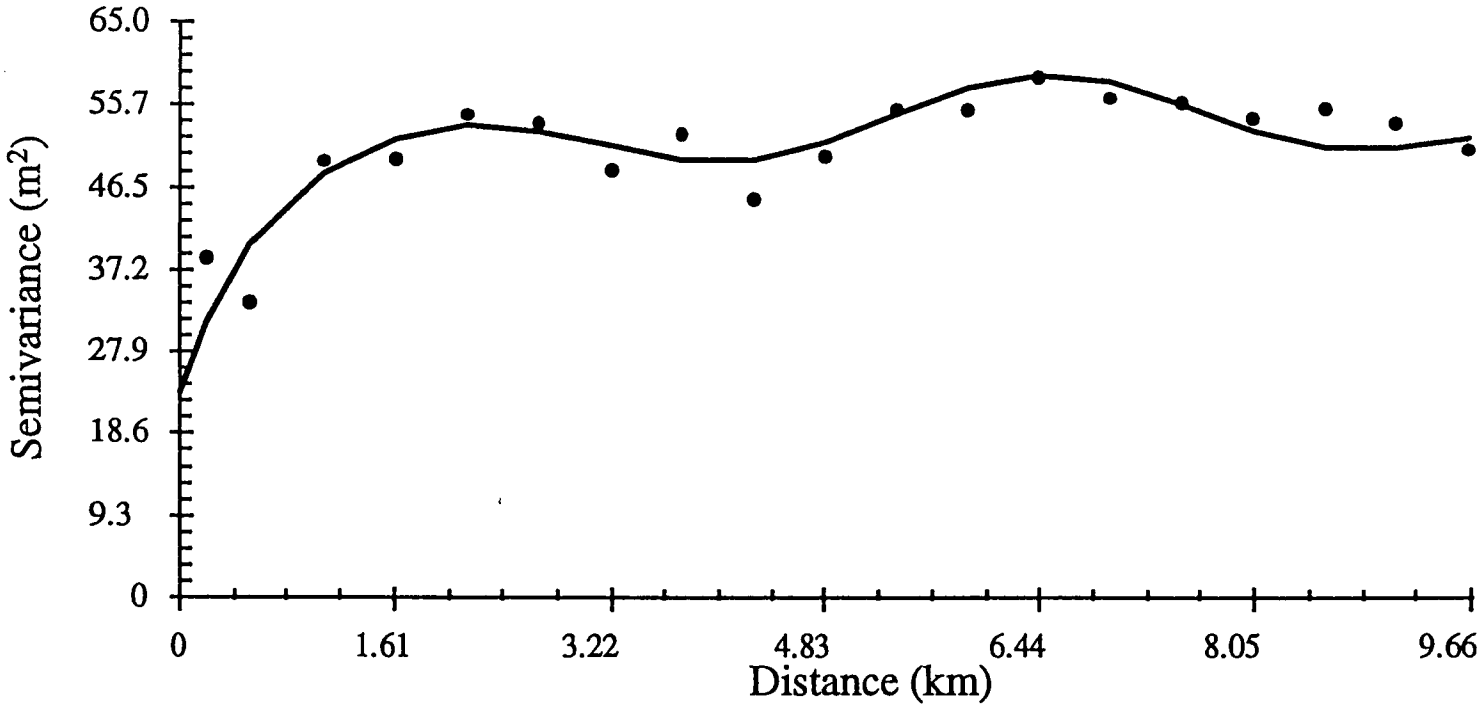

Figure A3.9: Direcrtional semivariogram in Zone 2. The direction is 0 degrees. The range is 1.61 km (1 mi). The sill is 53.4 m^2 (575 ft^2) and the nugget effect is 23.2 m^2 (250 ft^2). The lag distance is 1/3 of a mile (0.54 km). The hole effect present in the variogram is modeled by superimposing sine and/or cosine functions on the exponential model. Its purpose is to better identify the nugget sill and range parameters of the semivariogram.

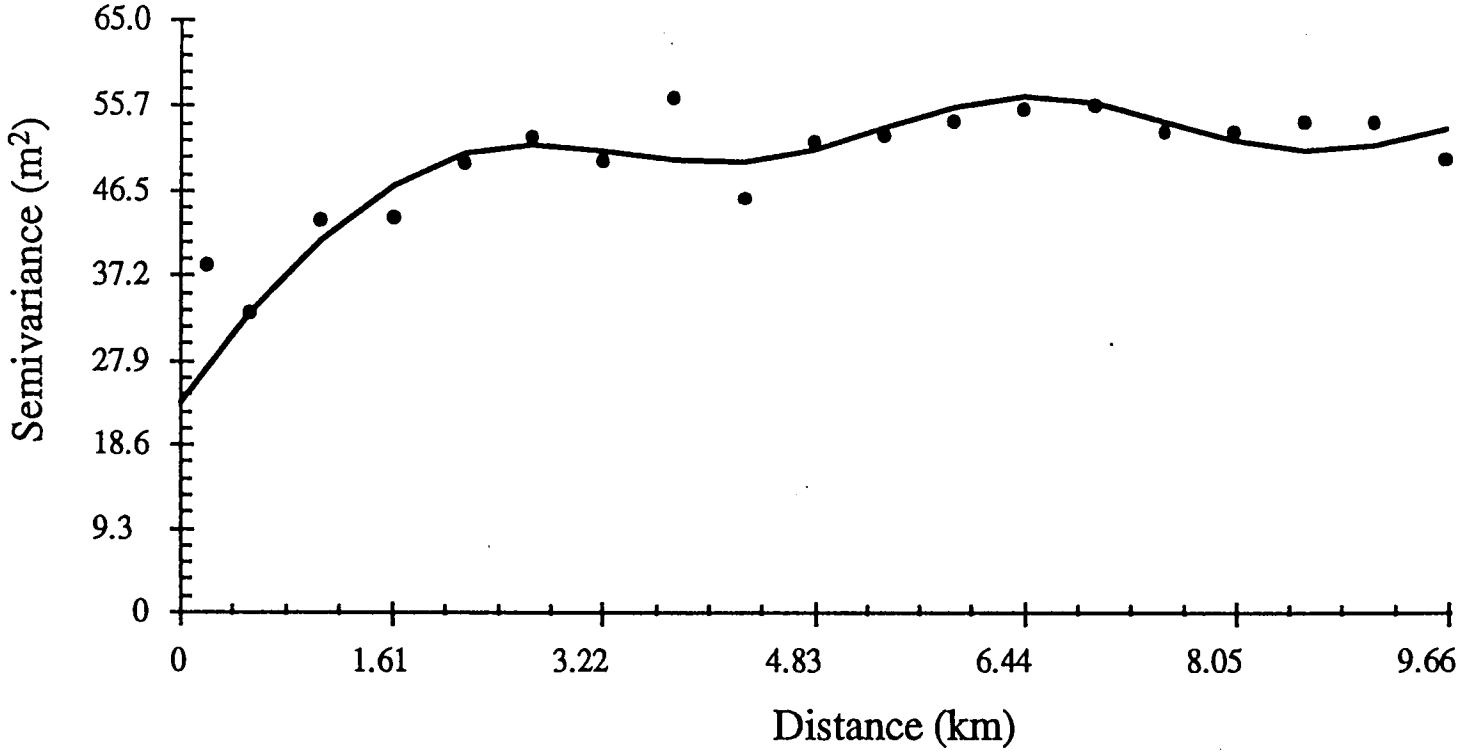

Figure A3.10: Direcrtional semivariogram in Zone 2. The direction is 22.5 degrees. The range is 4.02 km (2.5 mi). The sill is 53.9 m^2 (580 ft^2) and the nugget effect is 23.2 m^2 (250 ft^2). The lag distance is 1/3 of a mile (0.54 km). The hole effect present in the variogram is modeled by superimposing sine and/or cosine functions on the exponential model. Its purpose is to better identify the nugget sill and range parameters of the semivariogram.

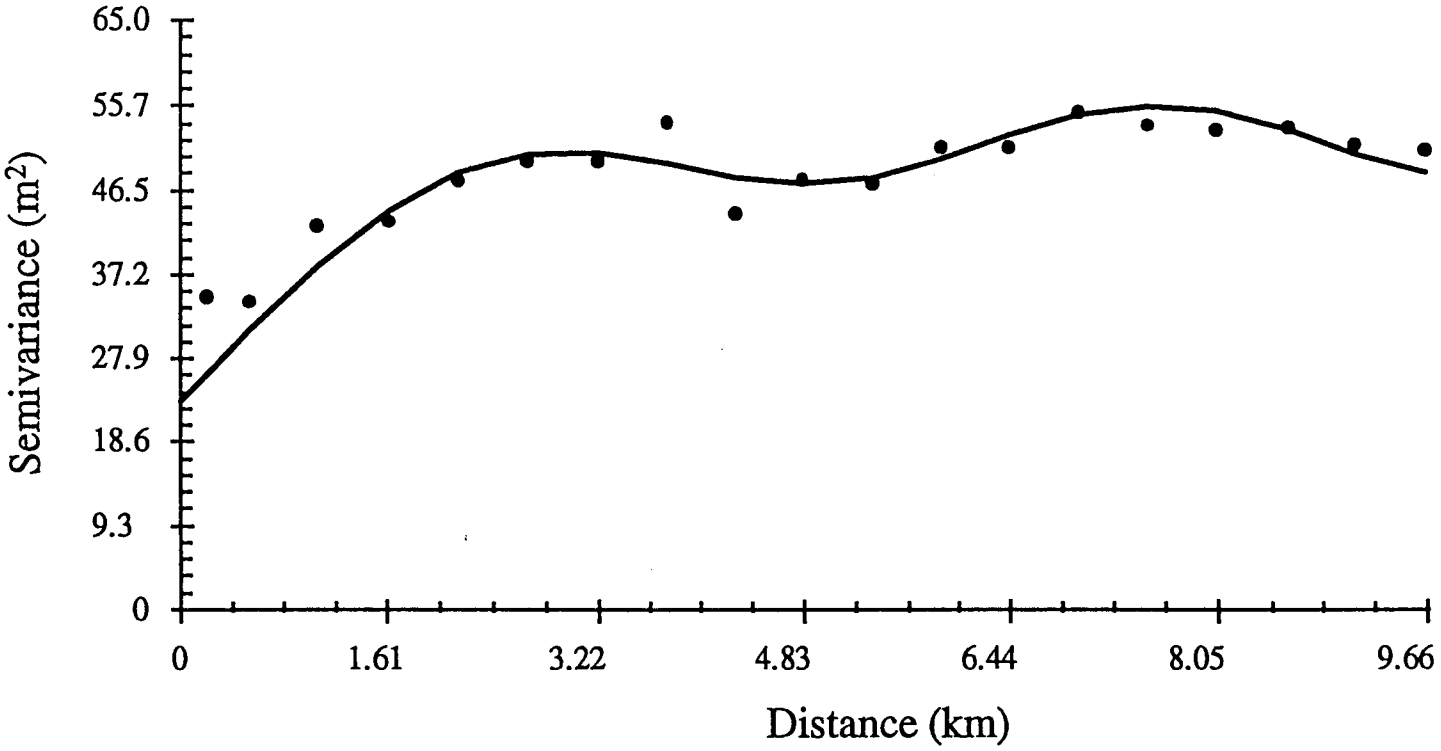

Figure A3.11: Direcrtional semivariogram in Zone 2. The direction is 45 degrees. The range is 4.83 km (3 mi). The sill is 52.0 m^2 (560 ft^2) and the nugget effect is 23.2 m^2 (250 ft^2). The lag distance is 1/3 of a mile (0.54 km). The hole effect present in the variogram is modeled by superimposing sine and/or cosine functions on the exponential model. Its purpose is to better identify the nugget sill and range parameters of the semivariogram.

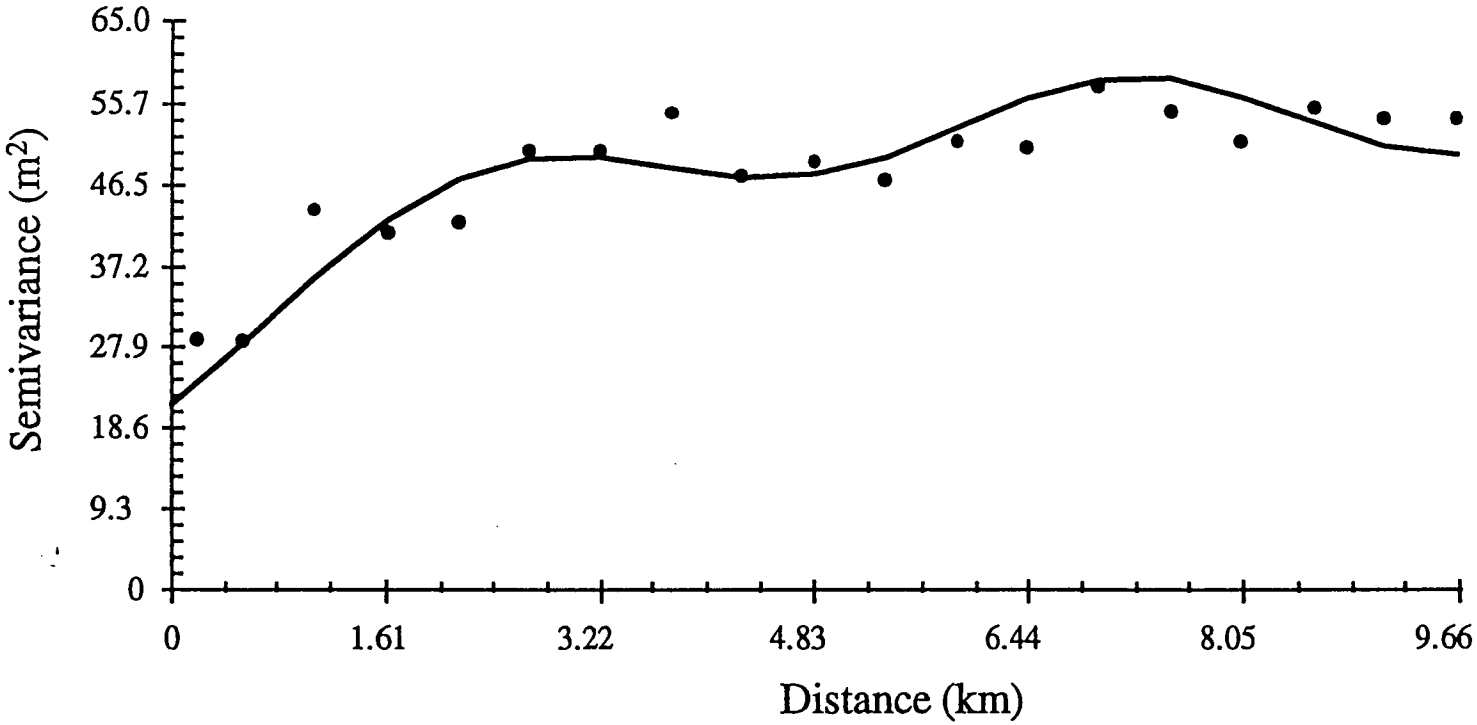

Figure A3.12: Direcrtional semivariogram in Zone 2. The direction is 67.5 degrees. The range is 6.44 km (4 mi). The sill is 54.8 m^2 (590 ft^2) and the nugget effect is 21.4 m^2 (230 ft^2). The lag distance is 1/3 of a mile (0.54 km). The hole effect present in the variogram is modeled by superimposing sine and/or cosine functions on the exponential model. Its purpose is to better identify the nugget sill and range parameters of the semivariogram.

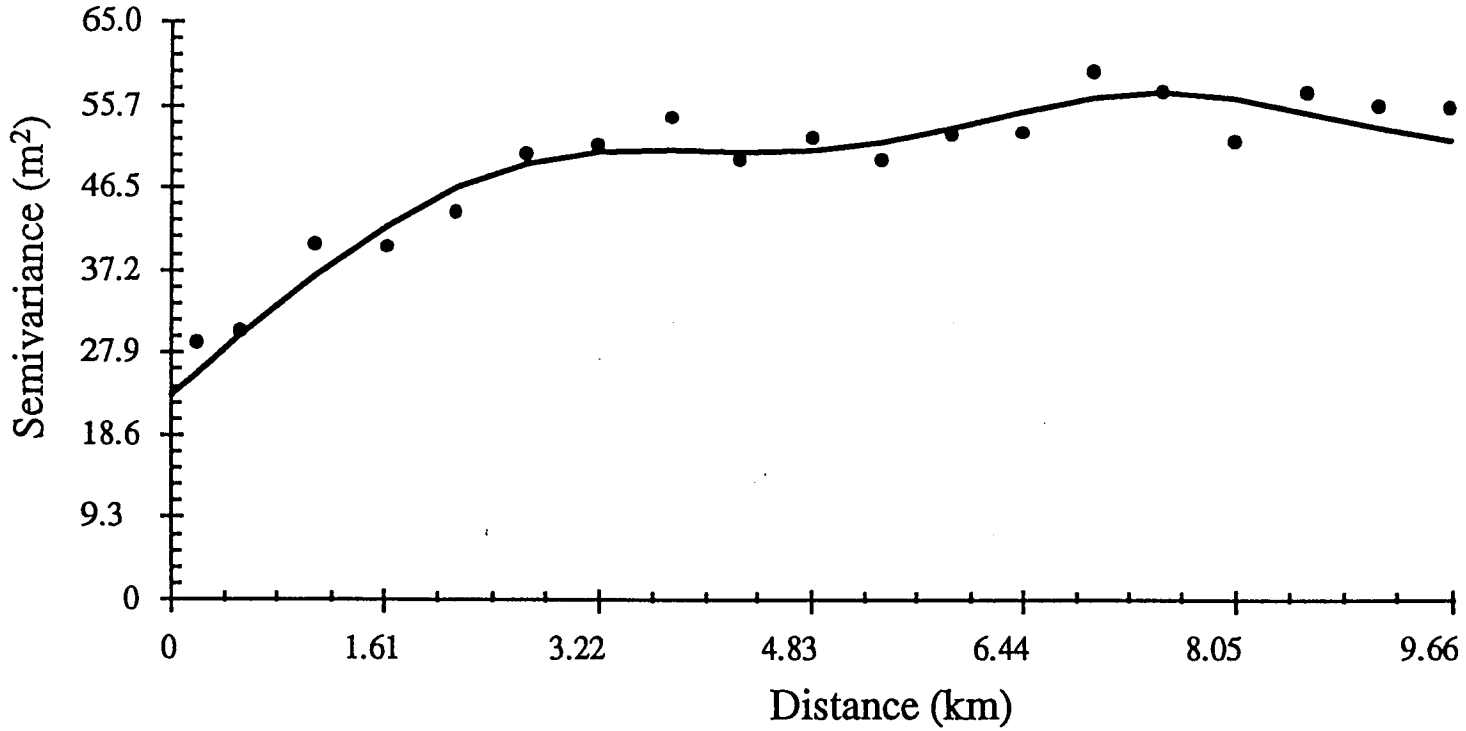

Figure A3.13: Direcrtional semivariogram in Zone 2. The direction is 90 degrees. The range is 6.44 km (4 mi). The sill is 55.7 m^2 (600 ft^2) and the nugget effect is 23.2 m^2 (250 ft^2). The lag distance is 1/3 of a mile (0.54 km). The hole effect present in the variogram is modeled by superimposing sine and/or cosine functions on the exponential model. Its purpose is to better identify the nugget sill and range parameters of the semivariogram.

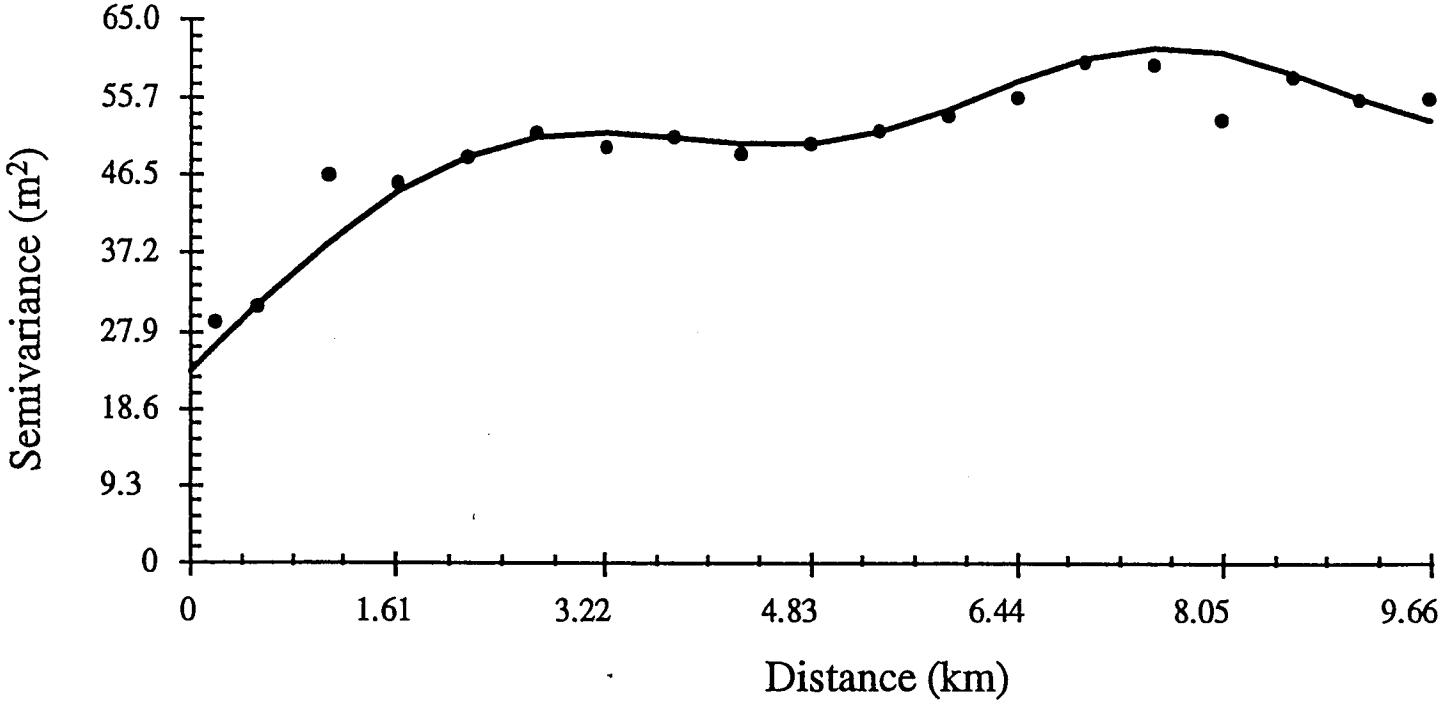

Figure A3.14: Direcrtional semivariogram in Zone 2. The direction is 112.5 degrees. The range is 4.83 km (3 mi). The sill is 55.7 m^2 (600 ft^2) and the nugget effect is 23.2 m^2 (250 ft^2). The lag distance is 1/3 of a mile (0.54 km). The hole effect present in the variogram is modeled by superimposing sine and/or cosine functions on the exponential model. Its purpose is to better identify the nugget sill and range parameters of the semivariogram.

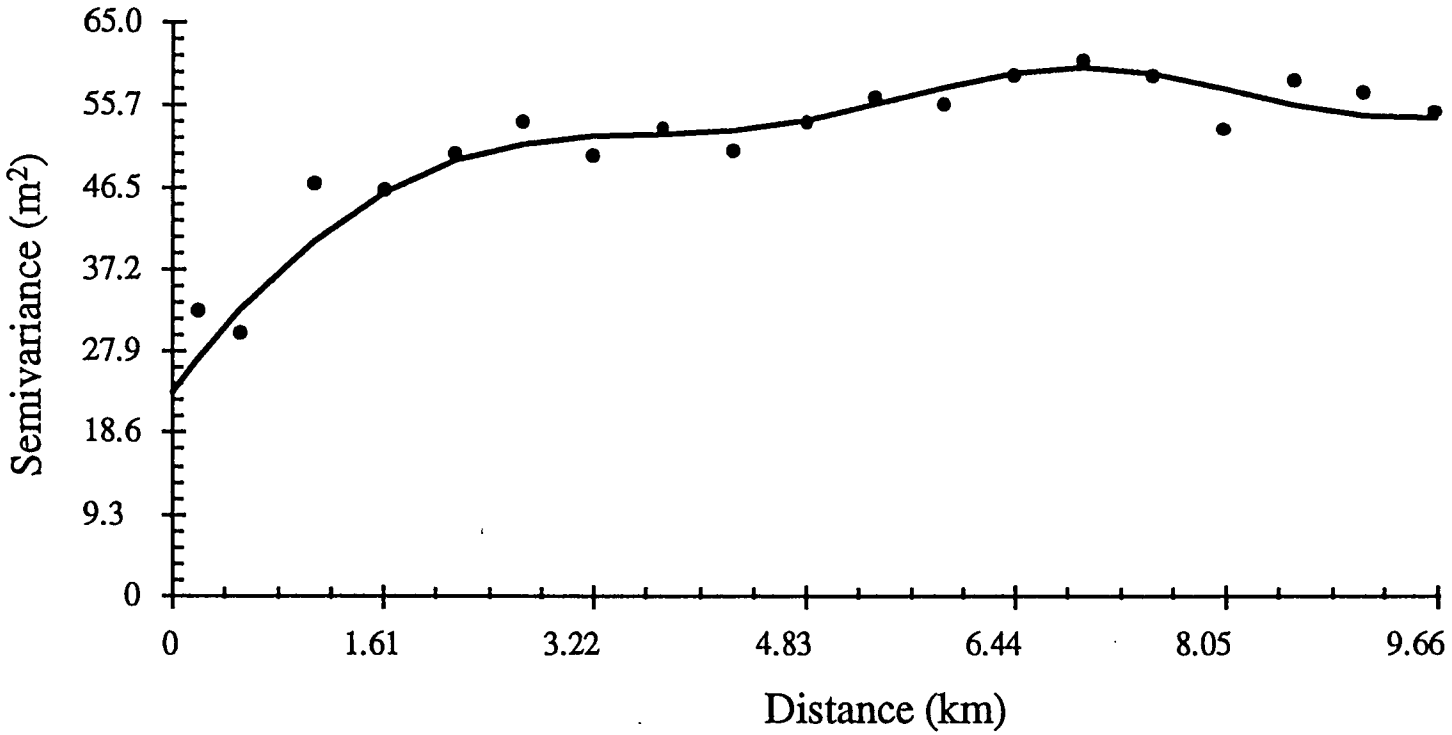

Figure A3.15: Direcrtional semivariogram in Zone 2. The direction is 135 degrees. The range is 4.34 km (2.7 mi). The sill is 56.7 m^2 (610 ft^2) and the nugget effect is 23.2 m^2 (250 ft^2). The lag distance is 1/3 of a mile (0.54 km). The hole effect present in the variogram is modeled by superimposing sine and/or cosine functions on the exponential model. Its purpose is to better identify the nugget sill and range parameters of the semivariogram.

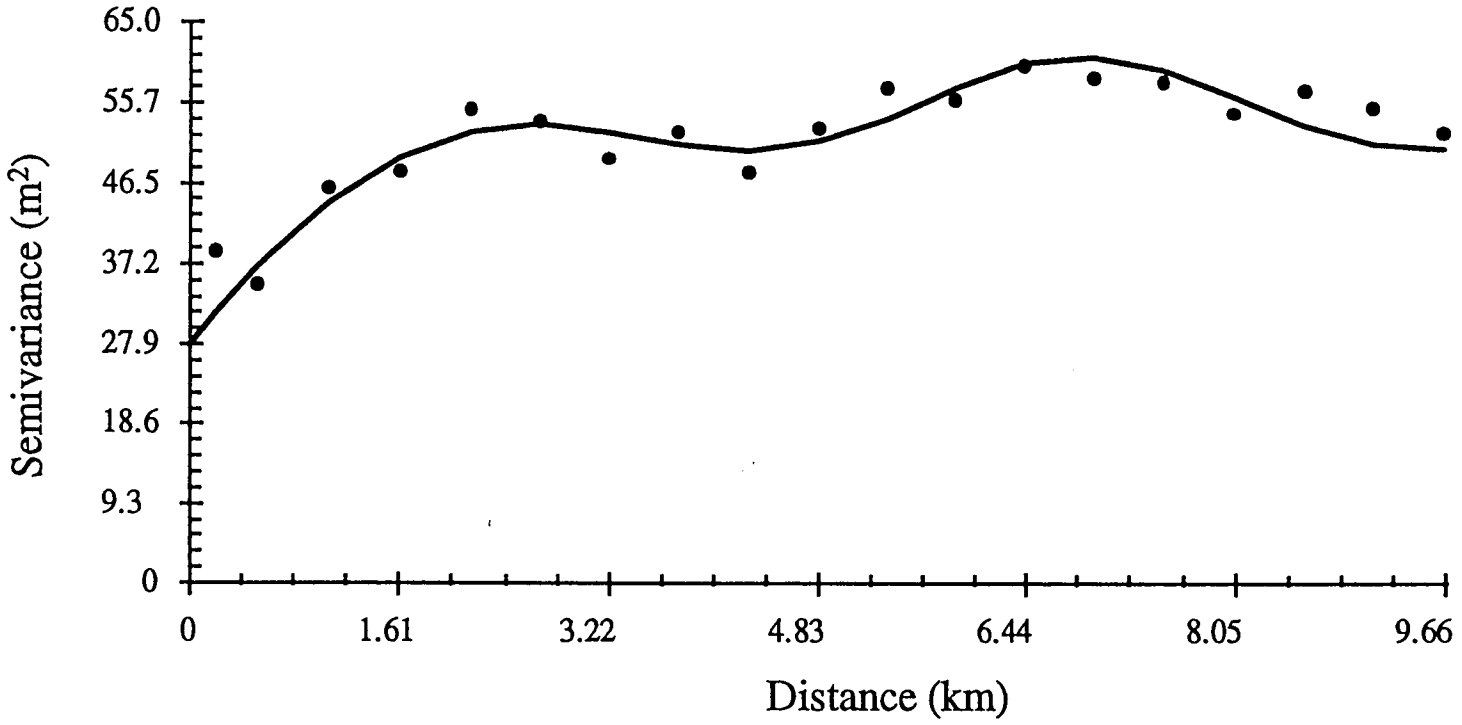

Figure A3.16: Direcrtional semivariogram in Zone 2. The direction is 157.5 degrees. The range is 3.22 km (2 mi). The sill is 54.8 m^2 (590 ft^2) and the nugget effect is 27.9 m^2 (300 ft^2). The lag distance is 1/3 of a mile (0.54 km). The hole effect present in the variogram is modeled by superimposing sine and/or cosine functions on the exponential model. Its purpose is to better identify the nugget sill and range parameters of the semivariogram.

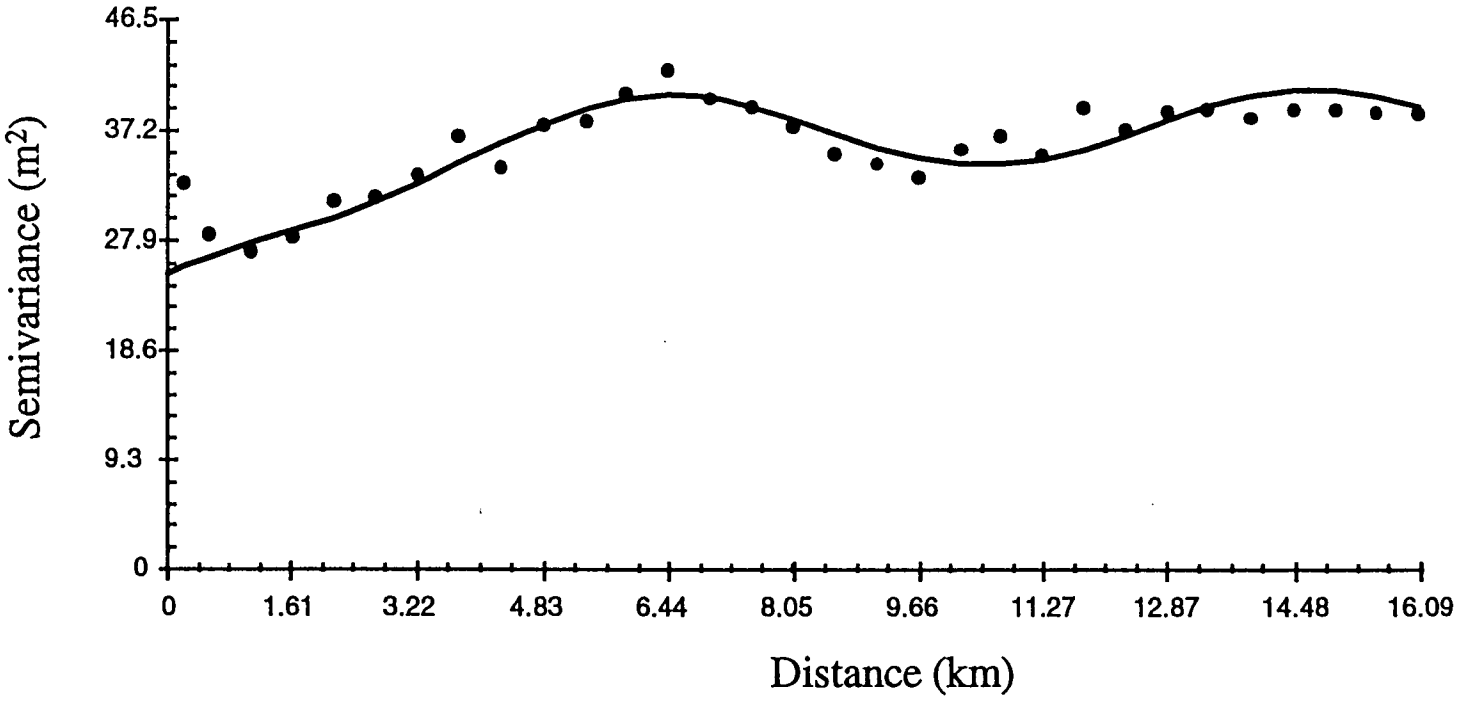

Figure A3.17: Direcrtional semivariogram in Zone 3. The direction is 0 degrees. The range is 6.44 km (4 mi). The sill is 37.6 m^2 (405 ft^2) and the nugget effect is 25.1 m^2 (270 ft^2). The lag distance is 1/3 of a mile (0.54 km). The hole effect present in the variogram is modeled by superimposing sine and/or cosine functions on the exponential model. Its purpose is to better identify the nugget sill and range parameters of the semivariogram.

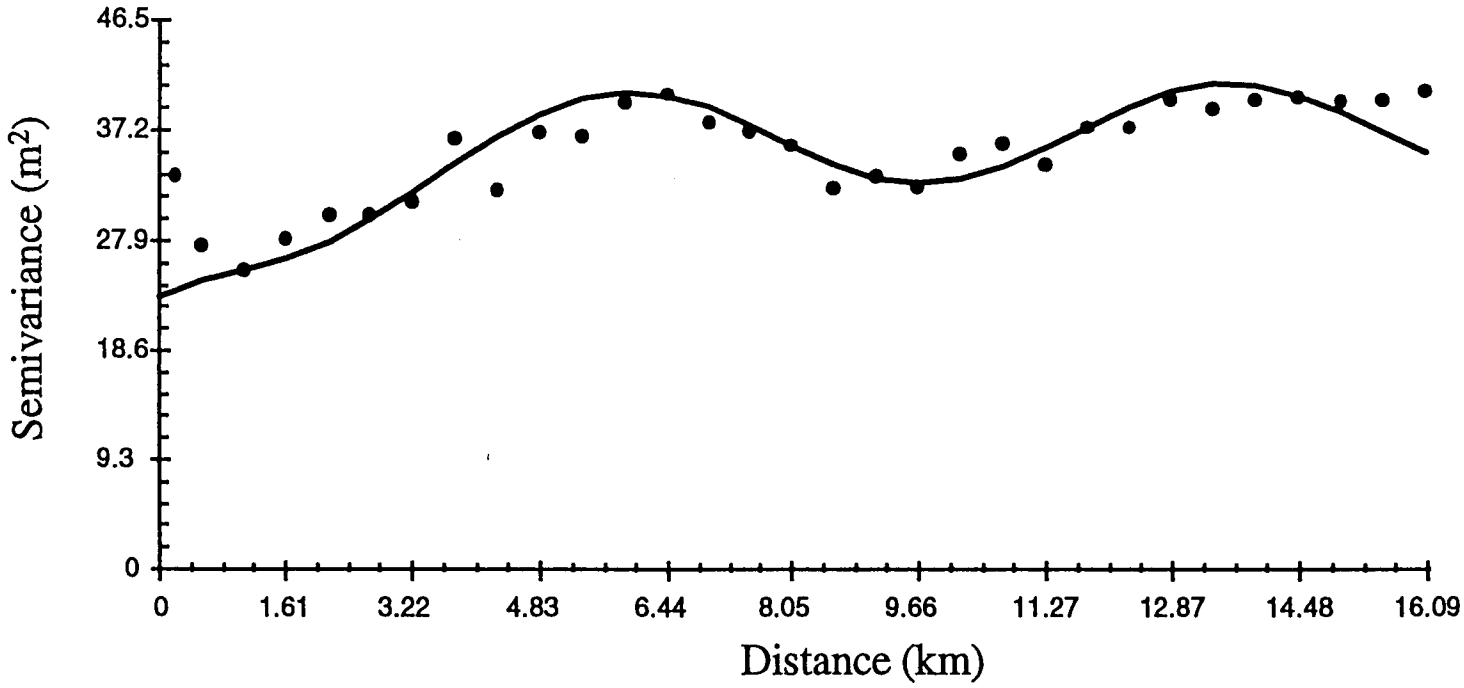

Figure A3.18: Direcrtional semivariogram in Zone 3. The direction is 22.5 degrees. The range is 6.44 km (4 mi). The sill is 37.2 m^2 (400 ft^2) and the nugget effect is 23.2 m^2 (250 ft^2). The lag distance is 1/3 of a mile (0.54 km). The hole effect present in the variogram is modeled by superimposing sine and/or cosine functions on the exponential model. Its purpose is to better identify the nugget sill and range parameters of the semivariogram.

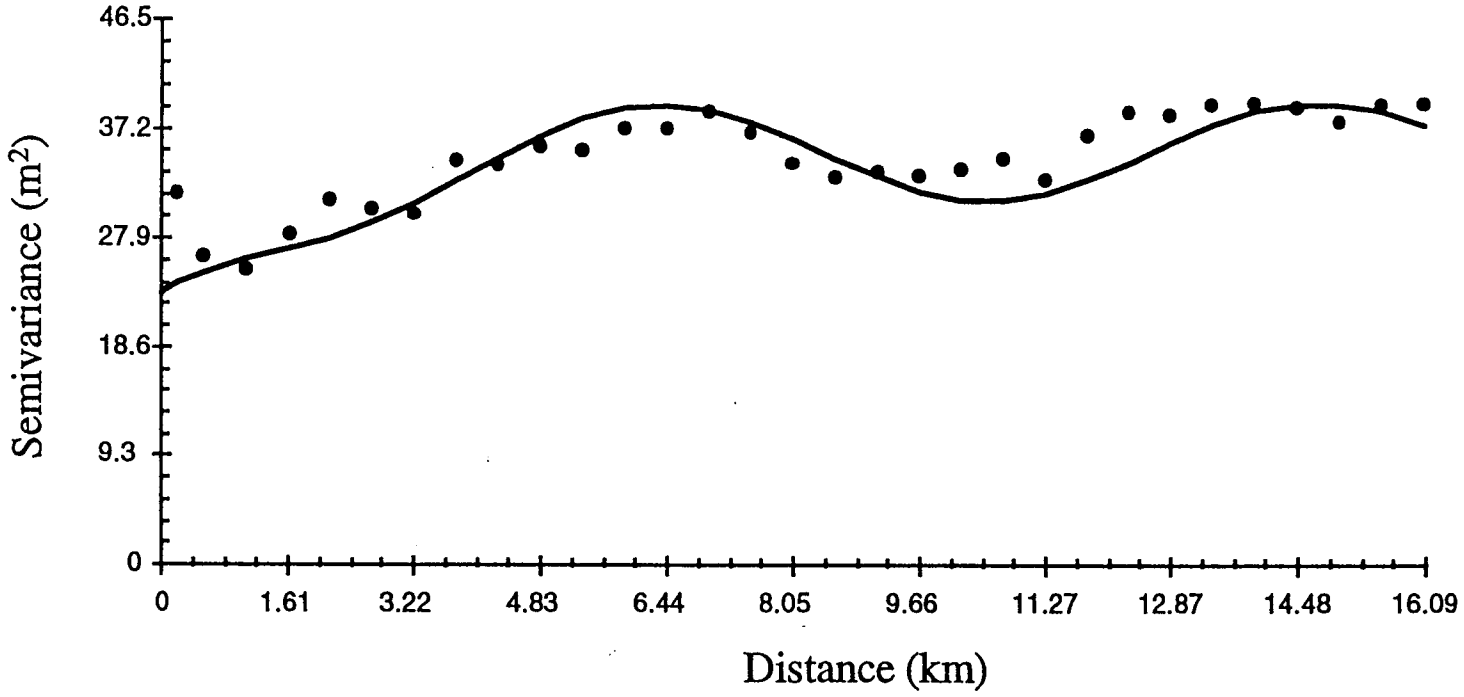

Figure A3.19: Direcrtional semivariogram in Zone 3. The direction is 45 degrees. The range is 4.83 km (3 mi). The sill is 35.3 m^2 (380 ft^2) and the nugget effect is 23.2 m^2 (250 ft^2). The lag distance is 1/3 of a mile (0.54 km). The hole effect present in the variogram is modeled by superimposing sine and/or cosine functions on the exponential model. Its purpose is to better identify the nugget sill and range parameters of the semivariogram.

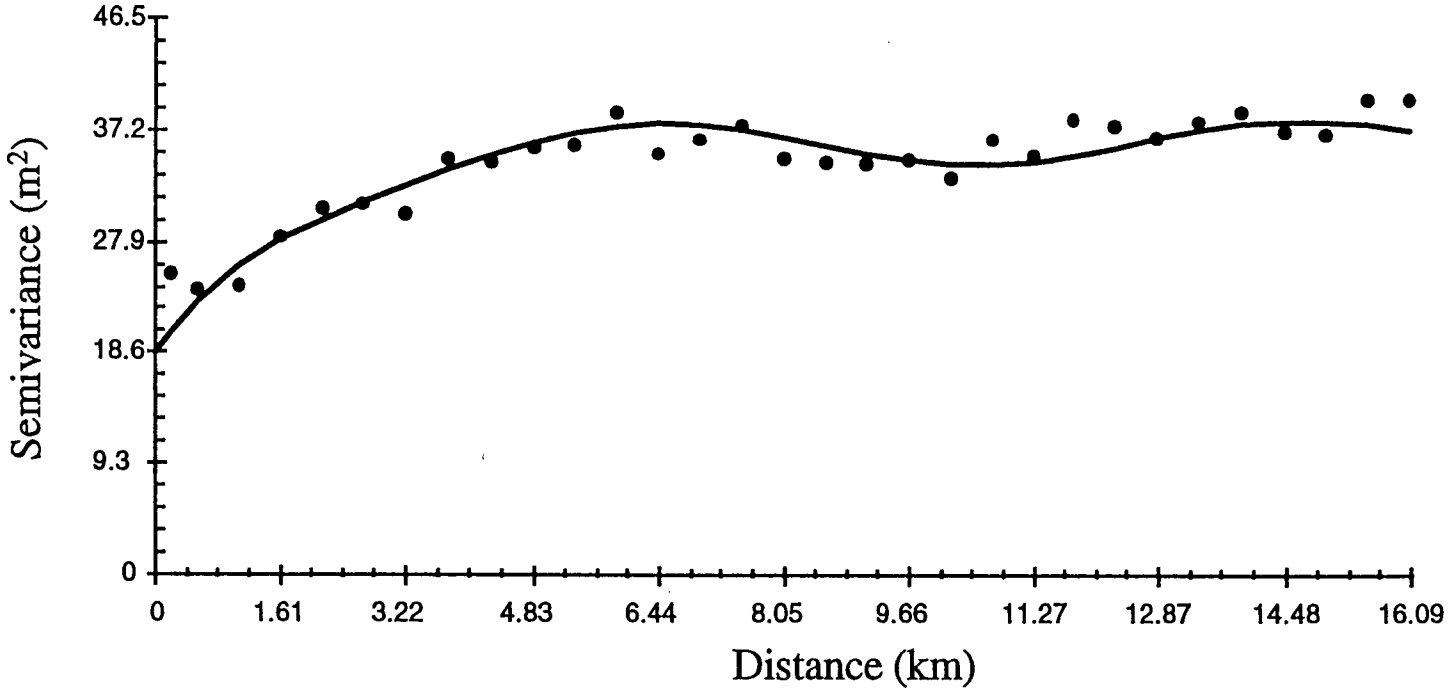

Figure A3.20: Direcrtional semivariogram in Zone 3. The direction is 67.5 degrees. The range is 4.83 km (3 mi). The sill is 36.2 m^2 (390 ft^2) and the nugget effect is 18.6 m^2 (200 ft^2). The lag distance is 1/3 of a mile (0.54 km). The hole effect present in the variogram is modeled by superimposing sine and/or cosine functions on the exponential model. Its purpose is to better identify the nugget sill and range parameters of the semivariogram.

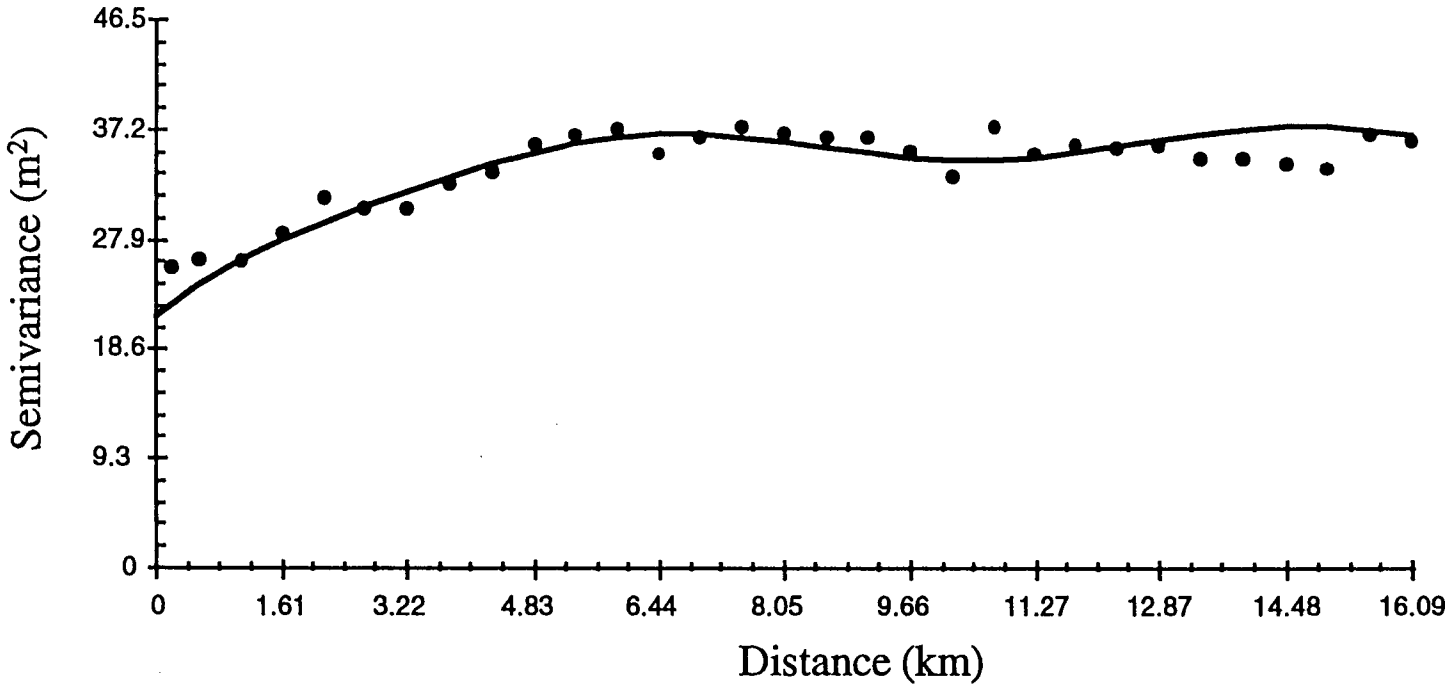

Figure A3.21: Direcrtional semivariogram in Zone 3. The direction is 90 degrees. The range is 6.44 km (4 mi). The sill is 36.2 m^2 (390 ft^2) and the nugget effect is 22.4 m^2 (230 ft^2). The lag distance is 1/3 of a mile (0.54 km). The hole effect present in the variogram is modeled by superimposing sine and/or cosine functions on the exponential model. Its purpose is to better identify the nugget sill and range parameters of the semivariogram.

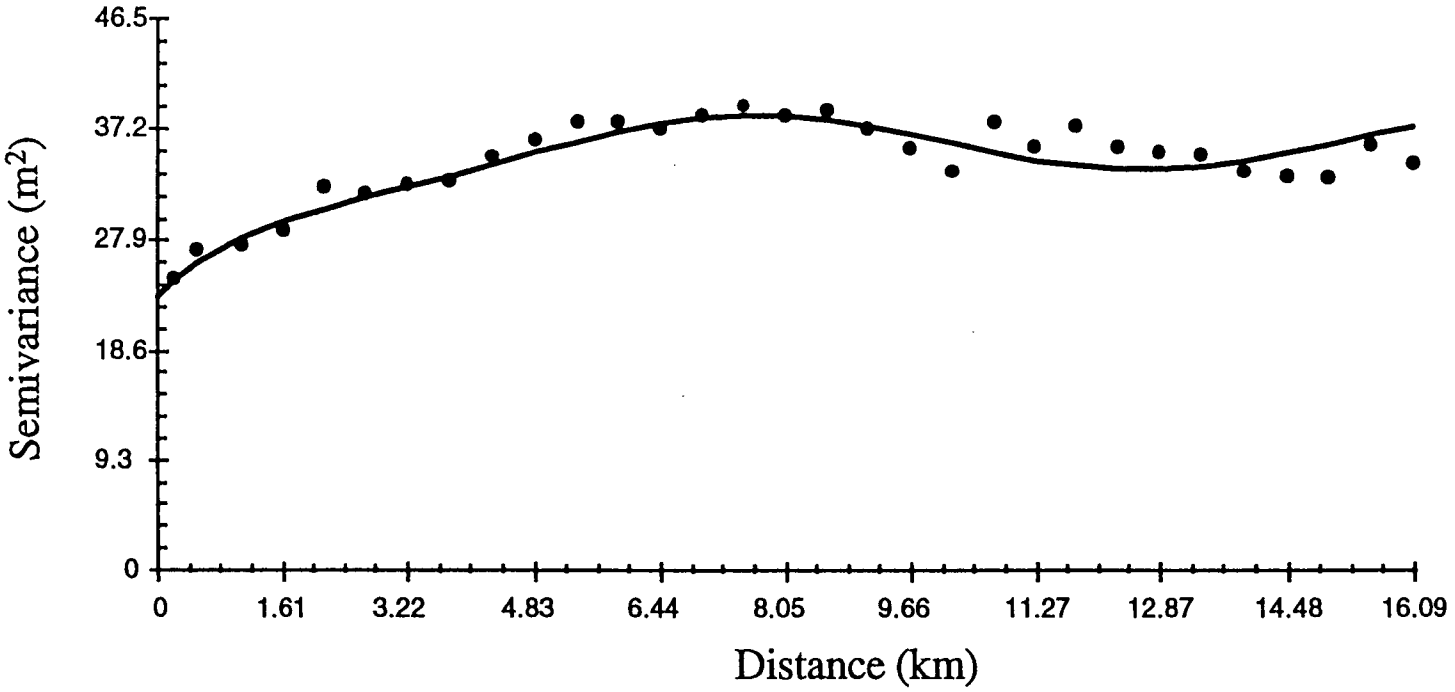

Figure A3.22: Direcrtional semivariogram in Zone 3. The direction is 112.5 degrees. The range is 4.83 km (3 mi). The sill is 36.2 m^2 (390 ft^2) and the nugget effect is 23.2 m^2 (250 ft^2). The lag distance is 1/3 of a mile (0.54 km). The hole effect present in the variogram is modeled by superimposing sine and/or cosine functions on the exponential model. Its purpose is to better identify the nugget sill and range parameters of the semivariogram.

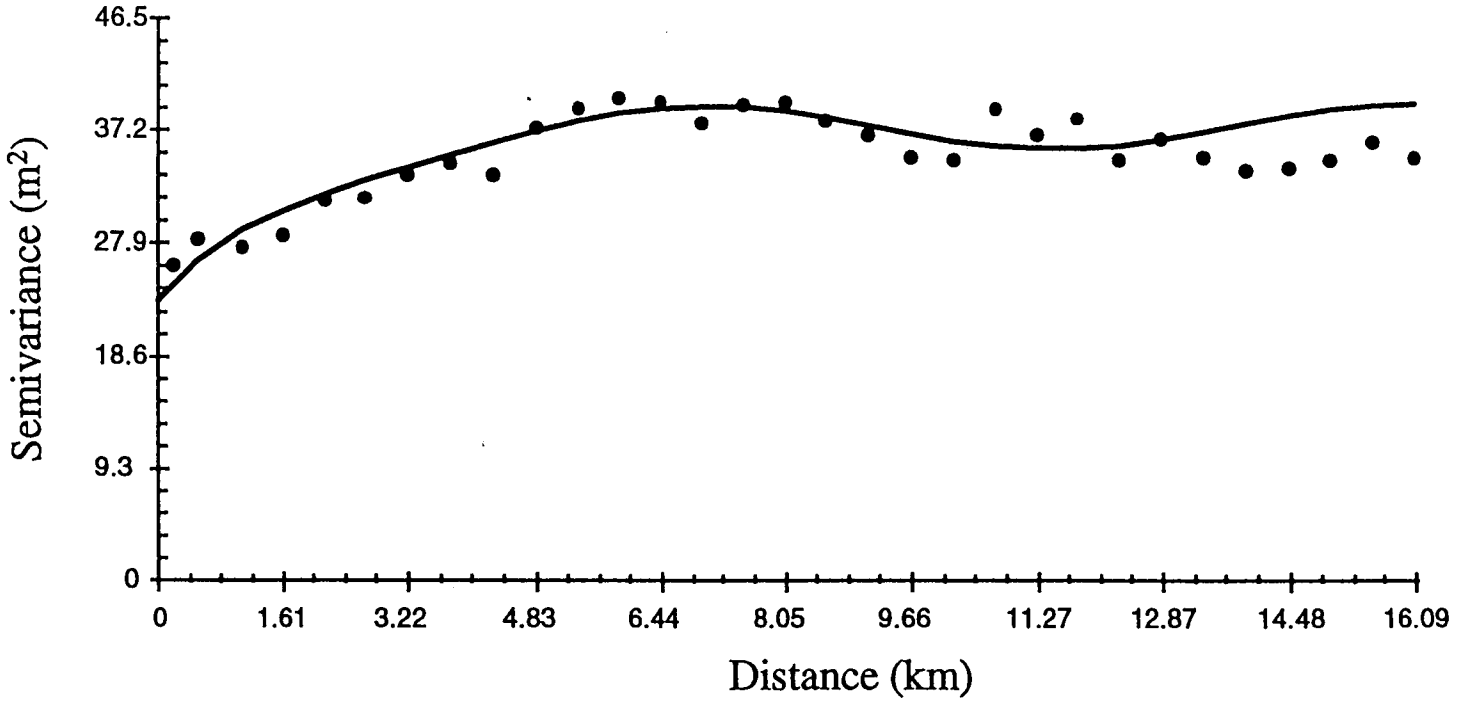

Figure A3.23: Direcrtional semivariogram in Zone 3. The direction is 135 degrees. The range is 4.83 km (3 mi). The sill is 37.6 m^2 (405 ft^2) and the nugget effect is 23.2 m^2 (250 ft^2). The lag distance is 1/3 of a mile (0.54 km). The hole effect present in the variogram is modeled by superimposing sine and/or cosine functions on the exponential model. Its purpose is to better identify the nugget sill and range parameters of the semivariogram.

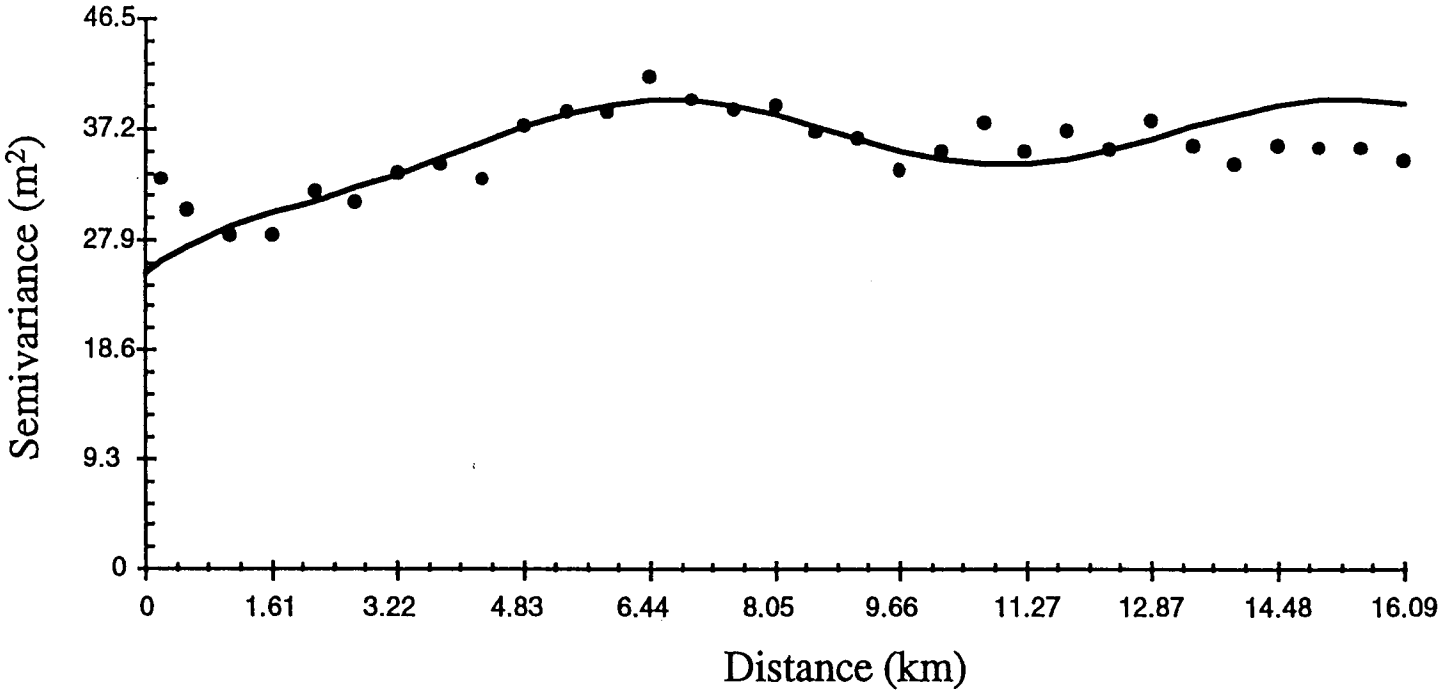

Figure A3.24: Direcrtional semivariogram in Zone 3. The direction is 157.5 degrees. The range is 4.83 km (3 mi). The sill is 37.2 m^2 (400 ft^2) and the nugget effect is 25.1 m^2 (270 ft^2). The lag distance is 1/3 of a mile (0.54 km). The hole effect present in the variogram is modeled by superimposing sine and/or cosine functions on the exponential model. Its purpose is to better identify the nugget sill and range parameters of the semivariogram.